

**Computer Simulation of Fundamental
Processes in High Voltage Circuit Breakers
Based on an Automated Modelling
Platform**



UNIVERSITY OF
LIVERPOOL

Thesis submitted in accordance with the requirements of the
University of Liverpool for the degree of Doctor in Philosophy

by

Yuqing Pei

November 2014

Department of Electrical Engineering and Electronics

The University of Liverpool

Acknowledgement

First of all, I would like to express my sincerest gratitude to my supervisor, Dr. Joseph D Yan, for his enthusiastic guidance, support, patience, and rigorous training over the period of my postgraduate research. He has helped me selflessly in all aspects of my life and work. I could not think of having a better advisor and mentor.

My special appreciation goes to Professor Michael T C Fang for his encouragement, insightful comments, and challenging questions. He is an extremely kind and helpful person and a great source of knowledge and wisdom.

My sincere thanks also go to my second supervisor Professor Joseph W Spencer for useful discussions, my colleagues Jian Liu and Quan Zhang for all the collaboration, discussion, generation and exchange of ideas, and their friendship.

Special acknowledgement must be addressed to Pinggao Group Co Ltd, a subsidiary of the State Grid Corporation of China (SGCC) for their financial support.

Last but not the least, my deepest gratitude is specially addressed to my parents, brother, sister-in-law, and my boyfriend, who all have been so loving all the time.

Abstract

Auto-expansion circuit breakers utilize the arc's energy to generate the flow conditions required for current interruption. The operation of this type of circuit breaker is extremely complex and its interruption capability depends on the whole arcing history as well as a number of geometric factors. On the other hand, circuit breaker development based on test is extremely expensive and time consuming. The accumulated understanding of the underlying physical processes so far enables arc models be used as a tool for optimum design of switchgear product such as high voltage circuit breakers. For academic research, there is often a need to study the performance of a newly developed arc model by inspecting the distribution of relevant physical quantities during a simulation and their sensitivity to model parameters in an efficient and convenient approach. However the effective use of computer simulation by design engineers has been hindered by the complexity encountered in model implementation.

This thesis presents the development and structure of an automated simulation tool, the Integrated Simulation and Evaluation Environment (ISEE), for the arcing process in gas-blast circuit breakers. The functionalities of ISEE are identified and developed based on the experience in real product design, which include visual creation and definition of components, automatic setup of arc models based on a commercial CFD software package as equation solver, simulation task management, and visualization of computational results in "real-time" mode. This is the first automated simulation platform in the community of switching arc simulation.

Using ISEE as the simulation tool, different designs of auto-expansion circuit breakers have been investigated to reveal the fundamental characteristics of the arcing process under different test duties. Before attempting to investigate the capability of an auto-expansion circuit breaker, the fundamental issue of determining the turbulence parameter of the Prandtl mixing length model is addressed. Previous studies on turbulence arcs were mostly concerned with simple converging-diverging nozzles. There has been little work on real circuit breaker nozzles. In order to calibrate the turbulence parameter, real arcing conditions including interrupting

currents, contact travels, and transient recovery voltages of two commercial circuit breakers, with rated voltage of 145 kV and 245 kV, have been used together with the geometry of the circuit breakers to calibrate the range of the turbulence parameter. The effect of nozzle ablation has been considered. All together 6 cases have been used for three circuit breakers with each pair of cases corresponding to a success and failure in its thermal recovery process. It has been found that a single parameter of 0.35 is applicable to all three circuit breakers with an auxiliary nozzle and a main nozzle of converge-flat throat-diverge shape. It must be noted that this value is obtained with the definition of thermal radius introduced in Chapter 3 and the assumption that the parameter linearly changes with the interrupting current from 0.05 at 15 kA to 0.35 at current zero.

Using the calibrated turbulence model, a computational study of the thermal interruption performance of a 145 kV, 60 Hz auto-expansion circuit breaker with different arc durations has been carried out in Chapter 4. The relation between pressure peak and current peak in the auto-expansion circuit breaker is discussed. It has been found that a larger average mass flux in the main nozzle indicates a better interruption environment, enabling the circuit breaker to withstand a larger rate of rise of recovery voltage after current zero. Another important finding is that the auxiliary nozzle plays an important role in an auto-expansion circuit breaker both at the high current phase and during the current zero period. Therefore, the proper design and use of an auxiliary nozzle is a key factor to enhance the thermal interruption capability of high voltage auto-expansion circuit breakers.

In Chapter 5 of the thesis, the transient pressure variation in auto-expansion circuit breakers was studied. The pressure variation has an extremely complex pattern and the pressure changes in different ways depending on the location in the arcing chamber. It is shown, for the first time, that the time lag between the current peak and pressure peak in the expansion volume can be explained by using an energy flow rate balance method, that is flow reversal occurs when the enthalpy exhaustion rate from the contact space equals the electrical power input. Following the flow reversal, a high enthalpy flow rate from the expansion volume into the contact gap first occurs for a short while (1 ms), which is followed by a high mass flow rate of relatively cool gas at less than 2000 K. This high mass flow rate causes a surplus in mass flow

rate into the contact gap and results in the last temporary pressure peak in the contact space before the pressure and flow field finally settle down for arc quenching at current zero. The pressure change under different conditions, i.e. different arc durations, different current levels and different length of the heating channel, has also been studied in details.

In summary the present research leads to original findings in three aspects of the operation of auto-expansion circuit breakers, i.e. the calibration of the turbulence parameter for the Prandtl mixing length model, interruption performance with different arc durations, and the transient pressure variation in the arcing process. The results are expected to provide useful information for the optimum design of auto-expansion circuit breakers.

Contents

Acknowledgement	ii
Abstract	iii
Contents	vi
List of Figures	ix
List of Tables	xvii
1. Introduction	1
1.1 Circuit Breaker in Power System.....	1
1.2 Types of Circuit Breakers.....	3
1.3 Interactions of Circuit Breakers with the Power System and Transient Recovery Voltage	8
1.4 Basic Physics of Interrupting Arcs.....	10
1.4.1 Gases in circuit breaker as a continuum medium	11
1.4.2 Plasma in thermal equilibrium.....	12
1.4.3 Arc instability (Turbulence)	14
1.5 Arc Models in Gas Flow	17
1.5.1 Integral method for arc in gas flow	18
1.5.2 Differential method for arc in gas flow	20
1.6 The Objective and Organization of The Thesis	22
References	24
2. The Development of an Integrated Simulation and Evaluation Environment (ISEE) for High Voltage Circuit Breaker	30
2.1 Introduction	30
2.2 Consideration of Switchgear Design Practice and Structure of the Simulation Platform	32
2.2.1 The overall structure	32
2.2.2 Division of the arcing process	35
2.2.3 Automated initiation and management of different phases in the simulation.....	38
2.3 Objects and Representation of Design Parameters Relating to Physical and Simulation Properties.....	38
2.4 Modelling of Arcs, Moving Component and Operation of Valves	41
2.4.1 The arc model built in ISEE	41
2.4.2 Moving components.....	51
2.4.3 Valve operation	53
2.5 Intelligent Process Control and Grid Generation in ISEE.....	56
2.5.1 Method of grid generation	57
2.5.2 Generation of input data files	65
2.5.3 Settings and initiation of the cold flow phase	68
2.5.4 Start of high current phase (Initiation of arc)	69
2.5.5 Start of current zero phase.....	70
2.5.6 Post arc zero phase.....	70
2.6 Information Exchange between Solver and ISEE-Visual Monitor.....	71

2.7	Conclusion.....	72
	References	74
3.	A Study on the Applicability of Prandtl Mixing Length Model to Arc Simulation of Commercial Gas-blast Circuit Breakers.....	77
3.1	Introduction	77
3.2	Definition of Arc Radius in Prandtl Mixing Length Model	78
3.3	Test Results for a 145 kV Auto-expansion Circuit Breaker	80
3.4	Simplifications on Geometry.....	84
3.5	No-load Case	87
3.6	Radiation Model Verification	89
3.7	Mass of Ablated PTFE	92
3.8	Calibration of Turbulence Parameter for Prandtl mixing length model in Current Zero Period	95
3.8.1	Current zero phase	95
3.8.2	Post current zero phase (post arc phase)	96
3.8.3	Discussion	100
3.9	Summery	103
	References	105
4.	A Comparative Study of Arc Behaviour in an Auto-expansion Circuit Breaker with Different Arc Durations.....	107
4.1	Introduction	107
4.2	The Whole Simulation Geometry	108
4.3	Comparison of Pressurization in the Expansion Volume	109
4.4	Flow Environment before Current Zero.....	118
4.5	Thermal Recovery Process	122
4.6	Critical Rate of Rise of Recovery Voltage (RRRV).....	124
4.7	Conclusions	128
	References	130
5.	Transient Pressure Variations following Flow Reversal and Their Implications towards the Interruption Performance of Auto-expansion Circuit Breakers	132
5.1	Introduction	132
5.2	Existing Study on Pressure Variation in Gas-blast Circuit Breakers	133
5.3	Verification of the Arc Model.....	136
5.5	Results	141
5.5.1	Mechanisms responsible for pressure variation.....	141
5.5.2	Different arc durations	158
5.5.3	Different current levels.....	166
5.5.4	Design parameter-channel length	168
5.6	Conclusions	172
	References	174
6.	Conclusions and Future Work.....	177
6.1	Major Contribution and Achievements	177
6.2	Summary and Conclusions	178
6.3	Future Work.....	180
6.3.1	Improvement for arc model based on measurement	180

6.3.2	Parallel processing	180
6.3.3	Radiation transfer and nozzle ablation.....	181
References	182

List of Figures

Figure 1.1: Diagram of a typical generation, transmission and distribution network[1].....	2
Figure 1.2: Major types of circuit breaker and their years in service	4
Figure 1.3: Plain air circuit breaker, diagram from [5] (left); and Air-blast circuit breaker nozzle system in 1926 [2] (right)	5
Figure 1.4: Cross section of vacuum interrupter, diagram from [6].....	6
Figure 1.5: Typical structure of a puffer SF ₆ circuit breaker.....	7
Figure 1.6: Typical structure of a 145 kV auto-expansion/self-blast SF ₆ circuit breaker.....	8
Figure 1.7: Short line fault (SLF) transient recovery voltage	10
Figure 1.8: Turbulent eddies in nozzle arc [26] near the current zero	14
Figure 1.9: Fast streak records of the arc in the vicinity of current zero at different axial positions as indicated with a, b, c, d, e (N ₂ , 23 bar, di/dt=-39A/us) [26].....	15
Figure 1.10: Velocity profile for a free jet flow and switching arc	16
Figure 2.1: The hierarchic structure of the proposed Integrated Simulation and Evaluation Environment (ISEE) for high voltage gas blast circuit breakers.	33
Figure 2.2: Typical geometry of an auto-expansion circuit breaker.....	36
Figure 2.3: An example of component represented using GraphicsPath.....	39
Figure 2.4: Diagram showing boundary conditions for the electrostatic potential equation (current continuity equation). The blue dotted lines are the 10,000 K isotherms approximating the conducting arc column. The equi-potential lines are perpendicular to the boundary surface representing a zero current density normal to the boundary faces.	46
Figure 2.5: Possible temperature profile of arcs and the emission (0 ~ R ₈₃) and re-absorption (R ₈₃ ~ R _{5k}) zones	47
Figure 2.6: A comparison of the NEC of pure SF ₆ , 50% SF ₆ – 50% PTFE, and pure PTFE vapour at 40bar which is the typical pressure in the arc at high current.	48
Figure 2.7: Diagram shows approximation of the rounded tip of a moving	

contact by flat tipped longitudinal rings, real geometry is assigned by black solid lines	51
Figure 2.8: Diagram (left) shows a valve in real circuit breaker, and (right) shows the simplified one in simulation.....	53
Figure 2.9: Diagram showing linear relationship between the six threshold value of force F_v and the number of rings of the divided cross sectional area of the valve hole (0,1,2,3,4,5, altogether 6 stages) that are kept open to flow.	54
Figure 2.10: Diagram shows the valve switches from closed to open state.....	55
Figure 2.11: Diagram illustrates the criteria of growing method for vertical grid lines	59
Figure 2.12: Flow chart of vertical grid line generating process.....	60
Figure 2.13: Diagram shows the process of growing vertical lines from corner SL	61
Figure 2.14: Diagram shows the process of growing vertical lines from corner SH	62
Figure 2.15: Diagram shows four components with green boundary in computation domain in wheat, red vertical grid lines divided whole domain into 23 blocks.....	63
Figure 2.16: Diagram shows the grid system divided by vertical and horizontal grid lines.	63
Figure 2.17: Diagram illustrates the criteria of growing method horizontal grid lines according to the blocks/patches those divided by vertical line in Figure 2.15.....	65
Figure 2.18: Diagram showing information flow in computer simulation of switching arcs based on PHOENICS. Blue rectangles – files to be prepared by user and will be automatically generated using ISEE platform; read circles- executables to be run during the simulation	66
Figure 2.19: Diagram shows the naming scheme for grid system	67
Figure 2.20: Required setting and files for each simulation stage	71
Figure 3.1: Contours of temperature and axial velocity component for (a) a nozzle arc at 1 kA DC with stagnation pressure of 1.12 MPa and exit pressure is near vacuum [8] (b) real circuit breaker with the instantaneous current of 5 kA, filling pressure of 0.6 MPa	80

Figure 3.2. Diagram shows the (a) contact and (b) nozzle of a 252 kV circuit breaker after L90 test (Pinggao) (c) PTFE surface of a test device (ABB) [16]	81
Figure 3.3: Current and travel curves for Test 92, 93 and 98, the slight difference between the travel curves are based on the scattering of the mechanical driver. Contacts separate at 9.8 ms, 10.6 ms and 11.4 ms for 92, 93 and 98, respectively. In simulation, arcs are initialised at 12.2 ms, 13 ms, and 13.8 ms for 92, 93 and 98, respectively.	83
Figure 3.4: Current and travel curves for Test 750 (thermal clearance) and 751 (thermal failure) (a) original test data and (b) smoothed data for simulation with arcs initiation at 19.66 ms and 6.2 ms for 750 and 751, respectively.	84
Figure 3.5: CAD drawing of the whole geometry of (a) 145 kV auto-expansion circuit breaker (b) 245 kV auto-expansion circuit breaker	86
Figure 3.6: Simplified geometry of (a)145 kV circuit breaker in simulation with 5 monitor points, P1 is the expansion volume, P2 in the heating channel, P3 in the middle section of main nozzle throat, P4 in the downstream of main nozzle, P5 in the compression volume (b) 245 kV circuit breaker	87
Figure 3.7: Comparison of pressure between prediction and measurement in (a) expansion volume (b) heating channel (c) middle section of nozzle throat (d) downstream region of the nozzle throat (e) compressor for the 145 kV circuit breaker, the measurement locations are given in Figure 3.6a.....	88
Figure 3.8: Pressure distribution at several typical time instants	89
Figure 3.9: Electric input ($U \cdot I$) and predicted PTFE ablation mass from simulation as a function of time in the arcing process for the 245 kV auto-expansion circuit breaker.	91
Figure 3.10: Measured specific ablation in an ABB test device versus peak current density. Applied peak current amounted from 4 to 64 kA. Arcing times were 5, 10 and 15 ms [16], comparing with predicted results of real auto-expansion circuit breaker simulation.	92
Figure 3.11: Predicted PTFE ablation on (a) auxiliary nozzle throat (b) main nozzle throat and (c) total ablated surface	94

Figure 3.12: Temperature distribution at current zero for (a) case 92, 93 and 98 (b) 750 and 751	96
Figure 3.13: Transient recovery voltage of test 92 and 93 for the 145 kV auto-expansion circuit breaker.....	98
Figure 3.14: Transient recovery voltage of test 750 and 751 within 600 us for the 245 kV auto-expansion circuit breaker.....	98
Figure 3.15: Post arc current with different turbulence parameter for (a) test 92 (b) test 93.....	99
Figure 3.16: Post arc current with different turbulence parameter for (a) test 750 (b) test 751	99
Figure 3.17: Axis temperature and electric field of Test 750 and 751 for 10us, 5 us before current, current zero and 0.5 us after current zero. These results were predicted with Tp_{I0} equal to 0.35.....	102
Figure 3.18: Profiles at critical cross section of main nozzle throat (a) radial temperature and turbulent eddy viscosity (b) mass flux (product of density and axial velocity)	103
Figure 4.1: Simplified geometry and computational domain of the 145 kV auto-expansion circuit breaker under investigation. The final position of the live contact is shown by the three dash lines near the live contact for different arc durations.	109
Figure 4.2: Predicted pressure rise in the expansion volume.....	110
Figure 4.3: Enthalpy flow rate at location A (assigned in Figure 4.1) in the flow guild channel at high current phase.	110
Figure 4.4: Temperature distribution with velocity field for short, medium and long arc duration at current peak of 56 kA from top to bottom, the time instant for live contact position is (a) 16.5ms (b) 19.5ms (c) 21.3ms (d) 23.5ms.....	111
Figure 4.5: Pressure records in the arcing chamber for (a) short (b) medium, and (c) long arc duration.....	115
Figure 4.6: Pressure distribution for long arc duration at current zero.....	116
Figure 4.7: Axis electric field 5us before current zero and 0.5us after current zero under dV/dt of 8kV/us.	116
Figure 4.8: Radial integrated energy balance of critical cross section with axial position 0.55 m at final current peak for (a) short (b) medium and (c)	

long arc duration. The curves present	117
Figure 4.9: Radial integrated energy balance at 500A for the short arc duration case, the meaning of each curve is same as Figure 4.7.....	118
Figure 4.10: Temperature 9.5mm away from axis at current zero.	120
Figure 4.11: Mass flux at critical cross section (axial position of 0.56 m) at current zero.	120
Figure 4.12:Radial temperature at critical cross section (axial position of 0.56 m) at current zero.	121
Figure 4.13: Mass flow rate at the axial position of 0.56 m versus pressure difference between (a) expansion volume and the middle of nozzle throat, i.e. P1-P3 in Figure 4.6; (b) heating channel and downstream of nozzle throat at current zero, i.e. P2-P4 in Figure 4.6.(c) heating channel and the middle of nozzle throat, i.e. P2-P3 in Figure 4.6 (d) upstream of nozzle throat and downstream of nozzle throat, i.e. P5-P4 in Figure 4.6.....	121
Figure 4.14: Axis temperature at current zero.....	122
Figure 4.15: Post arc current under different RRRV for short arc duration.....	124
Figure 4.16: Axis temperature 5 us before current zero and 0.5 us after current zero under dV/dt of 8 kV/us.	125
Figure 4.17: Temperature distribution with velocity field at current zero for short, medium and long arc duration cases, respectively.	127
Figure 4.18: Turbulent eddy viscosity at the cross sections with axial position 0.54 m and 0.56 m for short, medium and long arc duration at current zero. S_0.54m means the dynamic viscosity distribution in the radial direction at axial location 0.54 m.	128
Figure 5.1: Geometry used in simulation of auto-expansion circuit breaker in the present investigation, the position of monitoring point P1 is assigned.	137
Figure 5.2: Predicted pressure variation in the expansion volume of the auto-expansion circuit breaker specified travel curve of the driving mechanism for no-load case and arcing case at 40 kA.	139
Figure 5.3: Predicted and measured arc voltage for the given current waveform. The measured arc voltage has been corrected to exclude the voltage drop in the metallic conductors between the voltage measurement	

points.....	140
Figure 5.4: Arcing chamber with the monitor points P1- P11, P1 is in the expansion volume with position shown in Figure 5.1. The live contact tip position (a) at 29.7 ms (start of flow reversal), (b) 30.8 ms and (c) 32.3 ms (current zero).....	142
Figure 5.5: (a) Temperature and (b) pressure distribution with vector field at 18.9 ms	143
Figure 5.6: Temperature variation of the gas flow into the expansion volume at P3 in Figure 5.4	143
Figure 5.7: (a) Temperature and (b) PTFE concentration in the arcing chamber at 24 ms.....	144
Figure 5.8: (a) Temperature and (b) pressure distribution with vector field at 25.5 ms	145
Figure 5.9: Enthalpy flow rate ($\rho\omega \cdot 2\pi r dr$) and mass flow rate ($\rho\omega h \cdot 2\pi r dr$) from cross section A, B and C which assigned in Figure 5.4;.....	145
Figure 5.10: Total mass ($\rho\omega \cdot 2\pi r dr dt$) and enthalpy in/out ($\rho\omega h \cdot 2\pi r dr dt$) from cross section A, B and C which assigned in Figure 5.4; “-” means the flow travels in negative direction (positive direction assigned in Figure 5.4)......	146
Figure 5.11: Pressure variation for P1 to P11 with current waveform from arc initialisation to the final current zero with their location in Figure 5.4	147
Figure 5.12: The power flux normal onto the ablating surface, $Q_{ablation} = \xi(1 - \alpha) \iint_0^{R_{833}} q \cdot 2\pi r dr dz$, at main PTFE nozzle (M.N.) and auxiliary nozzle (A.N.), where ξ is the coefficient which is determined by the ablation surface incline, α is the reabsorption factor, q is the net radiation loss per unit volume and time.	149
Figure 5.13: Power and mass confined in the arcing chamber which is highlighted in flash box in Figure 5.4	150
Figure 5.14. (a) Temperature and (b) pressure distribution at 30.2 ms	151
Figure 5.15: Pressure variation at 5 monitoring points with their location in Figure 5.4.....	152
Figure 5.16: Temperature distribution at 29.7 ms at the instant of flow reversal. .	153
Figure 5.17: (a) Temperature and (b) pressure distribution with vector field at	

30.8 ms	154
Figure 5.18: Diagram showing the (a) enthalpy flow rate and (b) mass flow rate as a function of time out of the expansion volume (A_MFR), into the hollow contact (B_MFR), and out of the main nozzle (C_MFR). The sign of the values is with reference to the positive axial direction which is pointing from the hollow contact to the main contact.....	155
Figure 5.19: Temperature and flow field at current zero, in the heating channel (top) and in the arcing space (bottom).	157
Figure 5.20: Pressure rise in the expansion volume for different arc durations.....	159
Figure 5.21: (a) Mass and enthalpy flow rate (b) Total mass and energy into the expansion volume through cross section A for different arc durations.....	160
Figure 5.22: Temperature distribution at first current zero for short, medium, long arc duration cases at 21.8 ms, 23.6 ms and 25.5 ms, respectively	160
Figure 5.23: Temperature distribution at final current peak for short, medium, long arc duration cases at 27.1 ms, 28.9 ms and 30.8 ms, respectively	161
Figure 5.24: Pressure variation in the arcing space for different arc durations	161
Figure 5.25: Axis pressure at current zero for different arc durations.....	162
Figure 5.26: Axial direction component of axis velocity at current zero for different arc durations	162
Figure 5.27: Axis temperature at current zero, and 5 us, 30us and 50 us after current zero for different arc durations.	164
Figure 5.28: Critical electrical field E_{cr} at different pressures [21]	164
Figure 5.29. (a) Critical breakdown voltage at axis for different arc duration (b) Integrated critical breakdown voltage along the axis 50 us after current zero	165
Figure 5.30: Temperature and pressure at axis at current zero for L90 and L75 cases	167
Figure 5.31:..... Pressure in the arcing space at current zero for L90 and L75 cases
Figure 5.32: Critical breakdown voltage for L90 and L75	168
Figure 5.33. Pressure rise in the expansion volume for different channel length with (a) short arc duration (b) long arc duration.....	169

Figure 5.34: Pressure in the arcing space for different channel length with (a) short arc duration (b) long arc duration.....171

Figure 5.35: Total mass in the highlighted region with dash line in Figure 5.4 for different channel length with (a) short arc duration (b) long arc duration.....171

Figure 5.36: Critical breakdown voltage at axis for different channel length with (a) short arc duration (b) long arc duration.....172

List of Tables

Table 2.1: Main properties of PTFE nozzle component	40
Table 2.2: Main properties of Flow Inlet/Outlet virtual component make change to this table below for more and clear information.	40
Table 2.3: Concept and dimension of virtual component	41
Table 2.4: Source terms and diffusion coefficients for governing equations.....	42
Table 2.5: Parameters for SF ₆ and air	50
Table 2.6: Model parameters to simulation valve operation	55
Table 2.7: Growing Method of vertical lines from different points	58
Table 2.8: Three-Line-Method	62
Table 2.9: Growing method of horizontal lines from different point	64
Table 3.1: Information on type test of the 145 kV auto-expansion circuit breaker ..	82
Table 3.2: Erosion measurement on completion of the first round of type test on the 145 kV auto-expansion circuit breaker. The measurement was carried out using a Vernier Caliper.	83
Table 3.3: Specific ablation for three different auto-expansion circuit breakers from prediction.....	91
Table 3.4: Predicted PTFE mass ablation after each test without considering nozzle diameter variation due to PTFE ablation after each test	95
Table 3.5: Predicted and test nozzle throat variation for 145 kV circuit breaker	95
Table 3.6: Predicted ablated PTFE mass for 245 kV auto-expansion circuit breaker	95
Table 3.7: Predicted and test nozzle throat variation for 245 kV circuit breaker	95
Table 3.8: Summery of turbulence parameters for calibration cases	100
Table 4.1: Voltage across two sections of arc column separated by the stagnation point.....	123

Chapter 1

Introduction

1.1 Circuit Breaker in Power System

A typical power system, also called a grid, consists of three sub-systems, namely the generation, transmission and distribution systems. A generator generates electric power which is for most of the time fed into the transmission system or directly to the distribution system. The transmission system transmits the power from the generators to the destination over long distances, and the distribution system takes over from the transmission system to feed the power to a particular area or customer, on a continuous basis. The whole system must be kept in operation without major breakdown, to meet the users' demand. As illustrated in Figure 1.1, electric power is produced in the power generation plant, then through a step-up transformer the transmission voltage is increased to reduce power loss. At the end of the transmission line, a step-down transformer is used to decrease the voltage level and supply power to the customers. The objective of power system protection is to isolate faulty components from the rest of the network to avoid further damage to the network equipment, ensure reliable and stable operation of other parts of the grid. The most important functionality of a circuit breaker (Component 6 in Figure 1.1) is indeed to disconnect a faulty part of the network, thus serving as protective apparatus in the network.

International Electro-technical Commission (IEC) and American National Standards Institute (ANSI) defines a circuit breaker as “*a mechanical switching device, which is capable of making, carrying and breaking currents under normal circuit conditions and also making, carrying for a specified time and breaking currents under specified abnormal circuit conditions such as those of short circuit*”. Pure solid state switching devices do not have a test standard yet. Under normal condition, a circuit breaker is at the closed position, performing like a good conductor and

withstanding normal load currents. Only on certain occasions, it is needed to change the closed position to the open position. Therefore, it must be reliable in the static situations, but be effective instantaneously when it is instructed to disconnect an overload or a fault circuit. When a fault occurs, circuit breaker rapidly isolates the faulty part of a network by separating the two contacts with an electric arc formed between the arcing contacts. Before the arc is extinguished, it is able to withstand the specified current. After the circuit breaker fully opens, it acts as an insulator. It is the arc that provides the properties required to change the inter-contact impedance rapidly. Therefore, the arc is an essential component of the interrupting process.

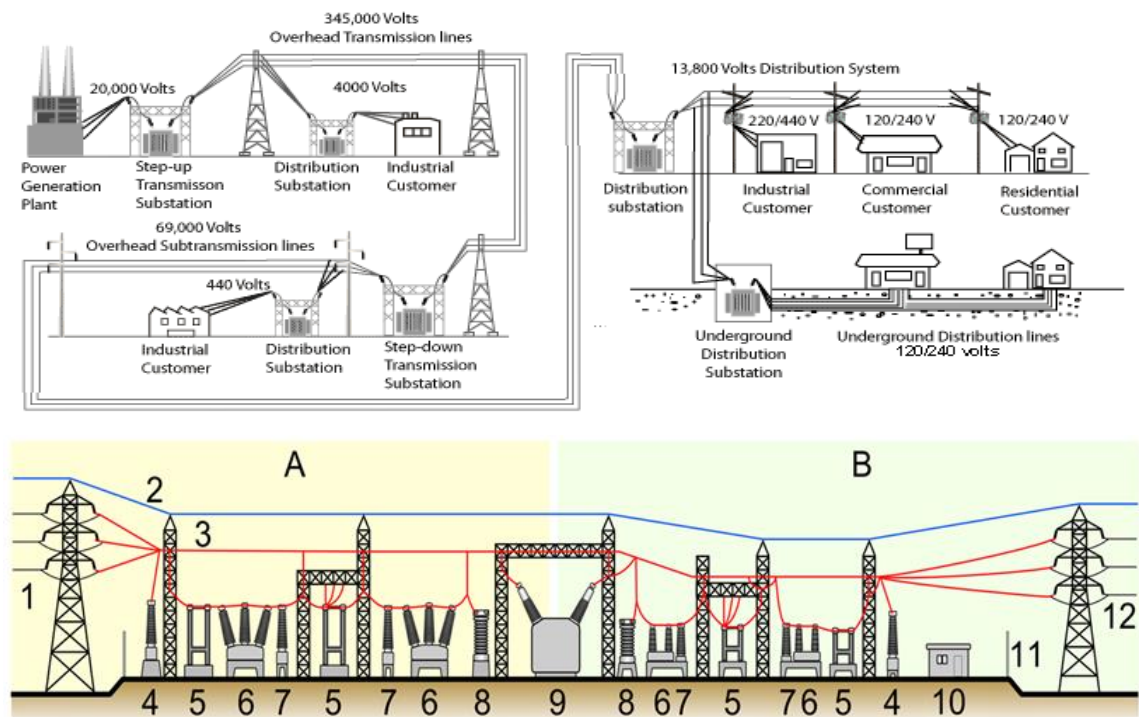


Figure 1.1: Diagram of a typical generation, transmission and distribution network [1]

A: Primary power lines' side, B: Secondary power lines' side, 1. Primary power lines
 2. Ground wire 3. Overhead lines 4. Transformer for measurement of electric voltage
 5. Disconnect switch 6. Circuit breaker 7. Current transformer 8. Lighting arrester 9.
 Main transformer 10. Control building 11. Security fence 12. Secondary power lines

The rate of impedance change from conductor to insulator for the medium between the arcing contacts is very important. If this rate is low, a long arc duration ($>20\text{ms}$) will generate a considerable amount of thermal energy in resistive elements leading to overheating and damage of hardware components. However, if the rate is too high, an extremely high voltage of $-L(di/dt)$ will be generated across the inductive elements causing over voltage damage. Severe current chopping by a circuit breaker is such a

typical example. Therefore, the magnitude of di/dt must be within an acceptable range. In an alternating-current (AC) circuit, the current passes two zero points in each cycle. Rapid impedance variation happens during the current zero periods, which is advantageously employed in AC circuit breakers for current interruption.

With the increasing of industry demand, to reduce the power loss, the network voltages have risen to ultra-high level. A number of ultra-high voltage AC transmission system have already been constructed in different parts of the world. For example, 2,362 km of 1,150 kV transmission system were built in the Former USSR, and 427 km of 1,000 kV AC transmission system have been developed in Japan (Kita-Iwaki power line). The State Grid Corporation of China (SGCC) started to run the first 1,000 kV AC power line between northern Shanxi province and center of Hubei province (Jindongnan-Nanyang-Jingmen, 650 km) in January 2009. As a result of the growth in network size, interruption of short circuits becomes the most arduous duty for circuit breakers, and the total break time required has also been reduced. For example, the early oil circuit breakers need a rather long interruption time of 10- 20 cycles [2], while with improved techniques new designs can now operate within 2 cycles. A brief history of circuit breaker development and their working principles are given in the section below.

1.2 Types of Circuit Breakers

Circuit breakers are commonly classified based on the insulating medium used for arc quenching. Although air is the first extinguishing medium that employed in the earliest switching device [3], it was not long before a better dielectric was needed and insulating oil soon appeared on the switchgear scene. The first 40 years of experience of circuit switching of high power was based on oil, which satisfied the requirement of uprating in both current and voltage during that time [3]. Air is free, abundant, and self-restoring after breakdown [2][4]. Self-restoring means the insulating properties recovery. Application of air to high voltage switchgear was first proposed at the British Electrical Research Association by Whitney and Wedmore in 1926 [3]. The earliest high power airbreak circuit breaker was then developed by Slepian at Westinghouse in 1929 [2]. The study of vacuum interruption was

undertaken by Sorensen and Mendenhall at the California Institute of Technology in 1923-26 [2]. The early developed vacuum circuit breaker at 1950s were only capable of switching about 4 kA r.m.s. and 20 kV r.m.s. [2]. In 1961, Ross put six vacuum breaking interrupters in series to switch the load current in 230 kV systems [2]. After that, High voltage vacuum circuit breaker (132 kV, 1200 A) started to be developed by Electrical Research Association (ERA) in the UK in 1967. The fundamental research on Sulphur hexafluoride (SF_6) was started in the 1950s. SF_6 was first used in gas blast circuit breakers in 1959 by Westinghouse. With increased knowledge on different insulating media, more types of circuit breakers were developed and put into service.

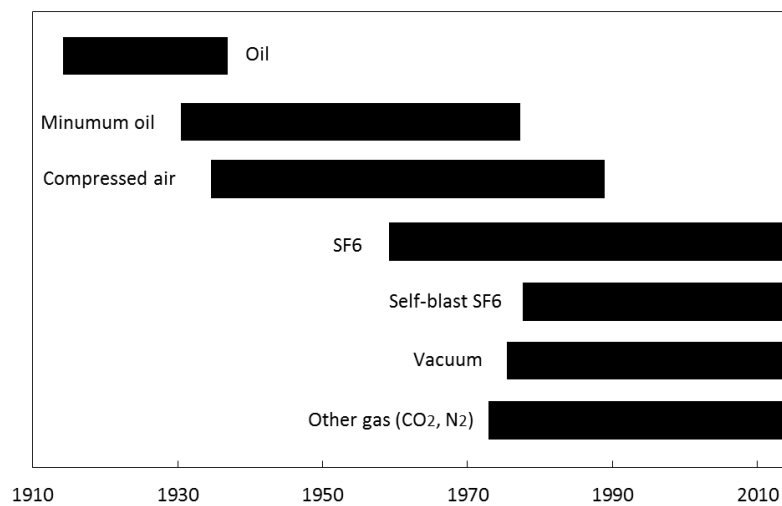


Figure 1.2: Major types of circuit breaker and their years in service

(a) Oil circuit breaker

Bulk oil circuit breaker (BOCB) and minimum oil circuit breaker (MOCB) are the two main types of oil circuit breaker. In a BOCB, the main contacts are immersed in oil which has dual function of quenching the arc as well as maintaining insulation. During the contract separation process, oil molecules dissociate under the high temperature of an arc. The high pressure hydrogen gas bubbles created by the arc energy is advantageously used to confine, compress and cool the arc. Meanwhile, the high pressure in the tank gives a risk of explosion. Unlike BOCB, a MOCB places the interrupting unit in interrupting chamber at live potential. The insulating oil is available only in interrupting chamber. MOCBs are generally similar with bulk one in construction but contain less oil. Thus, MOCB is designed to reduce the requirement of oil.

The oil has to be replaced after several faults clearances because of the gas generated decreases the insulation level of the oil. Despite the risk and frequent maintenance, oil remained a popular medium in the earlier years and was used until 1980s as shown in Figure 1.2. The rated voltage of BOCBs is between 11kV to 170kV, and 3.3kV to 33kV for MOCBs [2]. BOCBs are already obsolete as they are very bulky, high risk of fire and explosion and expensive to maintain.

(b) Air circuit breaker

In air-break (also called plain air) circuit breakers within low voltage level (<1 kV), the arc is chopped into a number of small arcs by arc-chute as it rises due to the heat and magnetic forces as Figure 1.3 shows. The arc has big voltage drop in its cathode and anode end. Cutting a long arc into small ones increases the total voltage drop. When the total voltage drop becomes larger than the system voltage, the arc cannot maintain and is extinguished. As Figure 1.3 shows, this type of circuit breaker has a high requirement on the size of arc chute.

Besides air-break circuit breakers, air-blast circuit breaker was another invention of Whitney and Wedmore in 1926 (Figure 1.3 right) [2], where the switching arc is confined and cooled by the high speed air flow through an insulating nozzle. Compared with oil circuit breakers, air-blast circuit breakers have no risk of fire hazard and need much less maintenance. Furthermore, arc quenching and breaking speed is much faster during the operation of circuit breaker. As the arc duration is shorter, the erosion on the contacts due to arc heating becomes less thus the service life becomes longer.

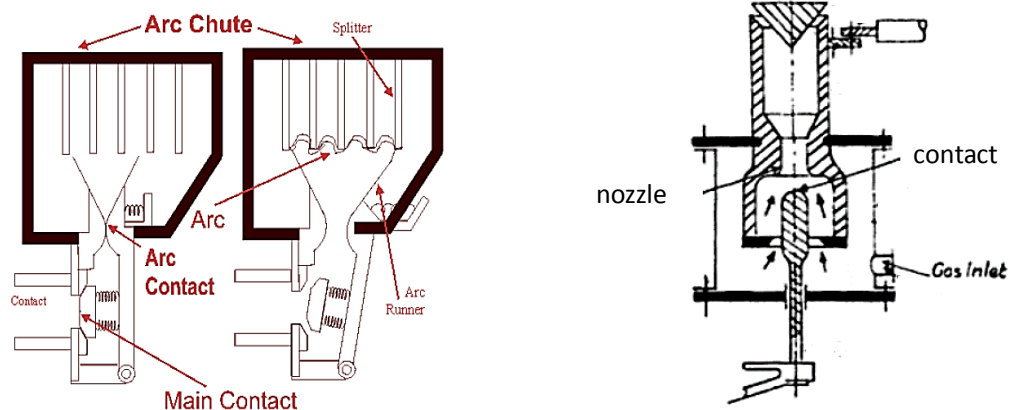


Figure 1.3: Plain air circuit breaker, diagram from [5] (left); and Air-blast circuit

breaker nozzle system in 1926 [2] (right)

(c) Vacuum circuit breakers

Vacuum circuit breakers have the simplest mechanical construction, which in principle consist of only a fixed and moveable contact located in a vacuum vessel as Figure 1.4 shown. When the contacts separated, an arc is burning in ionized metal vapor from contact erosion instead of ionized gas as in gas insulated circuit breaker. The collapse of ionisaion and vapour condensation is very fast at current zero thus the vacuum arc is extinguished. Vacuum circuit breakers are maintenance free during its expected lifetime since it is self-contained. However, the maximum service voltage per vacuum interrupter is still restricted to the order of 36 kV.

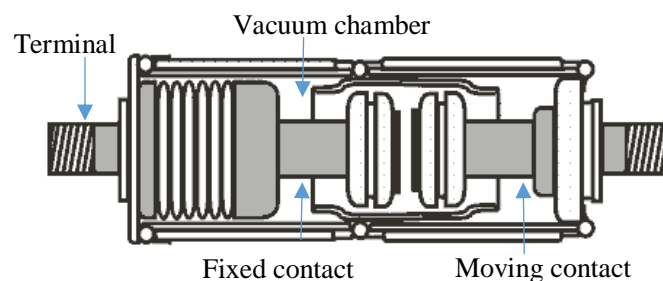


Figure 1.4: Cross section of vacuum interrupter, diagram from [6]

(d) SF₆ circuit breakers

SF₆ gas has high affinity for electrons, i.e. neutral gas molecule could absorb electron and form heavy negative ions, which will not attain sufficient energy for gas ionization in an applied electric field. Thus, SF₆ is an effective arc quenching gas. In addition, SF₆ has better dielectric strength than air and oil under specified atmospheric pressure, the breakdown strength of SF₆ at 1 bar 298 K is around 45 kV/cm [7]. Its dielectric strength is 2.5 times of that of air at atmospheric pressure, and is equal to that of oil at 3 atmospheric pressure. Besides excellent dielectric strength, it has good recombination property. At temperature of 1000 °C, SF₆ decomposes into SF₄, SF₂, S₂, F₂ and so on [2][4]. After arc extinction, the decomposed products recombine within about 1 microsecond, which means SF₆ has a unique ability of “self-heal”. Therefore, the particularity of SF₆ makes it become popular as arc quenching and insulating medium in circuit breakers.

SF₆ was first used in gas blast circuit breakers in 1959 by Westinghouse [8]. In the

1960s, the puffer system was applied to SF₆ circuit breaker [9]. In this puffer type circuit breaker as shown in Figure 1.5, SF₆ is compressed using operation mechanism when the contact opened, then the high pressure gas in the compression volume starts to rush into the arcing chamber and strongly blows the arc between the contact to be extinguished. Because the gas should be compressed during the very short time, the mechanical part required in such type of circuit breaker has to be powerful, which is an expensive part of the circuit breakers.

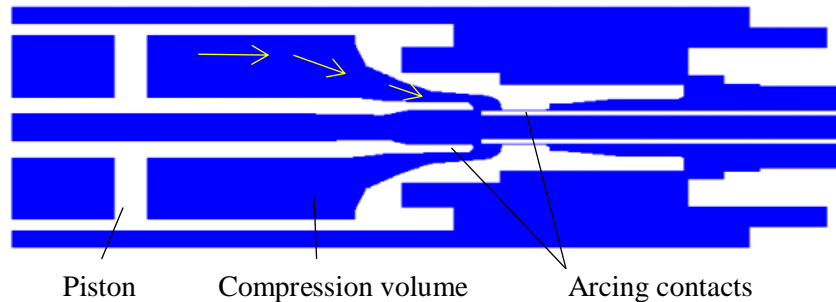


Figure 1.5: Typical structure of a puffer SF₆ circuit breaker

Then SF₆ was used in rotary arc circuit breakers in 1970 [9], which use a magnetic field to drive the arc move in working gas and achieve arc cooling. With more of understanding of arc interruption principle and arc thermodynamic characteristics, a new type circuit breaker, called self-blast SF₆ circuit breaker, (also called auto-expansion circuit breaker), was developed in the 1980s [10]. Self-blast circuit breakers as shown in Figure 1.6 have more different design ideas compared with puffer ones. The energy of the arc itself is utilized to increase the pressure of the gas in the expansion volume which creates high speed gas flow in the contact space at the current zero period to cool and subsequently quench the arc. The pressure rise in self-blast circuit breaker mainly depends on the arc itself rather than the mechanical force. Therefore, the technique significantly reduces the mechanical energy requirement for the operation of the circuit breaker, leading to lower product cost.

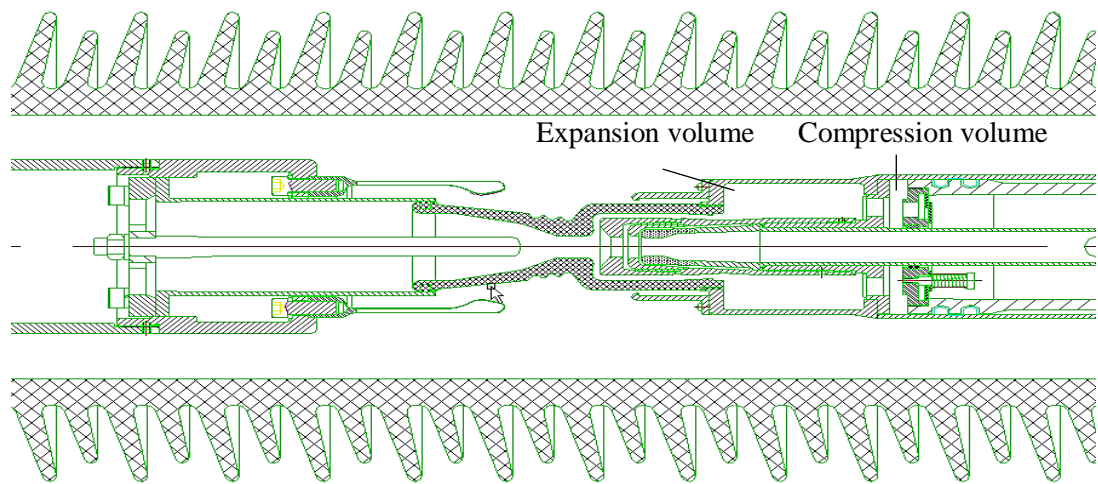


Figure 1.6: Typical structure of a 145 kV auto-expansion/self-blast SF₆ circuit breaker

SF₆ circuit breakers are the main switchgear equipment for distribution voltage through the high voltage class. However, SF₆ is able to last 3500 years [11] in the atmosphere and has high global warming potential. Thus air and CO₂ are proposed to replace SF₆ as the arc interruption medium by Patrick. A comparative study of the interruption perform and of these three gases was carried out in [12], which gives the ranking from low to high: air, CO₂, SF₆. In 2012, ABB 75 kV high-voltage breaker that uses CO₂ as the medium for arc quenching and insulation. By switching from SF₆ to CO₂ it helps reduce greenhouse gas emission by an equipment of 10 tons of CO₂ during the product's life cycle [13]. Work on SF₆ replacement is still at its very early stage. There is still much challenging issues to be studied and addressed.

1.3 Interactions of Circuit Breakers with the Power System and Transient Recovery Voltage

A circuit breaker is commanded to interrupt a short circuit current when a fault develops in the power network. The current is from the network. When the current is interrupted, the power system will experience a transient period and a transient voltage will be applied across the opened contacts of a breaker. This voltage after current interruption is called the transient recovery voltage (TRV). Generally speaking, network fault can be classified into two categories, terminal fault and short line fault (IEC 62271-100).

The terminal fault is defined as a fault occurring at or very near to the circuit breaker terminal. Thus, the reactance between the fault point and breaker can be neglected. Tests are required at 100%, 60%, 30% and 10% of rated short-circuit current with the corresponding TRVs and recovery voltages (ANSI/IEEE Std C37.09). The short line fault (SLF) is one of the most frequent met system fault conditions, which is caused by a fault on a transmission line, remote to (a few hundred meters to several tens of kilometers away) the terminals of a high voltage circuit breaker. Overhead transmission lines have distributed resistance, inductance, shunt conductance, and shunt capacitance. These electrical parameters determine the characteristic of TRV. Circuit breakers directly connected to overhead transmission lines need short line fault test, because the electromagnetic wave reflection from the fault location back to the terminal of the circuit breaker results in a very high rate-of-rise-of recovery-voltage (RRRV) during the initial saw-tooth portion of the TRV waveform as shown in Figure 1.7b. This leads to severe arc-quenching conditions for a circuit breaker. The investigation of interruption capability in my work focuses on SLF since it is more difficult to execute than the terminal fault [3].

For short line short breaking tests, IEC standard considers primarily the performance of SF₆ circuit breakers and specifies test duties corresponding to 90% and 75% of the rated short circuit breaking current [3]. The rate-of-rise of recovery voltage (dV/dt) in Figure 1.7c is expressed by [2]

$$\frac{dV}{dt} = Z_n \frac{di}{dt} \quad (1.1)$$

where Z_n is the equivalent natural impedance of the line which depends on the number and placement of conductors, and di/dt is the rate of change of current at the instant of current interruption. The period of the saw-tooth waveform is equal to four times the reflection time from the circuit breaker to the fault point which is less than 20 μ s [14].

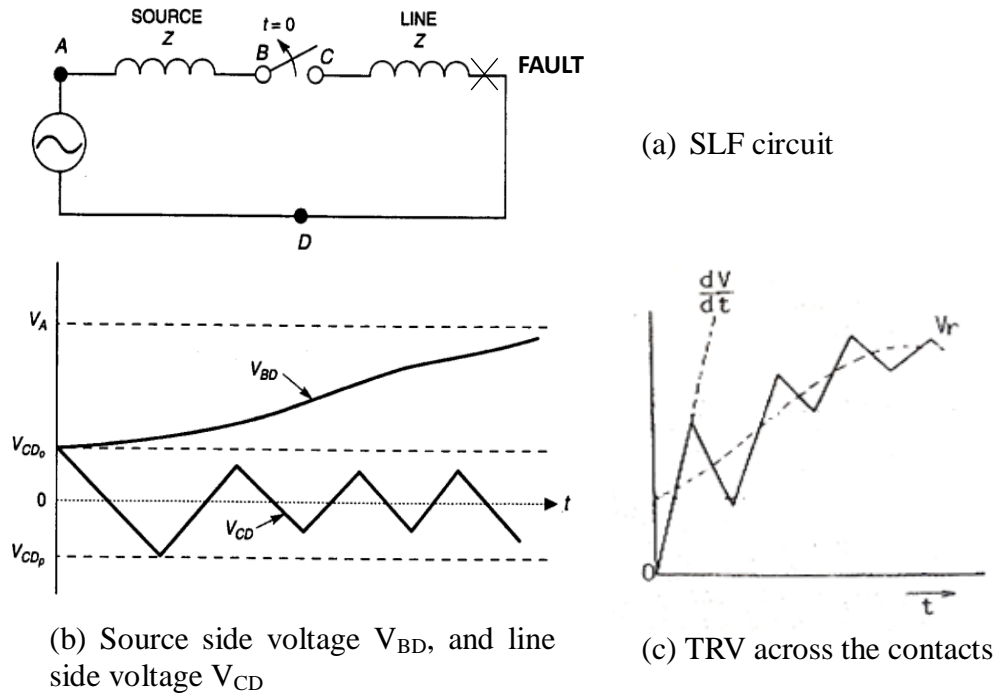


Figure 1.7: Short line fault (SLF) transient recovery voltage

1.4 Basic Physics of Interrupting Arcs

Switching arc is a type of high intensity electrical discharge sustained by an electric current flowing between two electrical contacts. When the contacts of a circuit breaker separate, the gas between them is ionized following breakdown and its temperature rises to a very high value (15,000 K to 35,000 K) with considerable electrical conductivity, thus the current can still pass through. An arc is considered to contain three physically distinct regions including two electrode regions and an inter-connecting plasma column [15]. The concept of plasma in local thermal equilibrium (LTE) will be discussed in section 1.4.2. To completely interrupt the current, the arc between the contacts gap should be quenched by changing the arcing medium from conducting plasma to insulating gas state. It is known that changing a state from gas to liquid, or from plasma to gas generally depends on temperature. On an AC circuit breaker, current crosses zero every half-cycle. Technically, it is easy to quickly cool the arc without electric input. To lead a successful current interruption, the circuit breaker should cool down the arc when a current zero of the alternating current is reached. Therefore, the investigation on arc characteristics, especially near the current zero becomes particularly important for circuit breaker design.

1.4.1 Gases in circuit breaker as a continuum medium

The medium in all blast-type circuit breakers is a flowing gas during the arcing process, either air or SF₆, and hydrogen in oil circuit breaker. The flowing gas cools the arc by strong convection. In SF₆ circuit breaker, the high speed gas flow causes arc instability, turbulence eddies are produced at the arc edge, which is an important mechanism for energy removal. In addition, it is the ionized gas that forms a “bridge” between two separated contacts. The bridge opening or closing depends upon the resistance of the arc. The resistance of the arc burning in gas blast circuit breakers changes gradually, which avoids current chopping and severe overvoltage.

The molecules of a gas are composed of atoms. Each of atom comprise a nucleus made up of a specific number of neutrons and protons. In a stable state, electrons move around the nucleus in fixed orbits with specific energy levels. When the gas is heated to a very high temperature due to an external heating source, some electrons receive energy and move to higher energy levels and leave atoms in an “excited” state, while some electrons are removed from atoms which make atoms in an “ionized” state. When atoms are in unstable state, electrons tends to move from one orbit to another. These changes are accompanied by absorption of energy from low energy level to high energy level, or release of energy from high energy level to low energy level. Radiation from arc plasma is a result of change in the energy levels of electrons, in the form of electromagnetic weave or described as absorption and emission of photons.

The pressure in a gas insulated circuit breaker is normally higher than atmospheric pressure. The mean free path, defined as the average distance travelled by a particle between two successive collisions, decreases with increasing pressure. It means that collisions between particles in switching arcs are sufficiently frequent so that particles are locked with each other and their macroscopic motion can be described by a common mass averaged velocity. Therefore, arc burning in high pressure (≥ 1 atm) is known as collision dominated plasma and can be treated as an electrically conducting fluid [16].

The arc temperature in gas blast circuit breakers is very high which is from 3,000 K to 35,000 K. The kinetic energy of particles in such a hot gas increases and energy

transfer due to collisions causes thermal ionization. The degree of ionization of a particle (molecule or atom) into several species (atoms, ions, or electrons) depends upon the temperature and pressure. It means that the variation of temperature and pressure could rapidly change particle density, which determines the gaseous material properties (i.e. density, viscosity, electrical conductivity, thermal conductivity and heat capacity). The material properties of the arcing medium as function of temperature, pressure, are essential elements for switching arc simulation. The concept of CTE and mass concentration in case of a gas mixture under the assumption of local thermal equilibrium (LTE) is described below.

1.4.2 Plasma in thermal equilibrium

To make the gaseous material properties predictable, there is a need to choose an adequate approximation of plasma state which can be described theoretically using classical statistical mechanics. Complete thermal equilibrium (CTE) is an ideal plasma state. If all the physical processes occurring in an arc are reversible and in detail balance, the arc is said to be in CTE. The gas particles in CTE satisfy the following four criteria [17].

- (a) The velocity of all particles follows Maxwell distribution;

$$dn_r = 4\pi n_r \left(\frac{m}{2\pi kT}\right)^{\frac{3}{2}} e^{-\frac{m_r v_r^2}{2kT}} v_r^2 dv_r \quad (1.2)$$

where v_r is the magnitude of the velocity vector, n_r the number density of species r , m_r the mass per particle, T the common temperature for all particle species and k is the Boltzmann constant.

- (b) The population density of excited states (atomic, vibrational and rotational) for each particle species follows the Boltzmann distribution:

$$n_{r,s} = n_r \frac{g_{r,s}}{Z_r} e^{-\frac{E_{r,s}}{kT}} \quad (1.3)$$

where $n_{r,s}$ is the number of particles of species r at an excited state s . $g_{r,s}$ is the statistical weight of the state s , $E_{r,s}$ its energy and Z_r the partition function of species r .

- (c) The number densities of charged particles can be described by Saha-Eggert equation.

$$\frac{n_{r+1}n_e}{n_r} = \frac{2Z_{r+1}}{Z_r} \frac{(2\pi m_e kT)^{\frac{3}{2}}}{h^3} e^{-\frac{\chi_{r+1}}{kT}} \quad (1.4)$$

where n_r and n_{r+1} are the number density of ion species in the (r)th and ($r+1$)th ionisation state respectively. n_e is the electron number density, χ_{r+1} the ionisation energy which is required to produce an ion in the ($r+1$)th state from the (r)th state, m_e the electronic mass and h the Planck constant.

(d) Radiation field within the arc obeys Planck's law for black body:

$$B_\nu d\nu = \frac{2h\nu^3}{c^2} \frac{d\nu}{e^{\frac{h\nu}{kT}} - 1} \quad (1.5)$$

where ν is the frequency, c the speed of light and B_ν is the radiation intensity of black body in $W/(m^2 \text{ ster})$. To achieve this an element in the arc will emit and receive the same amount of radiation at any time. So there should not be any radiative loss from the arc.

In practice CTE systems do not exist on the earth. The study of such a system is of importance as knowledge derived from such a system can be applied approximately to practical systems. Based on experimental evidence [18][19], Local Thermal Equilibrium (LTE), which satisfies the criteria (a), (b) and (c), is a good approximation of the plasma state for circuit breaker arcs. All chemical species in plasma are considered to have a common temperature in LTE.

In the recent 15 years, Gleizes and his colleagues proposed that during the decay of a circuit breaker arc, the arc plasma is subjected to strong blowing which leads to deviation from local chemical equilibrium (LCT), i.e. the population of chemical species differ from the equilibrium composition [20][21]. Moreover, after current zero, a transient recovery voltage is applied between the electrodes. Electrons gain the energy from the electric field much easier than heavy particles. Due to the low temperature (around 12,000 K), the energy transfer between electrons and heavy particles by collision may not be efficient enough, which leads to two temperatures (electron temperature T_e and heavy particles temperature T_h) in the residual arc plasma [22][24]. This two-temperature kinetic model of SF_6 arc plasma has been used to compute the transport coefficients and thermodynamic properties [20]-[24]. It has been indicated that consideration of the non LTE and non-LCE effect alone is not able to produce reasonable predictions for the critical RRRV values. On the other

hand it can be argued that the existence of turbulence in SF₆ arcs enhances not only the mass, momentum and energy transport process, but also increases the rates of chemical reactions around current zero, in a way similar to turbulent combustion, to render the plasma state closer to LTE and LCE . These issues collectively form one of the key research topics in the future to achieve quantitative prediction of the interruption capability of high voltage circuit breakers.

1.4.3 Arc instability (Turbulence)

Arcs in gas blast circuit breakers at current zero are burning in strong axial flow that is confined in PTFE nozzles. The interaction between the surrounding gas flow and arc plasma has been discussed in [25]. A hot arc column surrounded by cold flow forms a velocity shear layer due to pressure gradient and causes strong radial density gradient associated with large temperature difference. As a result, vorticities are generated in the arc edge as Figure 1.8 shown, which are known to cause instability. Turbulence is used to describe the instability of the flow field. The presence of turbulent eddies enhances mass and momentum transfer across regions where velocity and temperature gradient exist. As Figure 1.9 shows, at the high current phase, arc column fills most of the nozzle space and cold gas flow only occupies a thin annular layer near the nozzle surface. Turbulence does not significantly affect the arc behavior in this case. Around 5 μ s before current zero and after current zero, arc column is thin and surrounded by cold flow which easily deform the arc behavior. The turbulence started at location b which is on the downstream of nozzle throat, and becomes stronger along the location from c to e.

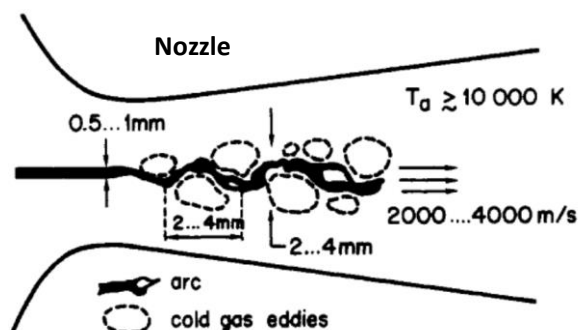


Figure 1.8: Turbulent eddies in nozzle arc [26] near the current zero

The importance of turbulence in circuit breaker arcs was recognized by both

experimental and theoretical study more than 30 years ago [27][28]. The instability of arcs burning in accelerating axial flow is usually caused in the boundary layer between the arc plasma and surrounding gas [15][29]-[32]. The work in [30] and [31] present the simulation results under both laminar and turbulent assumption. The work shows that the calculated RRRV and temperature profile have a good agreement with measurement. Therefore, turbulence should be considered in arc simulation, especially at low current.

The modelling of turbulent arcs normally follows the same line as that of a high temperature turbulent jet [23] as Figure 1.10 shows, because the radial temperature profile has very high gradient; the gas velocity has been strongly accelerated within the high temperature core (low density presents); this high velocity shear layer is usually attributed to as the cause of arc instability.

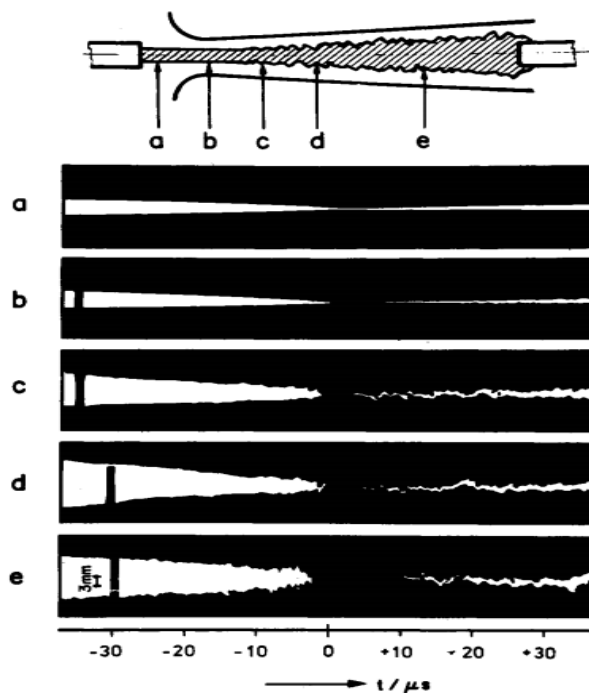


Figure 1.9: Fast streak records of the arc in the vicinity of current zero at different axial positions as indicated with a, b, c, d, e (N_2 , 23 bar, $di/dt = -39A/\mu s$) [26]

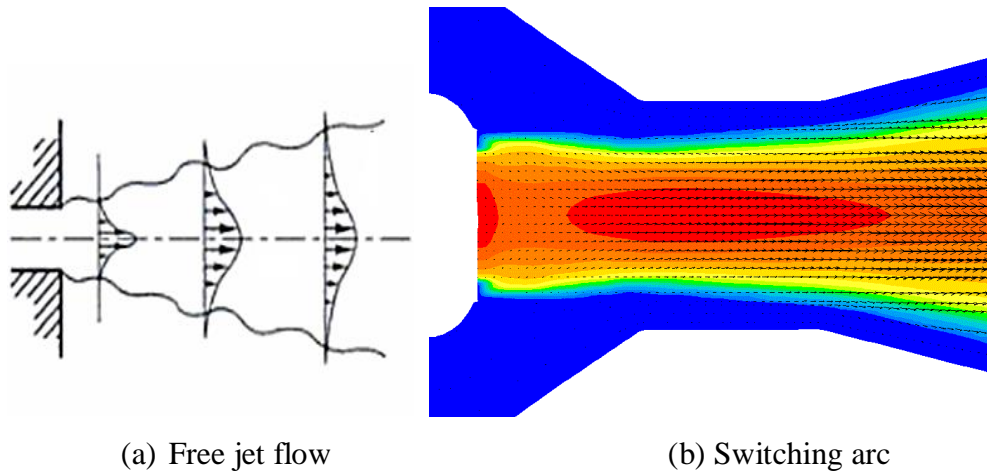


Figure 1.10: Velocity profile for a free jet flow and switching arc

Among a large number of turbulence model [25]-[37][38], the Prantl mixing length model [37][38] and the k-epsilon model family have been extensively utilized for simulations of turbulent nozzle arcs. The k-epsilon model consist of the standard k-epsilon [34][37][38] and its variants [36][37][39][40]. The viscosity introduced by the eddies that moves randomly in turbulent flow can be modelled as [37]

$$\mu_t = C_\mu \rho \lambda_c V_c \quad (1.6)$$

where C_μ is a constant and V_c are the length and velocity scale of the turbulent motion, respectively, λ_c is turbulent length. Turbulence models differ in the calculation of these two characteristic quantities.

Prantl mixing length model is the simplest turbulence model which is proposed in 1920.

It relates the turbulence length scale to the width of the jet. In arc simulation, this length scale marks the boundary of the high velocity core and is measured by the thermal arc radius.

$$\lambda_c = cr_\delta \quad (1.7)$$

Where c is a turbulence parameter. The velocity scale is expressed by

$$V_c = \lambda_c \sqrt{\left(\frac{\partial \omega}{\partial r}\right)^2 + \left(\frac{\partial v}{\partial z}\right)^2} \quad (1.8)$$

Thus the eddy viscosity is given by

$$\mu_t = \rho \lambda_c^2 \sqrt{\left(\frac{\partial \omega}{\partial r}\right)^2 + \left(\frac{\partial v}{\partial z}\right)^2} \quad (1.9)$$

In 1968, Harlow and Nakayama proposed the k-epsilon model [41]. In this

turbulence model, the characteristic quantities are related to the time-averaged turbulent kinetic energy, k and dissipation rate, ε , which are determined from

$$\frac{\partial \rho k}{\partial t} + \nabla \cdot \left(\rho \vec{V} k - \frac{\rho v_t}{\sigma_k} \nabla k \right) = \rho (P_k - \varepsilon) \quad (1.10)$$

$$\frac{\partial \rho \varepsilon}{\partial t} + \nabla \cdot \left(\rho \vec{V} \varepsilon - \frac{\rho v_t}{\sigma_\varepsilon} \nabla \varepsilon \right) = \rho \frac{\varepsilon}{k} (C_{1e} P_k - C_{2e} \varepsilon) \quad (1.11)$$

where P_k represents the generation of turbulence kinetic energy due to the mean velocity gradients, which is given by

$$P_k = v_t \left[2 \left(\frac{\partial w}{\partial z} \right)^2 + 2 \left(\frac{\partial v}{\partial r} \right)^2 + 2 \left(\frac{v}{r} \right)^2 + \left(\frac{\partial w}{\partial r} + \frac{\partial v}{\partial z} \right)^2 \right] \quad (1.12)$$

The turbulent length and velocity scale are respectively defined as

$$\lambda_c \propto \frac{k^{1.5}}{\varepsilon} \quad (1.13)$$

$$V_c \propto \sqrt{k} \quad (1.14)$$

Eddy viscosity is thus given by

$$\mu_t = \rho C_\mu \frac{k^2}{\varepsilon} \quad (1.15)$$

There are all together five turbulence parameters in this model, the values of which have been adjusted according to the test results for a range of fluid flows. The recommended values of the constants are [42]: $\sigma_k=1.0$, $\sigma_\varepsilon=1.3$, $C_{1e}=1.44$, $C_{2e}=1.92$, $C_\mu=0.09$.

Variant of the k-epsilon model like Chen-Kim [36] and RNG [39] model add additional term to the dissipation rate equation (1.11) of the standard k-epsilon model. The comparison of Prantl mixing length model, standard k-epsilon, Chen-Kim and RNG model have been done for SF₆ arc in a supersonic nozzle [37]. As there are no measurements available for verification, it is still difficult to say which turbulence model is the most appropriate for arc plasmas.

1.5 Arc Models in Gas Flow

Since arc was discovered in 1808, the improvement of knowledge regarding the physical processes is strongly needed because of its fast growing industrial application. Cassie [43] was the first person who proposed a mathematical model of arcs in gas flow in 1939. The arc column in Cassie's model was assumed to be cylindrical with constant temperature both in space and time, while its diameter

varies with current proportionally. This model could be applicable at the high current phase, while it cannot be used either at current zero period nor post arc period. The reason is that the rapid temperature variation of arc cannot be ignored.

In 1943, a model for low current arc was proposed by Mayr [45] assuming that the cylindrical arc column radius and the energy loss per unit length were constant, thus the temperature varied. However, the predicted results by Mayr's model still had discrepancy with test result [44].

Five years later, Browne [46] combined Cassie's model and Mayr's model by using former before current zero while latter for post arc period. This model did predict the features of arc to certain extent. However, it cannot provide any information about the physical processes occurring in the arc column, and its application still relies on test data to provide information on the relevant parameters such as arc time constant [47].

Conservation equations were firstly used to describe the arc behaviour by Elenbaas [48] in 1946. Elenbaas's model gives an energy balance between power output and power input, which is written as:

$$\frac{1}{r} \frac{\partial}{\partial r} \left(kr \frac{\partial T}{\partial r} \right) + \sigma E^2 = 0 \quad (1.16)$$

where the first term represents the heat conduction and the second one is Ohmic heating, the other variables have their conventional meaning. Obviously, this model is still too simple to represent all processes of energy transport, since the important aspects such as radiation and convection are not considered.

1.5.1 Integral method for arc in gas flow

At the middle of 1960s, the arc conservation equations became well known [49]. However, the solution of these conservation equations was difficult, because the computers at that time were not fast enough as well as the numerical method for the non-linear partial differential equation was not developed. Therefore, the integral method for arc physics was used instead of differential method in the late sixties and early seventies.

At the beginning of the 1970s, Swanson and Roidt [50]-[56] derived integral arc equations from basic differential equations assuming a boundary-layer flow. Combined with Topham's work [57] on arc analysis using integral method, the similarity between an arc in an axial flow and a hot boundary layer was clearly recognised and used to simplify the arc conservation equations. However, Swanson and Roidt's approach was not adopted by other researchers, because many assumptions and simplifications used to deal with the energy transport process, temperature profile, axial velocity across the arc etc. are not properly and have been proved not justified [50].

In 1975, another integral model which was developed by Lowke and Ludwig [58] obtained a successful achievement. The arc was assumed to be an electrically conducting channel with top hat temperature profile. Tuma et.al [59][60][61] extend it to investigate the transient behavior of nozzle arcs with the assumption of constant Mach number along the radial direction. The predictions by this method gives a good agreement with the experiments by Hermann et al [62] for a 2 kA N₂ arc in the steady state without introducing turbulence. However, at low current (below 500 A) the parabolic temperature profile assumption never yield satisfactory results.

During the same period with Lowke, a group of workers at Brown, Boveri & Co. (BBC) in Switzerland were engaged in an intensive experimental and theoretical investigation on arcs in gas flow [62]-[64]. The temperature, pressure, and electric field of a gas blast arc were accurately measured. A two zone model which consists of a high temperature arc zone with a constant temperature and a cold gas flow zone surrounding the arc was proposed to predict a 2 kA N₂ arc. This model successfully employed the turbulence momentum and heat transfer. The predictions also match well with experimental results. Therefore, the introduction of turbulence in N₂ arc causes much controversy by comparing the work of Lowke et.al and BBC workers.

Tuma and his co-workers [60][65] then introduced turbulence into arc model using Prantl mixing length model to study the free recovery and current zero behaviour of a gas blast arc in 1977. In order to account for the high thermal interruption capability of SF₆ over N₂ [60], it was found that the turbulence effect of SF₆ arc

should be three times larger than N_2 arc. Tuma indicated that the strong turbulence effect depends on the gas properties such as density and specific heat of SF_6 , which varies with temperature. Parameters, which control the turbulence strength and the radial profiles of temperature and axial velocity component, have to be calibrated so that the interruption capability agrees with experiment.

The most general form of boundary layer integral arc, together with external flow conservation equation was derived by Cowley [66] in 1974. Cowley's formulation then was extended by Chan [67] et al to include an energy conservation equation for the arc core. Thus, the models discussed above become special cases of this general formulation. This Liverpool-Cambridge arc model has then been used extensively for gas blast arcs. Based on this method, the scaling laws for high current phase [68] and a current zero model [69] by Fang were present in 1980. Then these models were used to investigate the effect of nozzle ablation with both dc and ac current [70]-[72]. From 1996 to 1997, this method was also used to predict the operation of puffer circuit breaker in the high current phase and current zero phase which takes into account of coupling with puffer compression chamber, PTFE ablation and moving contact [73][74]. There is no doubt that the integral method achieves remarkable success in elucidating and predicting arc behavior. Compared with the differential method, the computational costs are relatively low. However, for the current zero period integral method has only very limited success, because the shape factors, which is intruded to relate the arc thermal area to the external cool region, is difficult to correct.

1.5.2 Differential method for arc in gas flow

To solve the arc conservation equations of mass, momentum and energy, there is a need to give appropriate initial and boundary conditions. Due to the complexity of mechanisms in switching arcs such as radiation transport, turbulence mixing, and electrode sheath interaction, approximations have to be made to simplify the equations. Therefore, various models with different assumptions were derived for different arcing situations.

Till the early of 1980s, research development in the differential method started to have a significant progress. Ragaller et al [75] at BBC in 1982 predicted the dielectric recovery of a gas blast arc after current zero using a differential approach. A uniform radial pressure distribution is assumed to simplify the momentum equation. In addition, to solve the energy equation, the axial gradient of temperature is set to be zero. Because during the post current zero period, the current passing through the residual arc is rather small, the radiation loss and Ohmic heating are neglected. The prediction with strong turbulence is close to the measured dielectric recovery characteristic [76]. It was concluded that turbulence is a very important cooling mechanism after current zero. Flow downstream of the nozzle throat becomes turbulent before current zero.

In 1985, Mitchell et al [77] proposed a model with very different assumption from Ragaller et al [75] to investigate the dielectric behavior after current zero. The flow was considered to be laminar. Turbulence is absent from the model, while radiation is considered. Radiation emitted from the arc core is assumed to be fully absorbed in a single layer of one-cell thickness at the arc edge. Mitchell's model solved mass and energy equation. It assumes axial velocity component equal to zero, then extrapolated from the downstream with the axial pressure gradient. Their results of radial temperature profiles [77] are similar to those of Hermann and Ragaller [75] based on laminar flow for the period up to 200 μ s after current zero. In addition, the results given by Mitchell et al [77] of a steady state SF₆ arc at 1200A and 3.6bar indicated that the net emission coefficient given by Liebermann and Lowke [78] should be increased by a factor of 4.

At the same time as Mitchell et al, Lowke and Lee [79] investigated the thermal recovery process of a gas blast circuit breaker. They started the transient simulation from a steady state at 2kA before current zero without considering turbulence cooling. The approximated radiation model proposed is not proper. Their prediction indicates that N₂ was a better interrupting medium than SF₆, which obviously did not agree with the experimental [63]. The predicted RRRV for both N₂ and SF₆ showed one order of magnitude difference than the measurement [63].

Considerable progress was made at Liverpool University by Fang and his co-workers

[30][80][81] at the beginning of 1990s. An approximate radiation model [81] (detail described in section 3.6) was proposed and a proper account of radiation transport was achieved. The radiation model was based on the measurement of Ernst. et. al [82] for wall stabilized N_2 arcs and on the detailed radiation transport calculation of Shayler and Fang [83] for N_2 and of Liebermann and Lowke [78] for SF_6 . They have shown that for N_2 arcs theory based on laminar flow can give a reasonable prediction of the thermal interruption capability [80] but not for SF_6 [30]. Introduction of turbulence has been found necessary for SF_6 arcs. In 1999, considering all important physical processes, the arc behavior in an auto-expansion circuit breaker was successfully simulated by Yan [10]. Then, the work is repeated by Zhang [84], but using newly calculated properties of SF_6 and PTFE vapour, which improved the prediction in 2002. Recently, the behaviour of SF_6 arcs under shock conditions has been investigated by Fang et al [85][86].

1.6 The Objective and Organization of The Thesis

Computer simulation of circuit breakers based on commercially available CFD packages has been widely used as an aid to the development of circuit breakers. The user of such simulation tools needs to be familiar with arc physics, the setting up of the computation model for the circuit breaker in hand, monitoring and control of computational process, and extracting useful information from a vast amount of computing data. Thus, the use for such tools has a high requirement to design engineers. To make the simulation of switching arc be an easy task, an intelligent simulation platform called Integrated Simulation and Evaluation Environment (ISEE) is developed. The structure and development of ISEE is given in Chapter 2. The objective of the present work is using the newly developed simulation tool to improve the arc model (Chapter 3), investigate the arc behavior in several designs of auto-expansion circuit breaker and help the optimum design (Chapter 4,5,6).

Chapter 3 makes full use of measurement recovery voltages those provided by manufactures to give a calibration of turbulence parameter using Prantl mixing length model. The calibrated turbulence model is then used in the following investigations of the next chapters.

Chapter 4 presents a comparative study in a 145 kV, 60 Hz auto-expansion circuit breaker with different arc durations. The research findings show pressure peak in the expansion volume has a delay of 2.8 - 3.4 ms with reference to the current peak when the arc duration varies. A reasonable indicator of the interruption environment is the average mass flux in the main nozzle. The short arc duration case (12.25 ms) is the most difficult case with the lowest critical rate of rise of recovery voltage (RRRV) of 10 kV/ μ s, just above the initial system applied RRRV of 9 kV/ μ s. This is a result of insufficient gas flow cross sectional area between the live contact and the main nozzle to develop rapid gas flow for arc cooling. The auxiliary nozzle plays two roles. It provides blockage in the high current phase to reduce gas exhaustion from the main nozzle into the hollow contact; after current zero the hollow contact shares a considerable portion of the system recovery voltage, especially for the short arc duration case (36%). Therefore the proper design and use of an auxiliary nozzle is key to enhancing the thermal interruption capability of high voltage auto-expansion circuit breakers.

In Chapter 5, the important phenomena of pressure transient after flow reversal in a 245 kV ABB auto-expansion circuit breakers with different arcing conditions are detailed investigated. It gives design engineers a picture of how transient variations affect the interruption performance including thermal and dielectric recovery.

Finally, conclusions are drawn in Chapter 6.

References

- [1] M. Zuhaib, M. S. Alam, J. Ahmed, Gas insulated substation [Online] Available: http://www.slideshare.net/sharique_64/gas-insulated-substation-14315261
- [2] C.H. Flurscheim. Power circuit breaker theory and design. Peter Peregrinus Ltd, 1982.
- [3] K. Nakanish, Switching phenomena in high-voltage circuit breaker, 1991.
- [4] N.H. Malik, A.A. Al-Arainy, M.I. Qureshi, Electrical insulation in power systems, Taylor & Francis Group, 1998.
- [5] [Online]. Available: <http://www.electrical4u.com/air-circuit-breaker-air-blast-circuit-breaker/>
- [6] [Online]. Available: <http://www.electrical4u.com/vacuum-circuit-breaker-or-vcb-and-vacuum-interrupter/>
- [7] S. Saxena, M. Ali, A. Singh, K. Gandhi, Various types of circuit breakers used in power system for smooth working of the transmission line, MIT international journal of electrical and instrumentation engineering, Vol. 2, No. 2, pp106-111, 2012.
- [8] L. Hewitson, M. Brown, R. Balakrishnan, Practical Power System Protection, 2004
- [9] R.W. Blower, Distribution switchgear, Collins, 1986.
- [10] J. D. Yan, M. T. C. Fang, and W. Hall, The development of PC based CAD tools for auto-expansion circuit breaker design, IEEE Transaction on Power Delivery, Vol.14, pp.176-181, 1999.
- [11] F. Jakob and N. Perjanik, Analytical ChemTech International, Inc. Shlfur hexafluoride- a unique dielectric, 18th Technical conference-NETA, pp 53-68, 1996.
- [12] P.C. Stoller, M. Seeger, A.A. Iordanidis etc. CO₂ as an arc interruption medium in gas circuit breaker, IEEE Transaction on Plasma Science, Vol. 41, No.8, 2013.
- [13] "Switzerland: ABB breaks new ground with environment friendly high-voltage circuit breaker". Retrieved 7th June 2013.
- [14] R. W. Alexander, D Dufournet, Transient recovery voltage (TRV) for high-voltage circuit breakers, [Online]. Available: <http://webm.dsea.unipi.it/barsali/materiale/Dinamica%20e%20Controllo%20SE/TutorialTRVAlexander-Dufournet.pdf>
- [15] G.R. Jones and M.T.C. Fang, The physics of high power arcs, Rep. Prog. Phys., Vol. 43, pp. 1415-1465, 1980.

- [16] M.I. Boulos, P. Fauchais, and E. Pfender. Thermal plasmas fundamentals and applications, Vol. 1, Plenum Press, New York, 1994.
- [17] M.N. Hirsh and H.J. Oskam, Gaseous electronics, Vol. 1, Academic Press, New York, 1978.
- [18] E. Lewis, A.N. Prasad and G.R. Jones, Current zero spectroscopy of a high power SF₆ circuit breaker arc, Proceeding of Gas Discharge and Their Applications, Oxford, pp. 31-34, 1985.
- [19] A. Gleizes, A.A.M. Habib, M. Razafinimanana, M. Sabsabi and S. Vacquie, Departures from Saha equilibrium in SF₆ arc plasmas, Spectrochimica Acta, Vol. 45B, No. 7, pp. 789-797, 1990.
- [20] J. B. Belhaouari, J.J. Gonzalez and A. Gleizes, Simulation of a decaying SF₆ arc plasma: hydrodynamic and kinetic coupling study, J. Phys. D: Appl. Phys. Vol. 31, pp 1219–32, 1998.
- [21] R. Girard, J.B. Belhaouari, J.J. Gonzalez and A.A. Gleizes, Two- temperature kinetic model of SF₆ plasma, J. Phys. D: Appl. Phys. Vol. 32, pp 2890-2901, 1999.
- [22] R. Girard, J. J. Gonzalez and A. Gleizes, Modelling of a two-temperature SF₆ arc plasma during extinction, J. Phys. D: Appl. Phys. Vol. 32, pp1229–38, 1999.
- [23] H. K. Versteeg and W. Malalasekera, An introduction of computational fluid dynamics: the finite volume method (second edition), Pearson Education Limited, 2007
- [24] J. J. Gonzalez, R. Girard and A. Gleizes, Decay and post-arc phases of a SF₆ arc plasma a thermal and chemical non-equilibrium model, J. Phys. D: Appl. Phys. Vol. 33, pp 2759-2768, 2000.
- [25] H.K. Versteeg and W. Malalasekera, An introduction of computational fluid dynamics: the finite volume method 2nd edh (Harlow: Prentice-Hall), 2007
- [26] W. Hermann, U. Kogelschatz, L. Niemeyer etc. Investigation on the physical phenomena around current zero in HV gas blast breakers, IEEE Transaction on Power Apparatus and System, Vol. 95, No. 4, pp1165-76, 1976.
- [27] B.W. Swanson, and R.M Roidt, Boundary layer analysis of an SF₆ circuit breaker, IEEE Transaction, PAS-90, pp. 1086-1093, 1971.
- [28] W. Hermann, U. Kogelschatz, L. Niemeyer etc. Experimental and theoretical study of a stationary high-current arc in a supersonic nozzle flow, Phys. D, Vol. 7, pp. 1703-1722, 1974.
- [29] J.F. Zhang, M.T.C Fang and D.B. Newland, Theoretical investigation of a 2kA

arc in a supersonic nozzle, *J. Phys. D: Appl. Phys.* Vol. 25, pp 1197-204, 1987.

[30] M.T.C. Fang and Q. Zhuang, Current zero behaviour of an SF₆ gas-blast arc. Part I: Laminar flow. *J. Phys. D: Appl. Phys.*, Vol. 25, pp. 1197-1204, 1992.

[31] M.T.C. Fang, Q. Zhuang and X.J. Guo, Current zero behaviour of an SF₆ gas-blast arc. Part II: Turbulent flow, *J. Phys. D: Appl. Phys.*, Vol. 27, pp. 74-83, 1994.

[32] E. Schade, Recovery of switching arcs Proc. XVIIth Int.Conf. on the Phenomena Ionised Gases (Budapest) pp. 277-97, 1985.

[33] J. D. Yan, K. I. Nuttall and M. T. C. Fang, A comparative study of turbulence models for SF₆ arcs in a supersonic nozzle, *J.Phys. D: Appl. Phys.* Vol. 32, pp. 1401-6, 1999.

[34] B. E. Launder and D. B. Spalding, The numerical computation of turbulent flows, *Comput. Methods Appl. Mech. Eng.* Vol. 3 pp. 269-89, 1974.

[35] V. Yakhot, S. A. Orszag, S. Thangam etc. Development of turbulence models for shear flows by a double expansion technique, *Phys. Fluids A* 4 pp. 1510-20, 1992

[36] Y. S. Chen and S. W. Kim, Computation of turbulent flows using an extended K-epsilon turbulence closure model, Interim Report NASA CR-179204, 1987.

[37] Q. Zhang, J.D. Yan, M.T.C. Fang, Modelling of SF₆ arc in a supersonic nozzle. Part I: cold flow features and DC arc characteristics, *J. Phys. D: Appl. Phys.* Vol. 44, 025203 (9pp), 2011

[38] J.D. Yan, K.I. Nuttall and M.T.C. Fang, A comparative study of turbulence models for SF₆ arcs in a supersonic nozzle, *J.Phys. D: Appl. Phys.* Vol. 32, pp. 1401-6, 1999.

[39] Q. Zhou, H. Li, X. Xu etc. Comparative study of turbulence models on highly constricted plasma cutting arc, *J. Phys. D: Appl. Phys.* Vol. 42, 015210, 2009.

[40] R. Bini, N. T. Basse and M. Seeger, Arc induced turbulent mixing in an SF₆ circuit breaker model *J. Phys. D: Appl. Phys.* Vol.44, 025203, 2011.

[41] F. H. Harlow, Los Alamos Scientific Lab. Report LA-3854, New Mexico, 1968

[42] B. E. Launder and Spalding D. B. The numerical computation of turbulent flows, *Comput. Methods Appl.Mech. Eng.* 3 269-89, 1974.

[43] A. M. Cassie, Arc rupture and circuit severity: a new theory, CIGRE, Paper 102, pp. 1-14, 1939.

[44] M.T.C. Fang, H. Fung and H. Edels, Theory of electric arcs, *Proc. IEE*, Vol.120,

No.6, , p709, 1972.

[45] O. Mayr, Beitrage zur theorie des statischen und des dynamischen lichtbogens (contribution to the theory of static and dynamic arcs), Arch. Elect., Vol. 37, pp. 588-608, 1943.

[46] T. E. Browne, Trans. Am. Inst. Elec. Eng., Vol. 67, pp141-152, 1948

[47] Frind, G., Zeit. Angrew. Phys., Vol.12, pp. 231, 1966.

[48] W. Elenbaas, Phillips Research Report, Vol. 1, No. 5, 1946.

[49] J. G. Skifstad and S N B Murthy, IEEE Trans. Nucl. Sci. NS-11 93-103

[50] B.W. Swanson, and R.M. Roidt, Boundary layer analysis of an SF₆ circuit breaker arc, IEEE Trans., PAS-90, pp. 1086-1903, 1970.

[51] B.W. Swanson, R.M. Roidt and T.E. Browne, Arc cooling and short line fault interruption, IEEE Trans. PAS-90, pp. 1094-1102, 1970.

[52] B.W. Swanson, and R.M. Roidt, Thermal analysis of an SF₆ circuit breaker arc, IEEE Transaction PAS-91, pp. 381-389, 1972.

[53] B.W. Swanson, and R.M. Roidt, Some numerical solutions of the boundary layer equations for an SF₆ arc, Proc. IEEE., Vol. 59, pp. 493-501, 1971.

[54] B.W. Swanson, R.M. Roidt and T.E. Browne, A thermal arc model for short line fault interruption, ET-Z-A, Bd.93, pp. 375-380, 1972.

[55] B.W. Swanson, A thermal analysis of short line fault interruption, IEE Winter Power Meeting, Paper C-47, 1974.

[56] B.W. Swanson, Nozzle arc interruption in supersonic flow, IEEE Trans., PAS-96, 1977.

[57] D. T. Topham, The electric arc in a constant pressure axial gas flow. J. Phys. D, Vol.4, pp. 1114-1125, 1971

[58] J.J. Lowke and H.C. Ludwig, A simple model for high current arcs stabilised by forced convection, J.Appl. Phys., Vol. 46, pp. 3361-3367, 1975.

[59] F.R. El-Akkari and D.T. Tuma, Simulation of transient and zero current behaviour of arcs stabilised by forced convection, IEEE Trans., PAS-96, pp.1784, 1977.

[60] D.T. Tuma, A comparison of the behaviour of SF₆ and N₂ blast arcs around current zero, IEEE Trans., Vol. PAS-99, No. 6, pp. 2129, 1980.

[61] D.T. Tuma and H. Fong, Current zero deformation by interaction of gas-blast arc with test circuit, IEEE Trans., Vol.PAS-99, No.6, pp. 976, 1980.

[62] W. Hermann and E. Schade, Radiation energy balance in cylindrical nitrogen arc,

JQSRT, Vol. 12, pp. 1257-1263, 1972.

[63] W. Hermann, K. Ragaller, Theoretical description of the current interruption in high voltage gas blast circuit breakers, IEEE Trans. PAS, Vol. PAS-96, pp. 1546-1555, 1977

[64] W. Hermann, K. Ragaller and W. Schneider, Theory of high pressure arc in a strong axial gas flow, Proc. 10th Int. Conf. on Phenomena in Ionised Gases, pp. 199-201, 1971

[65] E. Richley and D. Tuma, Free recovery of the gas blast arc column, IEEE Trans. on Plasma Science, Vol. PS-8, pp. 405-410, 1980.

[66] M.D. Cowley, Integrated methods of analysing electric arcs : I. formulation, J. Phys. D. , Vol. 7, pp. 2218-2231, 1974.

[67] S.K. Chan, M.D. Cowley, and M.T.C. Fang, Integral methods of analysing electric arcs: III shape factor correlation for low radiation and laminar flow, J. Phys. D., Vol. 9, pp. 1085, 1976.

[68] M.T.C. Fang, S. Ramakrishnan, and H.K. Messerle. Scaling laws for gas blast circuit breaker arcs during the high current phase. IEEE Trans. Plasma Science, PS-8:357–362, 1980.-1099, 1976.

[69] M.T.C. Fang and D. Brannen. A current-zero arc model based on forced convection. IEEE Trans. Plasma Science, PS-7:217–229, 1980.

[70] W.H. Bu, M.T.C. Fang and Z.Y. Guo, The behaviour of ablation-dominated DC nozzle arcs, J. Phys. D: Appl. Phys. Vol. 23, pp. 175-183, 1990.

[71] M.T.C. Fang and W.H. Bu, Investigation of ablation dominated AC nozzle arcs, IEE Proc.-A, Vol. 138, pp. 71-77, 1991.

[72] M.T.C. Fang and D.B. Newland, DC nozzle arcs with mild wall ablation, J. Phys. D: Appl. Phys. 16, pp. 793-810, 1983.

[73] K.Y. Park and M.T.C. Fang. Mathematical modelling of SF₆ puffer circuit breakers i: High current region. IEEE Transactions on Plasma Science, 24:490–502, 1996.

[74] K.Y. Park, X.J. Guo, R.E. Blundell, M.T.C. Fang, and Y.J. Shin. Mathematical modelling of SF₆ puffer circuit breakers.ii. current zero region, IEEE Transactions on Plasma Science, Vol. 25, pp 967 – 973, 1997.

[75] K. Ragaller, W. Egli and K.P. Brand, Dielectric recovery of an axially blown SF₆-arc after current zero, Part II theoretical investigation, IEEE Transactions on Plasma Science, Vol. PS-10, pp. 154-162, 1982

[76] K. Ragaller, W. Egli and K.P. Brand, Dielectric recovery of an axially blown SF₆-arc after current zero, Part I experimental investigation, IEEE Transactions on

Plasma Science, Vol. PS-13, pp. 141-153, 1982

[77] R.R. Mitchell, D.T. Tuma and J.F. Osterle, Transient two dimensional calculations of properties of forced convection stabilised electric arcs, IEEE Transactions on Plasma Science, Vol. PS-13, pp. 207-213, 1985

[78] R.W. Liebermann and J.J. Lowke, Radiation emission coefficients for sulphur hexafluoride arc plasmas, JQSRT, Vol. 17, pp 253, 1976

[79] J.J. Lowke and H.E. Lee, A numerical study of a two dimensional circuit breaker arc during current interruption, proceeding of gas discharge and their applications, Oxford, pp. 54-56, 1985

[80] M.T.C. Fang and W.Y. Lin, Current zero behaviour of a gas blast arc, Part I: nitrogen, IEE Proc., Vol. 137, Pt. A, No 4, pp. 175-183, 1990

[81] J.F. Zhang, M.T.C. Fang, and D.B. Newland. Theoretical investigation of a 2ka dc nitrogen arc in a supersonic nozzle. Journal of Physics D: Applied Physics, Vol. 20, pp 368–379, 1987.

[82] K. A. Ernst, J.G. Kopainsky and H.H. Maehner, The energy transport, including emission and absorption in N₂ arcs of different radii, IEEE Trans., Vol. PS-1, No. 4, p3, 1973.

[83] P. J. Shyler and M. T. C Fang. Radiation transport in wall-stabilised nitrogen arcs, J. Phys. D: Appl. Phys, Vol.11 pp1743, 1978.

[84] J.L. Zhang, J.D. Yan, A B Murphy, W Hall and M T C Fang, Computational investigation of arc behavior in an auto-expansion circuit breaker contaminated by ablated nozzle vapour, IEEE Trans. Plasma. Sci, Vol. 30, pp 706-19, 2005.

[85] M.T.C. Fang, S. Kwan and W. Hall, Arc-shock interaction inside a supersonic nozzle, IEEE Trans. on Plasma Science, Vol.24, No.1, Pp.85-86, 1996.

[86] Q Zhang, J D Yan, M T C Fang, Current zero behaviour of an SF₆ nozzle arc under shock conditions, J. Phys. D: Appl. Phys. Vol.46, 2013.

Chapter 2

The Development of an Integrated Simulation and Evaluation Environment (ISEE) for High Voltage Circuit Breakers

2.1 Introduction

The interruption capability of high voltage gas blast circuit breakers, especially the more advanced generation of circuit breakers, i.e. the auto-expansion circuit breakers, depends on the design parameters (such as nozzle diameter, etc.) and operational characteristics (such as the contact travel, i.e. the velocity of a moving contact as a function of time) in a complex manner. Circuit breaker design in the early years (up to 1990) heavily relied on the experience and expertise of individual design engineers, which led to a long product development time with a typical duration of 2-5 years for each new product.

With significant advances in our understanding of the switching arc phenomenon [1], rapid increase in computing power, and the availability of robust computational fluid dynamics (CFD) packages, computer simulation of the switching process in commercial high voltage circuit breakers became a reality in the late 1990s and beginning of 2000s, as demonstrated by the work at the University of Liverpool [2][3], RWTH Aachen University [4], and Centre de Recherche en Calcul Appliqué [5]. Major international switchgear manufacturers also invested heavily to develop CFD based arc modelling tools to aid their product design [1][4][6][7] with the aim of reducing the development time and cost for high voltage circuit breaker products. Commercial CFD packages, such as PHOENICS [8], FLUENT [9], have been used to simulate the arcing process in high voltage circuit breakers with full differential arc models [2][10][11]. These models provide much more details of relevant physical quantities during the arcing process which otherwise are difficult to access for

measurement. It is increasingly true to say that computer based simulation is an essential part of the design process of high voltage circuit breakers, and is often viewed as an indicator of the technical competitiveness of a manufacturer.

An arc model has to be properly implemented in a well suited software package, either in-house or commercial, to not only define and solve the governing equations with proper initial and boundary conditions, but also represent all relevant hardware components in the arcing chamber, to produce sensible results compared with measurement. The commercial CFD packages are however developed for general computational purposes. The implementation of the arc model and setting-up of the initial and boundary conditions often require a substantial amount of coding and manual settings.

It is well known that switching arc is an extremely complicated phenomenon of a multi-physics nature. Design engineers who are in their early career and without adequate training and knowledge in arc physics and computational fluid dynamics experience extreme difficulties in correctly setting up the arc model using a commercial CFD package. Even for an experienced design engineer, it still takes a considerable length of time (several days to a week) to create the computational model for a circuit breaker.

It is found necessary to perform simulation of high current arcs differently from low current arcs in terms of grid density and total number of grids (cells) for adequate spatial resolution and computational efficiency [12]. Practically, the whole operation of a high voltage gas blast circuit breaker is conveniently divided into four stages (detail description given in Section 2.5). An early stage provides the initial conditions for a late stage. Traditional approach of arc simulation requires a user to manually perform the settings and restart the computation at the beginning of different stages, which leads to potential mistakes and unnecessary waste of time. Therefore, there is an urgent need for an automated simulation platform where accumulated experience and expertise can be embedded into the software environment to make the process of setting up the arc model automated, saving time and effort, and more importantly to release the design engineers from tedious and mechanical operations. Because of the complexity involved in arc simulation, there

has not so far been an automated system suitable for arc simulation for circuit breakers.

A newly developed simulation platform called Integrated Simulation and Evaluation Environment (ISEE) is described in this Chapter. It is based on the idea of Object Oriented Programming (OOP). ISEE aims to help design engineers set up an arc model for a circuit breaker in a rapid manner without involving coding or programming. The software environment is constructed in close match of industrial practice, following the sequence of machining mechanical parts, assembling into a prototype, test, modification, and re-test. For each stage in the simulation process, a user-friendly Graphic User Interface (GUI) is used for easy setting of the key parameters of the model and selection of functionalities of the simulation environment.

The overall structure of the simulation platform is presented in Section 2.2 with consideration of the real manufacturing process. The concept and properties of objects in real and simulation domains are considered in Section 2.3. Section 2.4 is devoted to a description of the arc models implemented in ISEE and also how ISEE deals with special objects like moving components and valve operations. The intelligence and novelty of ISEE is listed in Section 2.5. Information exchange between equation solvers and the Visual Monitor is explained in Section 2.6. Finally, conclusions are drawn in Section 2.7.

2.2 Consideration of Switchgear Design Practice and Structure of the Simulation Platform

2.2.1 The overall structure

The development of a high voltage circuit breaker (HVCB) product involves the following stages in sequence:

- initial design according to a given technical specification
- manufacturing of components
- assembly of a prototype from the components
- test and design analysis

- design changes and re-test

To align with and effectively aid the practical product design process, each of the above stages should ideally be mapped into the simulation environment. This means that the simulation process is divided into several distinctive phases according to each stage in the product design process, which allows design engineers to follow a unified procedure in both practical design and simulation. The hierarchic structure of the proposed simulation platform, ISEE, is shown in Figure 2.1.

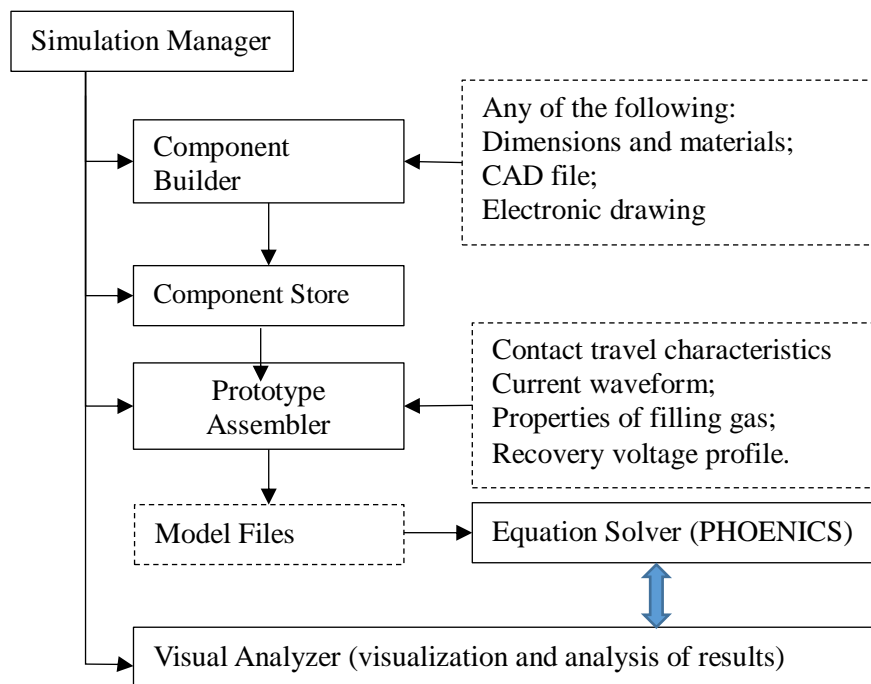


Figure 2.1: The hierarchic structure of the proposed Integrated Simulation and Evaluation Environment (ISEE) for high voltage gas blast circuit breakers.

A component is used in simulation to represent a mechanical part in a circuit breaker such as a nozzle, or a region in the computational domain with special settings or properties. The Component Builder is a Graphical user Interface (GUI) used as a tool to produce various components that make up the virtual system. The virtual system means a computer model established for a real system such as a circuit breaker. This stage corresponds to the practical stage where all hardware components are machined or made available before they are assembled into a circuit breaker.

In reality the quality and performance of a mechanical part is determined by its material, shape, dimensions, and its interaction with the environment. A material has

its own electrical, magnetic, physical and chemical properties. All the information for a mechanical part needs to be represented in a component, which is realized by the use of the concept of “class” and “object” in the Object Oriented Programming approach. More details will be given in Section 2.3. An object not only contains properties, but also has its behavior. Behavior means all defined operations relating to or using the properties of an object.

The *Component Builder* provides the user a tool to completely define a component, not only its shape but also all its properties, including computational requirements such as the grid size in the direction of each coordinate. Once a component is created and defined, it can be saved in a virtual *Store*. All components in the *Store* can be inspected or updated by a user at any time.

When all components are ready, a virtual product can be built. This is the role of the *Assembler*, a GUI based program. A computational domain is first defined to act as a space to contain the product, or the system. The components in the *Store* can be retrieved using mouse operation (click and drop) to form a virtual product in the computational domain. The position of a component can be adjusted using the mouse or by manual input of its positional coordinates if they are available. In addition, collision detection can be activated if necessary to ensure there is no overlap between components.

When the positional relationship among all components are fixed, a grid system is generated in a semi-automatic approach based on the coordinates of the vertices (corners) and side lines of each component. Information required for solving the governing equations, such as the inlet (for some of the circuit breakers inlet conditions may not be necessary) and outlet boundary conditions, Ohmic heating and radiation transfer as energy sources, Lorentz force as momentum sources, and nozzle ablation as surface sources of mass, momentum and energy, is automatically determines and set up based on interactions (communications) among different types of components (nozzle, fixed and moving contacts, piston, valves, etc). This process with high intelligence produces codes that are recognized by the chosen equation solver to perform the computation. In the present work, a commercial CFD package, PHOENICS, is used as the equation solver. Therefore two essential code files are

created, the q1 and Ground.for (explained in Section 2.5.2) files. The files will be compiled into an executive file to run.

Visual Analyser (VA) is a GUI that interacts with the equation solver and result files for the monitoring and analysis of the results. The VA interacts with the solution process in a “real time” mode to visualize the solved quantities as line distribution or colour contours. It is able to extract useful information from a huge amount of data in the result files generated by the simulation. Processed results in the form of animations, vector field for gas velocity and current density, etc. are generated and organized in an archive for the use of design engineers or for further analysis of researchers.

2.2.2 Division of the arcing process

The gas flow and arcing process during the operation of a high voltage circuit breaker is divided into four stages (phases) according to the features and characteristics of the arcing phenomenon. The schematic diagram of a typical auto-expansion circuit breaker is shown in Figure 2.2. During the circuit breaker operation, the piston is moving to compress the compression cylinder, which generates high pressure in the compression chamber. The valve between compression chamber and expansion volume operates when the pressure in compression chamber is higher than that in the expansion volume so that the gas can flow into the expansion volume. After the contact separation, the arc raised between the contacts gap starts to heat the gas and ablated PTFE vapour from the nozzle surface which then increases the pressure in the arc region and push the mixture into the expansion volume. The pressure in the expansion volume keeps increasing till the flow reversal occurs: gas starts to flow from the expansion volume to the arcing region and cool the arc. The leak valve attached with the piston releases gas to avoid the high pressure generation in the compression chamber to disturb the breaker motion.

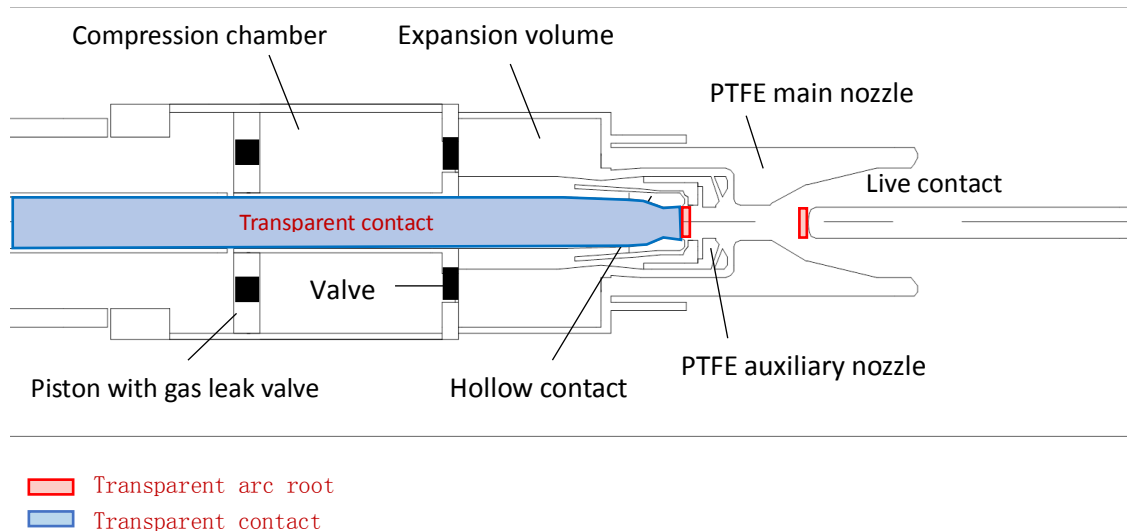


Figure 2.2: Typical geometry of an auto-expansion circuit breaker

In the operation of a commercial circuit breaker, one of the contacts has to reach a minimum speed when the contacts separate. This is realized by allowing the driving mechanism to accelerate the moving contact over a distance called “over travel”. The over travel of modern auto-expansion circuit breakers is in the range of 15 – 55 mm. during this period of contact acceleration, the cylinder is compressed by the piston, resulting in pressure rise in the cylinder and gas flow towards the nozzles. This period is called the “pre-arc” stage or cold flow phase.

In arc simulation, the breakdown of the contact gap immediately after contact separation is not considered due to its complexity. An arc is initiated when the two contacts separate with a distance of 5-8 mm. Thus the first phase, the cold flow (pre-arc) phase is defined as the period from the instant of contact movement to the instant when the contacts separate for a distance of 5-8 mm. This range of 5-8 mm is recommended in consideration of the computational grid size. It is rare that the two contacts separate with an exact distance at the end of a time step where results are saved for starting the arc process. It is expected that there are at least 7 finite volumes or cells as called in PHOENICS in the direction of the axis of the contact to properly initiate the arc and set up the “transparent arc roots” [6].

Arc is then imitated by initialing a hot column with the temperature gradually decreases from the axis toward the radial direction. If the current at the initial instant is very high, it needs to be ramped from 3 kA to the real value in a short time of

0.2ms for computational consideration. High current phase spans from the arc initiation to an instant corresponding to a current which is smaller than 15 kA before last current zero for reasons given in [6]. The authors of [6] found that the measured arc voltage has a surge around 15 kA before final current zero. The energy transport mechanism switches from radiation domination to turbulence domination. Thus, 15 kA is used to as a boundary of high current phase and current zero phase in arc simulation. The arc in this phase is supplied by the current source, thus, the intermediate current zero(s) are not considered and set to be 3000 A if it is smaller. Transparent contact and arc root as Figure 2.2 shows need to be defined to provide current collection from the arc column when the principle of current continuity is used to obtain the electric field in the high current phase, which is described in Section 2.4.1.3. In addition, the arc related Ohmic heating, radiation, Lorenz force and ablation are also required (Section 2.4.1.3 and Section 2.4.1.4).

After high current phase, the current becomes smaller than 15 kA. The period from the end of the high current phase to the final current zero is called current zero phase. The arc in this phase becomes very thin with the decreasing current. To capture the temperature gradient, the grid in the arc region within 2 mm from the axis has to be refined. The results in the refine part from the high current phase are interpolated to set the initial value to the extra grid cells. Turbulence model plays an important role in this phase which directly determines the accuracy of the prediction. The setting of turbulence parameters depends on the calibration of turbulence model in Chapter 3. Post arc phase starts from current zero point, the initial field based on the final time step of the current zero phase. In this phase, a linearly changed dV/dt is applied to calculate the post arc current. If the post arc current decreases to zero within a short time period ($< 15 \mu s$), the thermal interruption succeeds. The value of dV/dt , at which the arc will just be extinguished, is commonly known as the critical rate of rise of recovery voltage (RRRV). Thus, a set of cases need to be done to find the critical RRRV to evaluate the thermal interruption capability of the simulated circuit breaker or nozzle configuration. Since the current is very low ($< 1 A$) in this phase, the Lorenz force, and radiation is neglected. All the components are considered to be stationary in this short period.

2.2.3 Automated initiation and management of different phases in the simulation

Previous experience shows that it may take up to two weeks to perform a complete set of simulation for the interruption process in a high voltage circuit breaker. Most of the time has been spent on the settings of initial and boundary conditions and nozzle ablation, generation of the grid system, and the execution of simulation for different phases of the arcing process.

Manual initiation of each phase of the simulation is time consuming and prone to human mistakes. To start the high current phase firstly necessary information needs to be extracted from the results of the cold flow phase, as described in the previous section, which is time consuming using manual method. Secondly, the process of placing a hot conducting column in the contact gap requires many settings which were manually made in the past. In addition, grid refinement is needed in the current zero phase. The automation of these operations will lead to a considerable saving in the overall time required for the simulation.

In order to reduce the overall time for simulation and eliminate potential human mistakes in setting up the simulation, the *Simulation Manager* is created in ISEE to automate all the above time consuming operations. It is responsible for organizing and monitoring the actual computation of each phase of the simulation and keeping record of the general information of the result files. It works in the background and continuously monitors the simulation process. For example, when it detects that the cold flow phase is finished it will automatically extract information on contact separation, positions of each contact, the end time and time step, etc to produce necessary code files (Q1 and Ground.for, etc) to start the high current phase automatically. These detailed intelligent process controls are explained in Section 2.5.

2.3 Objects and Representation of Design Parameters Relating to Physical and Simulation Properties

Depending on the software development framework, an object can be given different

names in the software design process. For the present work Visual Studio C++ has been used. The mechanical parts in a real circuit breaker are represented by “components” in ISEE. A component that can be seen on a GUI is called a “Control” in Visual C++. Components are entities serving as the basic building blocks in Windows based programme [14]. To avoid ambiguity, the term “component” will be used in this chapter to refer to a mechanical part when it is mapped into the software domain.

In the framework of structured grid system in CFD applications [13], a component has a quadrilateral shape whose four side lines are named North, South, Low and High. A component in ISEE is created using a technique in Visual Studio called GraphicsPath [14] to accurately represent its shape, which is shown in Figure 2.3.

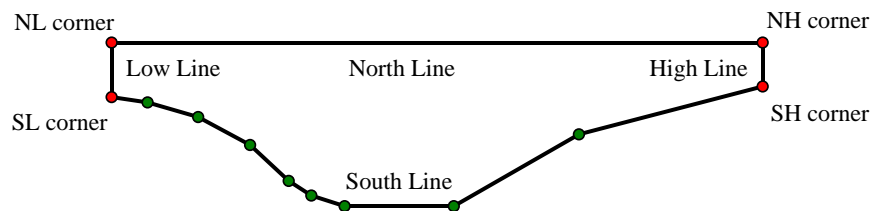


Figure 2.3: An example of component represented using GraphicsPath

There are many types of components with different roles and properties in a circuit breaker. For example a moving contact is different from a nozzle. Each type of component has a unique index so that a piston or a valve is differentiated. A collection of data and methods are encapsulated in an object, which means a component consists of properties and methods. In Object Oriented Design, an object is personified as human being. A property is a piece of information describing the state of an object (person). A method is also called a behavior, meaning what an object (person) can do. Table 2.1 and Table 2.2 list the properties which are defined for such as PTFE nozzle and Flow Inlet/Outlet, respectively. ISEE is able to simulate the movement of a component if its travel characteristics are given.

Table 2.1: Main properties of PTFE nozzle component

Name of Property	Role in Simulation
Coordinate values defining shape and position of an object (m), 2 values for each vortex plus intermediate values on the side lines if necessary.	For grid generation; visual display on GUI, collision detection between two components and allocation of solid cells in the computation domain
Spatial resolution (m)	Used to determine the number of radial and axial cells
Maximum number of cells	Limit for cell number for structured grid system.
Minimum number of cells	Limit for cell number for structured grid system.
Position of four corners in terms of cell position, 2 integer values for each vortex.	Used to allocate solid cells in the domain with a structured grid system to define the region occupied by a solid component.
Electrical conductivity ($\Omega^{-1}\text{m}^{-1}$)	To calculate potential distribution
Ablation surface	For calculation of ablation dimension
Density (kg/m^3)	For estimate of nozzle enlargement due to ablation.
Ablation energy (J/kg)	Calculate PTFE nozzle ablation.
PTFE vapour temperature (K)	Calculation ablation rate and specification of energy flux into gas domain.

Table 2.2: Main properties of Flow Inlet/Outlet virtual component make change to this table below for more and clear information.

Name of Property	Role in Simulation
Stagnation pressure (Pa)	To specify flow boundary conditions
Stagnation Temperature (K)	For use to compose energy flux into domain.
Gas constant	Equation of state in low temperature region.
Position, orientation and size of flow inlet/outlet	To determine flow domain boundary and impose appropriate boundary conditions which are assigned when this virtual component is constructed

To make the use of ISEE user friendly, boundary conditions and their location information, regions for Ohmic heating, radiation transfer and Lorentz force, and transparent contact region and their settings are also represented by components, although they are virtual in nature. The dimensions of a virtual component can be manually selected by the user or automatically detected by components communication after grid generated. In the manual mode, once the grid system is generated, user can define a region as a virtual component by mouse clicking the

four corners according a sequence of SL, SH, NH, NL corner. In the automatic model, different types of virtual components are defined due to different criteria which are listed in Table 2.3.

Table 2.3: Concept and dimension of virtual component

Index	Name	Concept	Region detection method
204	Transparent contact	A virtual contact which is used to fill the hole of hollow contact to provide current collection from a thin arc column	Axial: dimension same as hollow contact with the index of 215 Radial: from the axis to the South side of hollow contact object
214	Transparent arc root	A virtual component which locates in front of the tip of the contacts. No current can flow into the contact from the outside of the transparent arc root.	Axial: three cells Radial: its radius is calculated according to Equation 2.4.
215	Hot column	A virtual component is conducting to initiate the arc.	Axial: the gap length between two contacts Radial: it is calculated by Equation 2.4
216	Ohmic heating Radiation Lorenz force	A virtual component which is used to obtain energy source due to Ohmic heating, radiation, and Lorenz force	Axial: from the low side of computational domain to the final position of moving contact at the current zero Radial: from the axis to the south side of main nozzle with the index of 6
212	Inlet	A virtual component which is used to given inlet boundary condition	Axial: small thickness Radial: only allows manually setting
213	Outlet		
0	Grid component	A virtual component that is used to generate grid of special requirement in a particular space or region,	Only allow manually setting

2.4 Modelling of Arcs, Moving Component and Operation of Valves

2.4.1 The arc model built in ISEE

2.4.1.1 Governing equation

The circuit breakers under investigation in this thesis are all assumed rotationally

symmetric in geometry. The arc together with its surrounding gas flow is assumed to be in local thermodynamic equilibrium (LTE) state. Its behaviour can be mathematically described in a 2D cylindrical coordinate system by the time-averaged Navier-Stokes equations taking account of Ohmic heating, electromagnetic effect (Lorenz force), nozzle ablation, radiation loss and turbulence enhanced mass, momentum and energy transport. The general conservation equation is expressed in the following form:

$$\frac{\partial(\rho\phi)}{\partial t} + \frac{1}{r} \frac{\partial}{\partial r} \left[r\rho v\phi - r\Gamma_\phi \frac{\partial\phi}{\partial r} \right] + \frac{\partial}{\partial z} \left[\rho w\phi - \Gamma_\phi \frac{\partial\phi}{\partial z} \right] = S_\phi \quad (2.1)$$

where ϕ is the variable to be solved and, ρ , w and v represent respectively the density and axial and radial velocity components of a gas or gas mixture, The source term S_ϕ and the diffusion coefficient Γ_ϕ are listed in Table 2.4.

Table 2.4: Source terms and diffusion coefficients for governing equations

Equation	ϕ	Γ_ϕ	S_ϕ
Mass	1	0	0
Z-momentum	w	$\mu_l + \mu_t$	$-\partial P/\partial z + J_r B_\theta +$ viscous terms
R-momentum	v	$\mu_l + \mu_t$	$-\partial P/\partial r - J_z B_\theta +$ viscous terms
Enthalpy	h	$(k_l + k_t)/c_p$	$\sigma E^2 - q + dP/dt +$ viscous dissipation
PTFE mass concentration	c_m	$\rho(D_l + D_t)$	0
Current continuity	φ	σ	0

where μ is dynamic viscosity, P the pressure, j the current density and B the magnetic flux density. θ indicates the azimuthal direction of a cylindrical polar coordinates system. k is thermal conductivity, c_p the specific heat at constant pressure, σ the electrical conductivity, E the the electric field, q the the net radiation loss per unit volume and time. c_m the PTFE mass concentration, D the diffusivity, the subscript l denotes the laminar part of the diffusion coefficient and t the turbulent part.

2.4.1.2 Thermodynamic and transport properties of arcing medium

The filled gas in the auto-expansion circuit breakers under investigation is SF_6 . During the operation of an auto-expansion circuit breaker, the arc could burn in pure

SF₆, SF₆ and polytetrafluoroethylene (PTFE) mixture, or pure PTFE vapour depending on the nozzle geometry, contact travel and arcing history. The equation of state at room temperature for SF₆ gas takes the form of ideal gas law with a gas constant of 56 Jkg⁻¹K⁻¹ below 1000 K. However when the gas temperature increases, dissociation and ionisation take place and the equation of state no longer follows the ideal gas law. Since the arcing medium composition varies greatly with thermodynamic variables such as temperature and pressure [15], the equation of state cannot be expressed by a simple function. Therefore, the density ρ as a function of temperature and pressure and transport properties (laminar viscosity μ_l , the ratio of laminar thermal conductivity to the specific heat at constant pressure k/C_p , and electric conductivity σ) of SF₆ with different PTFE concentrations need to be calculated in advance. Many researchers have done this calculation for pure SF₆ and PTFE [16]-[19]. However, because of the differences in the atomic and molecular data used, there exist discrepancy between these data. By comparison, the data in [16] and [18] give the best agreement. In addition, the simulation results, like arc voltage using [16] and [19] are very close to each other. Therefore, the tabulated data in [16] are used in ISEE.

The local properties of the gas or gas mixture during the iteration process are obtained by interpolation [20]. According to Table 2.4, enthalpy (h) is solved for variable for the energy equation, and the temperature and transport properties mentioned above are derived from the enthalpy solution and pressure.

2.4.1.3 Ohmic heating and Lorenz force calculation

Ohmic heating (σE^2) and Lorenz force ($\vec{J} \times \vec{B}$) are included in the source term of energy and momentum conservation equations in Table 2.4, respectively. The electrical conductivity σ , is a function of temperature and pressure, which could be calculated by interpolation (section 2.4.1.2). At high current phase, the radial size of the arc column varies along the axial direction significantly and the radial current density component is comparable with the axial one, the electric field needs to be calculated by the so called “Non-slender arc model”, meaning the radial component of the electric field cannot be ignored and an electric potential equation has to be

solved. The Lorenz force is computed based on the axial and radial current densities and the azimuthal component of the magnetic field induced by the arcing current [15].

The electrical potential is calculated by solving the current continuity equation [21] as shown in Table 2.4, which is expressed as

$$\nabla \cdot (\sigma \nabla \varphi) = 0 \quad (2.2)$$

where σ is the electrical conductivity and φ the electrical potential. To solve such equation with only the diffusion term, the diffusion coefficient can never be zero in order that a solution exists in the whole domain. So for low temperature gas or insulating material, an electrical conductivity of $10^{-3} \Omega^{-1}\text{m}^{-1}$ is used. The radial and axial current density can then be calculated from the electrical potential distribution by

$$j_r = -\sigma \frac{\partial \varphi}{\partial r}; j_z = -\sigma \frac{\partial \varphi}{\partial z} \quad (2.3)$$

On all boundary surfaces of the domain for electric potential calculation except that intersecting with the current conducting contacts, a condition of zero current density is imposed, which is also the default PHOENICS boundary condition on walls [22], which means no current flow across the boundary. Because the boundaries for electric potential calculation is sufficiently away from the arc region, the electric field solution inside the arc column and in its vicinity is not affected by the use of the zero current density condition. The potential on the boundary surface where the live contact intersects with the boundary is set to zero.

A fixed current density J_{root} is specified in the arc root [3]. Thus the radius of the arc root is expressed as

$$R_{root} = \sqrt{\frac{I}{\pi J_{root}}} \quad (2.4)$$

where I is the current and $J_{root} = 1.5 \times 10^8 \text{ A/m}^2$ which produces reasonable results [3].

The arc column is rotationally symmetric and the magnetic field is dominated in the azimuthal direction of the axis of the arc column. Assuming the permeability of the arcing medium, μ_0 , to be homogenous and equal to $4\pi \times 10^{-7} \text{ H/m}$, the magnetic field

can be calculated by [2]

$$B_{\theta} = \frac{\mu_0 \int_0^r J_z 2\pi r dr}{2\pi r} \quad (2.5)$$

where J_z is the axial current density. The Lorentz force in radial and axial directions, as volumetric force sources in the momentum equations (Table 2.4), can be then expressed as:

$$f_r = -J_z B_{\theta} \quad (2.6)$$

$$f_z = J_r B_{\theta} \quad (2.7)$$

It has been mentioned that in the transparent arc root and in a section of the arc column joining the transparent arc root, the Lorentz force is calculated based on a uniform axial current density equal to J_{root} . In this case, the Lorentz force is reduced to

$$f_r = -\frac{\mu_0 J_{root}^2}{2} r \quad (2.8)$$

with $f_z = 0$.

During the current zero period, it is true that the radial arc column size does not change substantially along the axial direction and the radial component of the current density is negligible in comparison with that in the axial direction. Thus, the ‘‘slender arc model’’ is used to calculate the electric field. Moreover, the effect of Lorentz force is negligible since the current is low (<15,000A).

The axial electric field can therefore be conveniently calculated by the simplified Ohm’s law:

$$E_z = \frac{I}{\int_0^{R_c} \sigma 2\pi r dr} \quad (2.9)$$

where R_c is the radius of the conducting column, normally taken as the radial distance from the axis to the point where $T=3,000K$. Inside the nozzle the arc temperature in a slab may be larger than 3,000K. In this case R_c will be taken as the nozzle radius. The current density is then σE_z .

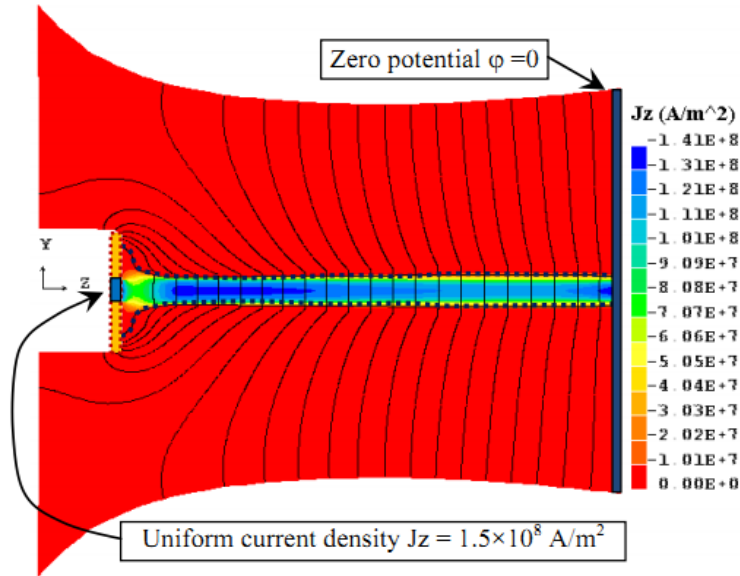


Figure 2.4: Diagram showing boundary conditions for the electrostatic potential equation (current continuity equation). The blue dotted lines are the 10,000 K isotherms approximating the conducting arc column. The equipotential lines are perpendicular to the boundary surface representing a zero current density normal to the boundary faces.

2.4.1.4 Radiation and ablation

A semi-empirical radiation transport model of Zhang et al [3] is used, which assumes a monotonic radial temperature profile (blue line) with a maximum temperature of T_m on the axis as Figure 2.5 shows. The arc core is defined as the region from the axis to the radial position of 83% of the maximum temperature, which is also called radiation emission zone. The total amount of radiation from the arc core is partly absorbed in the region between the core edge and the 5,000K/4,000K isotherm in the auto-expansion/puffer circuit breaker, where is called the re-absorption zone. The rest of the radiation reaches the PTFE nozzle wall and produces ablation.

In the energy conservation equation in Table 2.4, the net radiation loss per unit volume and time, q , is calculated by the net radiation emission coefficient (NEC) [23] in the arc core. The NEC depends on the temperature, pressure and arc radius. High temperature SF_6 gas and PTFE vapour both contain a significant proportion of fluorine element and their NECs are very close to each other for radiation radius larger than 1 mm [24] as shown in Figure 2.6. For example at a pressure of 4 MPa, which is typical for circuit breaker arcs, the difference between the NECs of SF_6 and

PTFE vapour is less than 20% for radiation radius between 1 mm and 10 mm. For computational efficiency, the NEC data of SF_6 is used in the present work.

Experience shows that to make reasonable temperature prediction at the arc centre, the NEC data from Lowke [25] has to be used with a specific definition of the radiation radius. For auto-expansion circuit breakers, the radial temperature profile varies substantially along the length of the arc column. In the main nozzle the temperature near the nozzle surface can be well above 4000 K and the radial temperature profile in the space between the two nozzles can become non-monotonic during the high current phase. Thus in the present work, the arc radius for the calculation of radiation emission is defined as the radial distance from the axis to the isotherm of $0.83T_{\max}$ for the high current phase (from arc initiation to the point of 15 kA magnitude before the final current zero) and the average of the two radii corresponding to $0.83T_{\max}$ and 5000 K in the current zero phase (from the end of the high current phase to the final current zero point). The use of the above two methods to define the radiation radius gives nearly identical radial temperature profiles while preventing numerical difficulties. More details of the radiation model can be found in [2] and [3]. The NEC data given in [25] is multiplied by a factor of 1.5, which produces reasonable arc voltage in the high current phase [16].

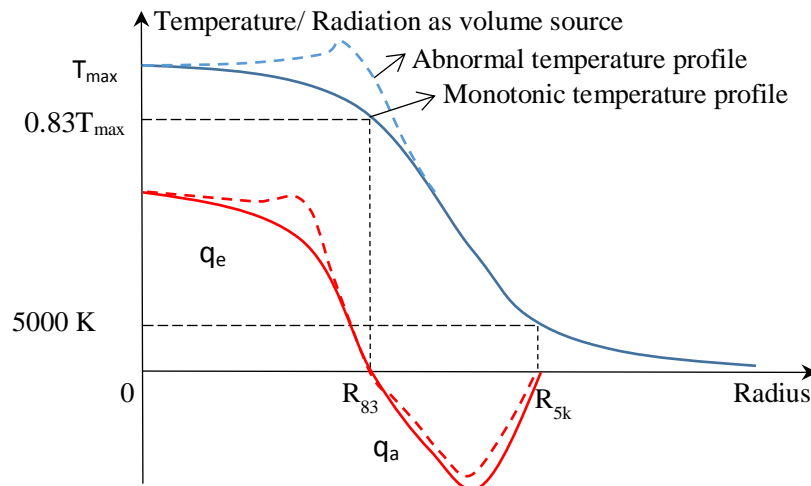


Figure 2.5: Possible temperature profile of arcs and the emission ($0 \sim R_{83}$) and re-absorption ($R_{83} \sim R_{5k}$) zones

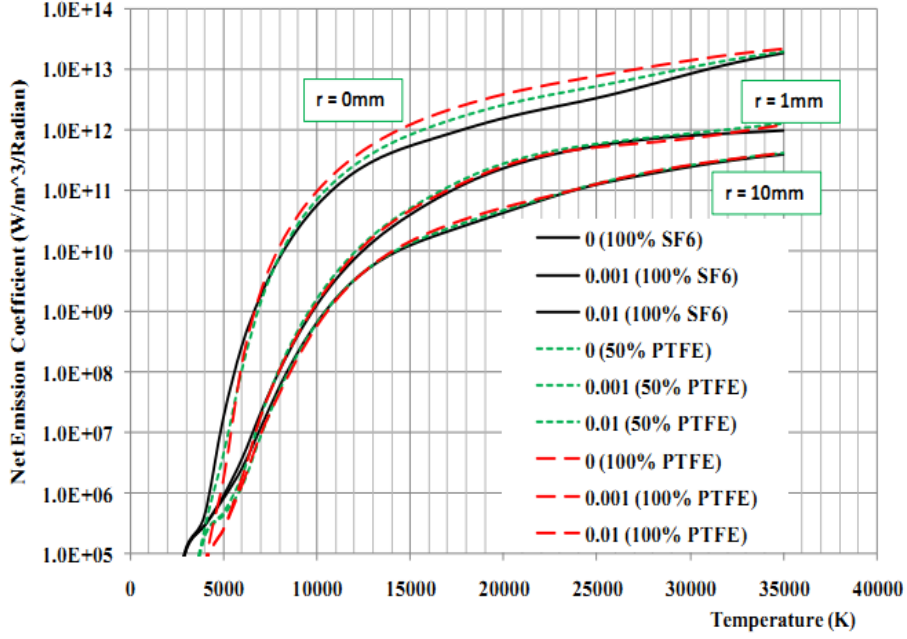


Figure 2.6: A comparison of the NEC of pure SF₆, 50% SF₆ – 50% PTFE, and pure PTFE vapour at 40bar which is the typical pressure in the arc at high current.

Radiation is emitted from the arc core. Once the volumetric radiation energy source is calculated, the total radiative flux from the arc core can be obtained by volume integration. 50% / 80% of this radiation flux is assumed to be absorbed at the arc edge in auto-expansion / puffer circuit breaker, respectively. The distribution of the negative volumetric energy source as a result of radiation re-absorption in the region from R_{83} to R_{5K} as a function of radius is given by:

$$q_a(r) = q_0 \left[1.1 - \left(\frac{R_{5K} + R_{83} - 2r}{R_{5K} - R_{83}} \right)^2 \right] \quad (2.10)$$

where R_{83} and R_{5K} is the radius at $0.83T_{max}$ and 5000 K, respectively. q_0 is a constant that can be calculated from the following expression

$$q_0 = \frac{0.5Q_{core}}{\int_{R_{83}}^{R_{5K}} \left[1 - \left(\frac{R_{5K} + R_{83} - 2r}{R_{5K} - R_{83}} \right)^2 \right] 2\pi r dr} \quad (2.11)$$

where Q_{core} is the total radiation flux from the arc core. The other 50% / 20% of Q_{core} reaches the nozzle wall producing nozzle ablation.

The radiation energy from the arc core is partly absorbed in the re-absorption zone, the rest of the radiation reaches the PTFE nozzle wall producing ablation. The effect of nozzle ablation is considered by solving a mass concentration equation for PTFE vapour. The amount of PTFE vapour injected into the flow domain is obtained by [24]

$$\bar{m} = \frac{Q_{noz}}{h_v} \quad (2.12)$$

where Q_{noz} is the radiation flux per unit length reaching the nozzle surface, \bar{m} is the rate of ablation per unit length as a mass source injected into the flow domain, and h_v is the energy required to break up the polymer PTFE chain and to raise the PTFE vapour from 300 K to 3400 K [26], which is equal to 1.19×10^7 J/kg.

The diffusion coefficient in concentration equation is expressed as $\rho(D_l + D_t)$ in Table 2.4, where D_l is the laminar diffusivity and D_t the turbulent diffusivity. D_l and D_t are respectively related to the local laminar viscosity and turbulent viscosity by the laminar and turbulent Schmidt number [27][29]:

$$D_l = \frac{\mu_l}{\rho S_{cl}}; D_t = \frac{\mu_t}{\rho S_{ct}} \quad (2.13)$$

The magnitude of S_{cl} and S_{ct} are around unity [15] and a value of 1.0 can be used for S_{ct} . The laminar viscosity is calculated in section 2.2 and the turbulence viscosity will be calculated in next section.

2.4.1.5 Turbulence model

Both Prantl mixing length model and k - ε turbulence model introduced in Section 1.4.3 are built in ISEE, which allow users to choose as required. The turbulence enhanced energy transfer is represented by a so-called “turbulent thermal conductivity”. It is not a material property and is given such a name only for convenience. The turbulent thermal conductivity is called k_t and we need to provide the solver with the term k_t/C_p . This term is also passed to the solver through a so-called turbulent Prandtl number defined as

$$P_{rt} = \frac{\rho v_t}{k_t/C_p} \quad (2.14)$$

where C_p is the capacity heat at constant pressure. The turbulence enhanced thermal conductivity cannot be directly obtained from a turbulence model and it has to be related to μ_t by assuming a value for turbulent Prandtl number for arc simulation. It is found that $P_{rt} = 1$ is sufficient since adjustable parameters appear in the turbulence model which are to be determined based on experiment for switching arc applications [28].

2.4.1.6 Boundary conditions

For a real circuit breaker, the arcing chamber is enclosed in an insulating tank with a high filling pressure and there is no forced gas inlet. When we take the whole tank as the system under simulation, there will be no gas exit. However, the simulation concentration is in and near the arcing chamber region, thus only outlet is needed when the computational domain is restricted. The pressures at the two exits are fixed as the value of filling pressure. While in an experimental arcing device, inlet stagnation pressure and temperature are normally specified. The inwards mass, momentum and energy fluxes are calculated by assuming isentropic expansion of gas from the stagnation pressure to the local pressure at the boundary cells. The boundary conditions provide fluxes of mass, momentum and energy into the boundary cells. Their values are determined by the stagnation pressure (P_0) and temperature (T_0) and local pressure in the boundary cells, P_{cell} :

$$\rho_0 = \frac{P_0}{R_g T_0} \quad (2.15)$$

$$w_{in} = \sqrt{\frac{2\gamma}{\gamma-1} R_g T_0 \left[1 - \left(\frac{P_{cell}}{P_0} \right)^{\frac{\gamma-1}{\gamma}} \right]} \quad (2.16)$$

$$\rho_{in} = \rho_0 \left(\frac{P_{cell}}{P_0} \right)^{\frac{1}{\gamma}} \quad (2.17)$$

$$T_{in} = T_0 \left(\frac{P_{cell}}{P_0} \right)^{\frac{\gamma-1}{\gamma}} \quad (2.18)$$

where γ is the ratio of specific heat at constant pressure (c_p) to specific heat at constant volume (c_v) of the gas. The values of the parameters for different gases used in this thesis are listed below:

Table 2.5: Parameters for SF₆ and air

Parameter	SF ₆	Air
γ	1.1079	1.4
R_g	56	287

The radial velocity on the axis is zero and all the radial derivatives of other dependent variables are set to zero ($\frac{\partial \varphi}{\partial r} = 0$). Besides, at the solid surfaces, the heat flux is set to zero (adiabatic), and a built-in wall function of PHOENICS [21] is applied.

2.4.2 Moving components

PHOENICS uses structure grids and is not able to accurately model the movement of a round tipped contact, either hollow or solid. However, in the real commercial circuit breaker, most contacts are round tipped, thus, there is a need to propose a method to deal with such moving component so that PHOENICS can handle it. In addition, the real process of valve operation will be simplified in simulation. The grid system is fixed once it is defined. In simulation, the electrode and piston is considered relatively traveling with the real moving mechanism like nozzle, because they have relative simple geometry. Within 2-dimensional system, the moving component are all rectangular. Even for a round-tip contact, it will be approximated as a set of flat tipped longitudinal rings like the following figure shows. The true minimum flow cross sectional area during the process of the live contact evacuating the main nozzle is $4\pi L(\delta L) + \pi(\delta L)^2$, where L and δL are the curvature radius and gap thickness of the round contact tip as shown in Figure 2.7, while a full length flat tip approximation gives much smaller gap area which is $\pi(R_N)^2 - \pi(R_C)^2$. The effective flow area can be sensitive to the shape of the contact tip, therefore, this approximation is necessary.

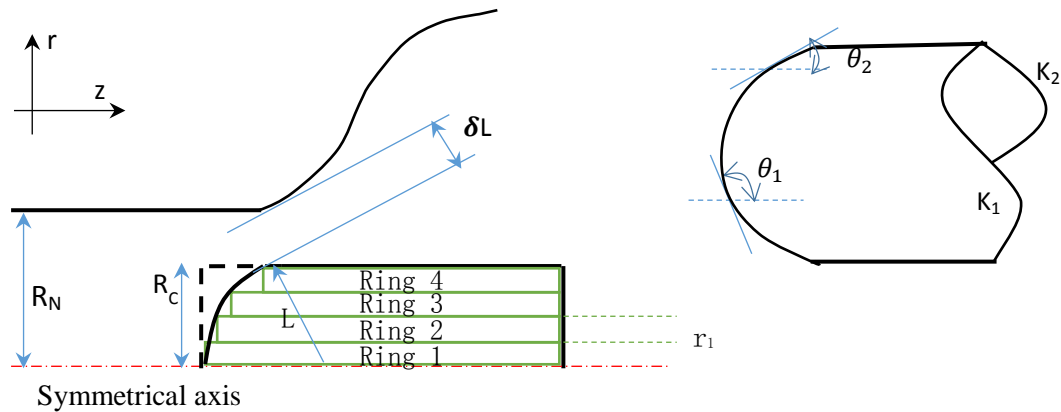


Figure 2.7: Diagram shows approximation of the rounded tip of a moving contact by flat tipped longitudinal rings, real geometry is assigned by black solid lines

The user may choose to describe the shape of the tip in one of the two ways, using an analytical description or by giving a set of points along the surface of the tip. In the second case, the points are fitted using least square method, so the coordinates of more intermediate points can be calculated and used. The polynomial can be expressed in the following form

$$z = a_0 r^n + a_1 r^{n-1} + \dots + a_{n-1} r + a_n; \text{ where } n > 1 \quad (2.19)$$

where z is the axial coordinate and r the radial coordinate. The axial coordinate as a function of the radial coordinate has to be used because on the contact tip surface r increases monotonically (start from the axis) while z can increase (hollow rounded tip contact) or decrease. When the number of points given is not sufficient to work out the intermediate points, equation (2.19) will be used to fit at least three points to obtain a segment of curve that approximates part of the surface of the tip.

To accurately approximate a round-tip contact, there is a need to use thin rectangle in gradual region ($\theta < 45^\circ$), while in steep region ($\theta > 45^\circ$), thick rectangular could be used. Therefore, the radial dimension of a rectangle could be determined by splitting the curve into multi-segments according to the criteria give below. As Figure 2.7 shows, the low side of contact is a curved surface, which is divided into multi-segments. This procedure is affected by three factors which are expressed below:

The corresponding curve length across a radial distance of (r_2-r_1) is:

$$\Delta L = \int_{r_1}^{r_2} (\sqrt{1 + f'(r)^2}) dr \quad (2.20)$$

where $z = f(r)$ is the function of LOW side of component of the contact object and r is the radial coordinate.

The slop angle variation over a segment of curve with a radial distance, Y , equal to r_2-r_1 is:

$$\Delta\theta = \max\{|\tan^{-1}(f'(r + \delta r)) - \tan^{-1}(f'(r))|\}, r \in [r_1, r_2 - \delta r] \quad (2.21)$$

Assume the maximum curve length, slop angle change and the corresponding radial distance of each split segments are ΔL_m , $\Delta\theta_m$ and ΔY_m , respectively. ΔY_m is fixed as 2 mm which is the radial distance of first split ring. ΔL_m is the corresponding curve length of 2mm radial distance for split component, $\Delta\theta_m$ is the degree with corresponding to ΔY_m .

The integration and calculation will start from a point on the curve and move towards the end of the curve. When the following condition is satisfied,

$$\text{Min} \left\{ \frac{\Delta Y}{\Delta Y_m}, \frac{\Delta\theta}{\Delta\theta_m} \right\} \geq 1 \quad (2.22)$$

the coordinates of the point will be used to construct a new component, i.e. it gives the radial extent of the component. ISEE is able to automatically approximate a

rounded tip moving component into a set of flat-tipped components so that PHOENICS can deal with. The movement of these moving components is realized by changing the material property index PRPS during the computation with consideration of energy balance.

2.4.3 Valve operation

Normally, the valves used in circuit breakers consist of a valve plate, a base plate and auxiliary spring. Real operation of valves result in huge difficulties in simulation, therefore, the operation of the valves is simplified as Figure 2.8 shows. In simulation, the valve will be in an open state if the force due to pressure difference on its two sides exceeds a threshold F_{pre} , otherwise, it will be in a closed state. The transition period between the two states due to valve inertia is very complex and is ignored in the simulation. To avoid excessively frequent operation of the valve under critical conditions, a minimum delay time, less than 0.5 ms, is applied to the valve.

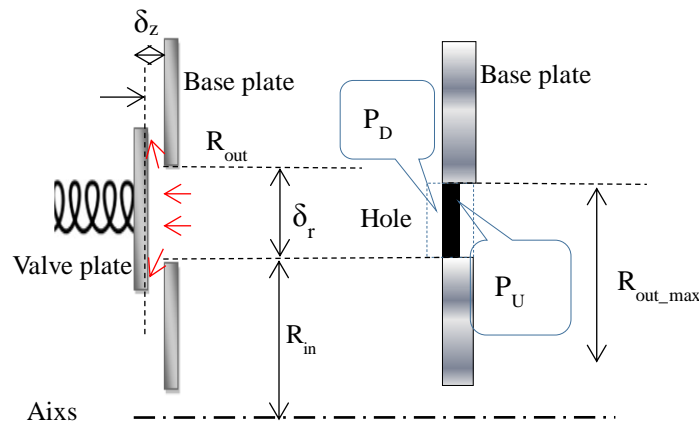


Figure 2.8: Diagram (left) shows a valve in real circuit breaker, and (right) shows the simplified one in simulation

In reality, the valve operates as a result of pressure difference. The flow cross sectional area is thus:

$$A_{gap} = 2\pi(R_{in} + \delta_r)\delta_z + 2\pi R_{in}\delta_z \quad (2.23)$$

When the spring achieves a maximum deformation (δ_{z_max}), the gas flow area achieves a maximum value A_{gap_max} . It also gives a threshold maximum force F_{max} on the plate, which can be expressed by

$$F_{max} = k \cdot \delta_{z_max} \quad (2.24)$$

where k is the spring constant. In the simulation for the valve, the control of the effective flow cross section area is achieved by controlling the radial extent of the valve hole that is open to gas flow. Thus, the equivalent maximum outer radius of the valve hole used in simulation can be calculated by

$$R_{out_max} = \sqrt{\frac{A_{gap_max}}{\pi} + R_{in}^2} \quad (2.25)$$

To work out an equivalent force that is applied on the valve plate, P_U is the sum of upstream pressure plus $0.5\rho w^2$, static pressure in downstream is P_D , the area of equivalent valve plate is A_{plate} , pre-force of spring is F_{re} and, then the following force balance equation is given:

$$F = (P_U - P_D)A_{plate} - F_{pre} \quad (2.26)$$

The whole valve hole, from R_{in} to R_{out_max} , is divided into five ring areas. The area that opens to gas flow is controlled by comparing the force, F , applied on the plate with the threshold maximum force F_{max} and preforce F_{pre} as Figure 2.9 shows.

Considering that in reality the valve plate has certain mass and it will result in an operational time constant. To allow the user to take this into account, an action time δt is introduced in Table 2.6, meaning that the minimum time interval between subsequent change of the valve hole area in terms of the number of ring areas with equal area as shown in Figure 2.9.

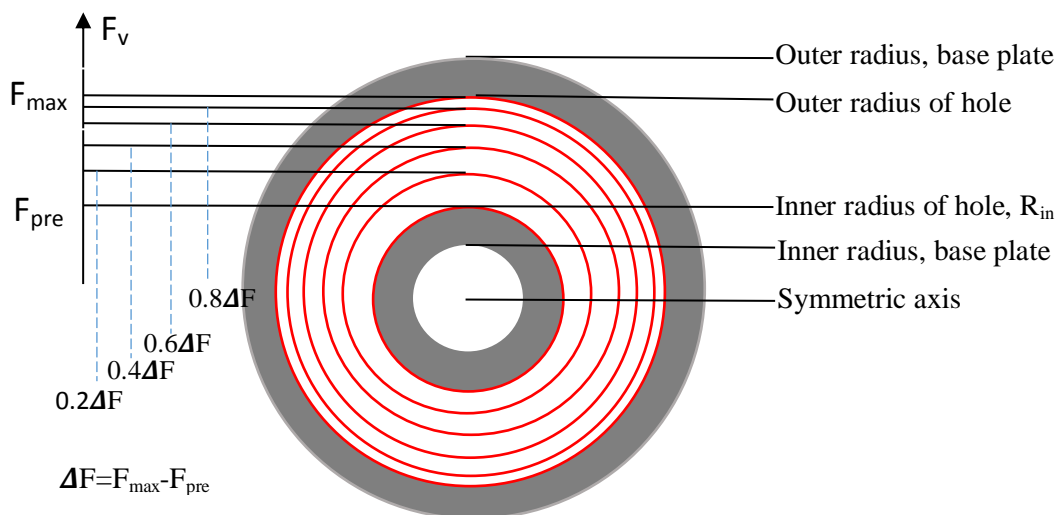


Figure 2.9: Diagram showing linear relationship between the six threshold value of force F_v and the number of rings of the divided cross sectional area of the valve hole (0,1,2,3,4,5, altogether 6 stages) that are kept open to flow.

Therefore, according to the above analysis of valve operation, its model parameters are listed in the following table.

Table 2.6: Model parameters to simulation valve operation

Parameters	Variable Name	Variable Name Setting in ISEE
Equivalent inner radius of valve holes	R_{in}	RVVIN
Radial thickness of equivalent valve hole used in model	$R_{out_max} - R_{in}$	DRVV
Perforce that the spring acts on the valve plate	F_{pre}	FPRE
Force to maintain full valve open	F_{max}	FMAX
Area of equivalent valve plate	A_{plate}	AREAONP
Valve operation time	δt	TDELAY
Valve open to which direction, 1 means open to left and 2 right	-	1LEFT2R

When the valve switches from closed to open state, the solid cells immediately change to gas cell, which leaves a vacuum. The gas from the upstream slab is used to compensate the vacuum. During this filling process gas expansion assumes isothermal at the average temperature in upstream slab. As a result, pressure in upstream slab will slightly decrease when the valve is opened or the flow passage size increases. When the valves switches from open to closed, the gas in the flow passage is pushed into the downstream before the solid material is filled in. The pressure in downstream slab will slightly increase when the valve is closed or the flow passage size decreases. Because of the small volume of the flow passage in comparison with the volume of upstream slab, mass, momentum and energy are all conserved during this process. The hole in simulation is always occupying one slab due to the computation reason.

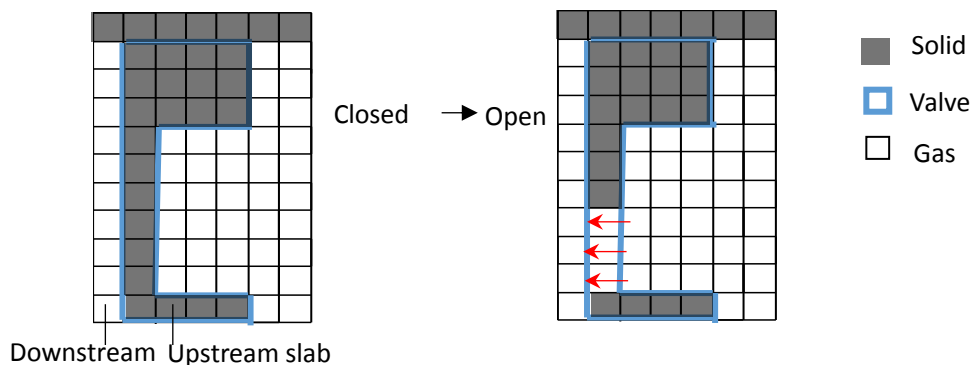


Figure 2.10: Diagram shows the valve switches from closed to open state

2.5 Intelligent Process Control and Grid Generation in ISEE

The automation of simulation of different phases of the arcing process is expected to produce significant savings in overall simulation time. Traditionally, the following processes are carried out manually.

- a) Definition of the geometry of the components in the computational domain is by individual points whose coordinates are obtained from drawings or CAD files. There exist methods to import the geometry of a circuit breaker from a CAD file into the arc simulation domain. However the user has to identify the solid and gaseous regions and make material settings.
- b) The inlet and outlet for fluid flow has to be identified and corresponding settings made.
- c) The region for Ohmic heating and Lorentz force has to be identified and necessary settings made.
- d) The region for radiation transfer has to be identified and necessary settings made.
- e) The size and position of a conducting hot column has to be determined and placed in the contact gap at the beginning of the high current phase for arc initiation.
- f) Ablating surfaces have to be determined and necessary settings made.
- g) Grid refinement for current zero period simulation is carried out manually.
- h) The critical rate of rise of recovery voltage (RRRV) is manually obtained by repeating the post arc current calculation with a large number of RRRV values.
- i) Grid generation, as further described below.

Grid generation is the most time consuming part for arc simulation. Especially for product optimal design, changing the geometry of one component in the computation domain needs re-definition of all the grid system, which renders optimal design a difficult and time consuming work. Furthermore, the quality of the grid may influence the convergence of the computation results. Therefore, to save simulation time, there is a strong need to produce a method which is able to generate structure grid automatically. It has been mentioned in section 2.3 that arcing simulation consists of four main stages. For each stage, different input files or boundary

conditions for solving the governing equations are required. The detailed implementation in ISEE will also be presented in this section.

2.5.1 Method of grid generation

Structured grids are generated automatically in *Assembler* after the virtual product is assembled. The method used here is called progressive aiming. A basic requirement in the grid generation process is that grid lines must follow the boundary lines of a quadrilateral component in 2D space. Therefore the Low and High sides of a component are always located on a “vertical” grid line and the South and North on a “horizontal” grid line. For a single grid line, the generation process starts with a point. With this start point, a vertical grid line will be grown in the positive radial direction until it achieves the North side of the overall domain. Then, with the same start point, the vertical grid line grows in the negative radial direction until it achieves the South side of the domain. The vertical grid lines are first allocated and the angles between intersecting lines have to be with the range of $90^\circ \pm \theta$ where θ is normally less than 10° as Figure 2.15 shows. For different start point, the growing method should be specified particularly. If a point/corner is contained by a component, this component is its Owner Component. One point/corner could have at most four owner components. All the different conditions for growing vertical lines are listed in Table 2.7.

Table 2.7: Growing Method of vertical lines from different points

Point Position		Growing Method (Growing direction is along the arrow, blue for up and green for down)
Corner SL	Only one owner component, see Figure 2.11 a.1;	Up: Vertical grid line grows in the positive radial direction following the path of the Low side boundary line; Down: Vertical grid line grows along the bisector of angle, whose two sides are default boundary line and South side of owner component;
	Shared by two component, see Figure 2.11 a.2;	Up: Vertical grid line grows in the positive radial direction following the longer path of the Low side boundary line; Down: Vertical grid line grows along the bisector of angle, whose two sides are South sides of two owner components;
Corner NL	Only one owner component, see Figure 2.11 b.1;	Up: Vertical grid line grows along the bisector of angle, whose two sides are default boundary line and North side of owner component; Down: Vertical grid line grows in the negative radial direction following the path of the Low side boundary line;
	Shared by two component, see Figure 2.11 b.2;	Up: Vertical grid line grows along the bisector of angle, whose two sides are North sides of two owner components Down: Vertical grid line grows in the negative radial direction following the longer path of the Low side boundary line;
Corner SH	Only one owner component, see Figure 2.11 c.1;	Up: Vertical grid line should grow in the positive radial direction following the path of the High side boundary line; Down: Vertical grid line grows along the bisector of angle, whose two sides are default boundary line and the nearest South side line segment of owner component;
	Shared by two component, see Figure 2.11 c.2	Up: Vertical grid line should grow in the positive radial direction following the longer path of the High/Low side boundary line; Down: Vertical grid line grows along the bisector of angle, whose two sides are South side line of two owner components;
Corner NH	Only one owner component, see Figure 2.11 d.1;	Up: Vertical grid line grows along the bisector of angle, whose two sides are default boundary line and the nearest north side line segment of owner component; Down: Vertical grid line should grow in the negative radial direction following the path of the High side boundary line;
	Shared by two component, see Figure 2.11 d.2;	Up: Vertical grid line grows along the bisector of angle, whose two sides are nearest north side line segments of neighbour component and owner component; Down: Vertical grid line should grow in the negative radial direction following the longer path of the High/Low side boundary line;
Side Point	see Figure 2.11 e.1	Up: Vertical grid line grows positive radial direction along the bisector of angle, whose two sides are nearest line segments; Down: Vertical grid line grows negative radial direction along the bisector of angle, whose two sides are nearest line segments;

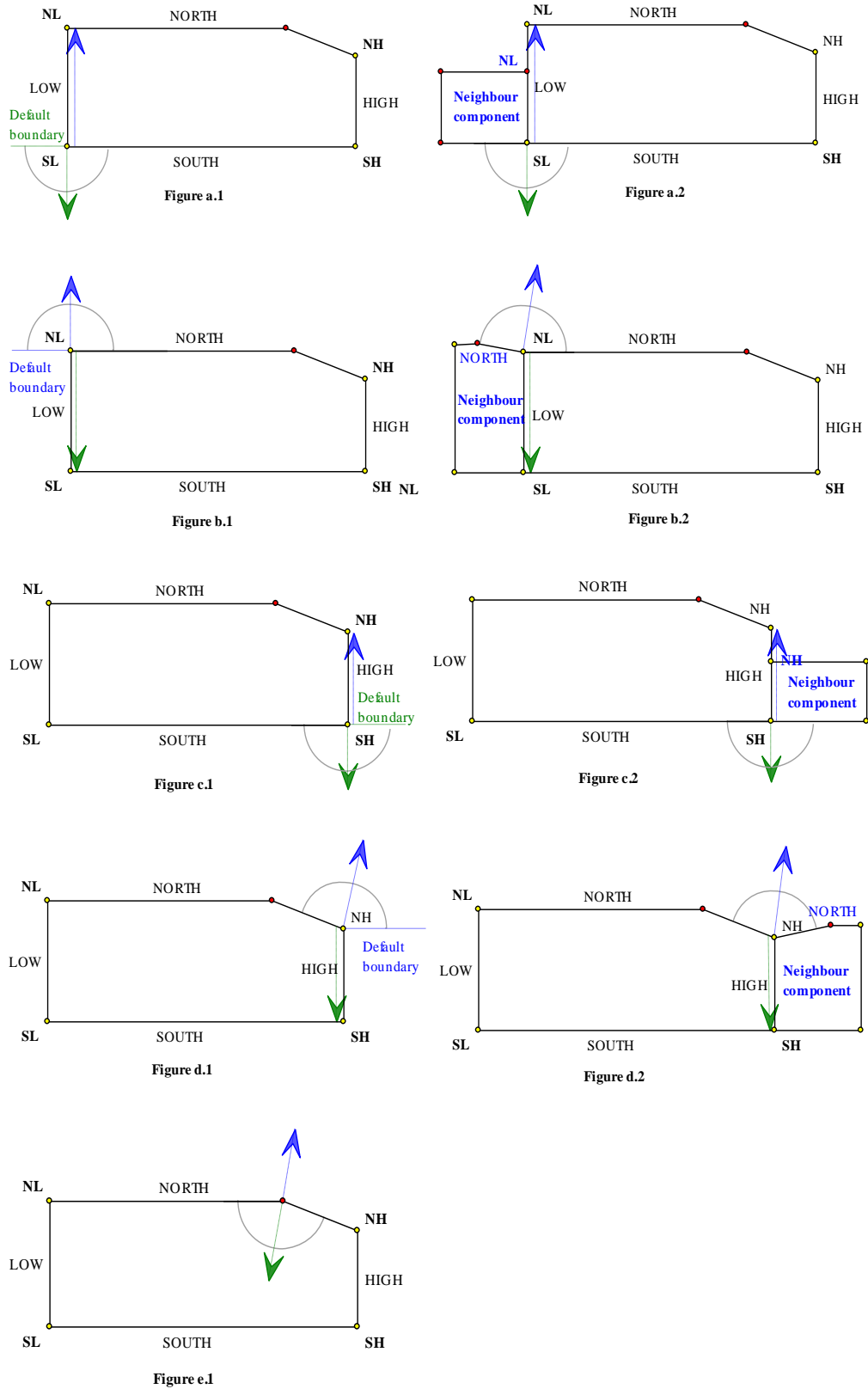


Figure 2.11: Diagram illustrates the criteria of growing method for vertical grid lines
 Figure 2.12 shows the flow chart of the process of vertical line generation. The corner index which is mentioned below, 1 represents corner SL, 2 means corner SH. According to the method described in Table 2.64 indicates vertical grid grow up

along the boundary side from corner SL to NL, or from SH to NH. Therefore, there is no need to involve corner NL and NH in that loop. The details about Tree-Line-Method are explained following this flow chart.

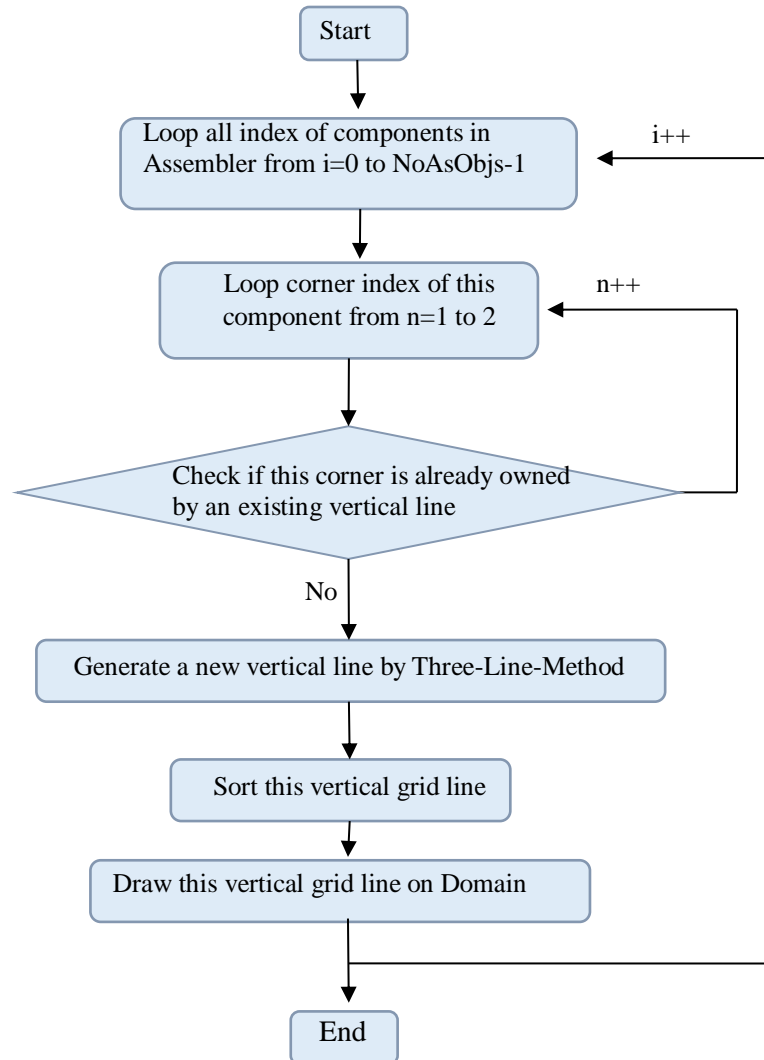


Figure 2.12: Flow chart of vertical grid line generating process

Like Figure 2.13 illustrated, vertical line grows from corner SL in plot ①. With the method in Table 2.7, firstly, the vertical line follows the Low side of component “FIXE” to corner SH in plot ②. Then producing three tentative straight lines (see Figure 2.13), the green and red dash lines are bilateral symmetry to the blue one. The angle is 5 degree which is sufficiently small for generating nearly orthogonal grid system. Secondly, check the intersection condition, combine Table 2.8, only middle line and right side line have intersection with component “NOZZ”, thus corner SL of “NOZZ” is the next point in plot ④. Plot ⑤ shows vertical line following the low

side of “NOZZ” to corner NL. Repeatedly, using Three-Line-Method to find the next grid point. None of tentative lines have intersection with any component, therefore, a point in domain north side is found in plot ⑦. Finishing growing up, this vertical line grows down, similar with the above, the final point is found in plot ⑨.

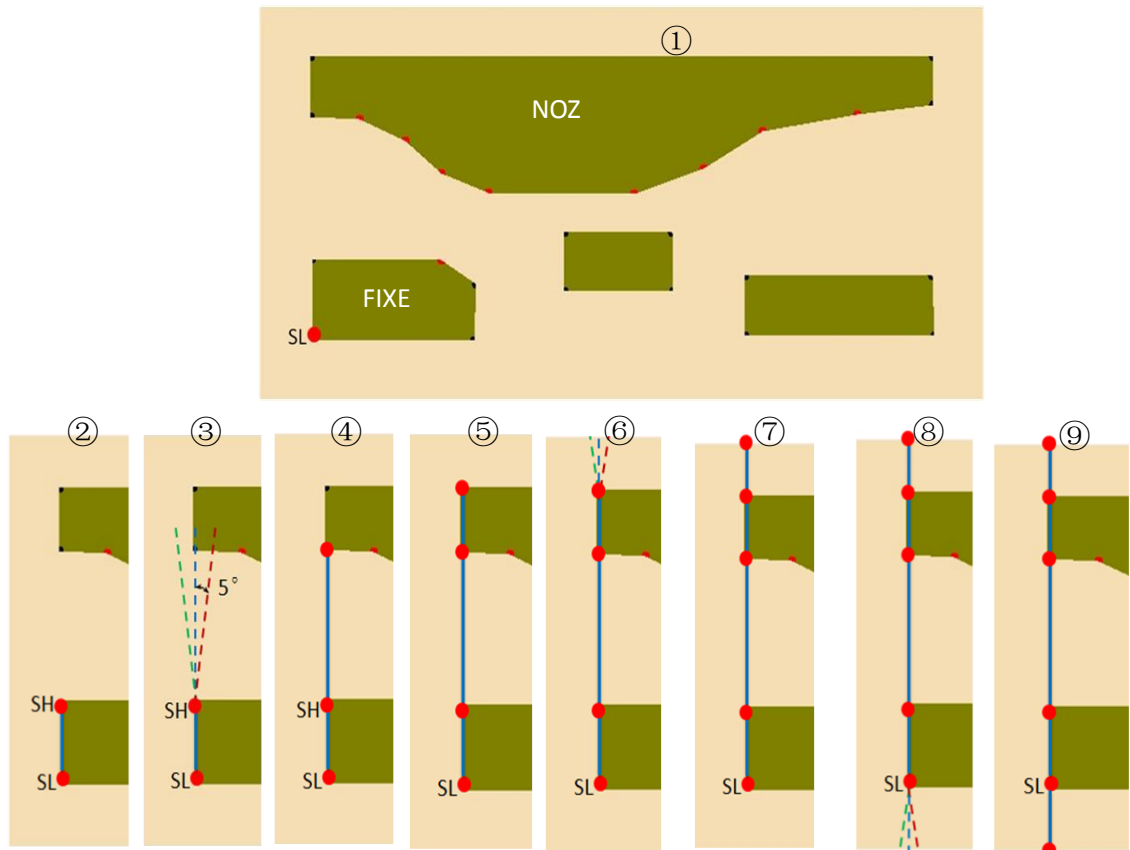


Figure 2.13: Diagram shows the process of growing vertical lines from corner SL

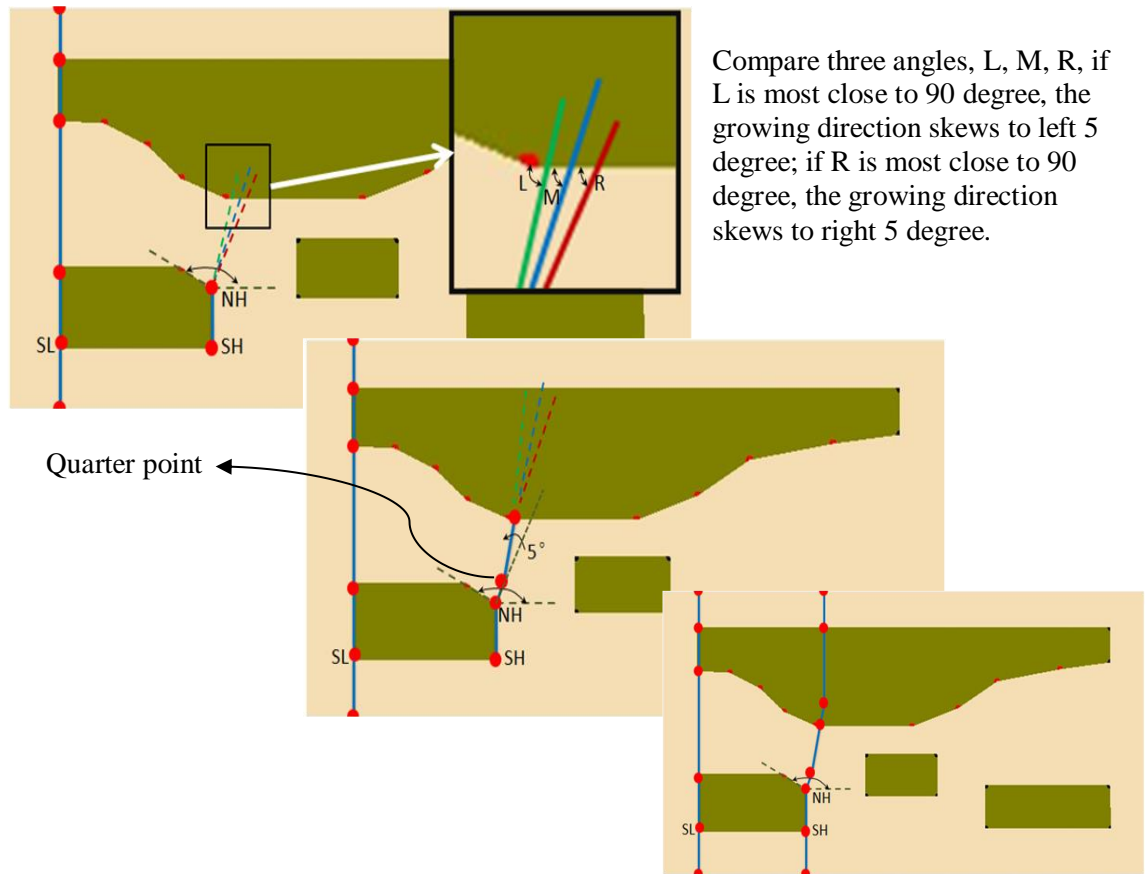


Figure 2.14: Diagram shows the process of growing vertical lines from corner SH

Table 2.8: Three-Line-Method

Intersection			Reorient	Next Point
L	M	R		
0	1/0	0	Skew the middle line 5 degree until the included angle with Domain side is between 80-100 degree	Locate on Domain side.(An example on plot ⑥ of Figure 2.13)
1	1/0	0	-	Corner SH of the intersect component
0	1/0	1	-	Corner SL of the intersect component (An example on plot ③ of Figure 2.13)
1	1/0	1	Compare the three included angle with the interested boundary side, find out the most close 90 degree angle of them. adjust the growing direction, 5 degree for one adjustment, until the angle is between 80-100 degree	Locate on a boundary side of a component (An example on Figure 2.14)

After all vertical lines are generated, the whole computational domain is divided into blocks/patches, which are demonstrated in Figure 2.15. Horizontal grid lines are generated based on these blocks. Similar to vertical grid line, a horizontal grid line will start to grow with a particular start point (a corner of an object) and keep

growing in the positive axial direction until it achieves the High side of domain, then it begins with the same point to grow towards the negative axial direction until it reaches the Low side of the overall domain. After the horizontal grid lines are generated, the whole computational domain is divided into more blocks. Since each component has properties of resolution in radial and axial directions which allow user setting the grid cell size, the divided blocks will inherit these properties and get the optimal value as users' requirement. Because of the rapid prototyping and convenience in grid generation, ISEE could be used to do the product optimization for design engineers.

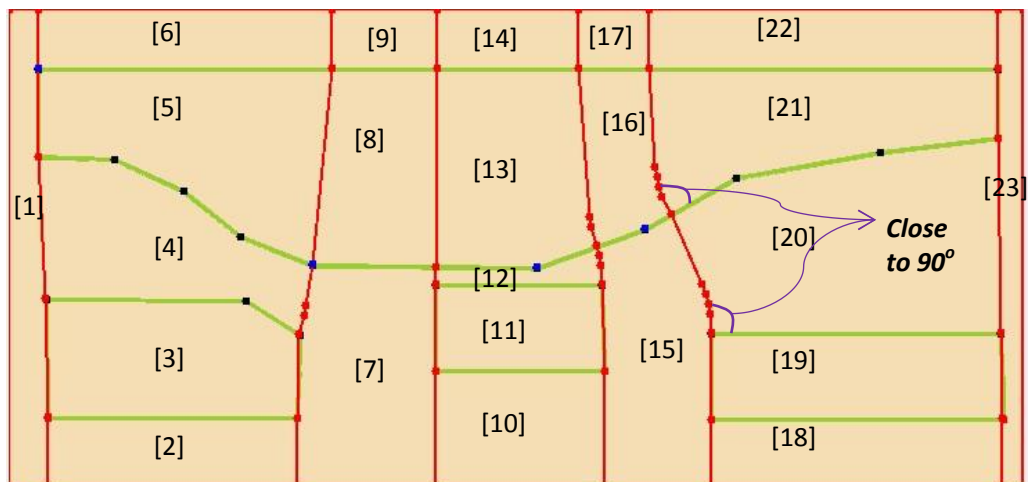


Figure 2.15: Diagram shows four components with green boundary in computation domain in wheat, red vertical grid lines divided whole domain into 23 blocks.

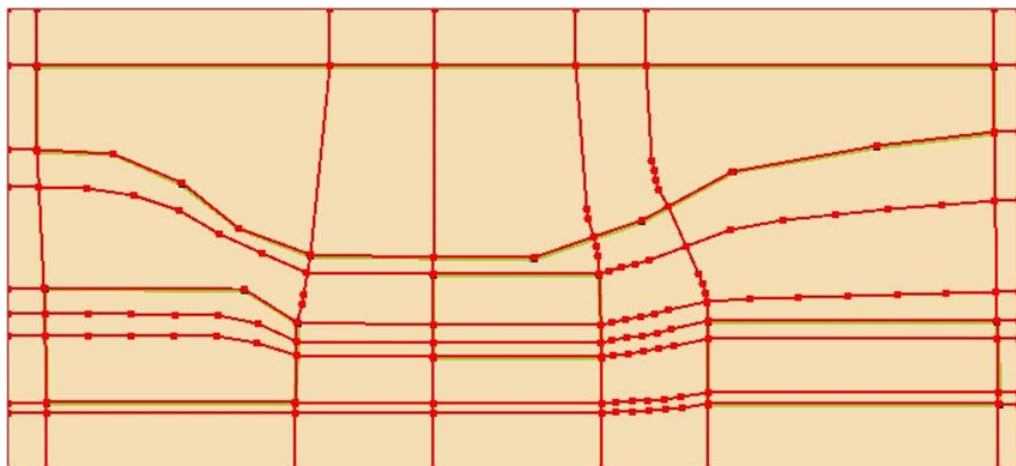


Figure 2.16: Diagram shows the grid system divided by vertical and horizontal grid lines.

Table 2.9: Growing method of horizontal lines from different point

Point Position	Growing Method (The patch mentioned below in shown in Figure 2.15)
Corner SL See Figure 2.17 A	Left: With the length ratio of the point on HIGH side of patch(7), find the corresponding point on LOW side, if no intermediate point exists on NORTH side, directly connect the two points on HIGH and LOW sides. Right: Horizontal grid line grows along the SOUTH side of patch (11)
Corner NL See Figure 2.17 B	Left: With the length ratio of the point on HIGH side of patch(7), find the corresponding point on LOW side, if no intermediate point exists on NORTH side, directly connect the two points on HIGH and LOW sides. Right: Horizontal grid line grows along the NORTH side of patch (11)
Corner NH See Figure 2.17 C	Left: Horizontal grid line grows along the NORTH side of patch (11) Right: With the length ratio of the point on LOW side of patch (15), find the corresponding point on HIGH side. If there is intermediate point exists on NORTH side, find five bisecting points respectively on SOUTH and NORTH sides of patch (15), and then connect them. According to the length ratio, find the intermediate point on horizontal grid line, in Figure C, there is an intermediate point beyond the area of patch (15), thus it is invalid and will not be involved in grid points, therefore, there four intermediate points in this case.
Corner SH See Figure 2.17 D	Left: Horizontal grid line grows along the SOUTH side of patch (11) Right: With the length ratio of the point on LOW side of patch (15), find the corresponding point on HIGH side. If there is intermediate point exists on NORTH side, find five bisecting points respectively on SOUTH and NORTH sides of patch (15), and then connect them. According to the length ratio, find the intermediate point on horizontal grid line.

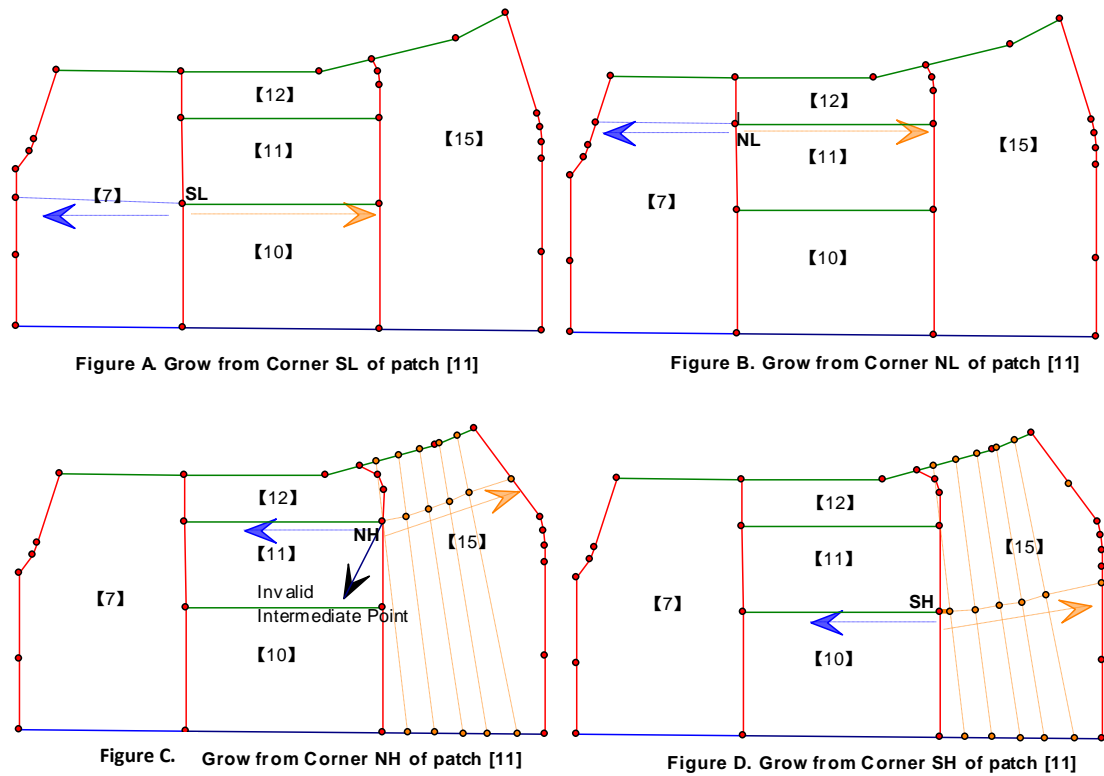


Figure 2.17: Diagram illustrates the criteria of growing method horizontal grid lines according to the blocks/patches those divided by vertical line in Figure 2.15.

2.5.2 Generation of input data files

Traditionally, using PHOENICS to simulate circuit breaker arcs requires the user to define the arc model through command file (Q1), data files (input data files such as material properties), and a PHOENICS specific user-interface subroutine written in Fortran (ground.for). Q1 and ground.for are the most important files for PHOENICS simulation. Figure 2.18 shows a flow chart describing the procedure of performing simulation using PHOENICS. The Q1 file is a collection of PHOENICS Input Language (PIL) commands, which defines the grid system, governing equations to be solved, sets the initial values for variables to be solved, boundary conditions, parameters for solution control and so on. Ground.for is a Fortran file accessible to PHOENICS users, which contains a set of subroutines. These subroutines contain important implementation of the arc model, such as the specification of mass, momentum and energy source terms, Lorentz force, calculation of material properties, and numerical algorithms for moving an object. The aim of this section is to give an explanation to the generation of various codes in the Q1 file.

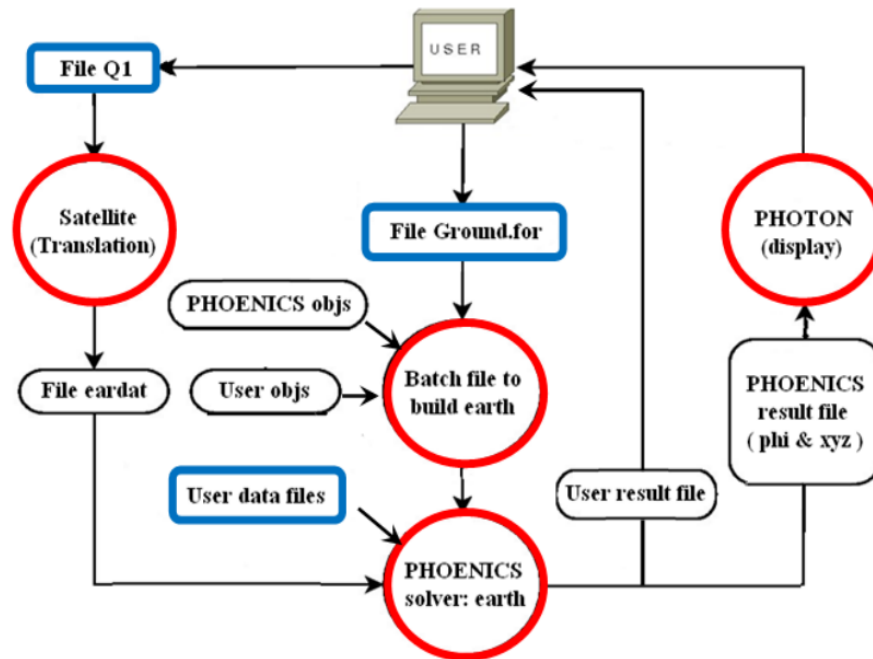


Figure 2.18: Diagram showing information flow in computer simulation of switching arcs based on PHOENICS. Blue rectangles – files to be prepared by user and will be automatically generated using ISEE platform; read circles- executables to be run during the simulation

a) Command for grid in Q1

Defining a grid system needs all the names of points, lines and frames with unambiguous rules. The grid generation for the whole domain needs satisfying the requirement for each individual object. A name, such as for a point or line, should be a string of up to four characters, the first of which must be alpha-numeric. To be compatible with PHOENICS, points and lines are generated using a unified naming scheme. This scheme divides the domain by Z-lines and Y-lines. Two letters are used to name the Y-lines. Starting with AA, AB, AC, ... to AX, AY, AZ, then continue with BA, BB, BC, ... , up to BX, BY, BZ, then CA, CB, CC, ..., the scheme can accommodate a maximum of 676 Y lines, which is sufficient. This is, however, not the actual names used for line segments appearing in Q1.

In Q1, points are first defined which are linked to form Z-line segments and Y-line segments. A combination of 4 letters or numbers is used to name a point, starting with PAAA to PAAZ like Figure 2.19 shows, then PAA0 to PAA9 on the Y-line AA. P means this variable is used as the name for a point. The number of points can be represented is 36, which should be enough for circuit breaker applications because these points are only needed to represent the corner points of objects, whether they

are solid objects or transparent objects.

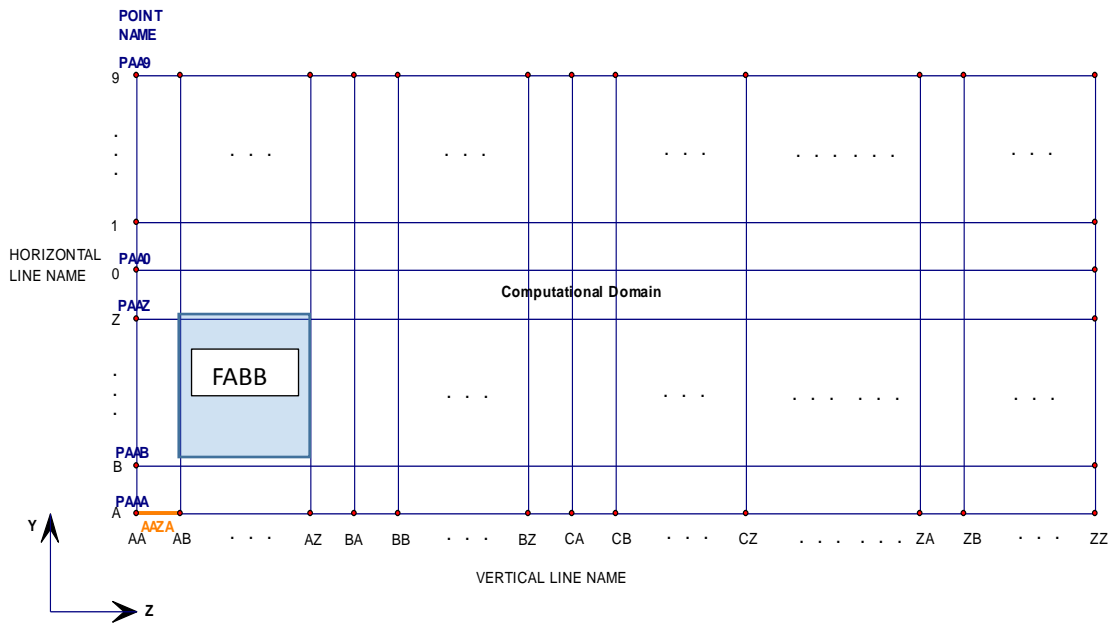


Figure 2.19: Diagram shows the naming scheme for grid system

After naming the points, the Y-line segments and Z-line segments are constructed. The Z- lines are named as, for instance, AAZA, which represent a Z-lines (3rd letter) with a starting point A (indicated by the 4th character) on Line AA (first two letters), namely the point PAAA. This line segment will logically end at the point PABA. Thus we can have a maximum of 36 Z-line segments (A~Z, 0~9) originating from Line AA. Similarly, Y-line segments are named as AAYA, with a starting point of A (4th character) and an ending point logically being PAAB, both of points are on Line AA.

A frame is constituted with points and lines, which highlighted with blue box in Figure 2.18. The name of a frame starts with the character of “F” and follows with the last three characters of the name of its lower-left corner point.

The format for point, line, and frame are listed below. The red characters in those commands will be replaced with the corresponding name and coordinates.

Set a point:

Format: GSET(P,pnam,xp,yp,zp)

pnam -- Name of the point, up to four characters; xp,yp,zp -- coordinate of the point

Set a straight line:

Format: GSET(L,lnam,pnm1,pnm2,nseg[,powr])

pnm1 -- Name of the point where the line starts. pnm2 -- Name of the point where the line ends. nseg -- Number of segments on the line, integer value or integer expression, in the range from 1 to 100. powr -- Distribution power string, normally set to be 1 which means average distribution.

Set a curve:

Format:

GSET(V,vnam,S,pnm1)

GSET(V,xvc,yvc,zvc)

GSET(V,vnam,E,pnm2)

vnam -- Name of the curve, a string of up to four characters, the first of which must be alpha-numeric. pnm1 -- Name of the point where the curve starts. pnm2 -- Name of the point where the curve ends. xvc, yvc, zvc -- coordinates of intermediate points

Set a frame:

Format: GSET(F,fnam,p1,m1,p2,m2,p3,m3,p4,m4)

fnam -- Name of the FRAME, a string of up to four characters, the first of which must be alpha-numeric. p1 -- Name of the first corner POINT. p2 -- Name of the second corner POINT. p3 -- Name of the third corner POINT. p4 -- Name of the fourth corner POINT. m1 -- List of intermediate points between the first and second corner points m2 -- List of intermediate points between the second and third corner points. m3 -- List of intermediate points between the third and fourth corner points. m4 -- List of intermediate points between the fourth and first corner points. If there are two or more intermediate points, they must be separated by a dot '.' in the list, ie P5.P6 if P5 and P6 are the names of intermediate points. When there is no intermediate point, use a hyphen, -, instead.

2.5.3 Settings and initiation of the cold flow phase

Users are allowed to run each phase of the simulation separately or run the

continuous whole arcing process. If a user chooses the former mode, he/she could do the required setting (as Figure 2.20 shows) before starting each stage, while if the latter one is chosen, all the required settings should be done before the pre-arc phase starts. The time step and relaxation factor will be set using default value based on more than twenty years' experience of Liverpool arc simulation.

There are two options for cold flow which are no-load mode and pre-arc phase. The simulation will stop at the final time step in the former case. A pre-arc phase is performed to obtain the initial conditions such as flow field for the high current phase. This stage is interrupted when the electrode and (transparent) contact separate 5-8mm. Then the arc is initialized with a hot conducting column in the contact gap.

In the cold flow phase, the only necessary virtual component that needs to be used in the Assembler GUI is inlet and/or outlet. The relevant parameters that are discussed in section 2.4.1.6 need to be assigned. When pre-arc phase finishes, a file named "AFTERCOLD.TXT" is generated which contains the required information for the high current phase such as final time instant, contacts gap dimension and position of the live contact. PHI is a file which records all field variables at the final time step for restarting the high current phase.

2.5.4 Start of high current phase (Initiation of arc)

Arc initiation is realized by adding a virtual component "hot column". The radial dimension of the "hot column" depends on the transient current magnitude, and the axial dimension is equal to the contact gap. The arc related virtual components, such as Ohmic heating, radiation, Lorenz force, transparent contacts and arc root will be also needed. Since the properties and source term for all types of component have been built in, the dimensions for these virtual components are only needed which is realized by communication of other components such as nozzle and contacts. Considering the convergence problem, before running the high current phase, the time step and relaxation control will be modified as well based on experience. These values from past experience are used to make settings which can also be modified according to the users' requirement. The simulation of high current phase is a restart

case based on the final step results from cold gas simulation.

2.5.5 Start of current zero phase

Normally, the arc in high current phase is fat, the radial cell dimension is around 0.25 mm which is sufficient to capture the temperature gradient. However, at the current zero phase, the current is below 15kA, the grid in the arcing region needs to be refined to simulate the thin arc column. The default size for arcing cell in 2 mm radially from axis is 0.02mm at the current zero phase. To realize the refinement, a virtual component with activated property called “refineObj” should be pre-defined before grid generation. The dimension of the refine component is determined by users according to the requirement. Therefore, from high current phase to current zero phase, the radial cell resolution will change from 0.25 mm to 0.02 mm. Because of this refinement, there are extra cells compared with the previous simulation stage, then the normal restart option cannot work anymore. The file “IOFIELD.TXT”, which has similar function of “PHI” but simple data format. The values for the extra cells are assigned by interpolate the results from high current phase.

2.5.6 Post arc zero phase

Thermal recovery is an important process in the interruption of a fault current. A linearly increased voltage at a given rate of rise (dV/dt) is applied to the contact gap immediately after current zero due to the interaction between the circuit breaker and the power system. In simulation, a critical rate of rise of recovery voltage (RRRV) is to be found by applying different values of dV/dt . The value of dV/dt , at which the arc will just be extinguished, is commonly known as the critical RRRV. The definition of critical RRRV has been given in section 2.2.2. The critical RRRV is commonly used to indicate the thermal interruption capability of a circuit breaker. Thermal recovery takes place within 10 μ s after the final current zero, thus in such a short time duration, the distance that a moving contact travels is negligible. No moving components are used in this phase. Ablation is also disabled because radiation reaching the nozzle wall is virtually none with an arc temperature of below 12,000K [25]. In each simulation corresponding to a given dV/dt , once the post arc

current reaches above a threshold value, such as 100A, the computation is stopped and a report is produced to indicate thermal failure at such a dV/dt . This is because once Ohmic heating becomes stronger than the energy loss due to convection and turbulent cooling for a considerable proportion of the thermal recovery period, the arc temperature will rise rapidly, leading to thermal re-ignition. A typical curve is shown in Figure 4.15 for a 145 kV auto-expansion circuit breaker. As the figure shows, multiple cases are started with different dV/dt values for the searching of the critical RRRV which is 10 kV/us for that case.

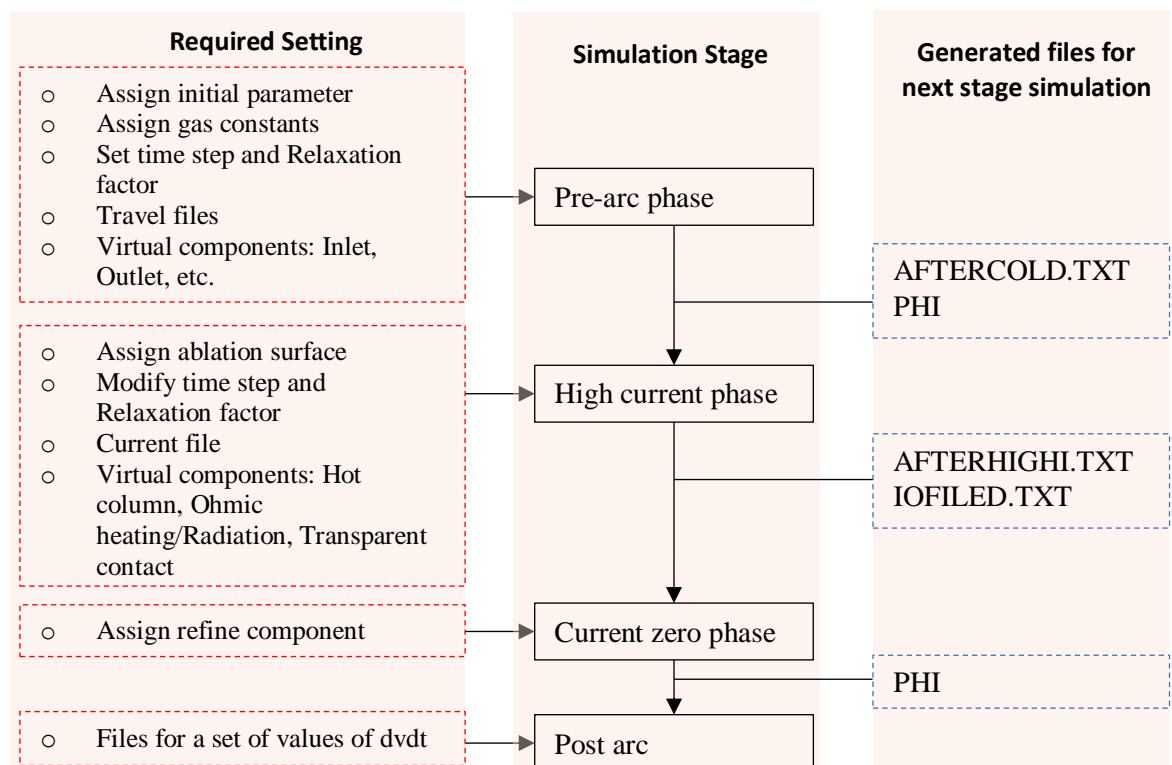


Figure 2.20: Required setting and files for each simulation stage

2.6 Information Exchange between Solver and ISEE-Visual Monitor

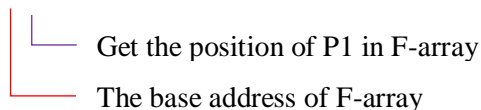
PHOENICS has been used for arc simulation for around 20 years. It was developed in 1990's and coded with Fortran 77 which is a fully procedure-oriented programming language. The current version is also single-threaded program. It is desirable to improve the performance and functionality. The main idea is to utilize the interface, Ground.for, provided by PHOENICS to implement the improvement. Mixed language programming which includes Fortran 77, Fortran 90, C++ and java is used.

Inversion of control (IoC), as one of the object-oriented programming techniques, has been used to bound the object coupling. It is implemented by Spring framework, which is an open source application framework and inversion of control container for the Java platform.

Ground.for contains an empty Fortran subroutine recognized by the PHOENICS solver, which provides interfaces for users to insert their own Fortran codes to influence the solution process. Ground.for also provides a binary code injection point, which means it can be executed as long as the customized function that may be defined using other languages is compiled to binary code. The definition of the binary code here is an obj (compiled but not linked file) or dll (dynamic link library) file.

PHOENICS uses the F-array to save the solved for variables and locate them in static and continuous memory addresses. Based on this feature, the data could be accessed without requesting in the main thread. It can be done by inserting the following code at the very beginning of computation, because the data can be obtained once the head address and the data structure are achieved. Therefore, the simulation results can be simultaneously displayed on GUI of Visual Monitor without any disturbance to computation.

```
CALL FARRAYINFO( F, LOF(ANYZ(P1,1)))
```



Get the position of P1 in F-array
The base address of F-array

```
Head address of P1= F + LOF(ANYZ(P1,1)) *4 // P1: float type
```

2.7 Conclusion

The structure and implementation of an integrated simulation and evaluation environment, the ISEE platform, has been described. The arc model incorporated in this platform is defined in details. The novelties of the work in this chapter can be summarised below:

- ISEE is developed using an object-oriented approach, closely aligned with

the practical design process and test process of high voltage circuit breakers. This makes the simulation process intuitively understandable and eliminates the traditionally time consuming model set-up approach.

- ISEE greatly reduces the overall time to complete the simulation of the whole circuit breaker interruption process by automatically generating the grid system and initiating the different phases of the simulation process.
- the use of mixing language programming adds parallel computation (calculation of material properties for example) to the solution process and more importantly, all variables can be visualised in the process of computation. This latter is extremely useful for researchers who need to investigate the causes of computational divergence by visually identifying the location and variables in the computational domain where computational instability first occurs.

This platform will be used in the following chapters to study the fundamental processes in the interruption process of different types of circuit breakers to gain new understanding and knowledge of the aerodynamic and thermal processes involved in the switching process.

References

- [1] M.T.C. Fang and E. Pfender, "Guest Editorial", IEEE Trans. On Plasma Science, Special Issue on High-Pressure Arcs and High-Frequency Thermal Plasmas, Vol. 25, No.5, pp. 807- 808, October 1997
- [2] J.D. Yan, M. T. C. Fang, and W. Hall, The development of PC based CAD tools for auto-expansion circuit breaker design, IEEE Trans. on Power Delivery 14, pp.176-181, 1999
- [3] J.F Zhang, M.T.C Fang and D.B Newland, Theoretical investigation of a 2kA arc in a supersonic nozzle, J. Phys. D: Appl. Phys. Vol. 25, pp. 1197-204, 1987.
- [4] M. Claessens, K. Moller and H.G. Thiel, A computational fluid dynamics simulation of high- and low-current arcs in self-blast circuit breakers, J. Phys. D: Appl. Phys. 30, pp. 1899-1907, 1997
- [5] P. Maruzewski, A. Martim, M. Reggio, and J-Y Trepanier, Simulation of arc-electrode interaction using sheath modelling in SF₆ circuit breaker, J. Phys. D: Appl. Phys., Vol. 35, pp. 891-899, 2002
- [6] J.L. Zhang, J.D Yan, A.B Murphy, W.Hall and M.T.C Fang, Computational investigation of arc behaviour in an auto-expansion circuit breaker contaminated by ablated nozzle vapour, IEEE Trans. Plasma. Sci, Vol. 30, pp 706-19, 2005.
- [7] J.D. Yan, S.M. Han, Y.Y. Zhan, H.F Zhao and M.T.C Fang, Computer simulation of the arcing process in high voltage puffer circuit breakers with hollow contacts, Proceedings of XVIIIth Symposium on Physics of Switching Arcs, Brno Czech Republic, pp 99-108, 2009.
- [8] PHOENICS is the name of a commercial CFD package developed by CHAM UK, Online help available: http://www.cham.co.uk/phoenics/d_polis/d_enc/encindex.htm
- [9] FLUENT is the name of a commercial CFD package developed by ANSYS, official website: <http://www.ansys.com/Support/>
- [10] X. Jiang, X. Li, H. Zhao, S. Jia, J.D. Yan etc. Analysis of the dielectric breakdown characteristics for a 252-kV gas circuit breaker, IEEE transactions of power delivery, Vol. 28, No.3, 2013
- [11] J.D. Yan, J.L. Zhang, K.Y. Kweon, C.M. Dixon and M.T C. Fang, Computer simulation of high voltage circuit breakers, Invited paper, Proceedings of the XVth Int. Conf. On Gas Discharges and their Applications, Toulouse, Vol. 2, pp. 1025-1034, 2004

- [12] M. Claessens, R. Starck, and G. T. Hans, Simulation of gas flow phenomena in high-voltage self-blast circuit breakers at heavy fault current interruption, IEEE Transactions on Plasma Science, Vol. 25, No. 5, 1997.
- [13] Introduction to body fitted coordinates [Online] Available: http://www.cham.co.uk/phoenics/d_polis/d_lecs/general/bfcintro.htm
- [14] Microsoft Visual Studio online help
- [15] J.L. Zhang, J.D. Yan, and M. T. C. Fang, "Electrode evaporation and its effect on thermal arc behaviour", IEEE Transactions on Plasma Science, Vol. 32, No. 3, 2004.
- [16] J.L. Zhang, J.D. Yan, A.B. Murphy, W. Hall and M.T.C Fang Computational investigation of arc behavior in an auto-expansion circuit breaker contaminated by ablated nozzle vapour, IEEE Transactions on Plasma. Science, 30, 706-19, 2005
- [17] L.S. Frost and R.W. Liebermann. Composition and transport properties of SF₆ and their use in a simplified enthalpy flow arc model. Proceedings of IEEE, 59(4): 474-485, 1971.
- [18] P. Kovitya. Thermodynamic and transport properties of ablated vapors of PTFE, alumina, perspex and pvc in the temperature range 5000-30,000 K. IEEE Transactions on Plasma Sci., PS-12: 38-42, 1984.
- [19] ABB Private communication
- [20] Y. Y. Zhan, Ph. D thesis "PC-based visual simulation of high pressure arc plasma", 2011
- [21] Boundary condition in PHOENICS. Retrieved from www.cham.co.uk/phoenics/d_polis/d_lecs/general/bcond.htm
- [22] J.L. Zhang, J.D. Yan, A.B. Murphy, W. Hall, and M.T.C. Fang. Computational investigation of arc behaviour in an auto-expansion circuit breaker contaminated by ablated nozzle vapour. IEEE Trans. on Plasma Science, Vol. 30, pp.706–719, 2002.
- [23] W.H. Bu, Fang M.T.C and Z.Y Guo, The behaviour of ablation-dominated DC nozzle arcs J. Phy. D: Appl. Phys. Vol. 23, 175-183, 1990
- [24] Private communication with Professor Vladimir Aubrecht of Brno University of Technology, Czech Republic.
- [25] R.W. Liebermann and J.J. Lowke, Radiation emission coefficients for sulfur hexafluoride arc plasmas J. Quant. Spectrosc. Radiat. Transf. Vol. 17, pp. 253-64,

1976.

[26] C.B. Ruchti and L. Niemyer 1986 Ablation controlled arcs. IEEE Trans. on Plasma Science, Vol. 14, pp. 423–434, 1986.

[27] A.B. Murphy and P. Kovitya, Mathematical model and laser-scattering temperature measurements of a direct-current plasma torch discharging into air. J. Appl. Phys., Vol. 73:pp. 4759–4769, 1993.

[28] M.T.C. Fang, Q. Zhuang and X.J. Guo, Current zero behaviour of an SF6 gas-blast arc. Part II: Turbulent flow, J. Phys. D: Appl. Phys., Vol. 27, pp. 74-83, 1994

[29] C.H. Chang and J. D. Ramshaw, Numerical simulation of nonequilibrium effects in an Argon plasma jet, Phys. Plasma, Vol.1, No.11, pp.3698-3708, 1994

Chapter 3

A Study on the Applicability of Prandtl Mixing Length Model to Arc Simulation of Commercial Gas-blast Circuit Breakers

3.1 Introduction

It is well known that arcs burning in SF₆ are turbulent [1]. In the current zero period, turbulence plays a critical role in shaping the arc behavior, especially the critical rate of rise of recovery voltage (RRRV) in the thermal recovery period. It has been shown in [2] that the Prandtl mixing length model is more advantageous over the k- ϵ model in terms of the range of applicability of the turbulent parameter and computational cost. However, the turbulence parameters in these two turbulence models need to be adjusted according to experimental results to obtain reasonable results for arcs around current zero. For Prandtl mixing length model, it has been found that the only turbulence parameter is sensitive to nozzle geometry [3], i.e. different nozzle geometries need different values of the turbulence parameter to produce satisfactory results. Nozzles with simple geometry have been studied for several cases in [2], [4] and [8]. Prandtl mixing length model is simple and less computationally costly than the k-epsilon model, thus it will be used in the simulation in this thesis. For commercial circuit breakers there has been little work on the applicability of the Prandtl mixing length model, which is the objective of the work in this chapter.

Modern auto-expansion circuit breakers employ almost exclusively a PTFE main nozzle with a shape of converging-flat-diverging [1][10]. In this section, two types of circuit breakers with such a type of main nozzle will be used to calibrate the turbulence parameter of the Prandtl mixing length model. It is expected that a range of the value of the turbulence parameter could be found by matching the prediction with measurement.

3.2 Definition of Arc Radius in Prantl Mixing Length Model

With the Prandtl mixing length model the eddy viscosity is related to the flow field by:

$$\mu_t = \rho(cR)^2 \sqrt{\left(\frac{\partial \omega}{\partial r}\right)^2 + \left(\frac{\partial v}{\partial z}\right)^2} \quad (3.1)$$

Where ρ is the density, the product of the turbulence parameter c and thermal radius R indicates the turbulence length scale. The definition of an arc radius R needs to reflect the jet flow features. Strictly speaking, Prandtl mixing length model is applicable to a flow field where there is a strong jet in a background gas and the distribution of axial flow velocity in the transverse direction is monotonic. In case of an arc, the radial temperature distribution needs to be monotonic as well to ensure a monotonic velocity distribution.

In the case of flow in a simple nozzle as shown in Figure 3.1a, the arc radius is defined by

$$R = \left(\frac{\theta_\delta}{\pi}\right)^{1/2} \quad (3.2)$$

where θ_δ is the thermal area of the arc given by

$$\theta_\delta = \int_0^\infty \left(1 - \frac{T_\infty}{T}\right) 2\pi r dr \quad (3.3)$$

where T_∞ is the temperature near the nozzle wall where the radial temperature gradient is negligible.

However, in a real an auto-expansion circuit breaker, there is tremendous difficulty in calculating a well-defined and reasonable thermal radius for the arc column due to much more complexity in the temperature field in comparison with that in a simple nozzle. In a real circuit breaker, there exists flow reversal, flow circulation and stagnation region (Figure 3.1b) at different locations in the arc region, resulting in complicated flow field and difficulty in defining an arc radius. The thermal radius R is a characteristic dimension of the arc column which is defined as the radial distance from the axis to the point of 5000K for the high current phase. The choice of 5000K is based on the observation that a large portion of the arcing space can sometimes be filled with hot vapour from nozzle ablation during the high current phase. In the current zero period and the subsequent post arc current calculation, R is defined as

the radius of 3000K isotherm. The choice of the turbulence parameter c is influenced by the definition of R . It has been found that a single value of c is not applicable for both high and low current arcs. Considering the arcing process in circuit breakers, it is correct to say that at high current the arc column fills most of the nozzle space and cold gas flow only takes a thin annular layer of the nozzle space. Turbulence cooling does not significantly affect the arc behaviour. At low current the arc column is thin and surrounded by cold flow. There is more space for the thin arc column to deform freely. In this sense the turbulence parameter c should be higher at lower current. Therefore, turbulence is a decisive factor in shaping the arc behavior in the current zero period and post arc phase. Thus, the calibration of the turbulence parameter relies on the measurement of the arc voltage and success/failure of the thermal recovery process.

It is proposed, based on the qualitative argument above, that the turbulence parameters are varied according to the instantaneous current, which is linked in general to the relative size of the arc column with respect to the confining nozzle. The turbulence parameter c , in Equation 3.1 is assumed to linearly change with the current. With this relationship, a fairly good agreement is obtained not only for the arc voltage around the peak for a 10kA case, but also around the extinction peak for a puffer circuit breaker [5]. The linear setting performs much better than the fixed parameter settings for c . Therefore, this linear relationship will be used here, the turbulence parameter c changes with the current between T_{p_HI} (0.05) to T_{p_I0} in the current zero phase, the relationship can be expressed as

$$T_p = T_{p_HI} + \frac{|I| - 1.5 \times 10^4}{0 - 1.5 \times 10^4} \times (T_{p_I0} - T_{p_HI}) \dots \dots \dots (3.4)$$

The turbulence parameter remains the value at current zero of T_{p_I0} for the post arc phase.

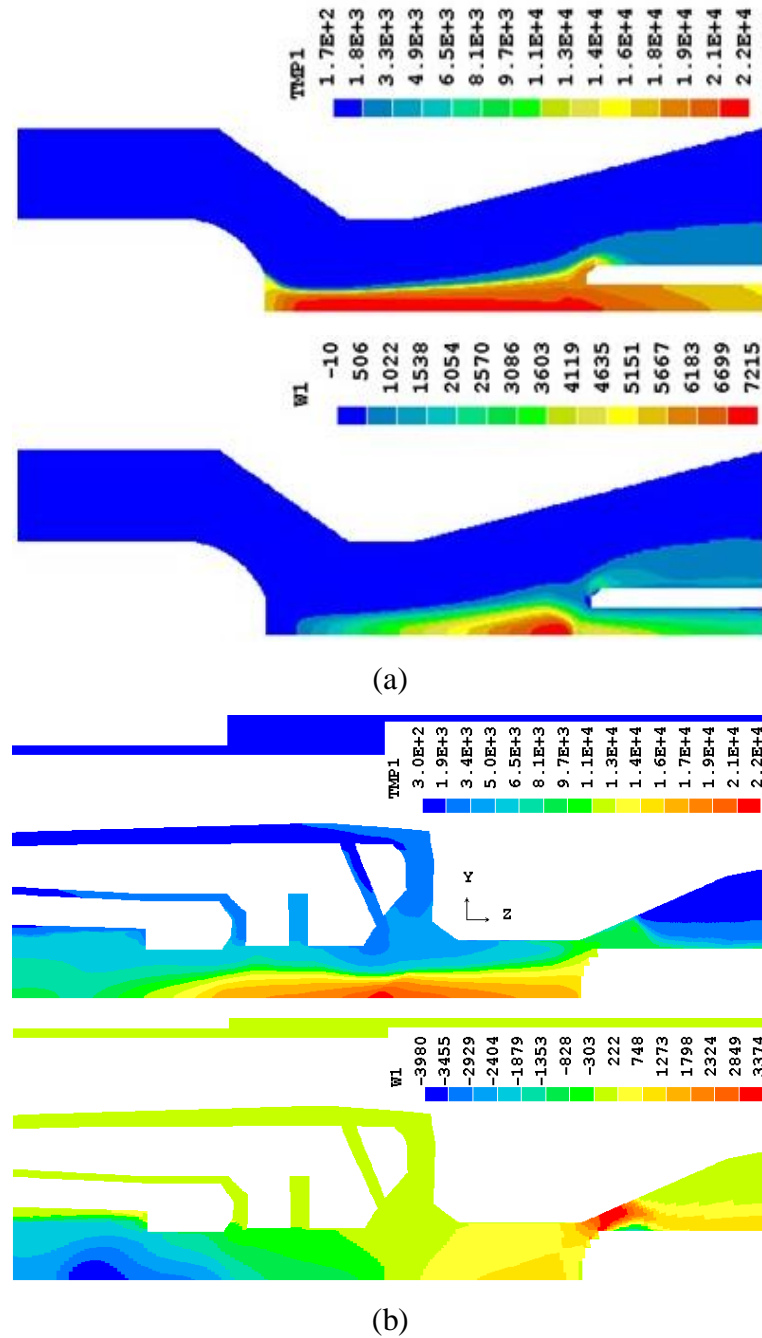


Figure 3.1: Contours of temperature and axial velocity component for (a) a nozzle arc at 1 kA DC with stagnation pressure of 1.12 MPa and exit pressure is near vacuum [8] (b) real circuit breaker with the instantaneous current of 5 kA, filling pressure of 0.6 MPa

3.3 Test Results for a 145 kV Auto-expansion Circuit Breaker

Test results and arc voltage measurement are scarce for commercial circuit breakers whose detailed structural information and material are available for use in research. In type test, the standard [IEC62271-100: 2008] requires several tests with different current levels or arc durations to be carried out consecutively. This imposes

constraints on visual check and measurement of contact erosion and nozzle ablation, both of which affect the interruption capability of the circuit breaker. Therefore, care has to be taken in using the test results to calibrate the turbulence parameter of the Prandtl mixing length model.

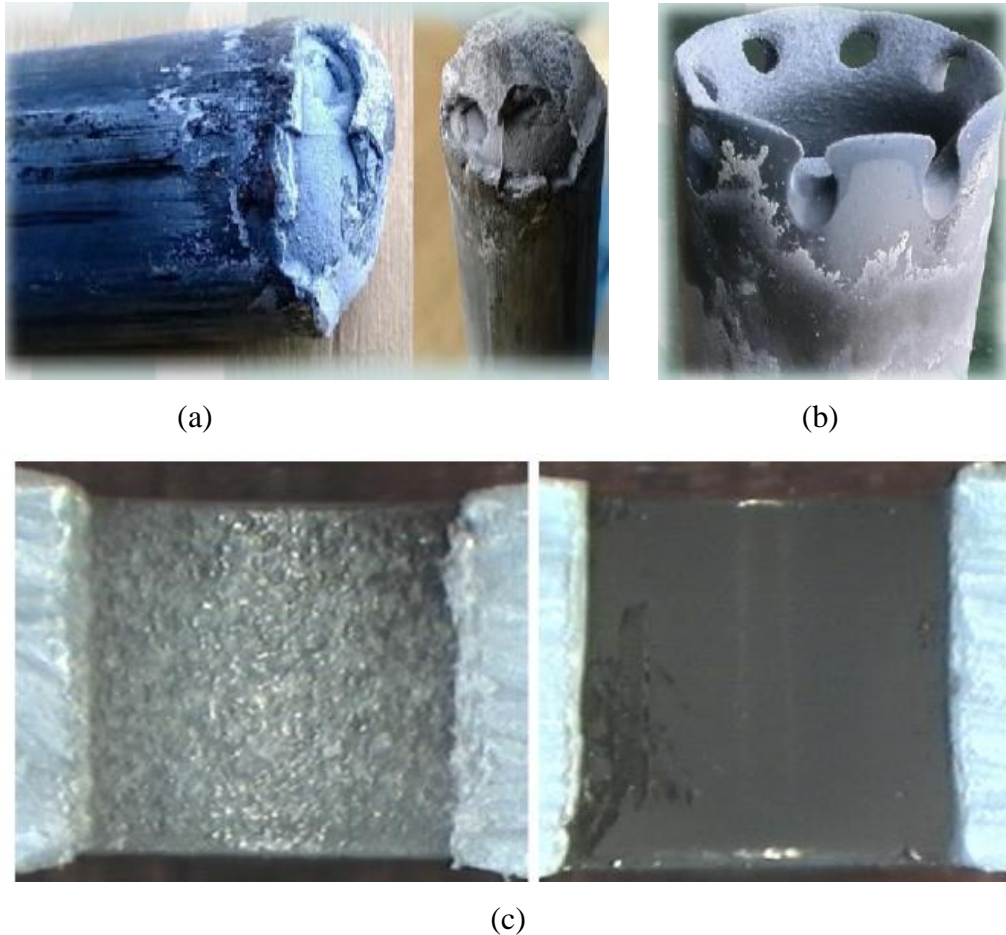


Figure 3.2. Diagram shows the (a) contact and (b) nozzle of a 252 kV circuit breaker after L90 test (Pinggao) (c) PTFE surface of a test device (ABB) [16]

Previous research has indicated that the nozzle diameter can substantially affect the interruption capability of puffer [3][11] and auto-expansion circuit breakers [12]-[14]. Therefore, the variation of nozzle diameter after each test should be considered to accurately define the real arcing conditions. However, the geometric change due to PTFE ablation and contact erosion is difficult to estimate. An example of eroded and ablated PTFE nozzle is given in Figure 3.2. It can be seen that the surface of both the contact and the nozzle is not smooth. The ordinary measurement (Table 3.2) using Vernier caliper cannot give accurate result, but an average value of multiple test values.

Two types of auto-expansion circuit breakers are used in this chapter. The first circuit breaker is a 145 kV auto-expansion circuit breaker (Pinggao). The other product is 245 kV circuit breaker (Reyrolle). In the absence of information it is assumed that the test was carried out with a newly assemble product without any previous tests. The test sequence 750 was followed by 751.

The 145 kV/40 kA auto-expansion circuit breaker passed Short Line Fault L90 test at KEMA after three rounds of test with a total cost of 4 million RMB (~400,000 pounds in 2012). After each failed round, the product was disassembled and overhauled with some new components including PTFE nozzle replacement. The results from the first round are chosen for the simulation work presented in this chapter. There were three tests in this round with test ID 92, 93 and 98. Test 92 started with a short arc duration suggested by the designer, which was 13 ms. The actual arc duration measured in the test was 13.6 ms, slightly longer than the suggested value. The circuit breaker passed Test 92. To search for the shortest arc duration, the arc duration in Test 93 was decreased by 1 ms from the nominal value of 13 ms to have a nominal value of 12 ms. The actual arc duration was 12.3 ms. The circuit breaker failed this test. Therefore, the short arc duration for the circuit breaker is 13 ms. Using a window of 7.5 ms which is calculated according to the relevant test standard, the long arc duration should be 20.5 ms although the actual arc duration in the test was 20.1 ms. The circuit breaker failed this long arc duration test, Test 98. The test data are summarised in Table 3.1 and Table 3.2, the current and contact travel curves are given in Figure 3.3. Detailed analysis of the results will be presented in the following sections before simulation is carried out.

For the 245 kV auto-expansion circuit breaker, only two tests were chosen in view of the facts that some important information is missing for the other cases. Both tests belong to the category of short arc duration interruption; however there is significant difference in the contact travel curves, as shown in Figure 3.4.

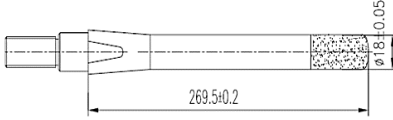
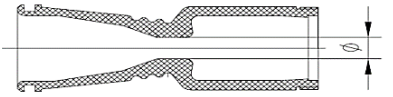

Table 3.1: Information on type test of the 145 kV auto-expansion circuit breaker

Test ID	T_{pre} (ms)		T_{real} (ms)	Result
92	Short	13	13.6	Pass
93		-1 (12)	12.3	Fail

98	Long	+7.5 (20.5)	20.1	Fail
----	------	-------------	------	------

* T_{pre} = predicted arc duration, T_{real} = real arc duration

Table 3.2: Erosion measurement on completion of the first round of type test on the 145 kV auto-expansion circuit breaker. The measurement was carried out using a Vernier Caliper.

Component	Diagram	Dimension change (mm)	Original (mm)
Stationary contact (solid contact)		Contact length due to erosion -1.2 (-0.4%)	269.5
Main nozzle		Throat diameter 22.1 (+5.2%)	21.0
Auxiliary nozzle		Throat diameter 21.3 (+12.1%)	19.0

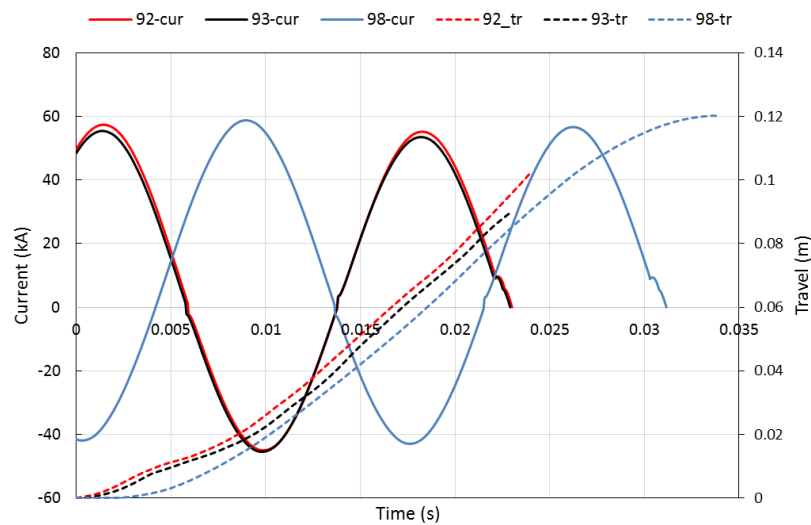


Figure 3.3: Current and travel curves for Test 92, 93 and 98, the slight difference between the travel curves are based on the scattering of the mechanical driver. Contacts separate at 9.8 ms, 10.6 ms and 11.4 ms for 92, 93 and 98, respectively. In simulation, arcs are initialised at 12.2 ms, 13 ms, and 13.8 ms for 92, 93 and 98, respectively.

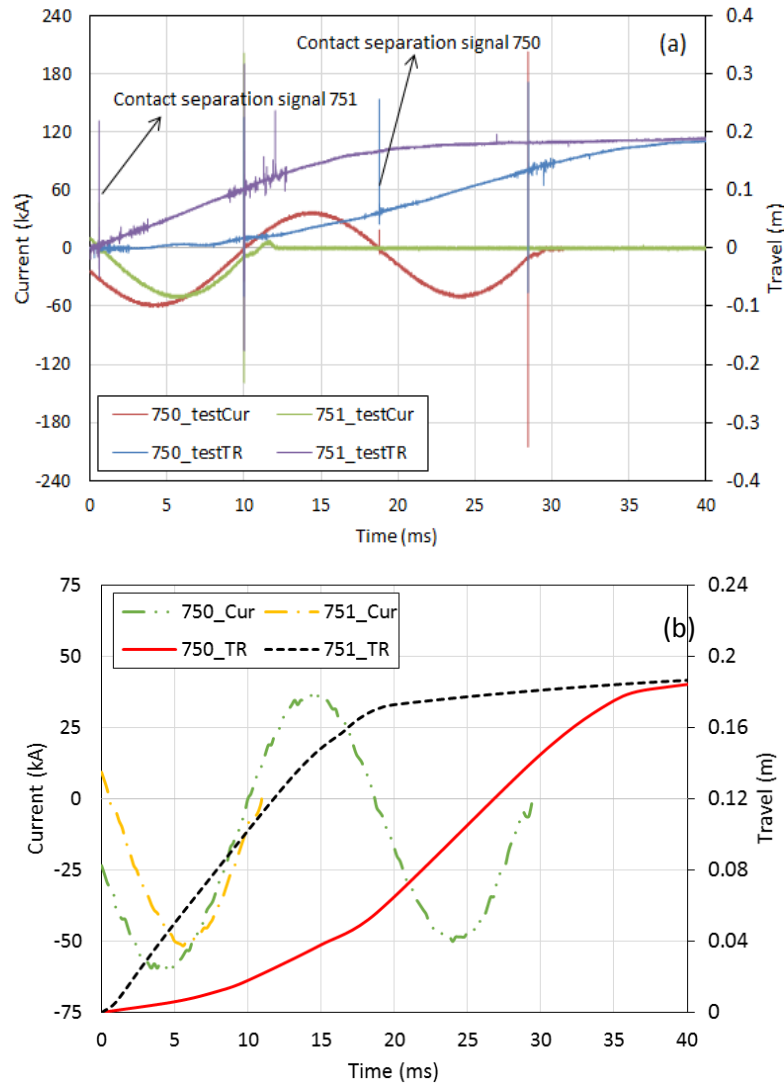


Figure 3.4: Current and travel curves for Test 750 (thermal clearance) and 751 (thermal failure) (a) original test data and (b) smoothed data for simulation with arcs initiation at 19.66 ms and 6.2 ms for 750 and 751, respectively.

3.4 Simplifications on Geometry

Modern auto-expansion (self-blast) circuit breakers employ geometries that are close to rotationally symmetry. To make the 2D axis-symmetric simulation model work possible, necessary approximations need to be made. In doing so it needs to be ensured that these approximations do not affect the correctness of the results and conclusions drawn in any significant terms.

Assumptions in simulation model:

- The rounded tips of the metallic field shapers (components A in Figure 3.5a) are replaced by square tips. This does not affect the arc behavior since they are sufficiently away from the arcing space.

- b) The piston, solid contact and a few key components are made move and the remaining components keep stationary in simulation, because the geometry of the nozzles are complex and hard to move in structured grid.
- c) Due to mechanical considerations, 6-8 holes in the wall of a hollow contact are used to provide flow passage to exhaust gas from the hollow contact into the immediate surrounding environment. 4-8 holes in the auxiliary nozzle are also used to provide a shortcut flow passage between the contact space and the expansion volume. The holes in PTFE auxiliary nozzle are approximated as a horn with equivalent flow cross sectional area because the arc model is axis-symmetric. The holes in the hollow contact are approximated as rings in a 2D model
- d) The round tip of a moving contact is approximated by a set of coaxial rings with flat tips. See Section 2.4.2 for more information.

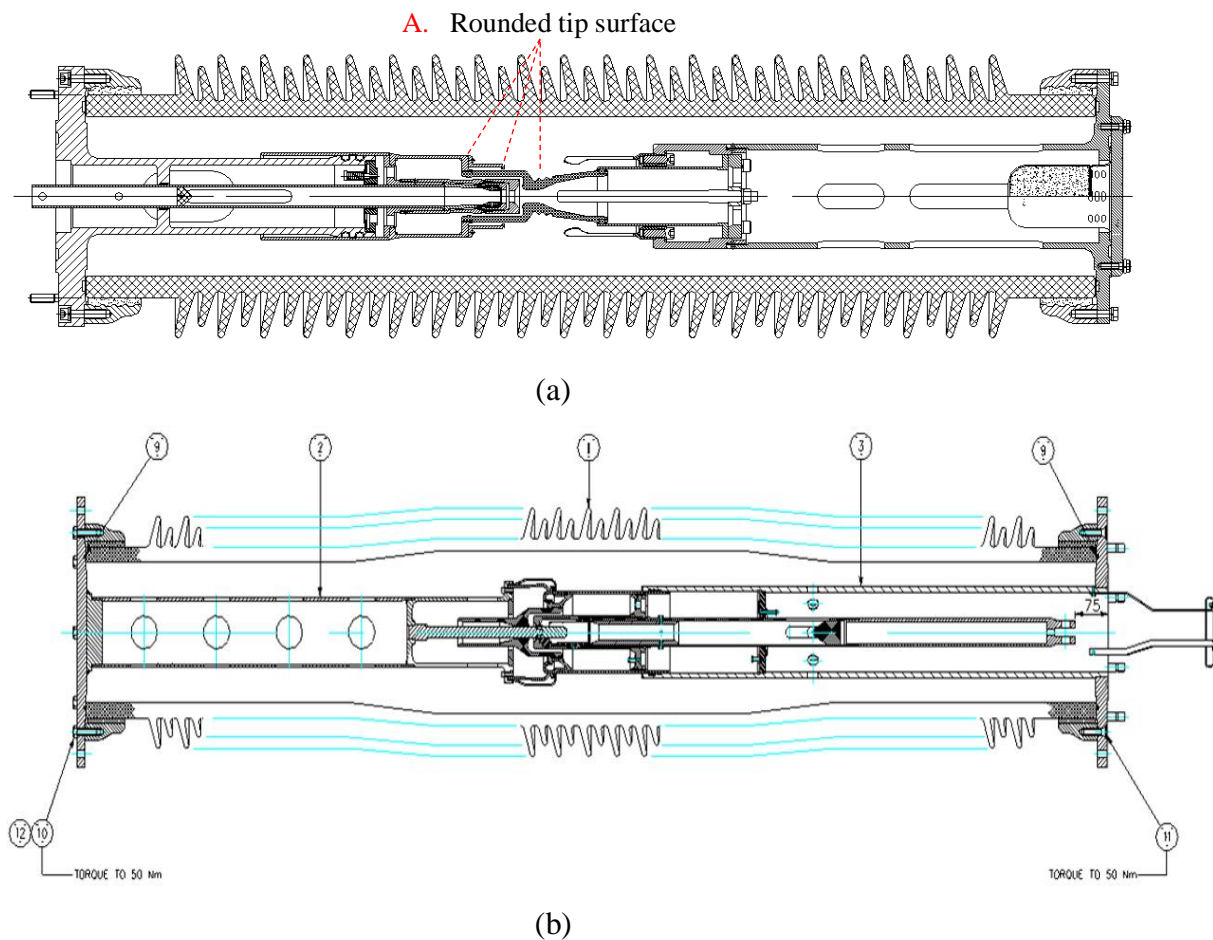


Figure 3.5: CAD drawing of the whole geometry of (a) 145 kV auto-expansion circuit breaker (b) 245 kV auto-expansion circuit breaker

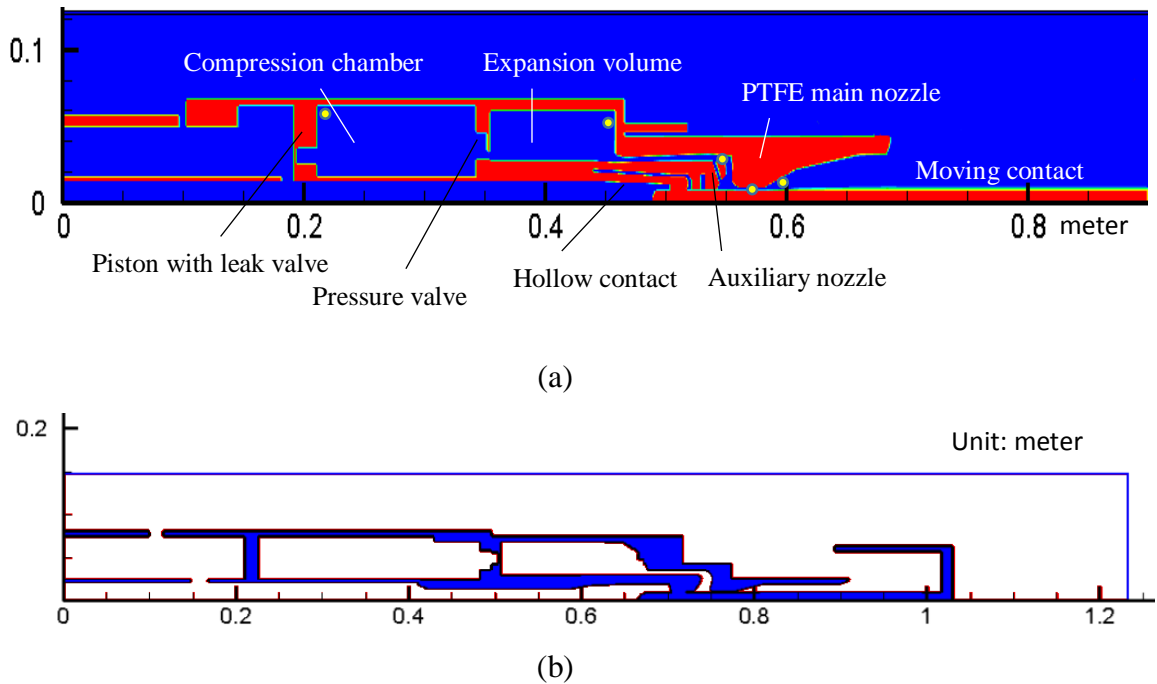


Figure 3.6: Simplified geometry of (a) 145 kV circuit breaker in simulation with 5 monitor points, P1 is the expansion volume, P2 in the heating channel, P3 in the middle section of main nozzle throat, P4 in the downstream of main nozzle, P5 in the compression volume (b) 245 kV circuit breaker

3.5 No-load Case

To verify the simplified geometry of the circuit breaker, a no-load case with a 0.7 MPa filling pressure (absolute) has been simulated and results compared with experimental data. The simulation results match reasonably well with the pressure measurement in the absence of an arc. It is noted that there is fluctuation around the peak pressure in the expansion volume and compression volume (locations shown in Figure 3.6a). The maximum difference is 0.1 MPa, 20 % of the absolute pressure rise. The inertia of the valve plate is hard to estimate, thus this fluctuation is caused by the frequent operation of the pressure relief valve in the simulation. For the pressure close to the nozzle, there is obvious difference (maximum 16%) between prediction and measurement. These regions could be occupied by arc with a load case, thus the pressure sensors were placed far away from the test points to avoid radiation disturb from arc. Tubes were used to connect the sensors and the test places. Therefore, the pressure propagation in the tube is an inevitable reason to cause this difference.

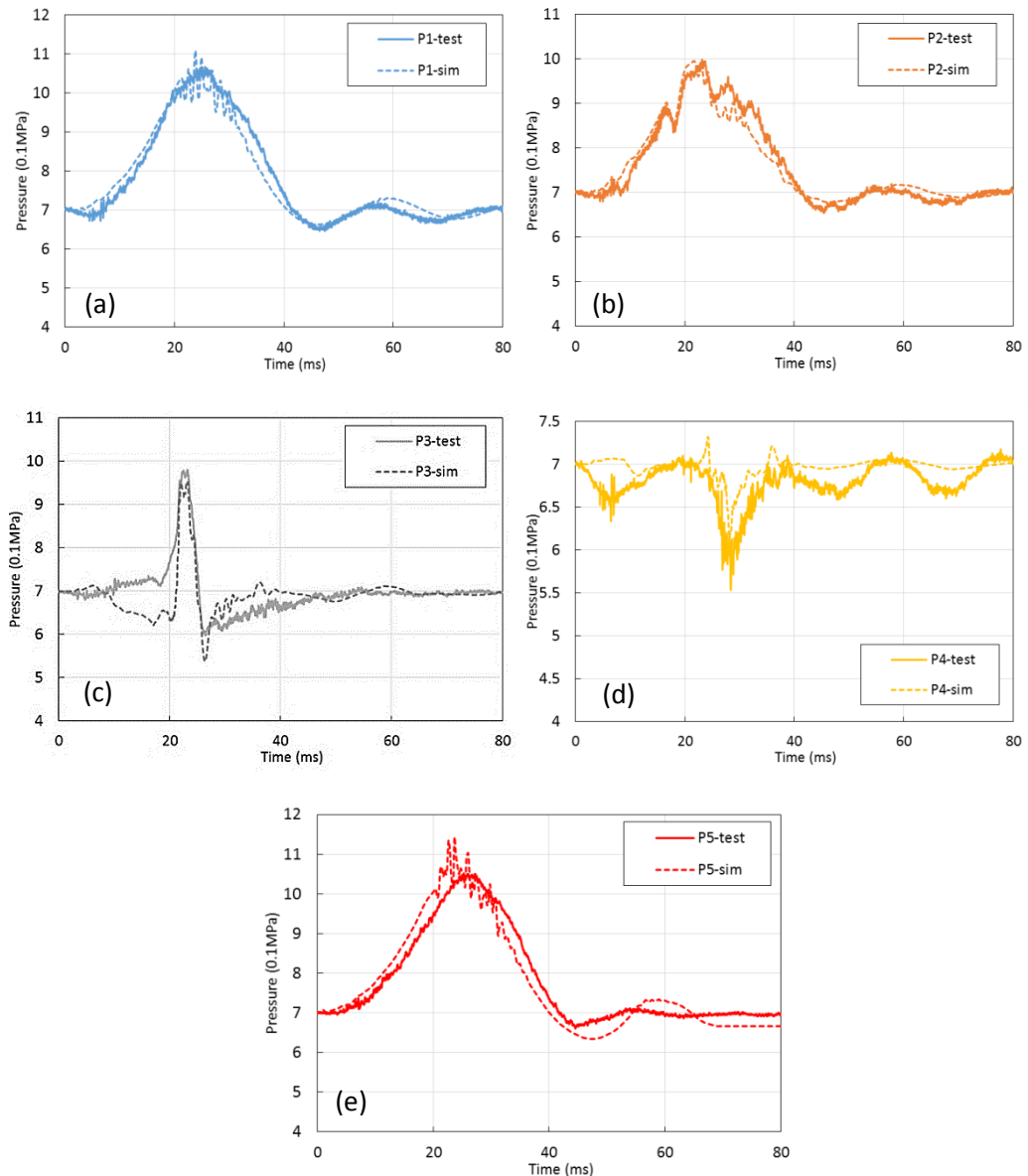


Figure 3.7: Comparison of pressure between prediction and measurement in (a) expansion volume (b) heating channel (c) middle section of nozzle throat (d) downstream region of the nozzle throat (e) compressor for the 145 kV circuit breaker, the measurement locations are given in Figure 3.6a

Figure 3.8 shows some typical time instants for pressure distribution. When the piston and live contact moving towards the downstream of the domain at the very beginning in (a), the gas in the compression chamber is compressed, and the valve between compression volume and expansion volume was pushed to open so that gas is rushing into the expansion volume. The pressure in the chamber is not uniform until the valve is fully open in (b). The flow field is established at that moment. When the live contact is about to leave the main nozzle in (c), the leak valve opens and relieves the pressure in the compression volume.

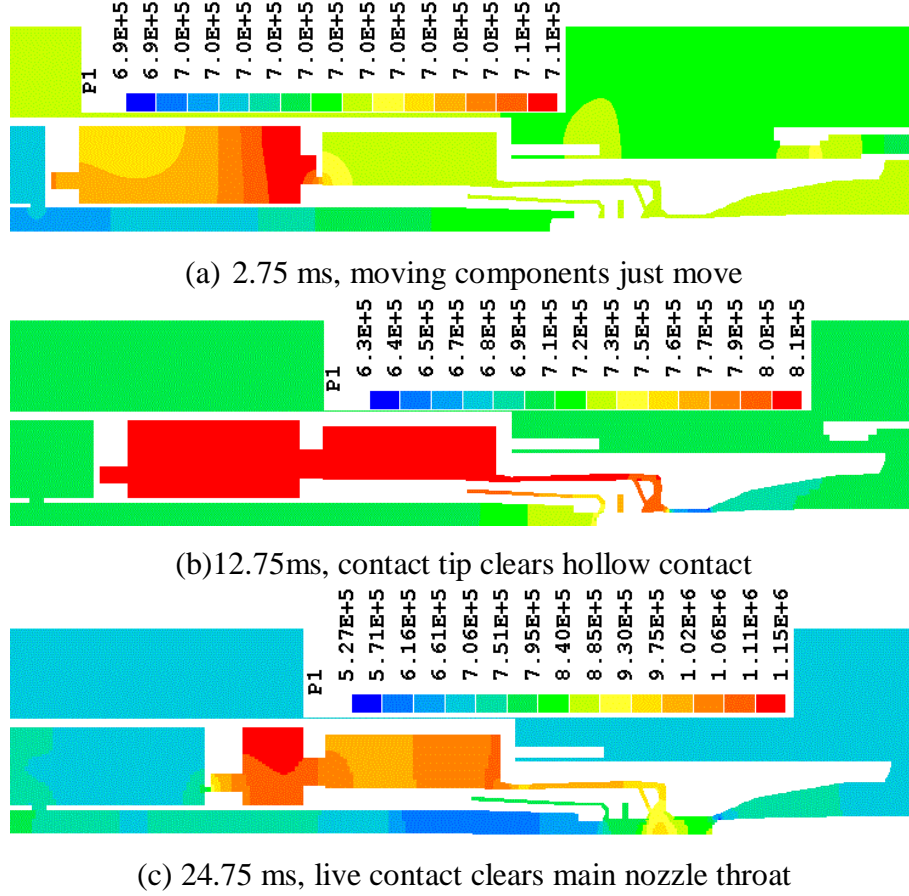


Figure 3.8: Pressure distribution at several typical time instants

3.6 Radiation Model Verification

To accurately calculate the mass of ablated PTFE, the radiation model that is described in Section 2.4.1.4, especially the radiation absorption at the arc edge, should be verified. This model assumes that 50% of the radiation flux from the arc core reaches the nozzle wall producing ablation. The power used for ablation is expressed by

$$Q_{ablation} = \xi(1 - \alpha) \int_{z_1}^{z_2} \int_0^{R_{833}} q \cdot 2\pi r dr dz \quad (3.5)$$

where ξ is the coefficient which is determined by the ablation surface incline, α the reabsorption factor which is equal to 0.5 for auto-expansion circuit breaker, and q the net radiation loss per unit volume and time, z_2-z_1 indicates the axial dimension of ablation surface. Thus, the evaporated PTFE mass is calculated by

$$m_{PTFE} = \frac{\int_0^t Q_{ablation} dt}{h_{PTFE}} \quad (3.6)$$

where h_{PTFE} is the energy required to break up the polymer PTFE chain and to raise the PTFE vapour from 300 K to 3400 K [15], which is equal to 1.19×10^7 J/kg.

A recent experimental study by ABB on PTFE ablation [16] in commercial high voltage circuit-breakers with rated short circuit currents of 40–63 kA present a relationship between specific ablation and peak current density, which will be used as a reference to verify our radiation model. The specific ablation is expressed by

$$\delta = \frac{m_{PTFE}}{\int_0^{t_{arc}} U_i(t)I_i(t)dt} \quad (3.7)$$

The peak current density is defined as

$$j_{peak} = \frac{I_{peak}}{A_n} \quad (3.8)$$

where A_n is the nozzle throat cross section.

Two methods were used to estimate the amount of ablated PTFE mass in [16]. The first method is to weigh the mass loss and the second method is to derive the mass loss from geometry change of the nozzle. The first method results in a specific ablation that is only half of the second one. The authors stated that the former method is more precise than the latter one in terms of the error bar. Therefore, it implies that the experimental result which is presented in Section 3.3 cannot be directly used to calculate the PTFE ablation. The experimental results from ABB [16] show a nearly constant specific ablation at high current densities ($j_{peak} > 1.2 \times 10^8 \text{ Am}^{-2}$), and the average value amounts to 26 mg/kJ. It is to be noted that the energy quoted here is the electrical power input integrated over time, not the radiative energy reaching the nozzle surface.

To match the experimental condition as much as possible, a 245 kV ABB auto-expansion circuit breaker is chosen to be under investigation. The detailed simulation condition is described in Chapter 5. The predicted PTFE ablation from simulation in Figure 3.9 is 7.28g. The total electrical energy input is 247 kJ. Thus the specific ablation is,

$$\delta = \frac{7.28 \times 10^3}{2.47 \times 10^2} = 29.5 \text{ mg} \cdot \text{kJ}^{-1}$$

and the peak current density $j_{peak} = \frac{53000}{3.14 \times 0.011^2} = 1.4 \times 10^8 \text{ A} \cdot \text{m}^{-2}$, which has a good agreement with the measurement deducted from total mass loss (blue triangle in Figure 3.10).

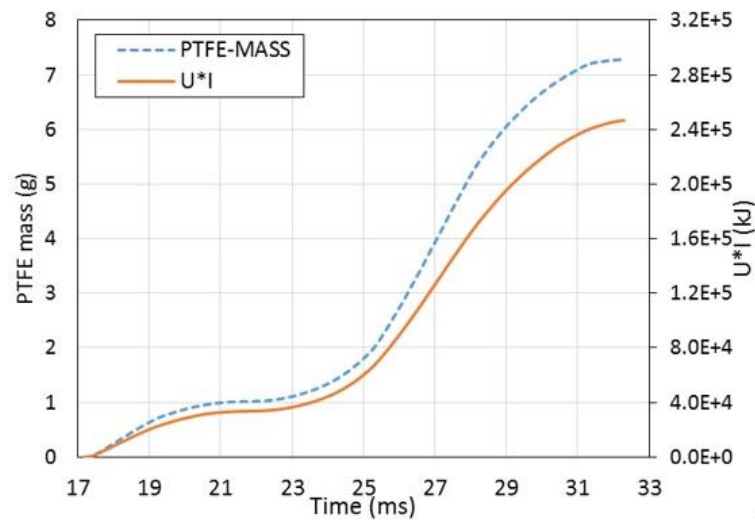


Figure 3.9: Electric input ($U \cdot I$) and predicted PTFE ablation mass from simulation as a function of time in the arcing process for the 245 kV auto-expansion circuit breaker.

Table 3.3: Specific ablation for three different auto-expansion circuit breakers from prediction

	ID	Radius of main nozzle (mm)	$\Sigma U \cdot I$ (J)	I_{peak} (A)	J_{peak} (A/m^2)	Mass of ablated PTFE (g)	Specific ablation (mg/kJ)	Arcing time (ms)
Pinggao 145kV/40kA/60Hz	92	10.5	1.77×5	5.52×4	1.59×8	3.47	19.6	10.81
	93	10.5	1.55×5	5.35×4	1.54×8	2.96	19.1	9.91
	98	10.5	4.17×5	5.67×4	1.64×8	9.11	21.9	17.40
Reyrolle 245 kV/ 50 kA/50 Hz	750	11.5	1.60×5	5.00×4	1.20×8	4.54	28.4	9.80
	751	11.5	3.06×4	4.84×4	1.16×8	0.87	28.4	4.75
ABB 245kV/50kA/50 Hz	-	11	2.47×5	5.30×4	1.39×8	7.28	29.5	15.11

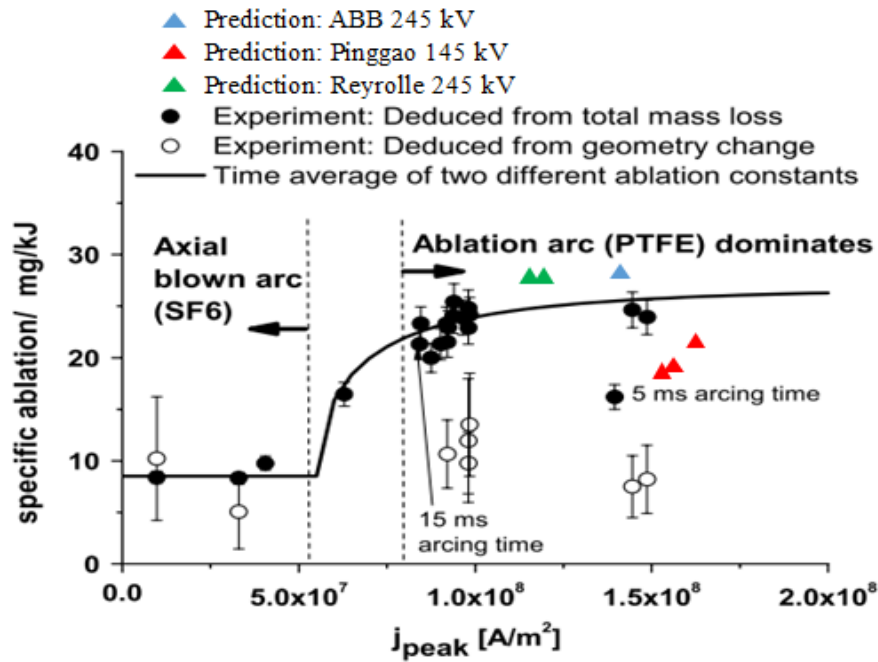


Figure 3.10: Measured specific ablation in an ABB test device versus peak current density. Applied peak current amounted from 4 to 64 kA. Arcing times were 5, 10 and 15 ms [16], comparing with predicted results of real auto-expansion circuit breaker simulation.

3.7 Mass of Ablated PTFE

The parameters of Pinggao the 145 kV circuit breakers are as follows:

- o rated voltage of 145kV,
- o rated interrupting short circuit current of 40 kA,
- o and a frequency of 60Hz,
- o initial filling pressure of 0.6 MPa in load case,
- o initial temperature 300K.

In the interruption simulation, the travel path curve of the moving contact is given by the manufacturer (Figure 3.3). Since the measurement data for PTFE ablation is rare, Table 3.2 only indicate gives the total increase of in nozzle diameter after three tests 92, 93 and 98. Therefore, to ascertain the arcing conditions for each test, it is needed to calculate the ablated PTFE vapour from the nozzle throat surface to determine the variation of nozzle diameter after each test.

As Figure 3.11 shows, the predicted amount of ablated PTFE vapour depends on the arcing current. In the first cycle of Test 98 (from 14 ms to 21 ms) the arc only ablates only half of the corresponding PTFE loss in the other two cases on the auxiliary

nozzle throat. This is because the magnitude of the current for Test 98 during this period is 70% of that for Test 92 and 93. The contact separation for these three cases at 21 ms are 83 mm, 79 mm and 74 mm. At that moment, the solid contact just entered the main nozzle for Test 98, the PTFE ablation surface exposed to the arc for Test 98 is the smallest. In the next half cycle of the arcing current, the current reaches its peak value when the solid live contact just passes the middle point of the main nozzle throat with a much larger ablating surface exposed to the arc radiation. Furthermore, the magnitude of the current in the second half cycle is 1.4 times of that in the first one. Therefore, the ablated PTFE vapour from the main nozzle throat increases substantially for the case of Test 98.

From the comparison (Table 3.4) of PTFE ablation between the short arc duration cases, Test 92 and Test 93 and the long arc duration case, Test 98, the ablation on the auxiliary nozzle throat takes a large percentage of total PTFE ablating surface for short arc durations, while for long arc duration case, ablation on the main nozzle throat takes more percentage than the auxiliary one. It indicates that for short arc duration cases, PTFE vapour from the main nozzle region has little contribution to the pressure rise. This means that pressurization in the expansion volume highly depends on the blockage of the hollow contact due to auxiliary nozzle ablation and arc clogging in the main nozzle. On the contrary, the main nozzle throat produced 59.2 % of the total PTFE vapour over the whole arcing process for the long arc duration case. Therefore, from the comparison of the predicted results for different test cases, the extent of nozzle ablation for long arc duration case is much more serious than in the short arc duration case.

Because of the uneven nozzle surface after short circuit current interruption in a real commercial circuit breaker, it is difficult to determine the exact nozzle conditions for use in simulation. To avoid possible influence of the nozzle surface, the cases with short arc durations, i.e. Test 92 and 93, are selected to calibrate the turbulence parameter of the Prandtl mixing length turbulence model because the variation of nozzle diameter due to ablation can be neglected for these two short arc duration cases in comparison with the long arc duration case.

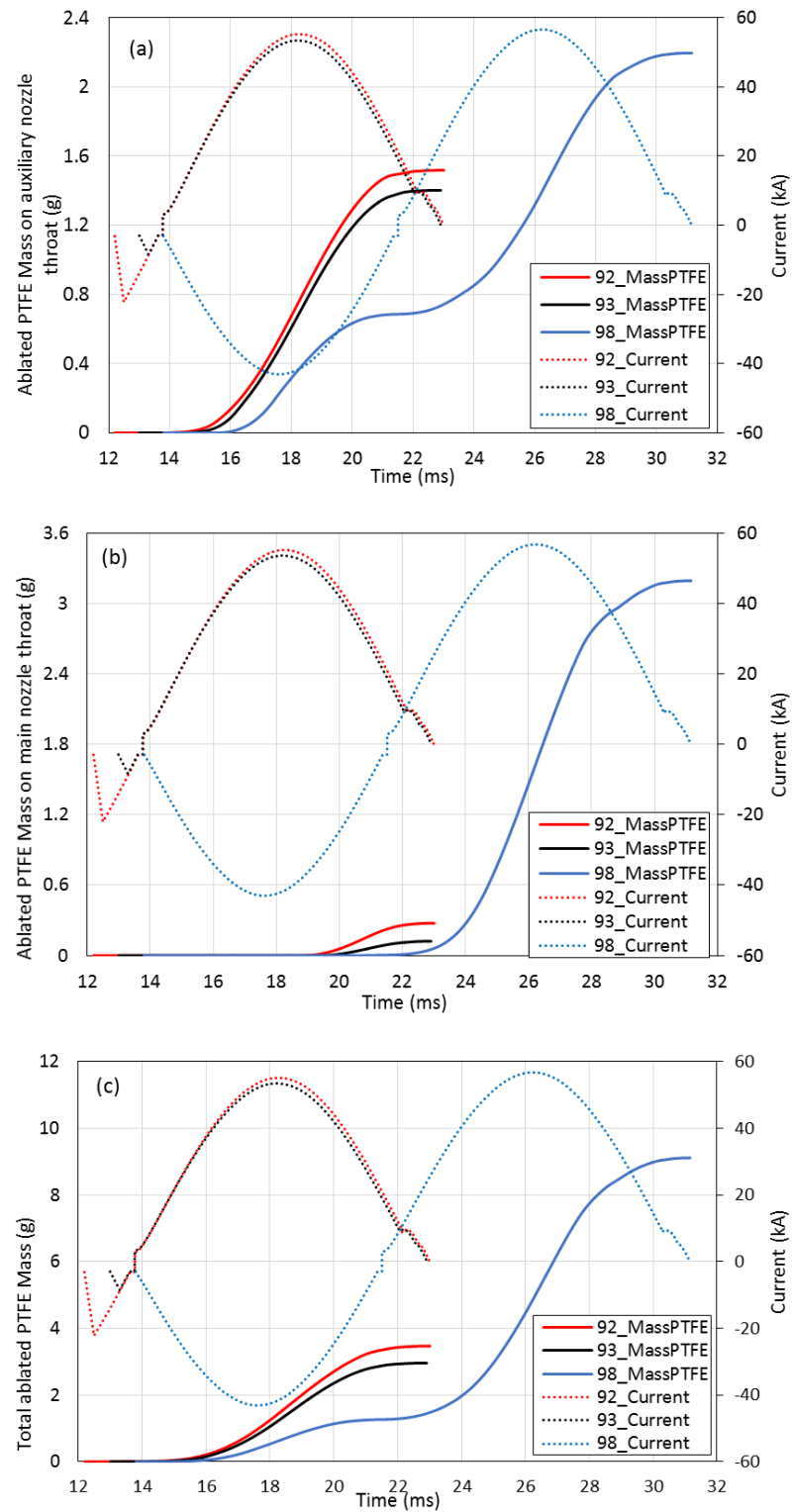


Figure 3.11: Predicted PTFE ablation on (a) auxiliary nozzle throat (b) main nozzle throat and (c) total ablated surface

Table 3.4: Predicted PTFE mass ablation after each test without considering nozzle diameter variation due to PTFE ablation after each test

Case	Auxiliary nozzle throat ablated mass				Main nozzle throat ablated mass				Total PTFE mass			
	Prediction			Test (g)	Prediction			Test (g)	Prediction			Test (g)
	g	%			g	%			g	%		
92	1.52	29.7	43.8	0.45	0.28	7.8	8.1	0.14	3.47	22.3	100	1.12
93	1.40	27.3	47.3	0.42	0.12	3.3	4.1	0.06	2.96	19.0	100	0.95
98	2.20	43.0	24.1	0.66	3.19	88.9	35.0	1.64	9.11	58.6	100	3.36
All	5.12	100	32.9	1.53	3.59	100	23.1	1.84	15.54	100	100	5.43

Note: (The length of flat section of the auxiliary nozzle and main nozzle throat are 9.5mm and 22.4 mm, respectively.)

Table 3.5: Predicted and test nozzle throat variation for 145 kV circuit breaker

Case	Prediction		Test	
	Auxiliary nozzle throat radius	Main nozzle throat radius	Auxiliary nozzle throat radius	Main nozzle throat radius
92	9.5 mm	10.5 mm	9.5 mm	10.5 mm
93	10.6 mm	10.6 mm	9.85 mm	10.54 mm
98	11.56 mm	10.64 mm	10.17 mm	10.56 mm
After 98	12.96 mm	11.55 mm	10.65 mm	11.05 mm

Table 3.6: Predicted ablated PTFE mass for 245 kV auto-expansion circuit breaker (The length of flat section of the auxiliary nozzle and main nozzle throat are 8.6 mm and 27.6 mm, respectively.)

Case	Auxiliary nozzle throat ablated mass			Main nozzle throat ablated mass			Total PTFE mass		
	g	%		g	%		g	%	
750	0.93	69.9	20.5	1.7	96.6	37.4	4.54	83.9	100
751	0.4	30.1	50.0	0.06	3.4	6.9	0.87	16.1	100
All	1.33	100	24.6	1.76	100	32.5	5.41	100	100

Table 3.7: Predicted and test nozzle throat variation for 245 kV circuit breaker

Case	Auxiliary nozzle throat radius	Main nozzle throat radius
750	11 mm	11.5 mm
751	11.7 mm	11.9 mm

Note: no measurement is available for these two cases

3.8 Calibration of Turbulence Parameter for Prandtl mixing length model in Current Zero Period

3.8.1 Current zero phase

The difference in contact travel curves and current waveforms in different cases directly results in different position of the solid live contact in the main nozzle at

current zero, as shown in in Figure 3.12. For Test 93 and 751, when the current passes the final current zero, the solid live contact still blocks in the main throat. The position of the solid contact determines the effective flow area between the contact and of the main nozzle, which influences the arc energy transport. In addition, the pressure in the expansion volume for Test 92 (or 750) is slightly higher than Test 93 (or 751). Thus the axial temperature for Test 92 and 750 are slightly higher than Test 93 and 751, respectively, which is in favour of arc extinction after current zero.

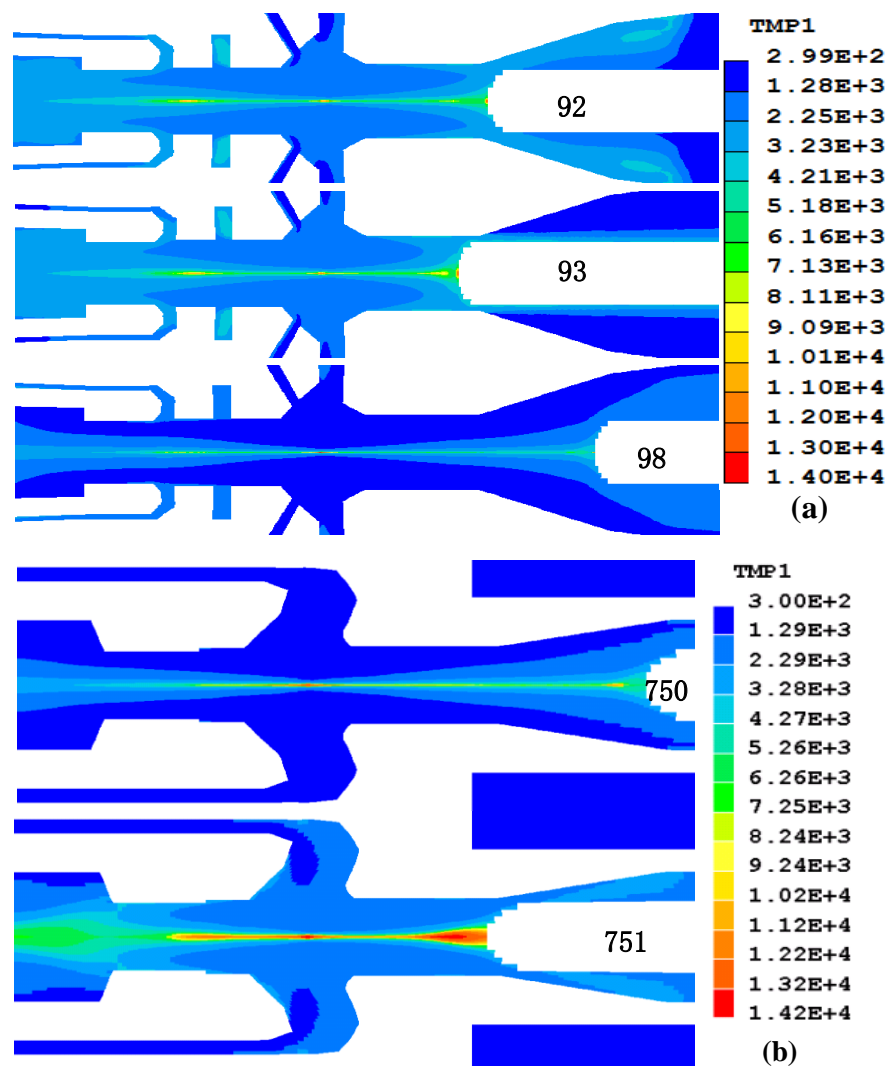


Figure 3.12: Temperature distribution at current zero for (a) case 92, 93 and 98 (b) 750 and 751

3.8.2 Post current zero phase (post arc phase)

After current zero, a low current still flows in the residual plasma in the contact

space under the action of the system recovery voltage. Ohmic heating occurs due to the energy input into the arc by the current while energy loss is mainly due to turbulence cooling. Strong turbulence cooling increases the rate of energy exchange between the residual arc and surrounding cold gas. The success or failure of thermal recovery is determined by the magnitude of post arc current and its change with time. It is therefore necessary to check whether the magnitude of post arc current decreases towards zero within a short time period. It is known that the fast increasing recovery voltage in the first saw-tooth part poses a more severe interruption condition for short line fault. Therefore, it is said that if the post arc current under the transient recovery voltage keeps a low value (< 0.1 A) within the first saw-tooth period, the interruption is successful.

The results at the end of the current zero phase is used as the initial condition for the calculation of post arc current. The resistance of the thin residue plasma in the contact gap is obtained by integrating the electrical conductivity of the hot gas which is expressed by

$$R = \frac{1}{G} = \int_{z_1}^{z_2} \left[\frac{dz}{\int_0^{R_{3K}} \sigma 2\pi r dr} \right] dz \dots\dots\dots (3.9)$$

where $(z_2 - z_1)$ is the arc length, σ electrical conductivity and R_{3K} is from axis to 3000 K isothermal. Then, the post arc current is calculated by Ohm's Law with a given dV/dt and time. In simulation, the turbulence cooling effect increases with the value of the turbulence parameter under the same flow conditions. Thus, the calibration process involves the adjustment of the turbulence parameter to match the thermal recovery result (success or failure) with the test result using the real transient recovery voltage in Figure 3.13.

For each case, a range of the turbulence parameter for current zero phase, i.e. Tp_I0 , is chosen to calculate the post arc current. From Figure 3.15, it is found that when the turbulence parameter is set to be larger than 0.3, the interruption results from prediction are consistent with the test 92 and 93 for 145 kV circuit breaker. However, when decreasing this value to 0.29, the arc of Test 92 cannot afford the increasing recovery voltage and breakdown at 1 μ s. Thus, for 145 kV circuit breaker, 0.3 is a critical value for prediction of turbulence cooling effect. The turbulence parameters for current zero larger than 0.3 will give a satisfactory prediction for thermal

recovery. To assess the applicability of this range of turbulence parameter that is calibrated from 145 kV circuit breaker, the second circuit breaker at 245 kV level are investigated in the same way, the predicted results are shown in Figure 3.16. The critical value is found to be 0.35 for this configuration. It is noted that Test 93 and 751 are two typical thermal failure cases, when the currents passing the final zero point, the position of live contacts are both in the outlet of main nozzle throat. The arcing time of the test 92 is considered as the shortest arcing time, the area between main nozzle and live contact has to be comparable with that of main nozzle throat. Therefore, it is concluded as the criteria for determination of the shortest arcing time.

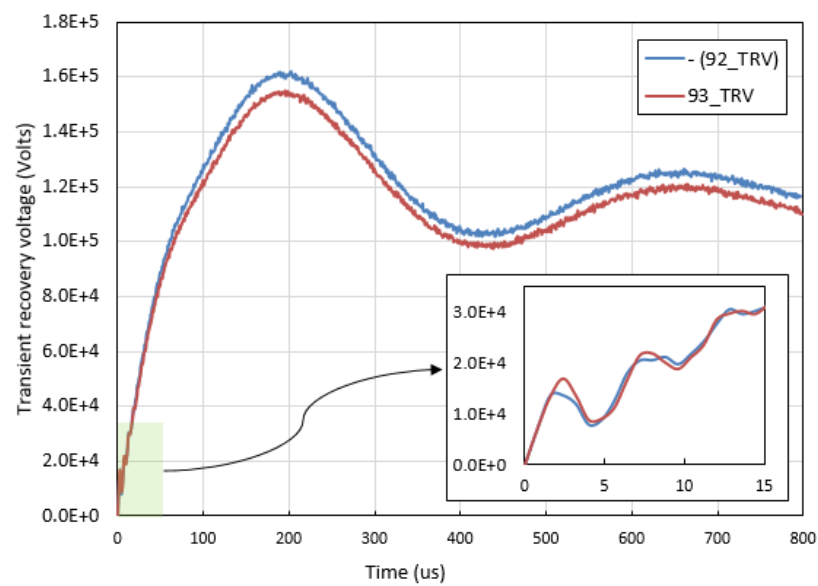


Figure 3.13: Transient recovery voltage of test 92 and 93 for the 145 kV auto-expansion circuit breaker

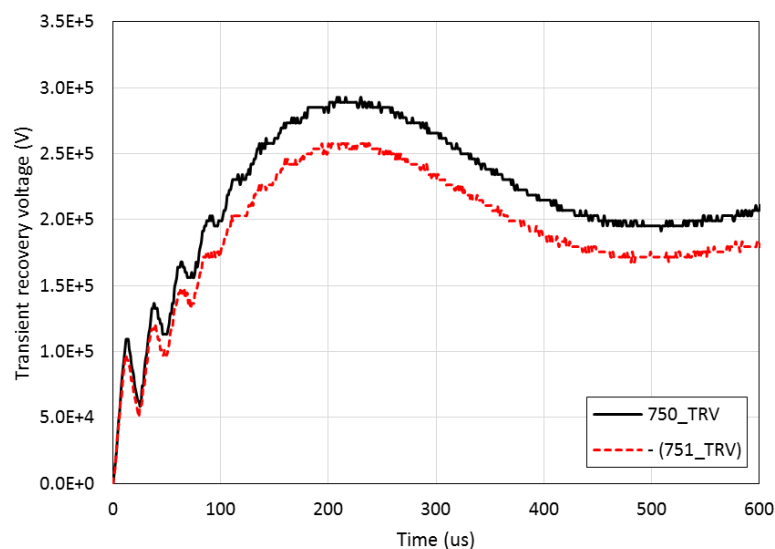


Figure 3.14: Transient recovery voltage of test 750 and 751 within 600 us for the 245 kV auto-expansion circuit breaker

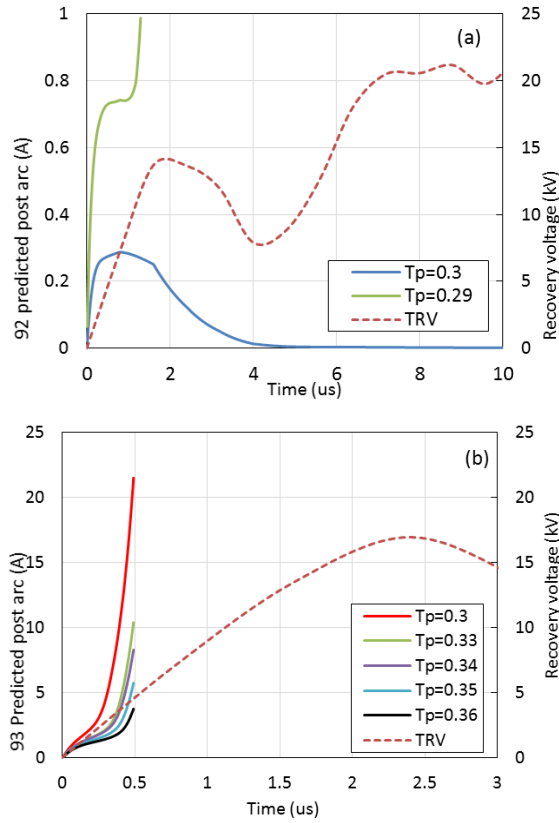


Figure 3.15: Post arc current with different turbulence parameter for (a) test 92 (b) test 93

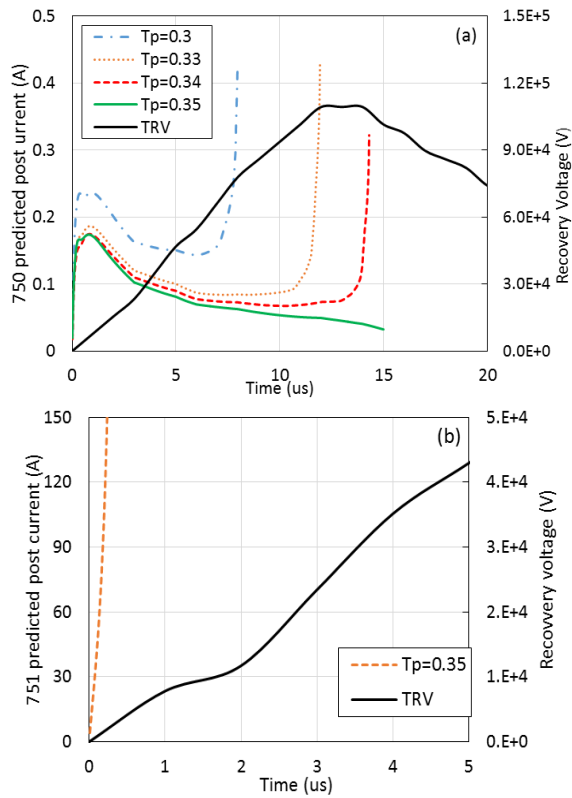


Figure 3.16: Post arc current with different turbulence parameter for (a) test 750 (b) test 751

Table 3.8: Summary of turbulence parameters for calibration cases

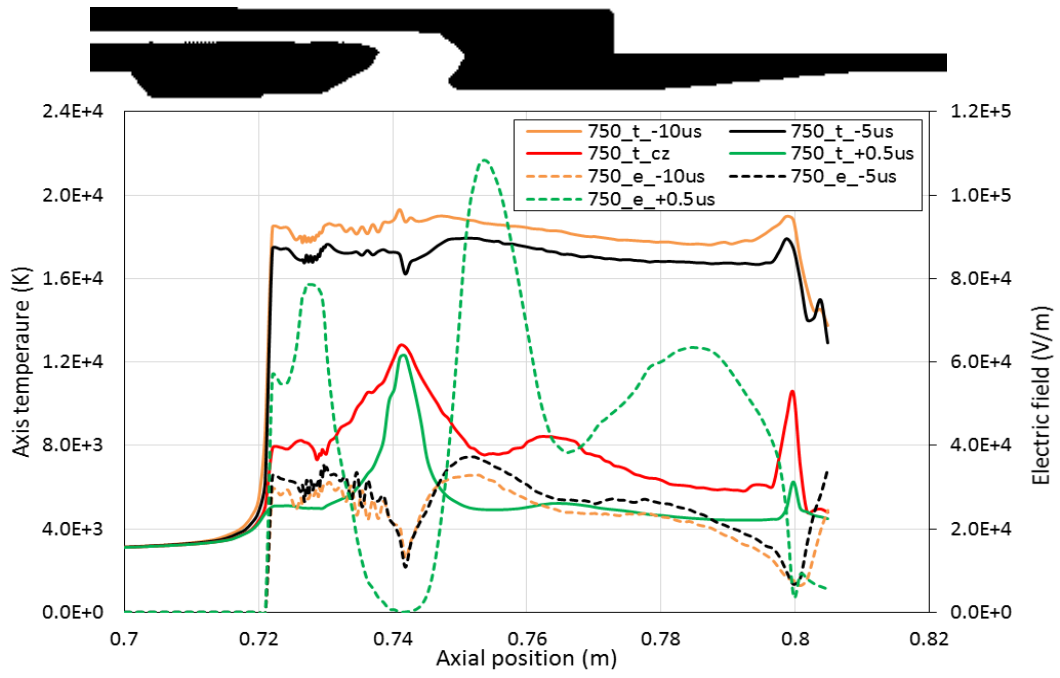
	Test 92	Test 93	Test 750	Test 751
Synthetic interruption result	Pass	Fail	Pass	Fail
Tp_I0=0.29	Fail	Fail	Fail	Fail
Tp_I0=0.30	Pass	Fail	Fail	Fail
Tp_I0=0.33	Pass	Fail	Fail	Fail
Tp_I0=0.34	Pass	Fail	Fail	Fail
Tp_I0=0.35	Pass	Fail	Pass	Fail

3.8.3 Discussion

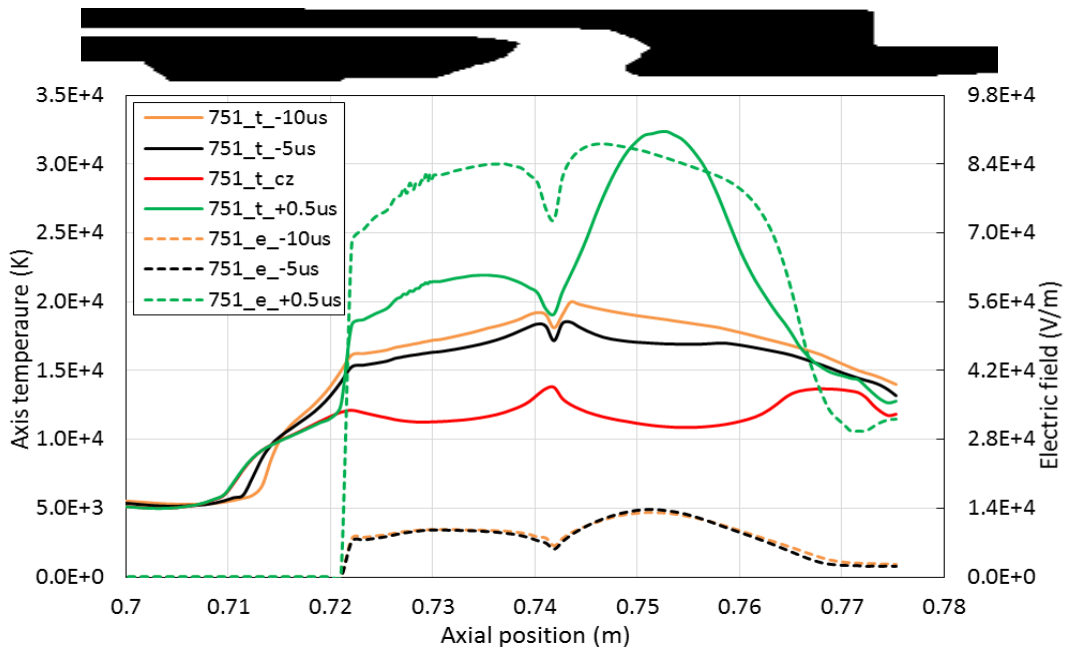
The analysis around the current zero for 145 kV circuit breaker will be given in Chapter 4. Thus in this section, only the predicted results of 245 kV circuit breaker will be presented. The temperature profiles at the axis for both Test 750 and 751 in Figure 3.17 indicate that significant temperature drop happens within 5 μ s before current zero. Test 750 gives a successful thermal recovery, most part of axis temperature except stagnation region with axial position of 0.74 m, all decrease below 5000 K. The electrical field increases rapidly 0.5 μ s after current zero. The arc length of Test 750 is 35 mm longer than Test 751, which can be observed from Figure 3.12. The distribution of recovery voltage 0.5 μ s after current zero is divided into three main parts: One is applied on the gas region in the auxiliary PTFE nozzle with the axial position of 0.727 m (Critical part 1); the second part is on the inlet of main nozzle throat with the axial position of 0.755 m (Critical part 2); the final one is carried on the downstream of main nozzle with the axial position of 0.788 m. This electric field of the 245 kV circuit breaker is similar with that of 145 kV circuit breaker with medium arc duration which is shown in Figure 4.7, Chapter 4.

For Test 751, the final contact tip still block in the main nozzle throat, the axis temperature is above 10,000 K, which rather high compared with that of Test 750. The temperature in front of the live contact is even higher than that in the stagnation region for Test 751. The radial temperature profiles in the middle of main throat nozzle those shown in Figure 4.11a indicate that the radius of arc for Test 750 is much smaller than that of 751 and the turbulence cooling is much stronger. Figure 4.11b. Because of the above reasons, the Test 750 provide an appropriate interruption condition at the current zero.

Before the current zero, the arc temperature in the two critical parts is lower than that of other parts. However, the mass flux at the current zero in the middle cross section of main nozzle throat for Test 750 is only 25 % of that for Test 751. Compared the mass flux of Test 750 with the short arc duration case of 145 kV circuit breaker presented in Figure 4.11b, it is found that the maximum value of these two cases is very similar. Since it has been concluded in Chapter 4, short arc duration is the most severe condition for successful thermal recovery, thus, 5000 kg/s/m^2 is a critical value for current interruption.



(a) Test 750



(b) Test 751

Figure 3.17: Axis temperature and electric field of Test 750 and 751 for 10us, 5 us before current, current zero and 0.5 us after current zero. These results were predicted with Tp_{I0} equal to 0.35.

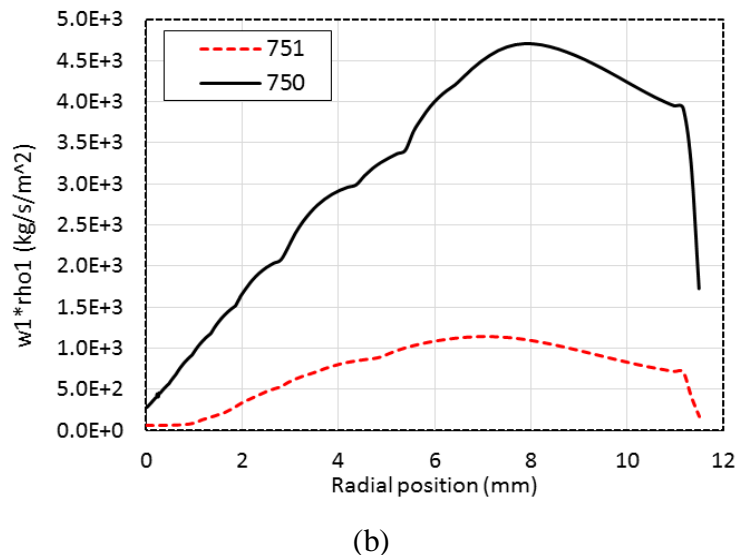
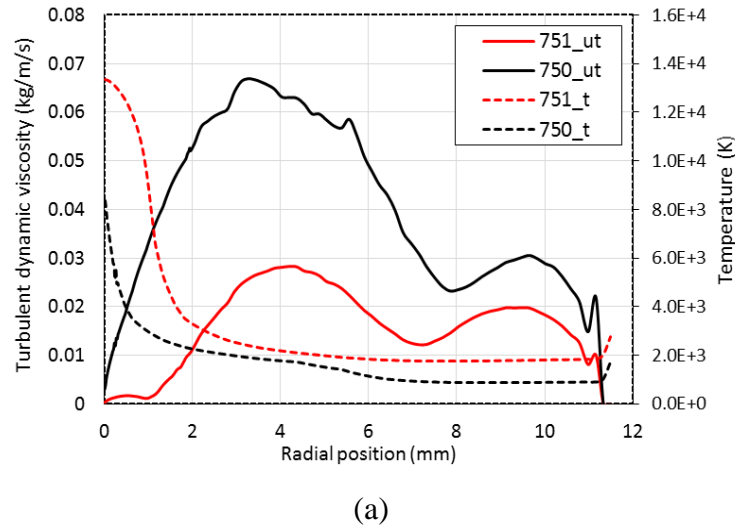


Figure 3.18: Profiles at critical cross section of main nozzle throat (a) radial temperature and turbulent eddy viscosity (b) mass flux (product of density and axial velocity)

3.9 Summery

Typical cases of real circuit breaker type test have been chosen to investigate the applicability of a single turbulence parameter for commercial auto-expansion circuit breakers. A considerable amount of effort is made to simulate the arcing processes in three circuit breakers to identify the range of the turbulence parameter based on test result of thermal failure or success. It has been found that the ranges for the three circuit breakers overlap at $c = 0.35$. This has the important implication that a single turbulence parameter is able to predict the thermal interruption capability of different designs of auto-expansion circuit breakers, making a step forward in the research

towards quantitative prediction of circuit breaker performance.

References

- [1] J.D. Yan, M.T.C. Fang, and W. Hall, The development of PC based CAD tools for auto-expansion circuit breaker design IEEE Trans. on Power Delivery 14, pp.176-181, 1999.
- [2] J.D. Yan, K.I. Nuttall and M.T.C Fang, A comparative study of turbulence models for SF₆ arcs in a supersonic nozzle, J.Phys. D: Appl. Phys. Vol. 32 pp.1401-6, 1999.
- [3] M.T.C. Fang, Q. Zhuang and X.J. Guo, Current zero behaviour of an SF₆ gas-blast arc. Part II: Turbulent flow, J. Phys. D: Appl. Phys., Vol. 27, pp. 74-83, 1994.
- [4] K. Song, B. Lee and K. Park, Calculation of the post-arc current in a supersonic nozzle by using the k- ϵ turbulence model, Journal of the Korean Physical Society, Vol. 45, No. 6, pp1537-1543, 2004.
- [5] J.D. Yan, S.M. Han, Y.Y. Zhan, H.F. Zhao and M.T.C. Fang, "Computer simulation of the arcing process in high voltage puffer circuit breakers with hollow contacts", Proceedings of XVIII Symposium on Physics of Switching Arc, Brno Czech Republic, pp 99-108, 2009.
- [6] Final version of L90 test and analysis, from Pinggao Group, Confidential
- [7] Test data sheet, provided by Reyrolle
- [8] Q. Zhang, J. D. Yan and M.T.C Fang, Modelling of SF₆ Arc in Supersonic Nozzle. Part I: cold flow features and DC arcs characteristics, J. Phys. D: Appl. Phys. Vol. 47, 215201, 2014.
- [9] J.L. Zhang, J.D. Yan, A.B. Murphy, W. Hall and M.T.C Fang, Computational investigation of arc behavior in an auto-expansion circuit breaker contaminated by ablated nozzle vapor, IEEE Trans. Plasma. Sci, 30, pp 706-19, 2005.
- [10] Q. Zhang, J.D. Yan and M.T.C Fang, Computer aided design studies of auto-expansion circuit breakers, Proceedings of the XIX International Conference on Gas Discharges and Their Applications, Beijing, China, 82-85, 2012.
- [11] Y. Yoshioka, M. Tsukushi, K. Natsui, A method and applications of a theoretical calculation for on-load pressure rises in puffer type gas circuit breakers, IEEE transaction on Power Apparatus and Systems, Vol. 98, No. 3, 1979.
- [12] J. Kim, C. Yeo, and Y. Yoshioka, Effect of various factors on gas blast

characteristics of auto-expansion circuit breaker, IEEE Trans. on Power delivery, Vol.25, No.3, 2010

[13] Y. Cao, X. Luo, H. Chunguang, L. Jing, The research on effect of nozzle throat diameter of high voltage SF₆ circuit breaker breaking capability, International Conference on Electrical Machines and Systems, ICEMS 2008.

[14] Y. Song, Y.P. Kim, J.S. Kang etc. Investigation of arc and flow characteristic of self-blast type circuit breakers by simulation, Abstracts IEEE International Conference on Plasma Science (ICOPS), 2013.

[15] C.B. Ruchti and L. Niemyer 1986 Ablation controlled arcs. IEEE Trans. on Plasma Science, Vol. 14, pp. 423–434, 1986.

[16] M. Seeger, J. Tepper, T Christen and J Abrahamson, Experimental study on PTFE ablation in high voltage circuit breakers, J. Phys. D: Appl. Phys. 39 pp5016-24, 2006.

[17] J. L. Zhang, J.D. Yan; M.T.C. Fang, Investigation of the effects of pressure ratios on arc behavior in a supersonic nozzle, IEEE Transactions on Plasma Science Vol.28 , pp 1725 – 1734, 2000

Chapter 4

A Comparative Study of Arc Behaviour in an Auto-expansion Circuit Breaker with Different Arc Durations

4.1 Introduction

Auto-expansion (self-blast) circuit breakers [1] are advantageous over puffer type gas circuit breakers (GCBs) [2][3] in that the former utilizes the energy of the arc to build up a high pressure reservoir in the high current phase which develops and maintains high speed gas flow in the nozzle during the current zero period to cool and quench the arc. The driving energy of an auto-expansion circuit breaker is thus considerably lower than that of a puffer circuit breaker of the same switching ratings. In comparison with a puffer circuit breaker, an auto-expansion circuit breaker has much more complex interruption behavior with different arc durations because of the fact that pressure build-up in the expansion volume (or heating chamber) depends on the arc's history [1].

A well-designed circuit breaker should ensure that the arc is always successfully quenched with the live contact being at all possible positions between the shortest and longest permitted arc durations. The shortest arc duration is normally found in type tests with a pre-defined procedure. With different arc durations the live contact is at different axial positions (different contact gap lengths) when the current passes its final zero point and a recovery voltage is subsequently applied. Variation in arc duration has two important implications. Firstly, the relevant position of the live contact tip in the main PTFE nozzle will determine the nozzle surface area that is exposed to arc radiation around the current peak(s) and subsequently the amount of PFFE vapour produced in the high current phase for pressurisation of the expansion volume. Secondly, the position of the live contact tip may affect the effective gas

flow area through the main nozzle and thus the development of flow field around the arc column at current zero, directly affecting the interruption capability of the breaker. The influence of arc duration on the interruption capability of auto-expansion circuit breakers has so far not been studied in details by computer simulation, as a result of long computational time and the availability of reliable arc models.

This chapter presents a comparative study of the arcing process in a commercial 145 kV auto-expansion circuit breaker with different arc durations by ISEE [4] which is introduced in Chapter 2. Analysis has been carried out through detailed energy balance, enthalpy flow rate, and distribution of temperature and flow fields at key instants to explain the relationship between the predicted critical RRRV of the breaker and the arc durations, using sinusoidal short circuit current waveforms and an identical contact travel curve. Information from this work is expected to be of interest to high voltage circuit breaker designers.

4.2 The Whole Simulation Geometry

Computation has been performed on a commercial auto-expansion circuit breaker, which is rated at 145 kV and 40 kA with a power frequency of 60Hz. The whole calculation domain is shown in Figure 4.1. The circuit breaker is initially filled with SF₆ at an absolute pressure of 0.6 MPa at 300 K. The pressure at the two exits, which are indicated by the parallel arrows in Figure 4.1, is fixed at 0.6 MPa. The arc model used has been described in section 2.4.1, which has been used previously to predict the pressure rise in auto-expansion circuit breakers [5] and arc voltage in a puffer circuit breaker [3], producing results matching reasonably well with measurement. The turbulence parameter used for current zero phase is 0.3 which is calibrated in Chapter 3.

The arc is initiated in simulation when the contacts separate at a distance of 8mm at 12.72 ms. The short, medium and long arc durations are 12.25 ms, 15.25 ms and 18.62 ms (from arc initialization to current zero) based on the type test results. The initial current is set to 3 kA and ramps up in 0.3 ms to the instantaneous value to start the arc and avoid computational difficulties. The influence of this artificial current

ramping has been studied and its influence is restricted to the first millisecond, thus its impact on the high current phase in terms of nozzle ablation and pressure built-up in the expansion volume can be safely ignored.

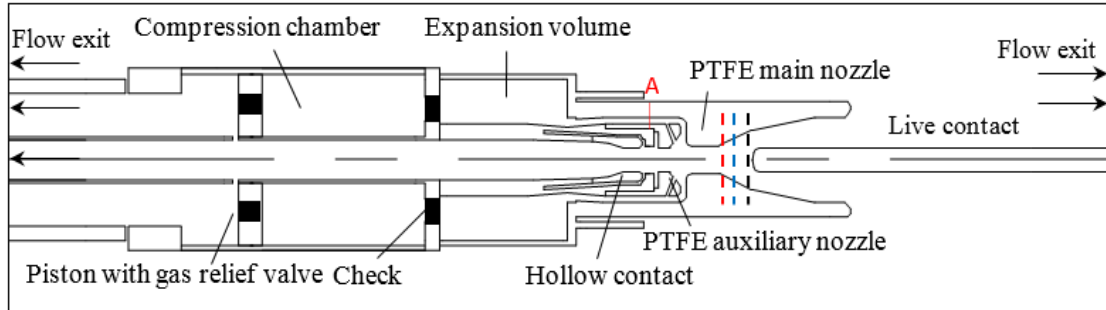


Figure 4.1: Simplified geometry and computational domain of the 145 kV auto-expansion circuit breaker under investigation. The final position of the live contact is shown by the three dash lines near the live contact for different arc durations.

4.3 Comparison of Pressurization in the Expansion Volume

Figure 4.2 shows the pressure variation in the expansion volume for different arc durations with identical peak values of the current. Before the live contact clears the tip of the auxiliary nozzle (tip position is indicated by Position a in Figure 4.4) at 16.5 ms, the relatively low rise of pressure (0.05 MPa from 12.7 ms to 16.5 ms) in the expansion volume for all three cases is mainly caused by the puffer action leading to gas compression. The arc is effectively isolated from the main nozzle and the heating channel (the annular channel connecting the nozzle and the expansion volume) by the live contact. The maximum pressure in the hollow contact shortly before 16.5 ms is around 10.6, 2.0 and 2.4 MPa for short, medium and long arc durations, respectively.

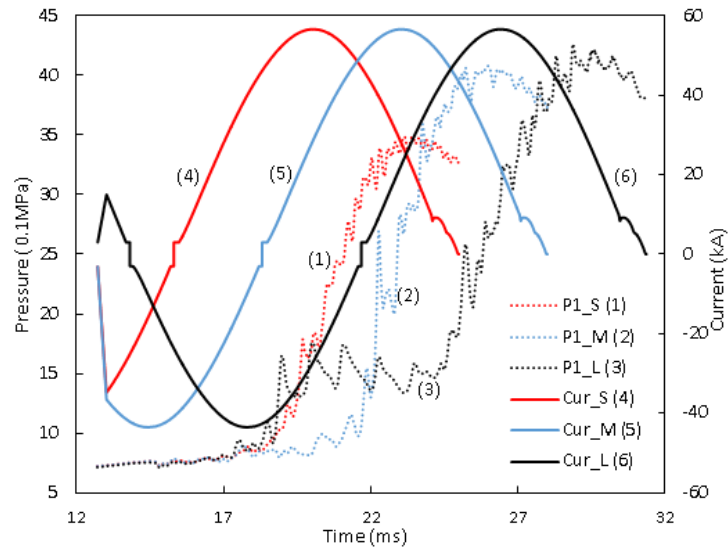


Figure 4.2: Predicted pressure rise in the expansion volume.

The hot gas inside the hollow contact rushes towards the heating channel when the live contact clears the auxiliary nozzle. However this process is not expected to lead to significant pressure rise in the expansion volume at the initial arcing stage because of the small volume of the hollow contact hole. As it was found in [6], pressurization in the expansion volume is closely associated with the thermal energy flux into it. This is shown in Figure 4.3. The enthalpy flux depends on two factors, i.e. the area of PTFE surface exposed to radiation and the magnitude of the instantaneous current flowing through the arc.

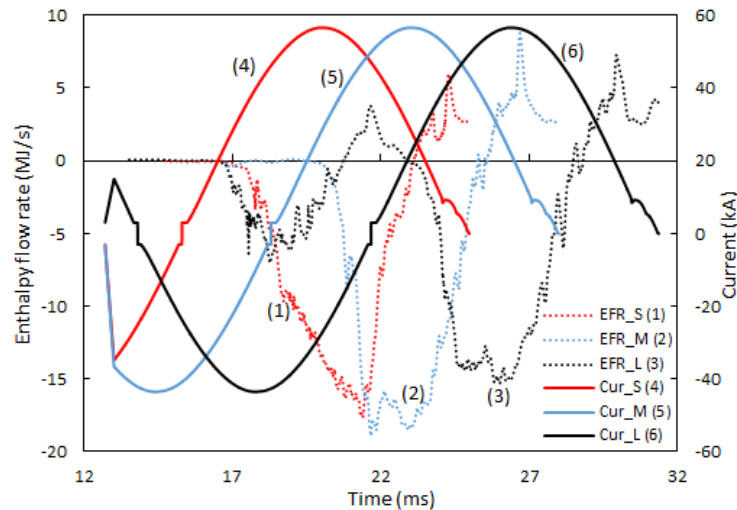


Figure 4.3: Enthalpy flow rate at location A (assigned in Figure 4.1) in the flow guild channel at high current phase.

The long arc duration case has the earliest enthalpy flux (recorded at location A of Figure 4.1) increase at 16.5 ms into the expansion volume because of the increasing

arcing current approaching its first peak located at 17.8 ms. It has a higher enthalpy flux than the short arc duration case because of the difference in the instantaneous current, leading to different level of ablation in the auxiliary nozzle. As a result, it has a high pressure rise in the expansion volume at the initial stage up to 19 ms for the long arc duration case. However, the enthalpy flux starts to drop soon after the current passes its first peak. Gas pumping completely stops at 20.7 ms when the current falls to 16 kA, which is evidenced by the zero enthalpy flux towards the expansion volume in Figure 4.3. During this period (before 20.7 ms) the arc is mainly burning in the auxiliary nozzle and space between the auxiliary nozzle and the main nozzle (Figure 4.4). The arc column is less confined in space and the radiation flux reaching the ablation surface is moderate (103 MW/m^2), which explains the lower enthalpy flow rate (-5 MJ/s) in comparison with the second half cycle of the long arc duration case (-15 MJ/s).

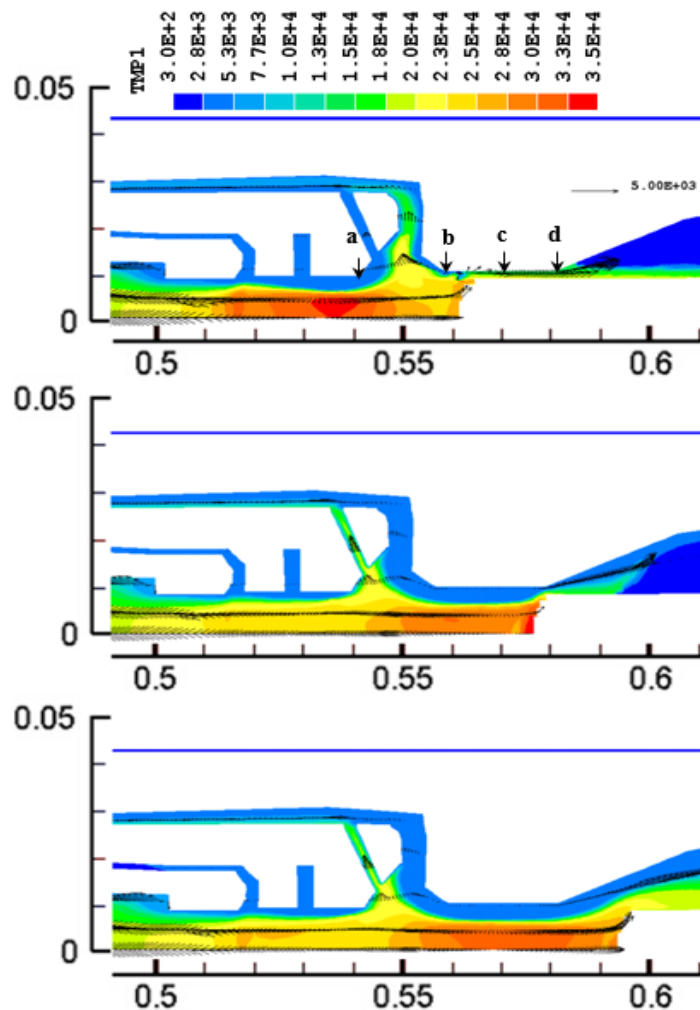


Figure 4.4: Temperature distribution with velocity field for short, medium and long arc duration at current peak of 56 kA from top to bottom, the time instant for live contact position is (a) 16.5ms (b) 19.5ms (c) 21.3ms (d) 23.5ms.

When the live contact tip moves through the flat throat of the main nozzle (distance between position b and c in Figure 4.4), the current approaches its zero point and there is virtually little ablation generated. A reverse flow period (from 20.7 to 22.8 ms) then occurs until the current reaches 20 kA in the second half cycle at 22.8 ms. At this time the arc burns in a considerable length of the flat throat of the main nozzle, exposed to much more ablating surface. In addition, the current goes through its peak of 56 kA, generating a much higher enthalpy flow rate (- 15 MJ/s) into the expansion volume. The pressure in the expansion volume also increases from 1.5 MPa to over 4.0 MPa in 5 ms (from 24 ms to 29 ms) before it drops to 3.8 MPa at current zero.

For medium arc duration, the enthalpy flow rate also increases (to -0.6 MJ/s) after 16.5ms, but lasts for a very short time (less than 0.5 ms), and then drops because the current is rapidly approaching its zero point before 18.3 ms. At 19.5 ms with an instantaneous current of 20 kA, the enthalpy rate begins to rise again. This indicates that 20 kA is a threshold current for the formation of an ablation dominated arc in the given configuration. In addition, from 19.5 to 23 ms (current peak), the live contact travels through the full length of the flat throat of the main nozzle. Due to the high current during this period, PTFE is effectively ablated which significantly increases the enthalpy flow rate to -18 MJ/s (Figure 4.3). Therefore, the pressure rapidly increases to the peak of 4.1MPa at 3 ms after the current peak because it takes time for the contact gap to be pressurized and then thermal energy is convected into the expansion volume.

As expected, the enthalpy flow rate in the short arc duration case experiences a delayed rise (Figure 4.3) between 17 ms and 18 ms in comparison with the long arc duration case because of the lower current level shortly before the live contact clears the auxiliary nozzle. The current already starts to drop after its positive peak when the tip of the live contact moves into the flat throat of the main nozzle around 20 ms. Its enthalpy flow rate into the expansion volume carries on increasing after the current peak until 21.5 ms because the flat nozzle of the main contact is still blocked by the live contact, which is different from the other two cases. The final position of the live contact tip at current zero is just outside of the exit of the main nozzle throat

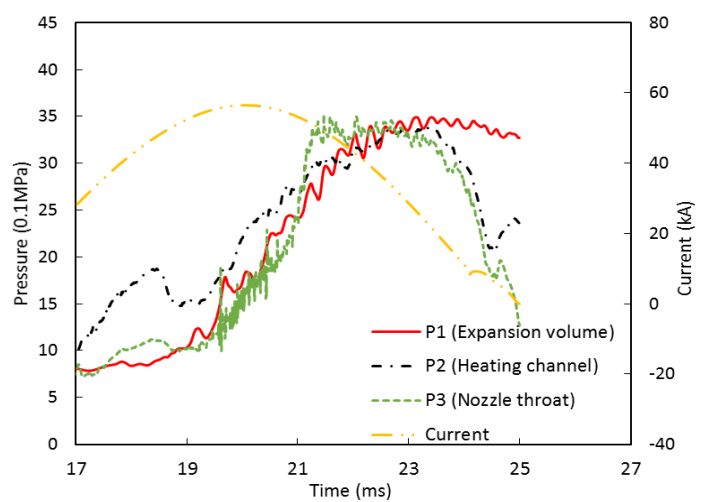
(see Figure 4.1). Since in the high current phase the main nozzle is blocked by the live contact and ablation in the auxiliary nozzle creates a stagnant region, vapour compression in the main nozzle rapidly established a high pressure zone and develops a high enthalpy flux (-17 MJ/s) towards the expansion volume (Figure 4.3).

For the geometry under investigation which is representative of modern auto-expansion circuit breakers, the final half-cycle of the current is mainly responsible for the pressurization in the expansion volume. In particular in the long arc duration case, the final half-cycle produces 77% of the total pressure rise in the expansion volume. While the fluctuation on the pressure curve is due to change in arc column size generating pressure waves propagating towards the expansion volume, the overall delay is caused by the development of the high pressure zone in the contact space and the motion of hot vapor across the length of the heating channel into the expansion volume.

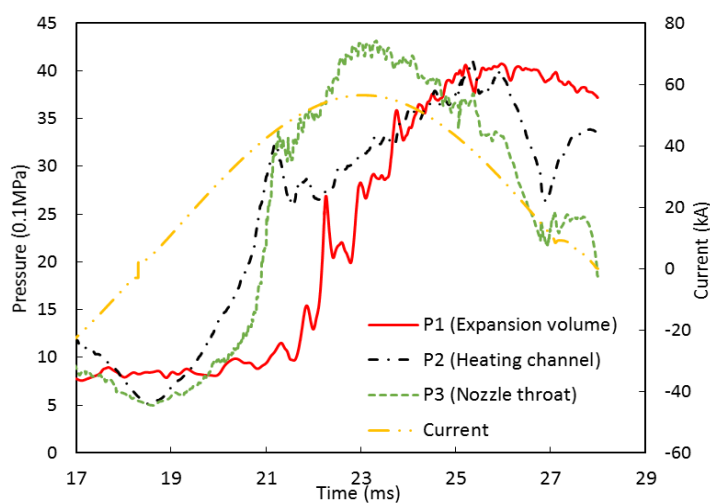
The delay between the current peak and the pressure peak in the expansion volume is respectively, 3.4, 2.9 and 3.2 ms for the short, medium and long arc duration cases. It is interesting to note that auto-expansion circuit breakers with overall different designs have very similar values for the delay between the last current peak and the last pressure peak in the expansion volume, with an average value of 3 ± 0.2 ms. Attempts have been made to identify the causes for this rather constant value of time delay. The length of the heating channel is 100 mm. It was found that the time taken for pressure to propagate from the contact space to the expansion volume is only a small fraction (~ 0.2 ms) of a millisecond.

Taking the short arc duration case as an example, pressure recorded at different positions (P1-P4 as shown in Figure 4.6) in the arcing chamber show that this delay consists of two stages, as shown in Figure 4.5a. The first stage (20 ms to 21.7 ms) is designated by rapid pressurization of the expansion volume when large pressure difference between expansion volume and nozzle throat exits. At 21.7 ms the pressures at P2 (in the heating channel) and P1 (in the expansion volume) reach the same level. In the second stage (21.7 ms to 23.4 ms) pressure at P3, the axially middle plane of the flat throat of the main nozzle, has reached a new height in its magnitude following vapour accumulation and flow field adjustment. This high

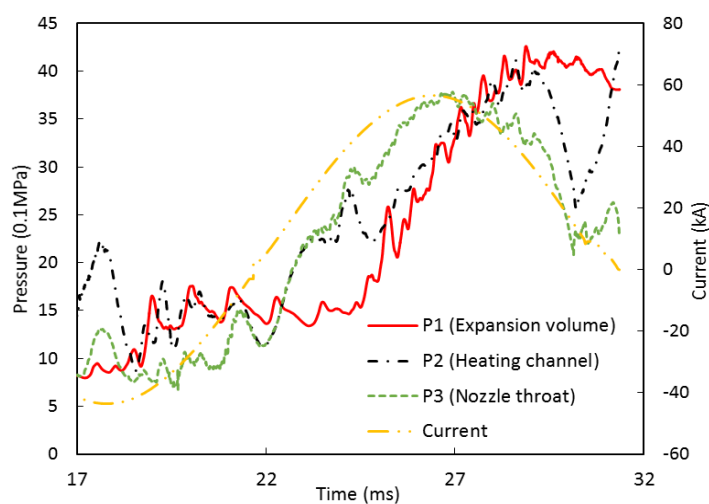
pressure drives further enthalpy flux into the expansion volume. With the pressure difference between the contact space and the expansion volume becoming smaller, the rate of rise of pressure also decreases until an instant (around 23.4 ms) the pressure difference becomes zero and pressurization vanishes. The use of a flat throated main nozzle and auxiliary nozzle of similar structure and comparable dimensions in modern auto-expansion circuit breakers (31.5 kA to 40 kA, 145 kV to 252 kV) gives the rather similar values in this time delay [1][6]-[8]. The other two cases shown in Figure 4.5 follow similar pattern of pressure variation and will not be repeated in detail.



(a)



(b)



(c)

Figure 4.5: Pressure records in the arcing chamber for (a) short (b) medium, and (c) long arc duration.

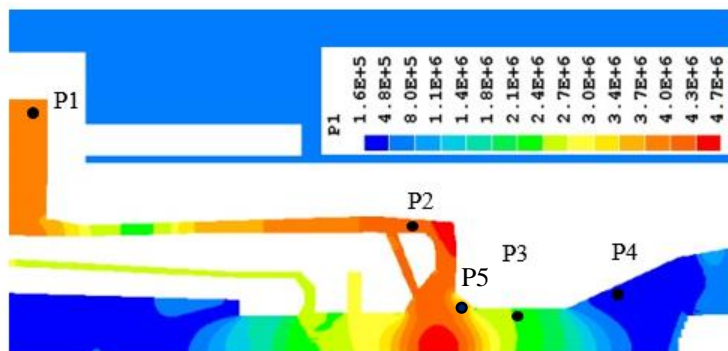


Figure 4.6: Pressure distribution for long arc duration at current zero

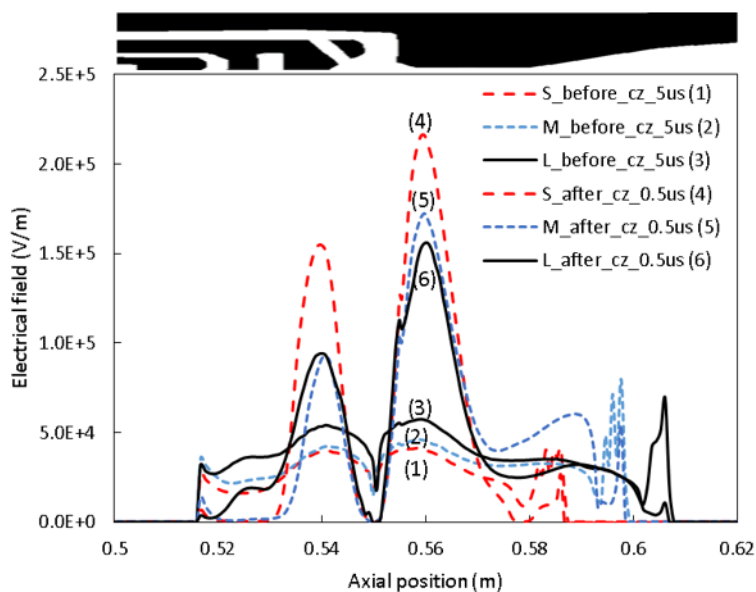
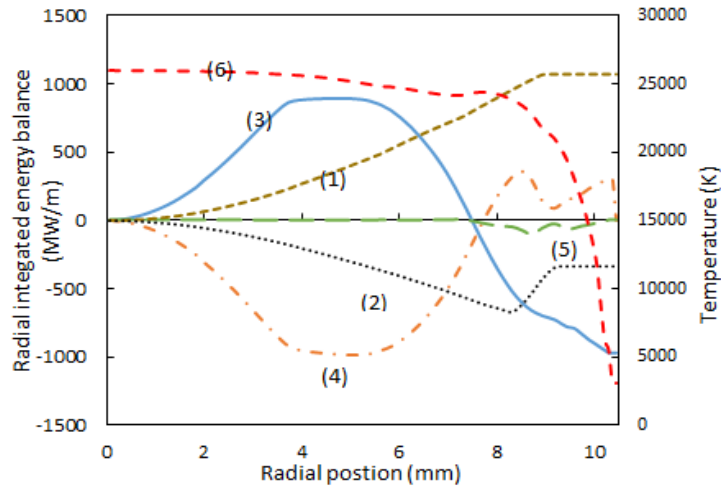
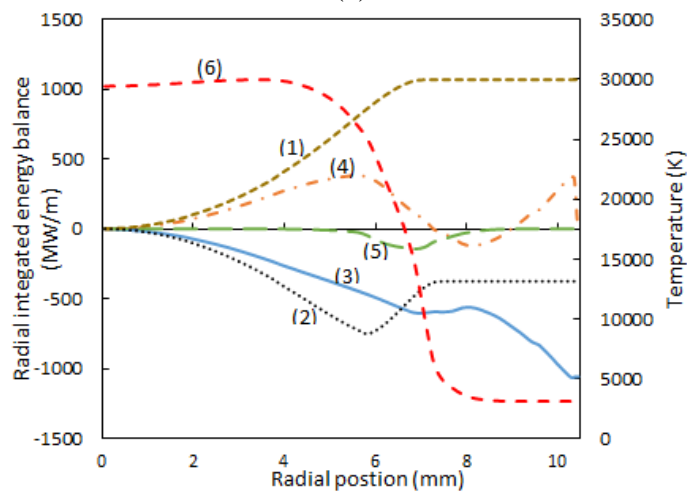


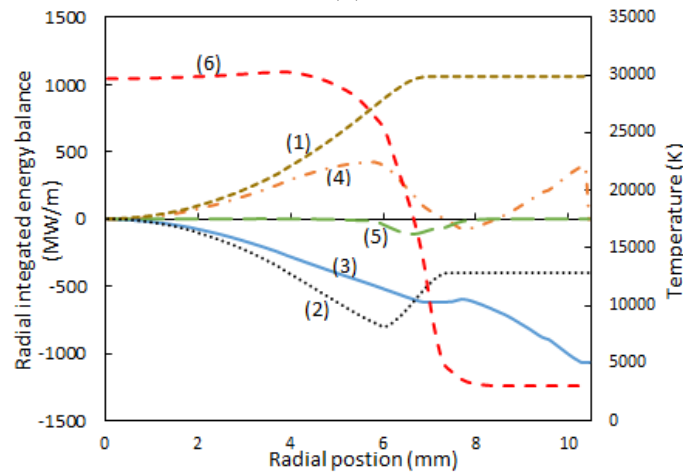
Figure 4.7: Axis electric field 5us before current zero and 0.5us after current zero under dV/dt of 8kV/us.



(a)



(b)



(c)

Figure 4.8: Radial integrated energy balance of critical cross section with axial position 0.55 m at final current peak for (a) short (b) medium and (c) long arc duration. The curves present

(1) Ohmic heating: $\int \sigma E^2 2\pi r dr$

(2) Radiation loss: $-\int q 2\pi r dr$

(3) Axial convection: $-\int \frac{\partial}{\partial z} (\rho \omega h) 2\pi r dr$

(4) Radial convection: $-\int \frac{1}{r} \frac{\partial}{\partial r} (r\rho v h) 2\pi r dr$

(5) Radial thermal and turbulence conduction: $-\int \frac{1}{r} \frac{\partial}{\partial r} \left(-r \frac{k}{c_p} \frac{\partial h}{\partial r}\right) 2\pi r dr$

(6) Radial temperature profile

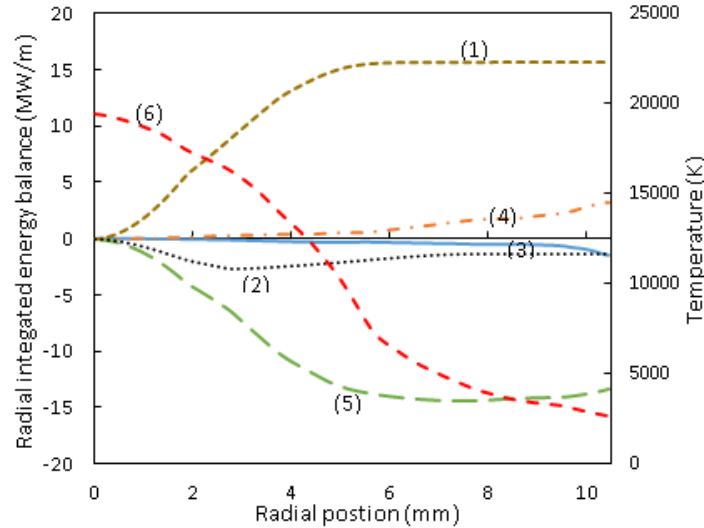


Figure 4.9: Radial integrated energy balance at 500A for the short arc duration case, the meaning of each curve is same as Figure 4.7.

4.4 Flow Environment before Current Zero

The quality of arc quenching at current zero depends on the flow field around the arc column. Both velocity and density affect the interruption process. From Figure 4.7, the region around an axial position of 0.56 m (corresponding to the left end of flat nozzle throat) and the region inside the auxiliary nozzle take up a considerable part of the recovery voltage. This means the arc temperature decays most rapidly in these two regions and arc resistance recovers to high values. In order to track the causes, energy balance is performed at the axial location of 0.56 m to identify the dominant energy transport mechanisms at several key instants before current zero.

Depending on the local flow field, energy transport at high current behaves differently from the low current arcs. For the short arc duration case at its peak current, convection dominates the energy transport process (curve (3) and curve (4) in Figure 4.8a). This is because at this instant the location for energy balance is close to the tip of the live contact, and energy is convected into the domain in the positive axial direction and convected out in the positive radial direction. For both medium and long arc duration cases, the live contact at peak currents has cleared the flat

nozzle throat and strong axial flow been established (Figure 4.8b and 8c). The net effect of axial convection on energy balance in the arc core becomes weaker. Ohmic heating and radiation dominate the energy transport process (curve (1) and (2) in Figure 4.8b and c). Approaching current zero, turbulence plays an increasingly important role. At 12 kA, the arc changes from radiation dominated to turbulent cooling dominated, turbulence cooling overtakes other mechanisms. At 500 A (30 μ s before current zero) turbulent cooling is the dominant mechanism for energy removal (curve 5 Figure 4.9).

Results in Figure 4.10 clearly show that at the current zero point, the axis temperature in the long arc duration case is the lowest and that of the medium arc duration case behaves similarly but is 300 K higher. In the short arc duration case the flat throat of the main nozzle is still partially blocked by the live contact and the arc column is larger, leading to a higher temperature near the nozzle wall. Cooling of the arc by the surrounding axial flow in the current zero period is a combined effect of gas velocity and density, determining the mass flow rate. Figure 4.11 shows that the axial mass flux of the surrounding gas flow is rather uniform in the majority part of the nozzle cross section (from a radius of 2.5 mm to 8 mm). The long arc duration case has the highest value of 1.64×10^4 kg/m²/s, which is 2.7 and 2 times higher than that of the short and medium arc duration cases, respectively. The arc column of the long arc duration case is thus thinnest in comparison with the other two cases (Figure 4.12). When the current reaches its zero point pressure drop in the auto-expansion volume from its peak value is normally within 10% of the maximum pressure rise (pressure peak minus the filling pressure) as shown in Figure 4.2.

A stronger flow (mass flow rate) from the expansion volume towards the nozzles is designated by a lower pressure difference between the expansion volume and the middle position of the flat nozzle throat (P3 in Figure 4.6), or a higher pressure difference between the heating channel (P2) and exit (P4) of the flat nozzle throat, as given in Figure 4.13. The main cause for this relationship is due to the fact that the pressure in the heating channel (P2) starts to recover shortly before current zero, at 24.6 ms, 26.95 ms, 30.22 ms for short, medium and long arc duration cases (details see Figure 4.5). Due to pressure reflection by the bent solid surface near P2, the pressure at P2 can become higher than that in the expansion volume (Figure 4.5c).

The pressure distribution for the long arc duration case has been given in Figure 4.6. It is this recovered pressure in the heating channel that supports the flow field and thus the mass flow rate near current zero.

For Figure 4.5c it should be noted that because the tip of the live contact clears the main nozzle throat before the current reaches its peak, the maximum pressure in the contact space is not at the middle of the nozzle throat in the pressurization stage. Instead the maximum pressure is close to the upstream end of the flat nozzle throat, which is responsible for pumping hot vapour into the expansion volume and raise the pressure to 4 MPa.

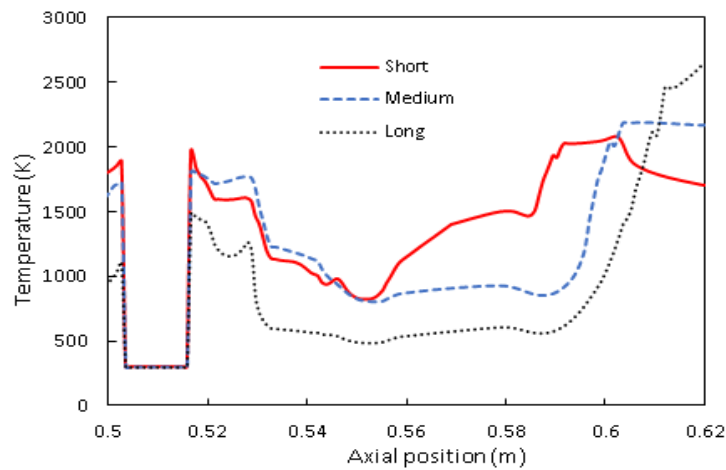


Figure 4.10: Temperature 9.5mm away from axis at current zero.

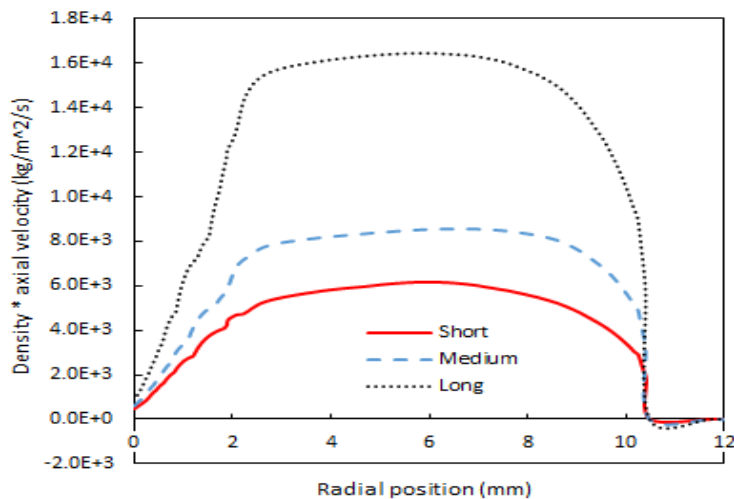


Figure 4.11: Mass flux at critical cross section (axial position of 0.56 m) at current zero.

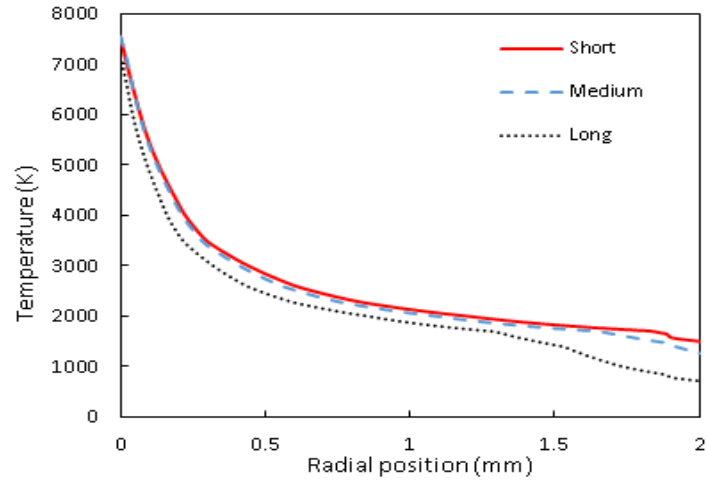


Figure 4.12: Radial temperature at critical cross section (axial position of 0.56 m) at current zero.

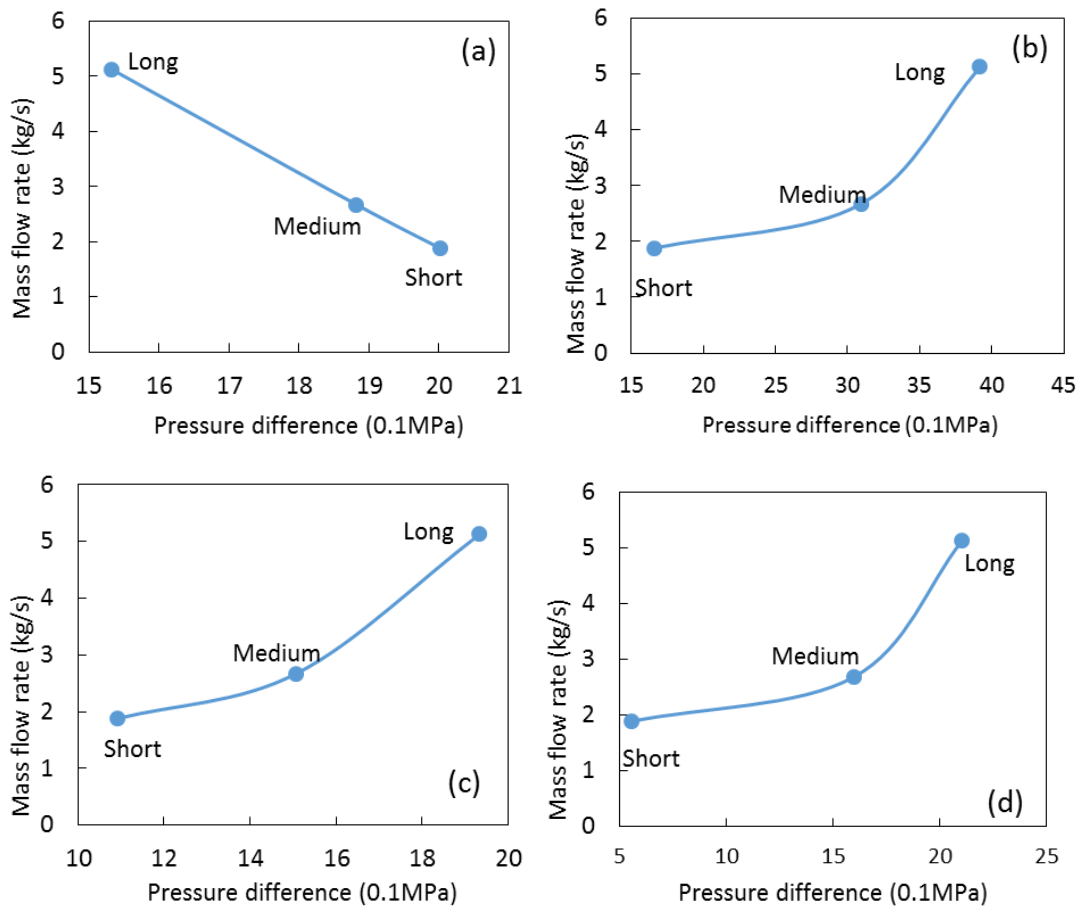


Figure 4.13: Mass flow rate at the axial position of 0.56 m versus pressure difference between (a) expansion volume and the middle of nozzle throat, i.e. P1-P3 in Figure 4.6; (b) heating channel and downstream of nozzle throat at current zero, i.e. P2-P4 in Figure 4.6. (c) heating channel and the middle of nozzle throat, i.e. P2-P3 in Figure 4.6 (d) upstream of nozzle throat and downstream of nozzle throat, i.e. P5- P4 in Figure 4.6

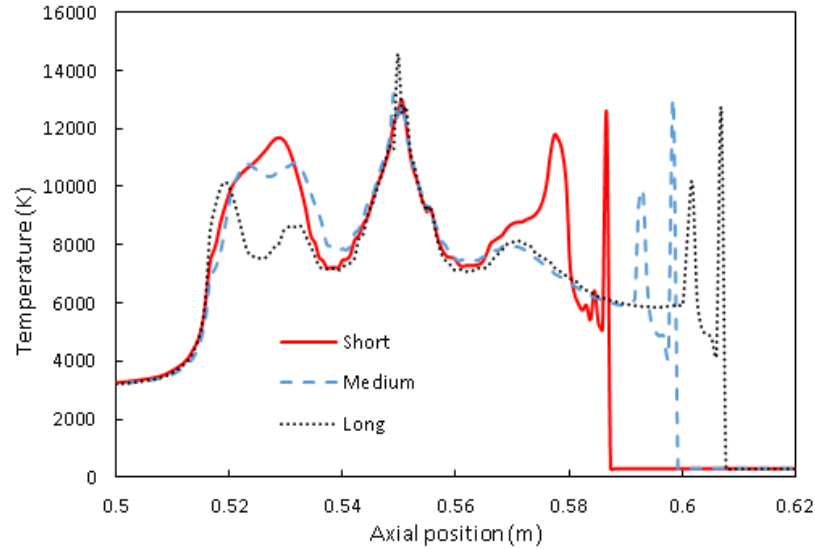


Figure 4.14: Axis temperature at current zero.

Turbulence enhanced momentum and energy transfer are most significant in the current zero phase of high voltage circuit breakers. Recently there is qualitative evidence that turbulence also contributes to the mixing of hot and cold gases in the expansion volume [10][11]. In the present work, a very small turbulence mixing length scale is used in the expansion volume of the breaker due to a lack of reliable information on the strength of turbulence mixing effect. The expansion volume is relatively long in comparison with its radial extent and hot gas flows towards the bottom of the expansion volume in the pressurization stage. It is well known that pressure rise in the expansion volume depends mainly on the energy flow rate into it, not the mixing of the gas. Our results show that gas temperature in the expansion volume after flow reversal is generally lower than 2000 K. It is not expected that any possible turbulent mixing of gas in the expansion volume would affect the results significantly in the present work.

4.5 Thermal Recovery Process

Figure 4.14 show that closely associated with the surrounding gas flow, arc temperature on the axis has two valleys after current zero, one near the tip of the auxiliary nozzle (axial position of 0.54 m) and the other near the left end of the flat throat of the main nozzle (axial position of 0.56 m). The arc temperature in the main nozzle for the short arc duration case remains above 8000 K, different from the other

cases. Results in Figure 4.7 and Figure 4.17 provide evidence that for the short arc duration case recovery voltage from the system has to be taken up by the gas in the auxiliary nozzle and a small section of the gas in the main nozzle. A comparison of voltage share for the three cases is given in Table 4.1. The current is 98 A at 5 μ s before the final current zero. It is clear that

- a) The gas in the auxiliary nozzle region takes about 40% of the arc voltage shortly before the final current zero and in the short arc duration case this figure is 46% because of the relatively shorter contact gap;
- b) Arc in the main nozzle is more rapidly cooled down to take an increased share of the recovery voltage after current zero (> 65%);
- c) In the short arc duration case the auxiliary nozzle region plays a more important role in the thermal recovery process in comparison with the other two cases.

Table 4.1: Voltage across two sections of arc column separated by the stagnation point.

Case		Auxiliary nozzle (V/%)		Main nozzle (V)	Total voltage (V)
5 μ s before C.Z.	S	936	46.3	1085	2021
	M	1071	38.3	1725	2797
	L	1402	39.2	2172	3575
0.5 μ s after C.Z.	S	1432	35.8	2568	4000
	M	789	19.7	3211	4000
	L	1208	34.0	2793	4000

At current zero a hot spot is formed in front of the live contact in all cases. This is due to the arc flow hitting the contact tip surface and causing a stagnation region with possible reverse flow (Figure 4.16). As a design guidance, the shortest arc duration for successful thermal interruption is achieved when the ring shaped flow cross sectional area between the tip of the live contact and the main nozzle equates the value of the nozzle throat cross section area shortly before the current zero point in the course of contact motion. At that moment, the circuit breaker is considered to establish adequate interruption ability because there is sufficiently large flow area to develop the gas flow at current zero. Comparing the flow field of three switching duties in Figure 4.16, the velocity in the short arc duration case is much lower than the other two cases because the blocking effect of the live contact. As a result, strong convection and turbulent cooling cannot be established in the main nozzle at current

zero for the short arc duration case.

4.6 Critical Rate of Rise of Recovery Voltage (RRRV)

The critical RRRV of a circuit breaker is a direct indicator of its interruption capability. It is a threshold value of dv/dt (or RRRV applied across the contact gap after current zero). Any dv/dt that is higher than this threshold value will eventually lead to thermal re-ignition. Computationally, for a specified set of arcing conditions, different dv/dt values are used to calculate the post arc current as a function of time. There will be two dv/dt values, one leading to thermal re-ignition and the other one leading to thermal recovery. The average of these two values can then be regarded as the critical RRRV.

The initial RRRV imposed by the network during a short line fault (SLF) is considerably higher than that during a terminal fault. In a 40 kA and 60 Hz scenario, the value of dv/dt is around 9 kV/ μ s in the first 2 microseconds, as evidenced in type test records and also in literature [12]. To investigate the variation in interruption capability, the critical RRRV is calculated for different arc duration cases after current zero. The computational uncertainty is less than 0.5 kV/ μ s.

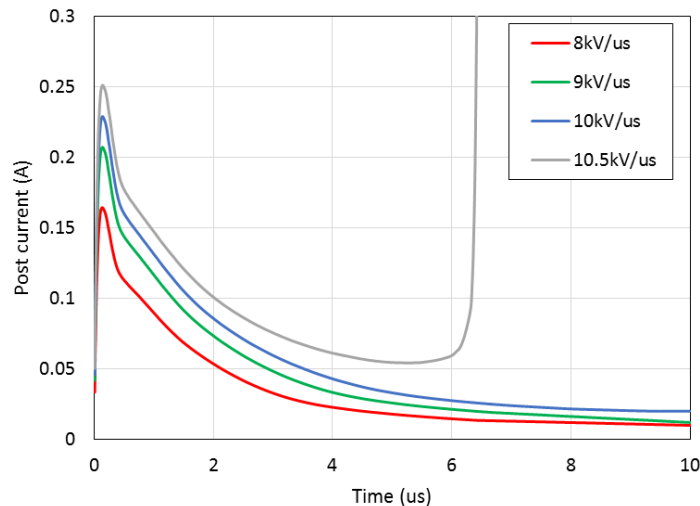


Figure 4.15: Post arc current under different RRRV for short arc duration

At 5 μ s before the final current zero point, the arc has the higher axis temperature in the long arc duration case (Figure 4.16). However, the temperature drops more rapidly after current zero leading to the lowest axis temperature at 0.5 μ s after

current zero, in comparison with those of the other two cases at the same axial position. This is a direct consequence of the strongest mass flux given in Figure 4.11. The turbulent eddy viscosity at current zero is shown in Figure 4.18 at two axial positions of 0.54 m and 0.56 m, respectively. It is evident that turbulent cooling is strongest in the long arc duration case. Its critical RRRV is thus expected to be the highest. The circuit breaker under investigation successfully passed all test duties. The predicted critical RRRV using a turbulence parameter of 0.3 is 10 kV/ μ s, higher than the applied RRRV of 9.0 kV/ μ s. The critical RRRV for the medium and long arc duration cases are both higher than 12 kV/ μ s. Despite the uncertainty in the turbulence parameter, it appears that a value of 0.3 produces a reasonable critical RRRV for the short arc duration case. The much higher critical RRRV for the other two cases indicates that this circuit breaker has a rather large margin in its interruption capabilities. It can also be argued that the short arc duration case is the most difficult switching duty for this type of auto-expansion circuit breaker and one of the design focuses should be with the careful choice of the shape and dimension of the auxiliary nozzle based on the consideration in section 4.5.

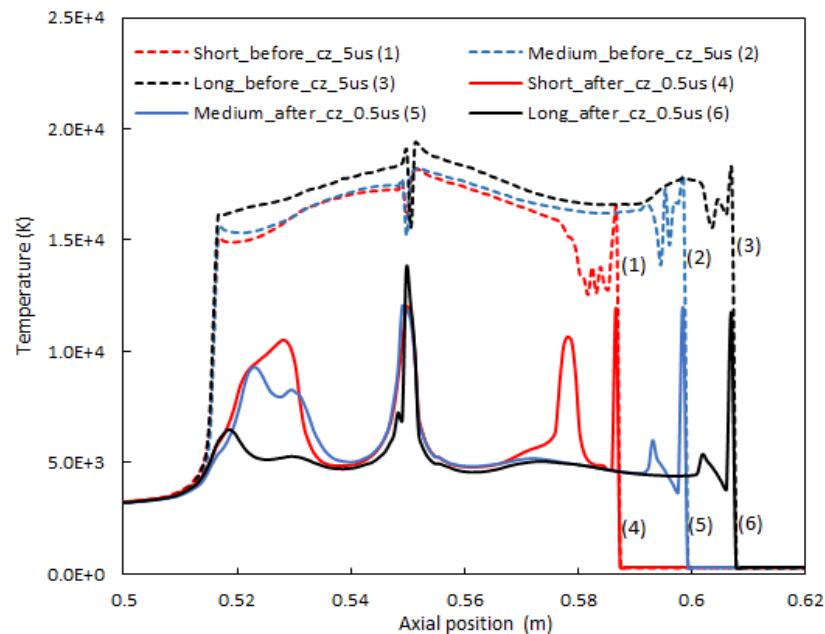


Figure 4.16: Axis temperature 5 μ s before current zero and 0.5 μ s after current zero under dV/dt of 8 kV/ μ s.

There is recognition that deviation from local thermal equilibrium (LTE) and local chemical equilibrium (LCE) exists in the current zero period due to the fact that the time constants of chemical reactions differ significantly and electrons cannot pass

their energy gained from the electric field to heavy particles in an efficient way during the short time scale. This problem has been investigated in several publications [13]-[16]. It has been indicated that consideration of the non LTE and non-LCE effect alone is not able to produce reasonable predictions for the critical RRRV values. On the other hand it can be argued that the existence of turbulence in SF₆ arcs enhances not only the mass, momentum and energy transport process, but also increases the rates of chemical reactions around current zero, in a way similar to turbulent combustion, to render the plasma state closer to LTE and LCE. These issues collectively form one of the key research topics in the future to achieve quantitative prediction of the interruption capability of high voltage circuit breakers.

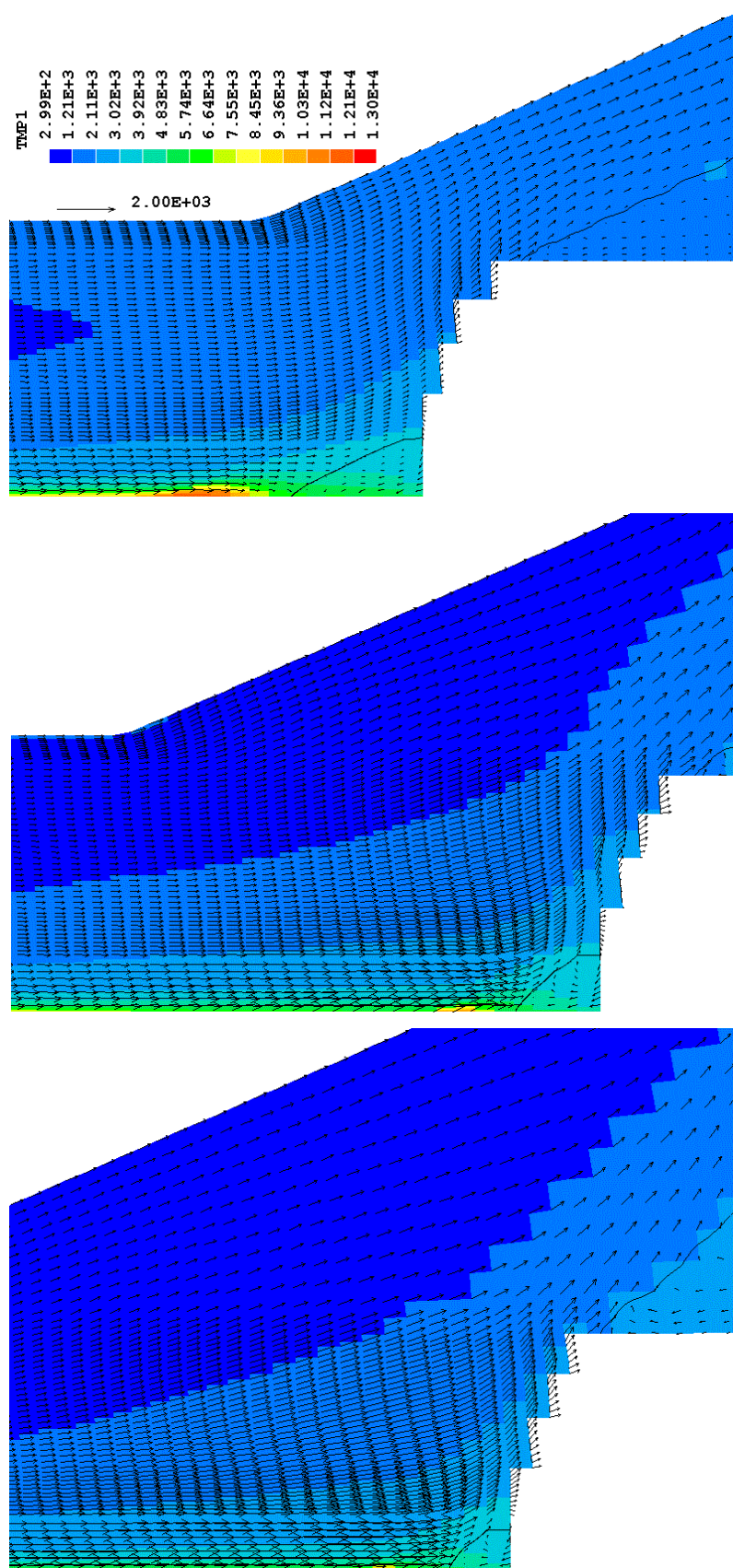


Figure 4.17: Temperature distribution with velocity field at current zero for short, medium and long arc duration cases, respectively.

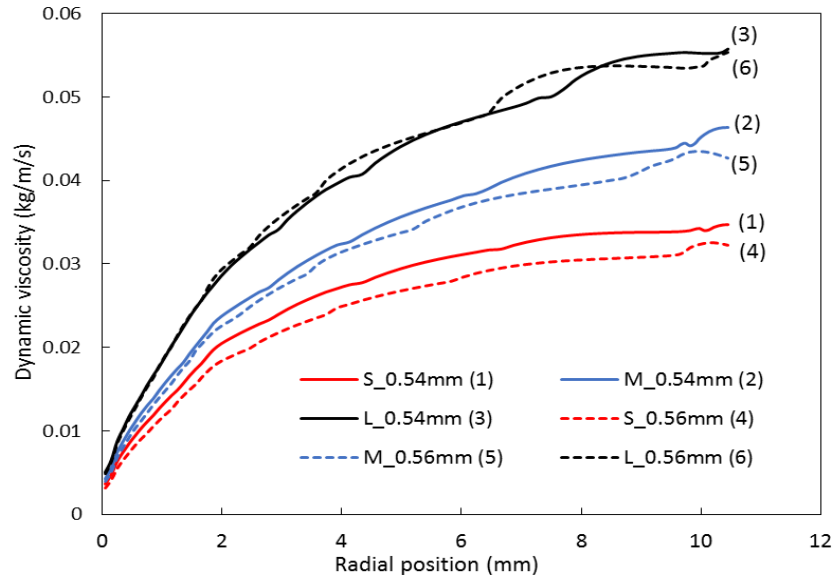


Figure 4.18: Turbulent eddy viscosity at the cross sections with axial position 0.54 m and 0.56 m for short, medium and long arc duration at current zero. S_0.54m means the dynamic viscosity distribution in the radial direction at axial location 0.54 m.

4.7 Conclusions

The behavior of a 145 kV, 60 Hz auto-expansion circuit breaker with different arc durations and symmetrical short circuit current waveforms is computationally studied. The value of the turbulence parameter, which is key to quantitative prediction of the thermal interruption capability of gas blast circuit breakers, is carefully selected based on type test results.

- a) The final half-cycle of the current is mainly responsible for the pressure rise in the expansion volume (77% for the long arc duration case). The auxiliary nozzle plays an important role in the pressurization process by creating a stagnation zone inside its hole to force the pressure in the contact gap to rise rapidly providing an enthalpy flux into the expansion volume. The peak enthalpy flow rate into the expansion volume is 17 MJ/s, 18 MJ/s and 14 MJ/s for short, medium and long arc duration cases, respectively. The pressure drop in the expansion volume from its peak value is within 10% when the current reaches its final zero point, implying that only a small fraction of the heated gas in the expansion volume flows out to establish the necessary flow field in the nozzles for arc quenching after current zero. The delay in time between the current and pressure peaks in the expansion

volume is 3 ms, a rather constant value for different designs of auto-expansion circuit breakers.

- b) When the current falls from its final peak toward the zero point the arc evolves from radiation and convection dominated cooling into a turbulent cooling dominated regime. The transition takes place at 12 kA. The increase in arc resistance is closely associated with the mass flow rate out of the expansion volume. At current zero the mass flow rate in the main nozzle is linearly related to the pressure drop over the heating channel. Due to the partial blockage of the main nozzle by the live contact, the arc column in the short arc duration case is hotter and larger in the main nozzle in comparison with the other two cases, leading to inferior interruption capability.

- c) After current zero the system recovery voltage is shared by two sections of the contact gap divided by the flow stagnation point between the main nozzle and the auxiliary nozzle. The gas in the auxiliary nozzle region takes about 35% of the recovery voltage in the short arc duration case, which is the most difficult interruption duty of the three cases studied. It is evident that the auxiliary nozzle plays an important part in both the pressurization process and the thermal recovery period, especially for short arc duration cases. Therefore, the dimension and location of the auxiliary nozzle should be a key technical consideration in the design of high voltage auto-expansion circuit breakers.

References

- [1] J.D. Yan, M.T.C Fang and W. Hall, The development of PC based CAD tool for auto-expansion circuit breaker design IEEE Trans. Power Delivery, Vol. 14, pp. 176-81, 1999.
- [2] K.Y Park and M.T.C Fang, Mathematical modelling of SF₆ puffer circuit breakers i: High current region IEEE Trans on Plasma Sci., Vol. 24, pp. 490–502, 1996.
- [3] J.D. Yan, S.M. Han, Y.Y. Zhan etc. Computer simulation of the arcing process in high voltage puffer circuit breakers with hollow contacts, Proceedings of XVIIIth Symposium on Physics of Switching Arcs, Brno Czech Republic, pp. 99-108, 2009.
- [4] Y. Pei, Q. Zhang, J.D. Yan, M.T.C Fang, Intelligent computer simulation tools for HV circuit breakers and issues related to simulation, in Electric power equipment-switching technology (ICEPE-ST) 1ST international conference, Xi'an China, pp. 435-439, 2011.
- [5] J.L. Zhang, J.D. Yan, A.B. Murphy, W. Hall and M.T.C Fang, Computational investigation of arc behavior in an auto-expansion circuit breaker contaminated by ablated nozzle vapor IEEE Trans. Plasma. Science, Vol. 30, pp. 706-19, 2005.
- [6] T. M. Wong, J.D. Yan, X. Ye, J. Abrahamsson and M.T.C Fang Global Thermal and Aerodynamic Environment in High Voltage Auto-Expansion Circuit Breakers. Proceedings of XVII Symposium on Pysics of Switching Arc. Local Organisation Comiittee, Brno, pp. 37-46, 2007.
- [7] V.K. Liau, B.Y. Lee, K.D. Song, and K.Y. Park, Computational investigation of arcing phenomena in 245 kV hybrid circuit breaker Japanese Journal of Applied Physics, 46, 1674 – 1679, 2007.
- [8] Q. Zhang, J.D. Yan and M.T.C Fang, Computer aided design studies of auto-expansion circuit breakers Proceedings of the XIX International Conference on Gas Discharges and Their Applications, Beijing, China, pp. 82-85, 2012.
- [9] C.M. Franck and M. Seeger, Application of high current and current zero simulation of high voltage circuit breaker Contrib. Plasma Phys. Vol. 46, pp. 787-797, 2006.
- [10] R. Bini, N. T. Basse and M. Seeger, Arc-induced turbulent mixing in an SF₆ circuit breaker model, J. Phys. D: Appl. Phys. Vol. 44, pp. 25203–12, 2011.

- [11] J.J. Gonzalez, P. Freton, F. Reichert and D. Randrianarivao, Turbulence and magnetic field calculations in high-voltage circuit breakers, *IEEE Trans. on Plasma Science*, Vol. 40, pp. 936-944, 2012.
- [12] R. W. Alexander, D. Dufournet, Internets: Transient recovery voltage (TRV) for high-voltage circuit breakers, [Online]. Available:
<http://webm.dsea.unipi.it/barsali/materiale/Dinamica%20e%20Controllo%20SE/TutorialTRVAlexander-Dufournet.pdf>
- [13] J.B. Belhaouari, J.J. Gonzalez and A. Gleizes Simulation of a decaying SF₆ arc plasma: hydrodynamic and kinetic coupling study, *J. Phys. D: Appl. Phys.* Vol. 31 pp. 1219–32, 1998.
- [14] R. Girard, J.B. Belhaouari, J.J. Gonzalez and A. Gleizes, A two- temperature kinetic model of SF₆ plasma, *J. Phys. D: Appl. Phys.* Vol. 32, pp. 2890-2901, 1999.
- [15] R. Girard, J.J. Gonzalez and A. Gleizes, Modelling of a two-temperature SF₆ arc plasma during extinction *J. Phys. D: Appl. Phys.* Vol. 32 pp. 1229–38, 1999.
- [16] J.J. Gonzalez, R. Girard and A. Gleizes, Decay and post-arc phases of a SF₆ arc plasma a thermal and chemical non-equilibrium model, *J. Phys. D: Appl. Phys.* Vol. 33, pp. 2759-2768, 2000

Chapter 5

Transient Pressure Variations following Flow Reversal and Their Implications towards the Interruption Performance of Auto-expansion Circuit Breakers

5.1 Introduction

High voltage gas-blast circuit breakers rely on the generation of high speed gas flow in the contact space during the current zero period to cool the arc and subsequently interrupt the fault current. In a puffer type circuit breaker, flow in the contact space is established by the relative movement of a piston in a cylinder (the puffer) [1]. In an auto-expansion (self-blast) circuit breaker a high pressure reservoir is formed in the high current phase as a result of nozzle ablation that generates a high pressure zone in the contact space driving pressurized hot nozzle vapor (PTFE vapor) into a storage space, known as the expansion volume [2]. When the arcing current approaches its final zero point, the pressure in the contact space starts to drop quickly and the pressurized expansion volume drives gas into the contact space to establish the required high speed gas flow for arc extinction.

The pressure in the contact space is also affected by the relative movement of the contacts and the size of the arc column by changing the gas flow path and the effective flow cross sectional area, respectively. As a result, gas pressure in the arcing chamber, especially in the contact space, experiences rapid change well beyond the current zero point [3][4][5] The time scale for pressure variation is much shorter than the period of the alternating short circuit current, thus having a “transient” nature.

Gas pressure is an important parameter in shaping the interruption capability of gas-blast circuit breakers. It affects the interruption process in several ways. Firstly, in the high current phase the arc voltage is affected by the pressure. A higher pressure leads to a higher arc voltage and smaller arc radius [6]. Thus, the pressure will affect the energy dumped in the contact space and radiation loss from the arc core as well. Secondly, in the current zero period arc cooling effect is controlled by the mass flow rate through a nozzle, affecting the critical rate of rise of recovery voltage (RRRV) in the thermal recovery process [5]. The mass flow rate depends on gas velocity and density and the latter is determined by temperature and pressure. Thirdly, with a system applied recovery voltage after current zero the dielectric strength of the gas in the contact gap is a function of gas composition, density and temperature [7] and the density is proportional to pressure. A lower pressure and higher temperature in the contact gap results in a lower particle density and larger mean free path, which means free electrons obtain more kinetic energy between two successive collisions increasing the likelihood of electron avalanche and breakdown of gas through the formation of streamers and leaders [7]. Therefore, a well-designed circuit breaker should aim towards achieving highest possible pressure in the contact space. Understanding the pattern and causes of transient pressure variation during the operation of a circuit breaker is an important aspect for optimum design.

5.2 Existing Study on Pressure Variation in Gas-blast Circuit Breakers

There has been a sizeable amount of work devoted to the pressure variation in puffer circuit breakers [3][4][8][10][11]. However, most of the studies focused on the pressure in the compression volume, where it is relatively easy to perform pressure measurement.

Pressure measurement in a model puffer circuit breaker was taken in [8][10]. Different from a modern puffer circuit breaker, the nozzle in [8] was a converging-diverging nozzle without a flat throat. The contact space is connected to the puffer through a short passage [8] with larger cross sectional area [8][10]. The pressure in the compression volume generally keeps increasing until the end of the mechanical travel at different current levels, filling pressures and arc durations [8].

The reason for the difference in the pressure pattern can be explained by the fact that the absence of a flat nozzle throat in the model puffer circuit breaker decreases the effect of nozzle clogging, which results in the pressure variation directly dependent on the piston compression rather than the gas backflow due to nozzle clogging. It was believed that with a high level of arcing current, fast pressure variation can be caused by aerodynamic resonances within the arcing chamber and nozzle assembly [8]. This will be discussed later in Section 5.4 when the results are presented.

Results from a theoretical study on puffer circuit breaker in [4] support the conclusion that increasing the size of the compression volume could increase the gas pressure and density not only in the compression volume itself but also in the contact space at current zero, thus improving the dielectric recovery performance. However, the reason has not been clearly explained. It is believed that by increasing the compression volume more gas is available for compression and a higher pressure in the contact space can be maintained for a longer time. In addition, for different arc durations, an optimum mechanical travel of a contact due to appropriate operating force, can be found to withstand the highest recovery voltage through its influence on pressure and flow field, which is verified by experimental test and computer simulation in [11].

More recently pressure measurement was taken for a modern 252 kV puffer circuit breaker [3]. Pressure variations at four locations, i.e. inside the expansion volume, upstream, downstream, and at the middle of the main nozzle throat, were recorded for a no-load case and several arcing cases with a current between 20 kA and 50 kA (rms value). The measured pressure wave oscillates with a high frequency after the arc is initiated. In the authors' opinion, this is caused by pressure reflection inside the insulating tube connecting the measurement point and the pressure sensor. The implication of using the insulating tube is investigated only for the no-load case. Although the measurement results show that the tube only causes mild oscillation in the no-load case, it still needs to be cautious about the validity of the pressure measurement in a high current case. When PTFE particles of 1 – 2 mm in diameter were added to the tube a damping effect was observed, removing the high frequency oscillation. The trend lines with and without damping are close to each other, which are expected to reflect the general pressure variation pattern.

Compared with puffer circuit breakers, the process to establish the required gas flow conditions in the contact space in an auto-expansion circuit breaker during the current zero period is much more complicated with the existence of a unique “flow reversal” phenomenon, i.e. a transition between pressurisation of the expansion volume with hot vapour inflow and discharge of pressurised gas mixture from the expansion volume into the contact space. The interruption performance of an auto-expansion circuit breaker depends on the whole arcing history. It is thus expected that pressure variation in the arcing chamber is more abrupt than that in a puffer circuit breaker due to the fact that pressurisation of the expansion volume is closely coupled to the arc characteristics, different from the puffer circuit breaker where pressurisation is provided by an independent mechanical driving mechanism.

Up to date there has been very limited work to study the transient pressure variation in the arcing chamber of an auto-expansion circuit breaker. It was observed in [2][12] that the pressure fluctuates with large amplitude (around 20% of the peak value) in the expansion volume with SF₆ as the filling gas. However, there is no pressure record near the contact space since measurement of pressure in the contact space is extremely difficult as a result of the potential damage to the pressure sensors by strong arc heating and radiation. Early pressure measurement in the contact space was carried out in a used circuit breaker design [13] that is completely different from the modern ones, thus the pressure measurement does not provide much useful information to explain the transient pressure variation in modern auto-expansion circuit breakers. The effects of various factors including interrupting current level, arcing time, nozzle throat length and diameter etc. on the pressure variation in the expansion volume and compression volume have been investigated in a modern auto-expansion circuit breaker [14]. However, the influences of transient pressure variation on the interruption capability have not been mentioned.

The transient pressure variation in auto-expansion circuit breakers, especially that after flow reversal, is an important phenomena. A clear understanding is essential to product optimum design, which is not available up to date. The present work is devoted to elucidating how the transient pressure variation is formed during the interruption process of the breaker and how the key design parameters affect it. A model 245 kV auto-expansion circuit breaker of typical modern design is used in this

study. The arc model is verified by measurements in Section 5.3. Typical results obtained under different switching conditions are presented and analysed in Section 5.3. Conclusions are drawn in Section 5.6.

5.3 Verification of the Arc Model

Direct pressure measurement near electric arcs is extremely difficult due to the hostile environment, i.e. high temperature, strong optical radiation and high voltage. The insertion of a tube between the measurement point and the pressure sensor to shield heat, radiation and electric interferences bring additional complexity in interpreting the sensor output [15][16]. Therefore direct verification of the transient pressure variation prediction from the CFD simulation is prohibitively difficult for locations inside or close to the arc column.

In terms of computer simulation of the transient pressure variation in the contact space, the accuracy and reliability of the results from a proven CFD package with satisfactory solution convergence are controlled by a number of factors, which are given below:

- The total energy dumped into the arcing space and size of arc column. It can be shown that the arc voltage is very sensitive to the size of the arc column for a given current. A small segment of confined arc column can take up a considerable proportion of the overall arc voltage. Therefore, agreement in arc voltage is a key indicator of reasonable prediction of arc size and total energy dumped into the contact space. A reasonably predicted arc column size will lead to correct flow cross sectional area, especially in the main and auxiliary nozzles where flow is most confined.
- Mass rate of ablated PTFE material. Pressurisation of the expansion volume is a direct consequence of pressurised contact space. It can be shown that the maximum pressure in the expansion volume is closely related to the maximum pressure that can be reached near the nozzle surface (not the pressure on the axis that is sensitive to magnetic pinch effect in the conducting core of the arc column) in the contact space due to nozzle ablation. Therefore pressure prediction inside the expansion volume well matching the measurement indicates proper calculation of the radiative energy

flux reaching the nozzle surface that directly causes nozzle ablation. It also shows reasonable modelling of the pressure wave propagation inside the heating channel and expansion volume.

- Geometric change due to moving components in the arcing chamber. In the absence of an arc (no-load case), accuracy of pressure prediction is affected mainly by the method of modelling the moving components which change the gas flow passage in the operation of the breaker. Pressure measurement near the contact space is also relatively easy to perform. Therefore reasonably well predicted pressure variation in comparison with measurement in a no-load case serves as an indication of the appropriateness of the method to model the moving components in the CFD domain and validity of any geometric approximation.

There is strong argument to have confidence in the predicted transient pressure variation in arcing cases if reasonable agreement with measurement can be shown for the above three aspects. To this end the model used in the present work has been applied for simulation of the operation of an auto-expansion circuit breaker in next section for which measurement is available for comparison.

A schematic diagram of the circuit breaker under investigation is given in Figure 5.1. Geometric approximation has been made to some of the components moving in the simulation. The rounded tips of components A and B are replaced by rectangular shaped tips to numerically move these components. These approximations will not affect the flow field around the arc column. The rounded tip of the live contact is approximated by a set of coaxial rings with flat tips moving in the simulation according to the travel characteristics of the driving mechanism.

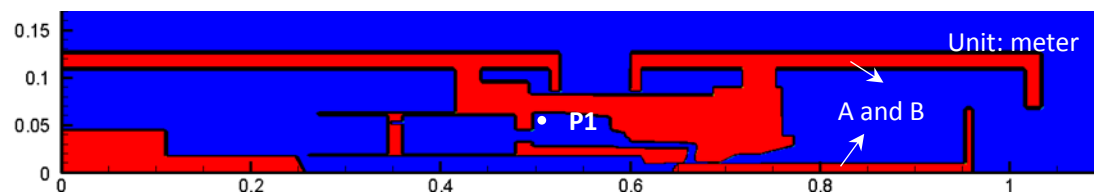


Figure 5.1: Geometry used in simulation of auto-expansion circuit breaker in the present investigation, the position of monitoring point P1 is assigned.

The arc model is set up by ISEE, an automated circuit breaker arc simulation

platform which allows a user to conveniently define the circuit breaker components, generate a grid system, specify the ablating surface areas and boundary conditions, configure the moving characteristics of movable components, manage different phases of the arcing process, and visualise the user required results [5]. The initial filling pressure of SF₆ is 0.6 MPa at a temperature of 300 K. The arc is initiated when the contacts separate at a distance of 8 mm at 17.2 ms. The initial current is set to 3 kA and ramped up to the true instantaneous current value in 0.3 ms. The validity of this method has been verified in previous work [18].

The measured travel curves of the contact together with the pressure variation in the expansion volume are given in Figure 5.2 for a no-load case and an arcing case. The two curves start to differ significantly at around 25 ms when the current reaches a high level and the pressure inside the expansion volume increases rapidly. The maximum difference between pressure prediction and measurement is 0.3 MPa, 5 % of the measured pressure. This level of agreement validates that the geometric approximation and the numerical scheme to move the components are reasonable.

The weak effect of arcing on the pressure variation in the expansion volume can be demonstrated by looking into the pressure variation in the no-load case and load case in Figure 5.2. Before 19 ms, the pressure variation in the expansion volume does not have significant difference between the no-load and arcing case because it is mostly caused by piston compression before the live contact moving into the main nozzle throat. Between 19 ms and 25 ms, measured pressure in the expansion volume shows that the local pressure is disturbed by the arc but not significantly affected. The predicted pressure at location P1 is more disturbed, possibly because the sudden insertion of a hot column in the contact gap, generating a stronger pressure wave propagating into the expansion volume. The pressure inside the expansion volume starts to increase rapidly at 25 ms when the tip of the solid contact moves into the main nozzle throat.

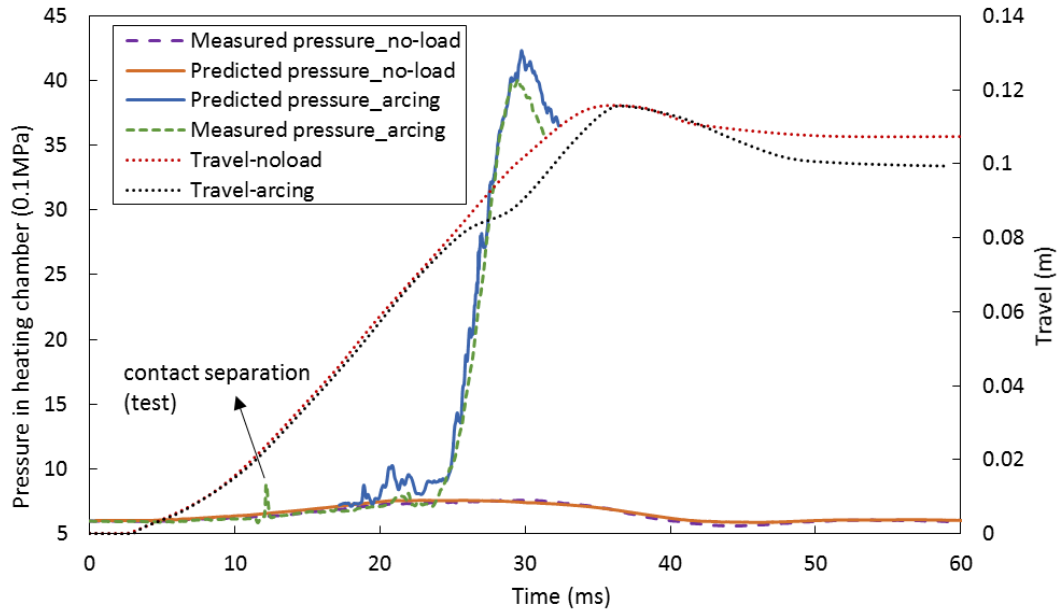


Figure 5.2: Predicted pressure variation in the expansion volume of the auto-expansion circuit breaker specified travel curve of the driving mechanism for no-load case and arcing case at 40 kA.

A comparison of the predicted and measured arc voltage is given in Figure 5.3. There is good overall agreement between the prediction and measurement. In the test, the contacts separation signal is generated at 12 ms. A complete and sustained contact separation should be identified from the arc measurement. There is noticeable arc voltage only until around 17 ms in the measurement. In the simulation the arc is initiated at 17.2 ms with a contact separation of 8 mm. In the first 2 ms of arcing (17.2 ms – 19.2 ms), the predicted arc voltage is higher than that from the measurement. This discrepancy is expected because the exact arc shape and temperature immediately following the breakdown of the contact gap is not known and an arbitrary hot column of 5 mm radius with a central temperature of 28,000 K is chosen to start the arc. In addition, the arc may not be axisymmetric at its very initial stage in reality. The higher predicted arc voltage indicates that the chosen hot column is smaller than that in the reality. Following its initiation the arc column adjusts itself according to the physical mechanisms represented by the governing equations. Previous work has shown that the influence of the uncertainty in initiating the arc is limited to the first 2 ms. Since the contact gap is relatively small, this uncertainty will not have a significant effect on the whole arcing process. By 20 ms the predicted arc voltage (238 V) is much closer to the measurement of 210 V.

The arc voltage is over-predicted from 25 ms to 27 ms, but well predicted for the rest of the arcing period. Theoretically, the arc voltage is largely determined by the size of the arc column, electrical conductivity of the arcing gas, and arc length. For a given current, a good agreement between predicted and measured arc voltage indicates that the predicted arc column size is reasonable and close to that of real operation. Preliminary results have clearly shown that the arc voltage is extremely sensitive to the size of the arc column [19]. A smaller arc column diameter leads to a higher arc temperature. However, the electrical conductivity above a certain temperature (30,000 K) is no longer sensitive to the temperature. Therefore the arc column size is the most influencing factor for total arc voltage.

In addition, the arc column size determines the effective flow cross area in the main nozzle throat. By predicting a reasonable arc column size, we have confidence in modelling the flow field and pressure variation in the arcing chamber. Over the period from the instant of arc initialization to the time corresponding to the pressure peak, the maximum pressure variation (rise) is 3.3 MPa in test and 3.5 MPa from simulation. Considering the possible experimental uncertainty, a 6.9 % relative difference is acceptable. The model has also been applied to other circuit breakers and the prediction agrees with measurement of pressure and arc voltage, such as in [2].

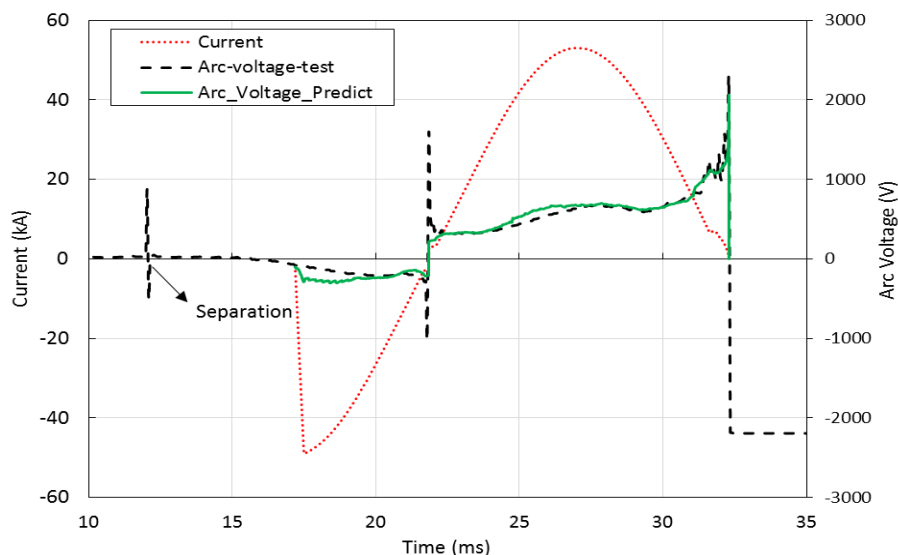


Figure 5.3: Predicted and measured arc voltage for the given current waveform. The measured arc voltage has been corrected to exclude the voltage drop in the metallic conductors between the voltage measurement points.

5.5 Results

On the basis that the arc model produces reasonable agreement between arc voltage prediction and measured values and also between predicted and measured pressures for the no-load and arcing cases, confidence is built up on the results of pressure variation. In producing the results below, the influence of grid system and boundary conditions have been checked carefully to ensure that the results are trustable. It is to be noted that in the simulation the nozzle and the hollow contact reassembly and the cylinder stay stationary and the solid contact and the piston move.

5.5.1 Mechanisms responsible for pressure variation

5.5.1.1 Pressure variation in the expansion volume

Variation in gas pressure is a consequence of temperature and gas density according to the equation of state of the gas, as described in Chapter 2. The change in temperature and density is not separable because the mass, momentum and energy equations are coupled. The root cause for the rapid pressure variation lies with the changing arc current and movement of the mechanical parts, especially the contact and piston.

The pattern of pressure variation in the arcing chamber is studied by recording the pressure changes at 11 locations, as shown in Figure 5.4. The first point P1 is inside the expansion volume and its position shown in Figure 5.1. The pressure near the nozzle wall such as P6 will be different from that on the axis such as P8 in the high current phase due to magnetic pinch effect. The positions of the solid contact tip at three different instants are also given for reference.

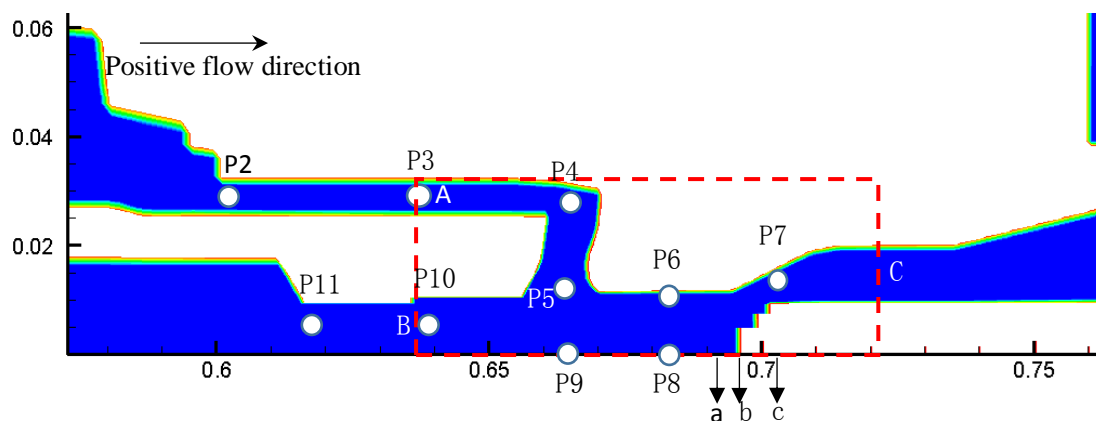


Figure 5.4. Arcing chamber with the monitor points P1- P11, P1 is in the expansion volume with position shown in Figure 5.1. The live contact tip position (a) at 29.7 ms (start of flow reversal), (b) 30.8 ms and (c) 32.3 ms (current zero)

As shown in Figure 5.2 and Figure 5.3, the arc is initiated at 17.2 ms. At this instant the pressure in the expansion volume is increased to 7.2 bar from its original value of 6.0 bar, the SF₆ filling pressure. The pressure variation in the expansion volume stays at a moderate level until 24 ms. During this period (17.2 – 24 ms), the piston moves a distance of 30.3 mm and the pressure increases by only 1.8 bar. This pressure variation is a combined effect of the piston movement and arcing. However the effect of arcing is expected to be small. The magnitude of the current changes from 3 kA to 23 kA. The arc column is confined in the hollow contact up to 18.9 ms and only a limited amount of hot gas runs into the heating channel causing mild pressure patch as shown in

Figure 5.5. The temperature in the heating channel (Point 3) increases rapidly after 18.9 ms (Figure 5.6), indicating hot vapor starts to flow towards the expansion volume when the arc column extends into the space between the main and auxiliary nozzles (Figure 5.7) and leading to a temporary surge of enthalpy flow into the expansion volume from 18.9 to 21ms, as shown in Figure 5.9.

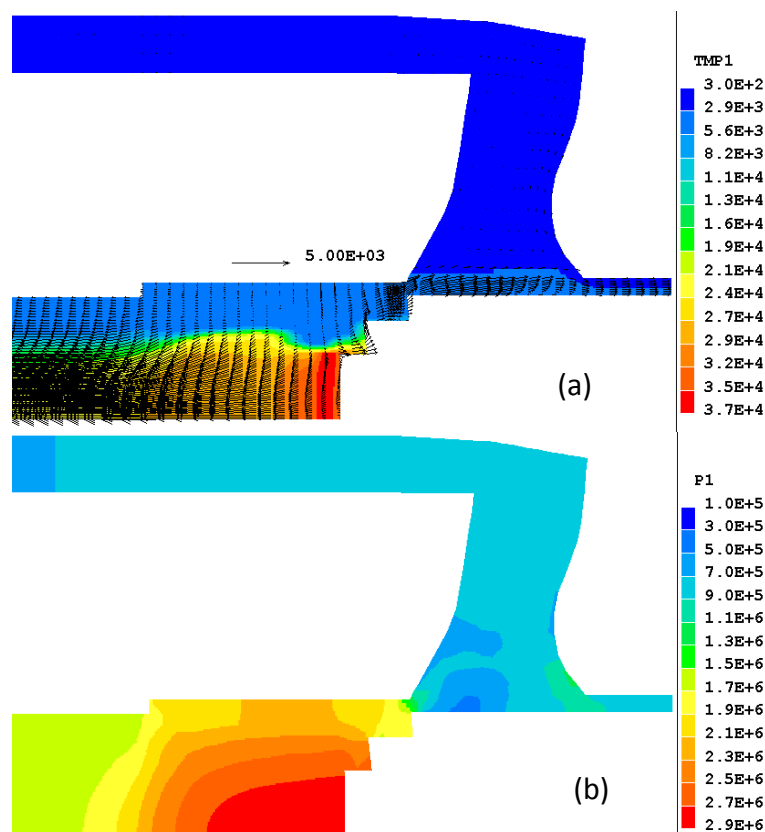


Figure 5.5. (a) Temperature and (b) pressure distribution with vector field at 18.9 ms

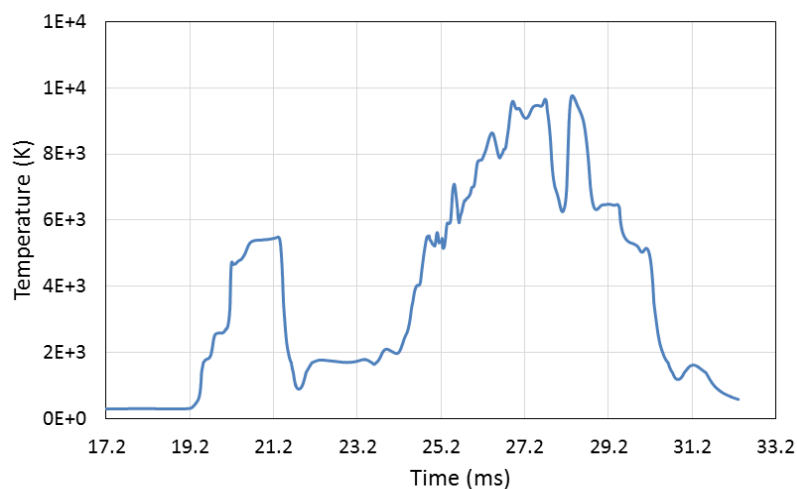


Figure 5.6: Temperature variation of the gas flow into the expansion volume at P3 in Figure 5.4

When the current is approaching the first zero point at 22 ms, the temperature in the heating channel drops to a low level, around 2,000 K. There is a small amount of energy flow out from the expansion volume from 21ms to 23 ms (Figure 5.9). The growth in arc length as a result of continued contact movement and increase in arc current generates more vapor from the PTFE surface (auxiliary nozzle and also the

surface of the heating channel). The current reaches 23 kA at 24 ms. The tip of the solid contact just moves into the main nozzle throat starting to generate PTFE vapor (Figure 5.7). These two factors combine to build up a high pressure zone around the arc column and pump hot gas towards the expansion volume. The enthalpy flow rate through the cross section A in the heating channel reached its maximum value 1.7×10^7 J/s at 26.8ms (Figure 5.9) when the live contact travels to the middle of main nozzle throat (Figure 5.8). Meanwhile, the gas is exhausted from the hollow contact with a high enthalpy flow rate (1.2×10^7 J/s). From Figure 5.10, the total mass flow out from the arcing space through cross section B (hollow contact) and C (main nozzle exit) are almost the same, however the former dominates the energy loss process. The pressure rise is shown in Figure 5.11. As already explained in [22] the pressure rise in the expansion volume is more affected by the thermal energy flux brought with the vapor than the mass flux.

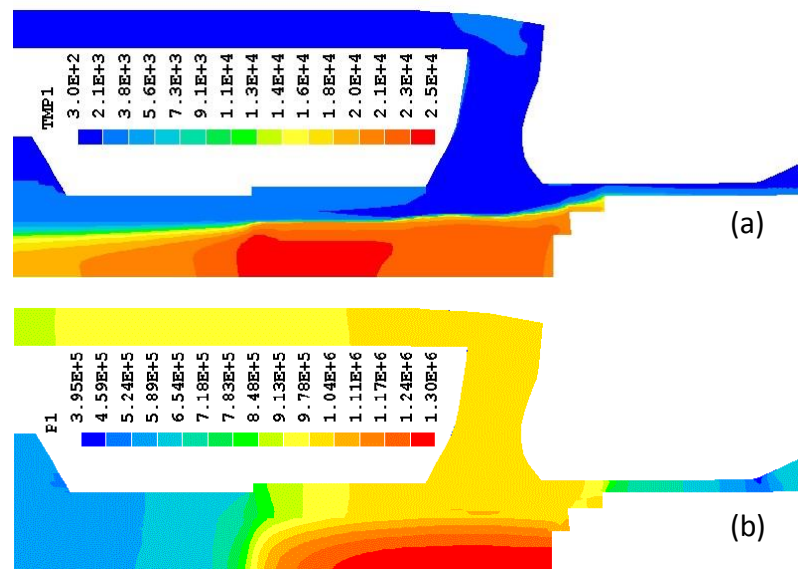


Figure 5.7: (a) Temperature and (b) PTFE concentration in the arcing chamber at 24 ms

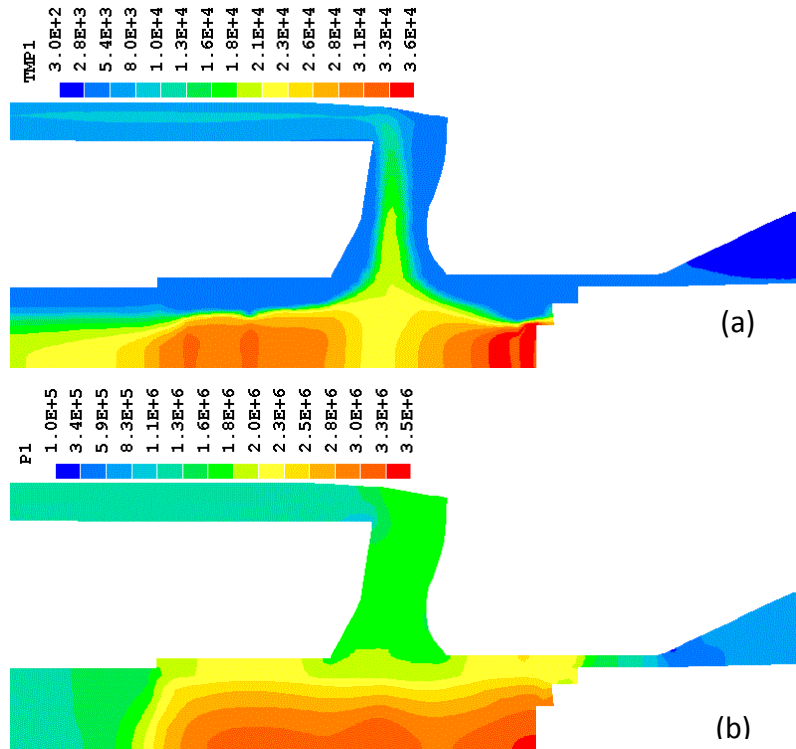


Figure 5.8: (a) Temperature and (b) pressure distribution with vector field at 25.5 ms

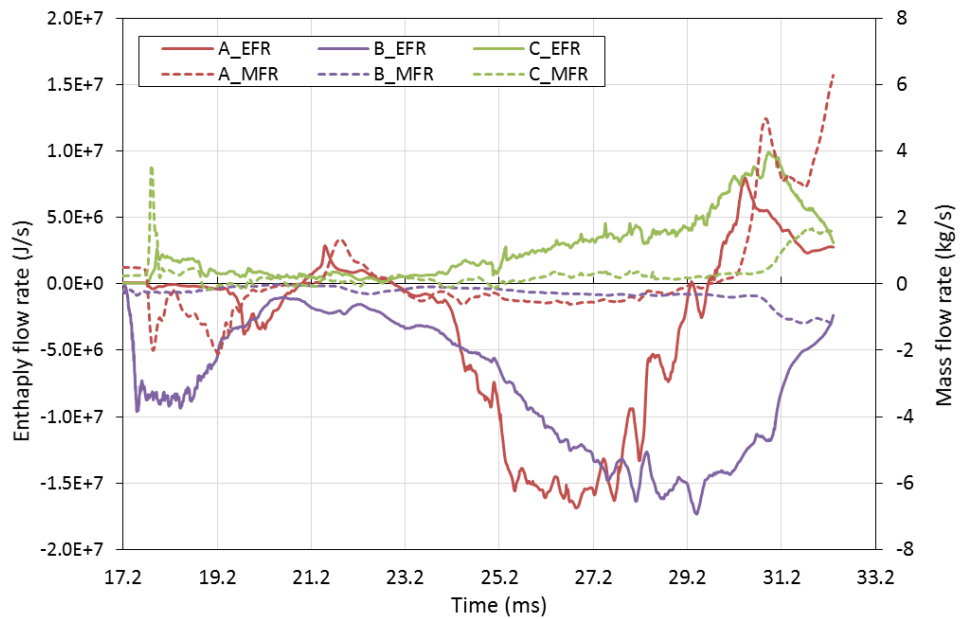


Figure 5.9: Enthalpy flow rate ($\int \rho \omega \cdot 2\pi r dr$) and mass flow rate ($\int \rho \omega h \cdot 2\pi r dr$) from cross section A, B and C which assigned in Figure 5.4;

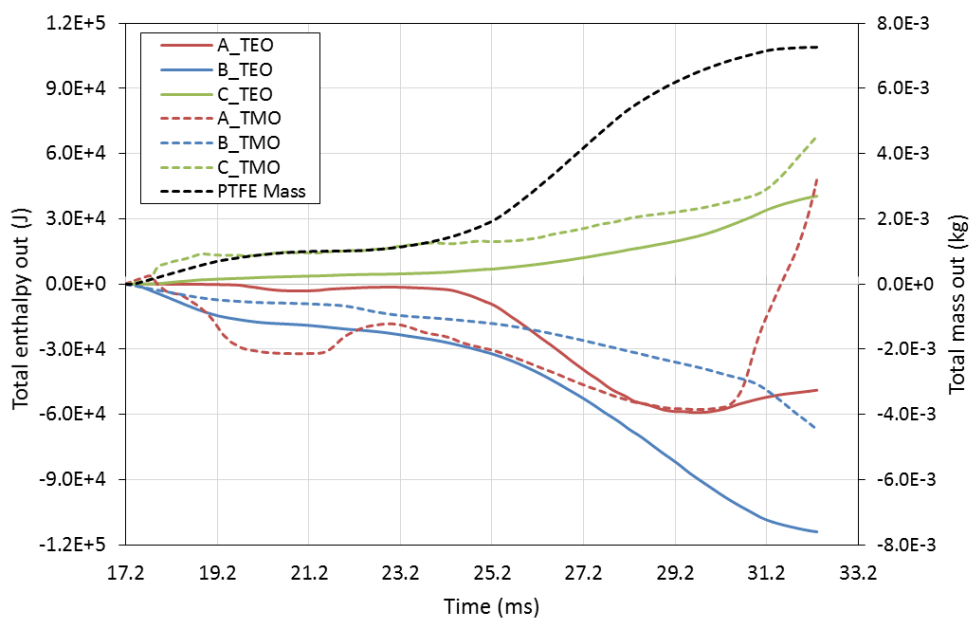


Figure 5.10: Total mass ($\iint \rho \omega \cdot 2\pi r dr dt$) and enthalpy in/out ($\iint \rho \omega h \cdot 2\pi r dr dt$) from cross section A, B and C which assigned in Figure 5.4; “-” means the flow travels in negative direction (positive direction assigned in Figure 5.4).

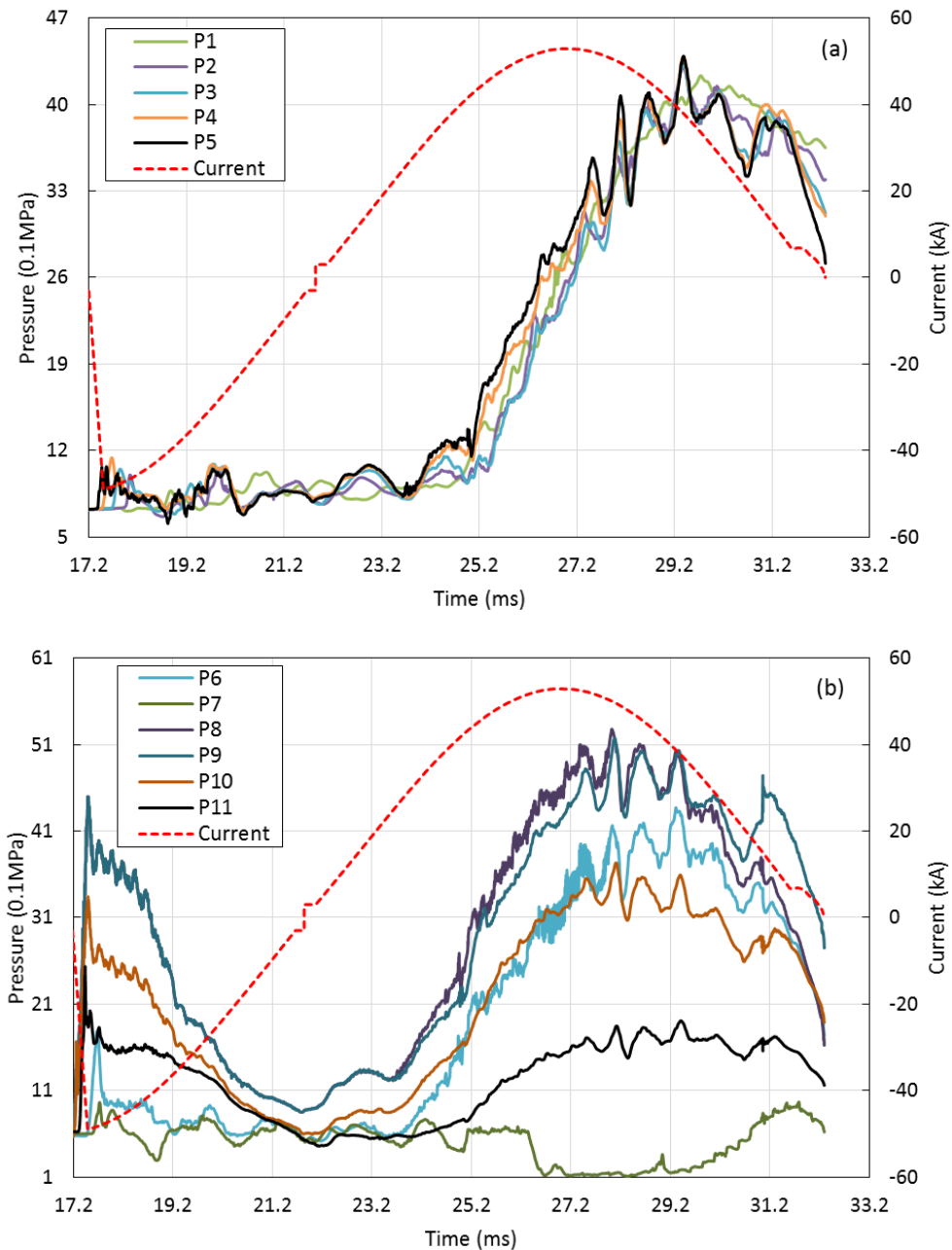


Figure 5.11: Pressure variation for P1 to P11 with current waveform from arc initialisation to the final current zero with their location in Figure 5.4

The initial gas mass and enthalpy contained in the expansion chamber is respectively 17.2 g and 6.6 kJ. Figure 5.9 clearly shows that the enthalpy flux in the expansion volume starts to increase at a high rate at 24 ms. A total of 58.7 kJ of enthalpy flows in the expansion volume at 29.2 ms, which is 8.9 times the original enthalpy content of SF₆. It is clear from Figure 5.6 that the vapor has an increasing temperature when the current increases in the period from 24 ms to 27 ms where the current reaches its peak. On the other hand, the maximum mass increase in the expansion volume with

reference to that at 17.2 ms is 4 g at 29.2 ms, it is only 23% of the initial mass of SF₆ (17.2 g). It is therefore the thermal content of the PTFE vapor that is responsible for the pressurization of the expansion volume.

5.5.1.2 Pressure variation in the arcing space

The inflow of hot vapor into the expansion volume is a result of the pressure difference between P4 (inlet of heating channel) and P1 (expansion volume). From Figure 5.11a, it can be seen that before 24 ms, the pressure in the expansion volume (P1) and that at the entrance of the heating channel (P4) does not follow a clear order in their largeness. As discussed above the overall pressure change is largely influenced by the piston movement and hot vapor generated by the short length arc. From 24 ms, the pressure starts to increase rapidly at P4 and P5. Between 24 ms and 27.5 ms, it follows $P5 > P4 > P1$, as expected from the pumping mechanism. It is this pressure difference that pumps the vapor into the expansion volume.

The root cause for the pressurization process in the expansion volume is the ablation of the PTFE nozzles. Ablation is caused by arc radiation interacting with the PTFE material. Figure 5.12 depicts the radiative power received by the two nozzles in the arcing process. The solid contact tip moves out from the auxiliary nozzle at 20.8 ms when the current is approaching the first zero point, thus the power flux hardly reaching the main nozzle surface. It can be seen that before 22 ms, the arc radiation only interacts with auxiliary nozzle. After the first current zero, the arc radiation is almost equally divided between auxiliary and main nozzle. Radiation reaching the main nozzle surface starts to overtake that on the auxiliary nozzle at 25.9 ms when the arc column extends into the main nozzle at high current, causing severe ablation.

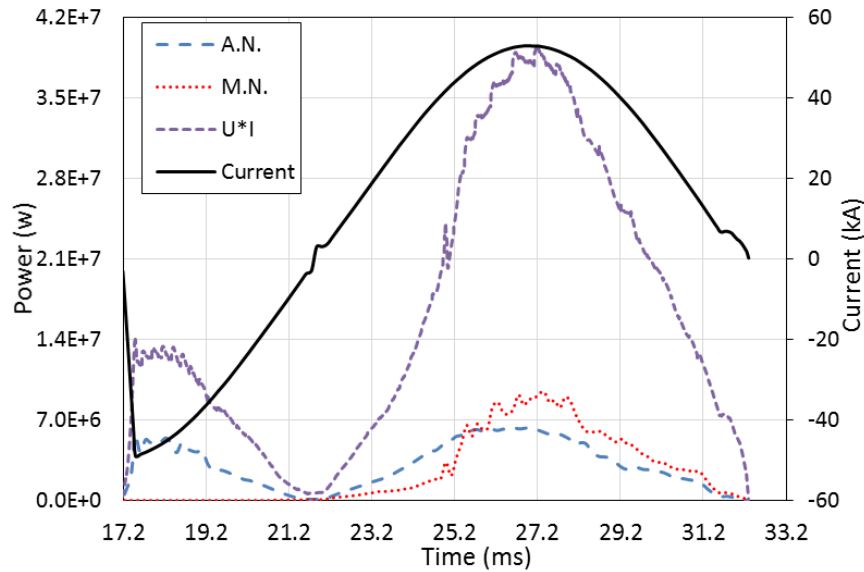


Figure 5.12: The power flux normal onto the ablating surface, $Q_{ablation} = \xi(1 - \alpha) \iint_0^{R_{833}} q \cdot 2\pi r dr dz$, at main PTFE nozzle (M.N.) and auxiliary nozzle (A.N.), where ξ is the coefficient which is determined by the ablation surface incline, α is the reabsorption factor, q is the net radiation loss per unit volume and time.

A striking feature of the pressure variation pattern is that the pressure at P4 and P5 starts to oscillate from 27.5 ms when the current starts to drop from its peak value, which is in agreement with the pressure measurement [8][9][15]. The reasons are complicated because multiple mechanisms are operating and closely coupled during this period.

When the arc current starts to drop, electrical power input starts to reduce, which immediately leads to a reduction in the radiation reaching the nozzle wall for PTFE ablation, as shown in Figure 5.12, through temperature decrease. On the other hand, the mass of gas mixture flowing out of the arcing zone through the hollow contact, the exit of the main nozzle and the heating channel towards the expansion volume is mild (Figure 5.9), which is not expected to have a strong influence on the onset of the pressure variation. The mass in the arcing space remains relatively constant, as given in Figure 5.13. It does not have any oscillations corresponding to the pressure oscillation. Thus the change in mass is unlikely to be a factor responsible for the pressure variation.

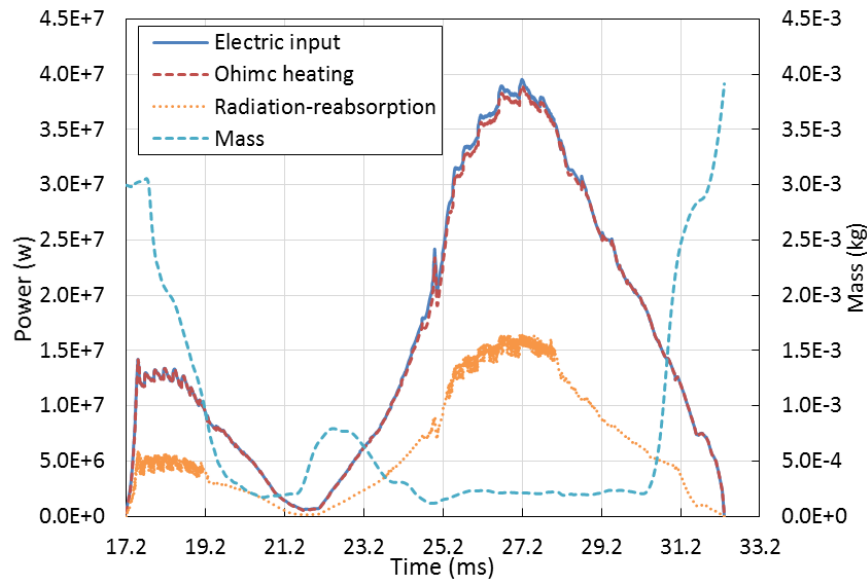


Figure 5.13: Power and mass confined in the arcing chamber which is highlighted in flash box in Figure 5.4

The next factor to be considered for the pressure oscillation is the ablation of PTFE. The total ablation rate as a function of time is proportional to the radiation reaching the ablating surfaces (Figure 5.13). It can be seen that there is no matching oscillatory pattern starting at 27.5 ms. Thus nozzle ablation, although contributing to the onset of pressure drop in the arcing space, it is again not a factor controlling the oscillation of pressure.

Thus the remaining factors can only be energy- related or aerodynamic related, i.e. propagation of pressure waves. One obvious feature in the energy flux in Figure 5.9 is that both the energy fluxes into the expansion volume and the hollow contact have oscillatory behavior starting at 27 ms. The energy flux out through the exit of the main nozzle does not change abruptly because the main nozzle is still blocked by the solid contact. In view of the fact that the mass fluxes do not oscillate, it is pretty certain that it is the energy related process and pressure wave propagation that is responsible for the pressure variation from 27.5 ms and 30.2 ms. The turning point in Ohmic heating from increasing to decreasing is a critical point for the onset of large pressure oscillation. It is also to be noted that the pressure in the heating channel (P2 and P3) and near the arc column (P4 and P5) start to be in phase and unified in the period from 27.5 ms to 30.2 ms in Figure 5.11.

Flow reversal is a term used in the operation of an auto-expansion circuit breaker to signify the transition of gas flow from being into the expansion volume to being out from the expansion volume. It is a direct consequence of the reduced pressure in the contact gap as a result of decrease in arcing current, in the period several milli-second before the final current zero. It is the starting point to build up the flow field in the contact gap to prepare for arc quenching at current zero.

For the circuit breaker under investigation, the flow reversal occurs at 29.7 ms soon after the pressure inside the expansion volume reaches its maximum and the mass flow rate in the heating channel change from negative to positive, as indicated in Figure 5.10. At this point, the instantaneous current already drops to 32 kA from its peak value of 52 kA. As a result, the arc column size rapidly shrinks and the radiation reaching the nozzle surface becomes half or even less than half of the radiative power at the peak current (Figure 5.13). The shrinkage in arc size and reduced PTFE ablation both contribute to the rapid reduction in pressure in the contact space, which triggers the flow reversal. The pressure and temperature distribution at 30.2 ms are given in Figure 5.14.

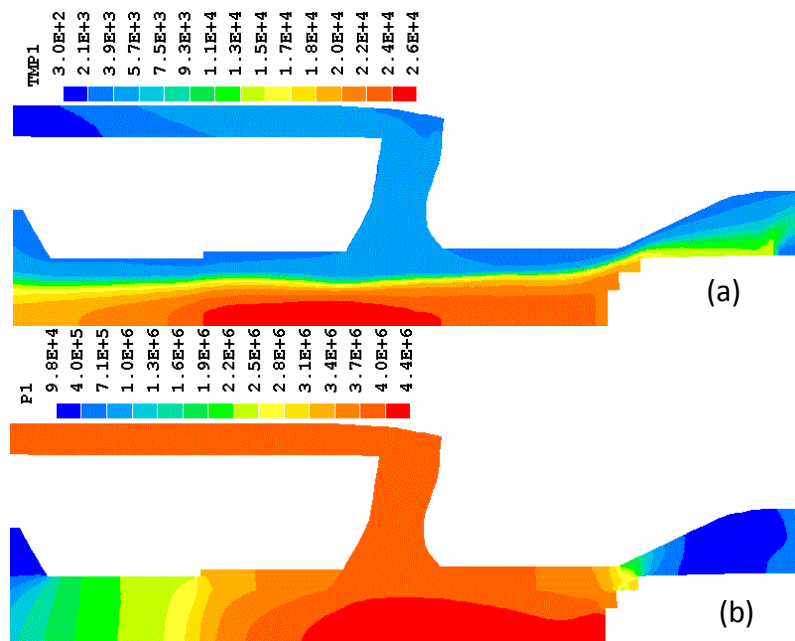


Figure 5.14: (a) Temperature and (b) pressure distribution at 30.2 ms

Before flow reversal, 3.8g of SF₆-PTFE gas mixture is pumped into the expansion volume, bringing an energy of 6×10^4 J into the expansion volume. This leads to a

pressure rise of 3.5 MPa. At the instant of flow reversal at 29.7 ms, pressure in the heating channel (P2 and P3) and near the arc (P4 and P5) all reach their lowest value of approximately 3.9 MPa (Figure 5.15) while the pressure in the expansion volume reaches its highest value of 4.2 MPa. Although during the period between 27.2 ms to 29.7 ms there are oscillations and the pressure in the contact space is temporarily lower than that in the expansion volume on several occasions, the temporary pressure difference is not able to overcome the momentum of the vapour moving into the expansion volume. It only reduces the mass and enthalpy fluxes into the expansion volume (Figure 5.9).

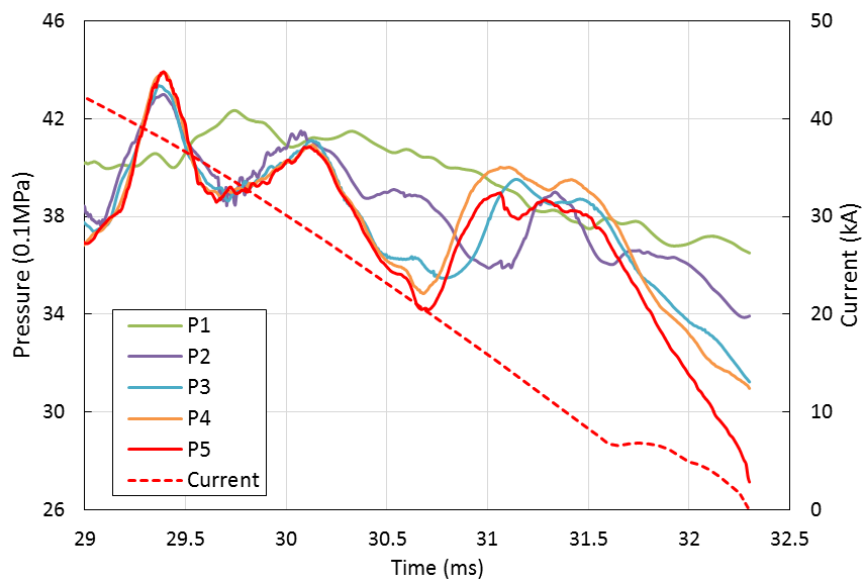


Figure 5.15: Pressure variation at 5 monitoring points with their location in Figure 5.4.

The lag between flow reversal (pressure peak in the expansion volume) and peak current is 2.6 ms, from 27.1 ms to 29.7 ms. Examining the enthalpy and mass fluxes over this period in Figure 5.9 and neglecting the oscillations, it becomes clear that the mass and enthalpy fluxes out of the main nozzle and the hollow contact remain rather constant. The only significant change is the enthalpy and mass fluxes into the expansion volume. The reduction of the enthalpy flux is a direct consequence of the reduction in electrical power input into the contact space and nozzle ablation. The injection of PTFE vapour not only adds mass into the flow domain, but also recovers the energy loss from the arc column through radiation.

The average enthalpy flux into the hollow contact is 14.5 MJ/s and that exhausted

from the main nozzle is 4 MJ/s in the period from 27.1 ms to 29.2 ms. At the point of flow reversal the enthalpy flux into the expansion volume is zero. Neglecting the change of enthalpy content in the contact gap, the above two enthalpy fluxes should be balanced by the Ohmic heating. Equating the sum of the above two fluxes with the Ohmic heating curve in Figure 5.13, then an estimated flow reversal time can be obtained, which is 30.3 ms, giving a time lag of 3.1 ms. It is 0.6 ms after the computed flow reversal time, or 23% of the time lag of 2.6 ms after the current peak. It can be concluded that flow reversal is triggered by the inadequate power supply from the current with respect to enthalpy exhaustion out of the contact gap. Once flow reversal starts, enthalpy flux into the contact gap from the expansion volume quickly increases (29.7 ms to 30.4 ms in Figure 5.9). Since the gas temperature inside the expansion volume is generally low (Figure 5.16), soon after flow reversal, cool gas flows out from the expansion volume (temperature drop in Figure 5.6 for P3) and the high enthalpy flux is replaced by high mass flux of the cool gas from the expansion volume (Figure 5.9 at 30.3 ms). As a result, the mass stored in the contact space increases rapidly (Figure 5.13). The arc column and velocity field at 30.8 ms are given in Figure 5.17.

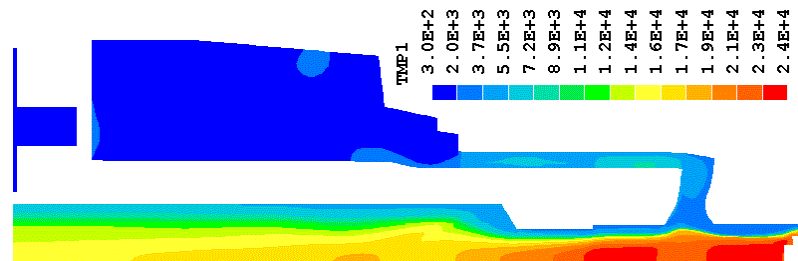


Figure 5.16: Temperature distribution at 29.7 ms at the instant of flow reversal.

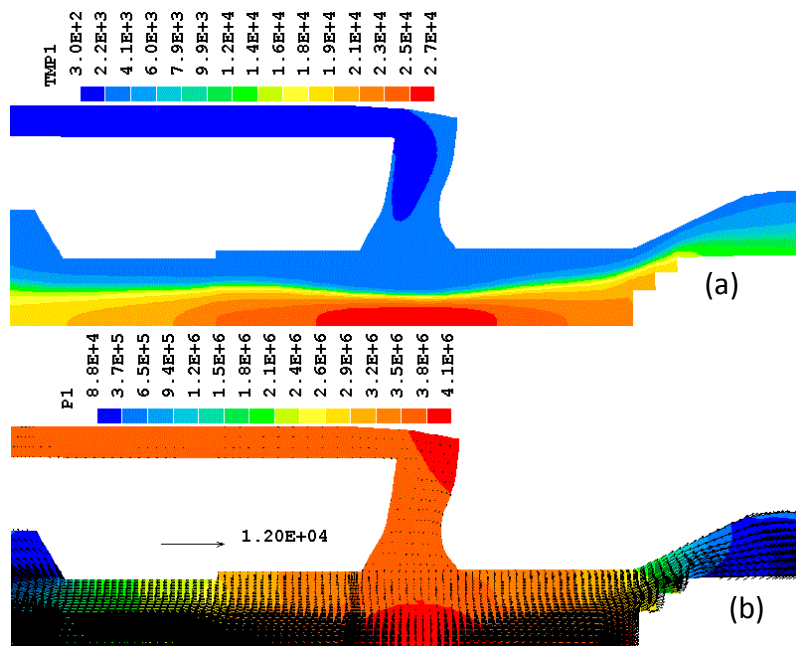


Figure 5.17: (a) Temperature and (b) pressure distribution with vector field at 30.8 ms

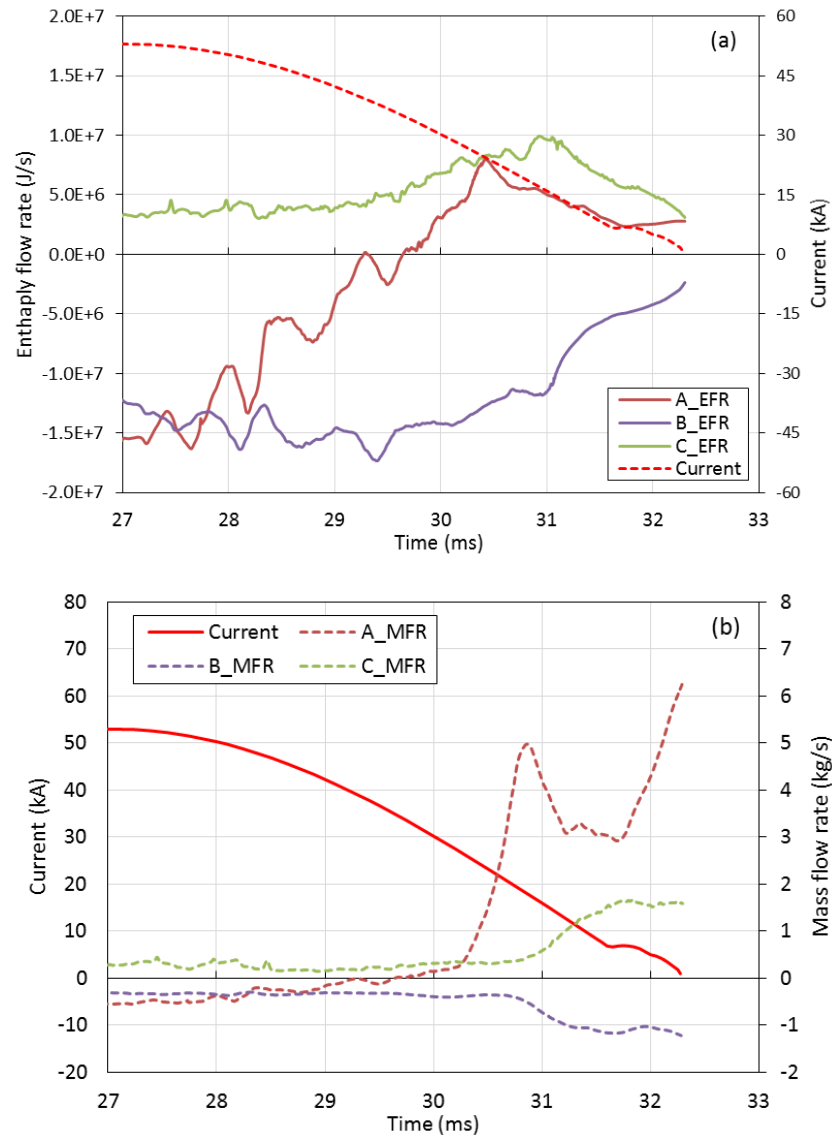


Figure 5.18: Diagram showing the (a) enthalpy flow rate and (b) mass flow rate as a function of time out of the expansion volume (A_MFR), into the hollow contact (B_MFR), and out of the main nozzle (C_MFR). The sign of the values is with reference to the positive axial direction which is pointing from the hollow contact to the main contact.

5.5.1.3 Flow field at current zero

As discussed above the pressure inside and near the arc column drops to their minimum at 30.7 ms (Figure 5.11) as a result of insufficient energy supply to maintain the energy exhaustion from the two nozzles. At this instant, the cool gas from the expansion volume rushes out due to the pressure difference. The gas is of

low temperature (1500 K, Figure 5.6) and high mass flux (Figure 5.9). It is interesting to see that at this instant the enthalpy flow rate into the contact gap is much lower than that out of the contact gap (Figure 5.18a). The enthalpy rate is 8.08 MJ/s out of the main nozzle, 11.5 MJ/s that into the hollow contact, and 5.5 MJ out of the expansion volume into the contact gap (Figure 5.18a). The electrical power input is 12 MJ/s. The power input rate is 17.5 MJ/s, slightly lower than the out rate of 19.6 MJ/s. However, the mass flow rate pattern is very different. The mass flow rate into the hollow contact is 0.38 kg/s, 0.35 kg/s out of the main nozzle, close to each other. The mass flow rate from the expansion volume is however much larger, reaching 2.97 kg/s or 4 times the sum of the two outgoing mass fluxes. In addition there is a PTFE ablation rate of 0.4 kg/s. This temporary surplus of mass inflow into the contact gap results in a pressure surge with a peak value of 3.9 MPa at 31.1 ms. The rapid change in pressure and flow field generates pressure waves and it can be seen that the pressure at P2 which is close to the expansion volume behaves very differently from that at P4 while P2 continues to decrease from 30.7 ms to 31.1 ms, P4 keeps increasing in Figure 5.15.

The pressure and flow field adjust themselves over the period from 31 ms to 31.5 ms and finally settle down to their individual values. The pressures at different locations start to move towards different values from 31.5 ms, depending on their location in the domain. At current zero the pressure drop is in the order of expansion volume (P1), entrance of expansion volume (P2), entrance of heating channel (P3), upstream of main nozzle throat (P4) and near the stagnation point (P5), following the path of flow. The pressure drops by 1 MPa from inside the expansion volume to the point near the stagnation point, as shown in Figure 5.15. Figure 5.11 also shows that the pressure at the arc centre (P8) equalises with that near the nozzle surface (P6) when the magnetic pinch effect at low current becomes insignificant. Pressure further downstream, such as that in the hollow contact (P11) and at the exit of the main nozzle throat (P7) becomes much lower than that near the stagnation point (P5) as expected. The arc column and flow field at current zero are given in Figure 5.19.

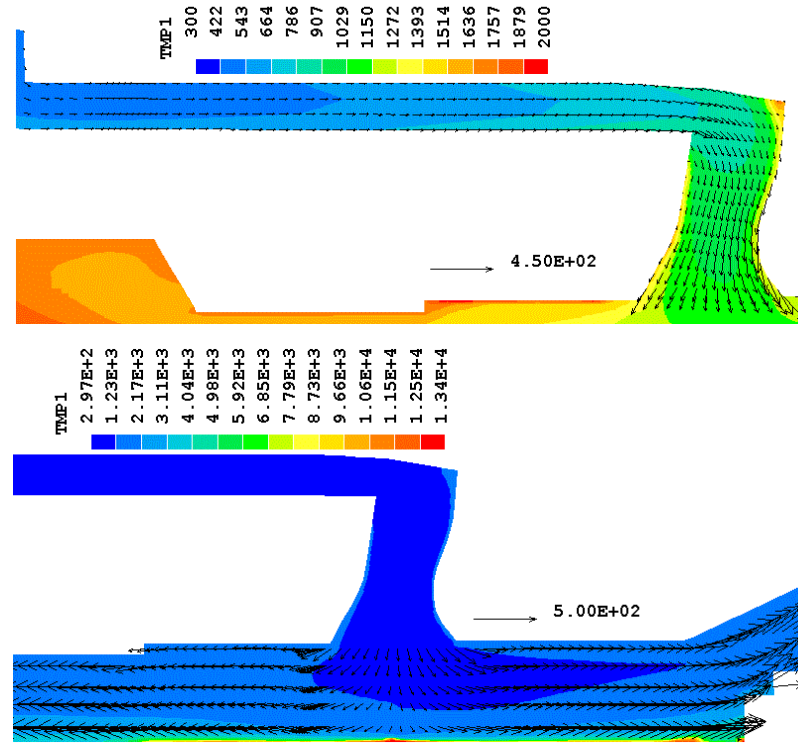


Figure 5.19: Temperature and flow field at current zero, in the heating channel (top) and in the arcing space (bottom).

From the above discussion it can be concluded that:

- The pressure oscillation before and around the peak current is a result of energy related process and pressure wave propagation;
- Flow reversal in auto-expansion circuit breakers is triggered by an insufficient electrical power supply, leading to an overall cooling of the gas and therefore pressure drop in the contact gap;
- Immediately after flow reversal an inrush of energy followed by an inrush of mass from the expansion volume results in a surplus of mass inflow with respect with gas outflow from the contact gap, leading to a temporary pressure increase in the contact gap;
- The pressure and flow field takes about 0.5 ms to adjust themselves to finally establish the flow and pressure field for arc quenching in the current zero period.

The time lag between the current peak and pressure peak is controlled by the enthalpy exhaustion rate through the hollow contact and the main nozzle exit. Flow

reversal takes place when the enthalpy exhaustion rate equals the electrical power input after the current peak. In this sense, a higher power frequency such as 60 Hz will result in a smaller time lag.

5.5.2 Different arc durations

A circuit breaker needs to perform different switching duties in their service with different arc durations. In this section the transient pressure variation with different arc durations is studied. Three cases are used with arc duration of 18.8 (long), 16.9 (medium) and 15.1 (short) ms at the same current levels. The contact travel is the same for all three cases. The filling pressure is 0.6 MPa absolute.

5.5.2.1 Comparison of pressure rise in the expansion volume

The pressure variation in the expansion volume for all three cases are given in Figure 5.20. The general profile is similar to that discussed in Section 5.5.1. Despite the difference in the arc duration, the pressure peak is more or less the same. In the first arcing stage up to 24 ms. The arc is burning in the hollow contact or in the interspace between the two nozzles. In the short arc duration case the current is rapidly approaching the current zero point and nozzle ablation does not contribute much to the expansion volume, therefore the pressure in the expansion volume remains low. In the long arc duration case the arc burns at its peak current around 20 ms and this induces much ablation in the auxiliary nozzle (Figure 5.21a). As a result the pressure rise in the expansion volume is more significant, reaching an average of 1.8 MPa in the process of oscillation.

The pressure in the expansion volume in the short arc duration case reaches its peak earlier because the current in this case increases towards its peak value when the tip of the solid contact moves into the main nozzle throat. Because in this case the main nozzle is blocked by the solid contact so nozzle ablation by arc radiation is most effective in pumping the nozzle vapor into the expansion volume. In the long arc duration case, despite the initial pressure rise, the arc current passes its zero point when the solid contact tip moves into the main nozzle, discharging some of the gas from the expansion volume (Figure 5.21a) when the current approaches its peak, the

solid tip already clears the main nozzle throat and a significant part of the vapour from nozzle ablation is directly discharges in the exhaustion volume downstream and does not contribute to pressurization of the expansion volume. This is why in the second half cycle of the current the pressure rise in the expansion volume is only 2.3 MPa, which is lower than that in the short arc duration case which is 3.2 MPa. In addition, the mass flow rate from the expansion volume at current zero is highest in the short arc duration resulting in a steeper pressure drop just before the current zero point. The total mass and enthalpy flowing into the expansion volume are given in Figure 5.21b. The temperature distribution at the first current zero and peak current are respectively given in Figure 5.22 and Figure 5.23.

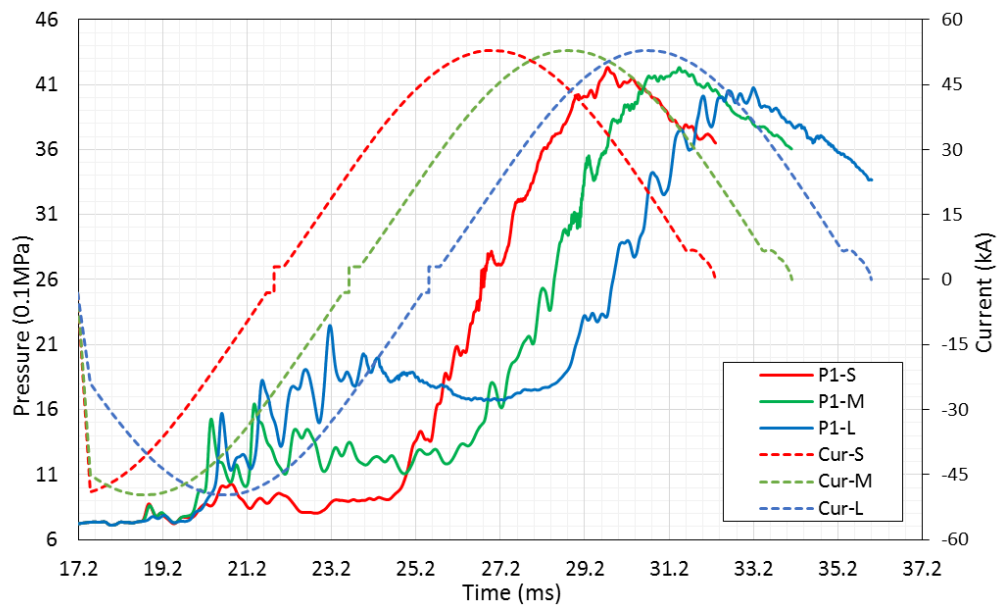


Figure 5.20: Pressure rise in the expansion volume for different arc durations

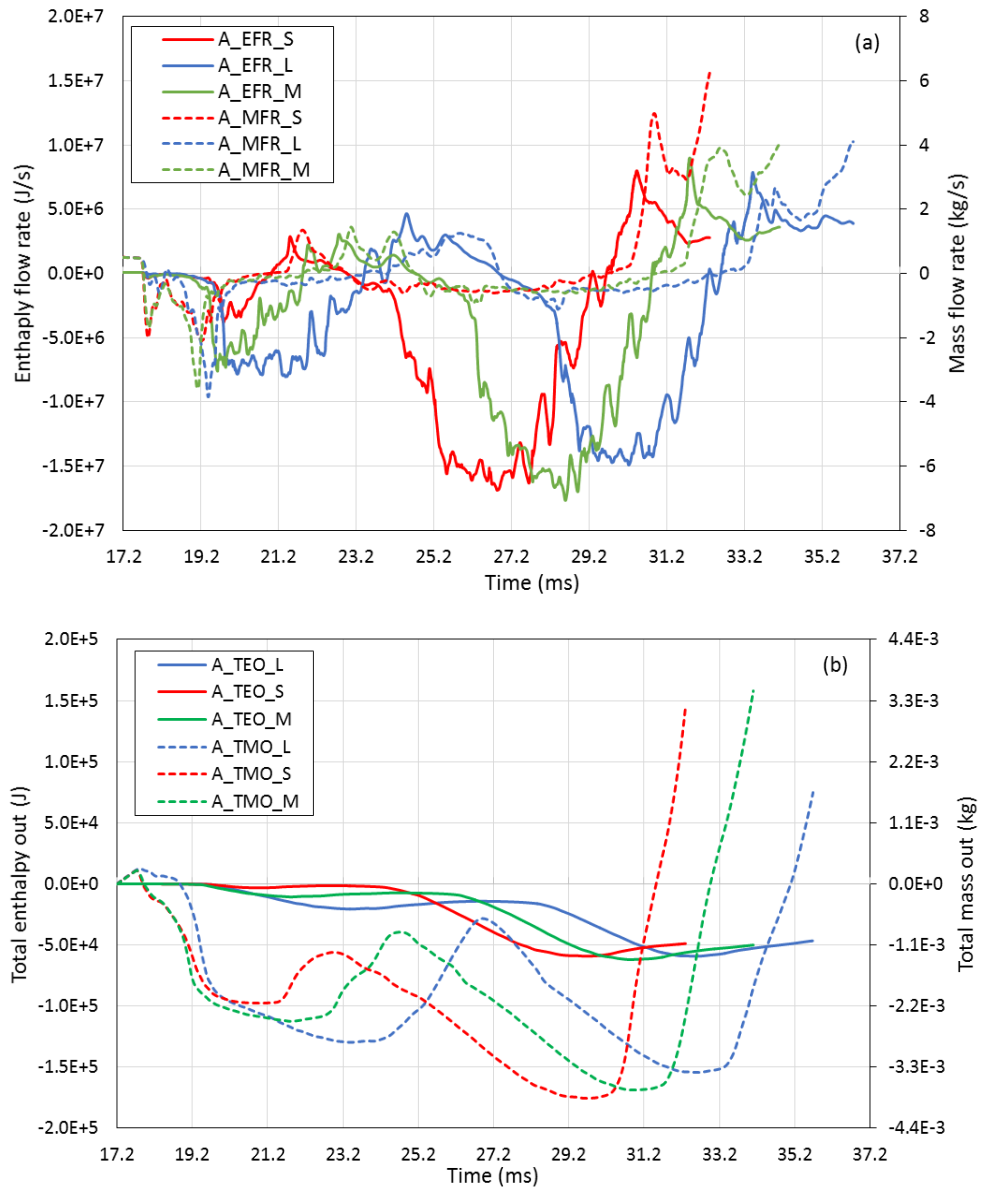


Figure 5.21: (a) Mass and enthalpy flow rate (b) Total mass and energy into the expansion volume through cross section A for different arc durations

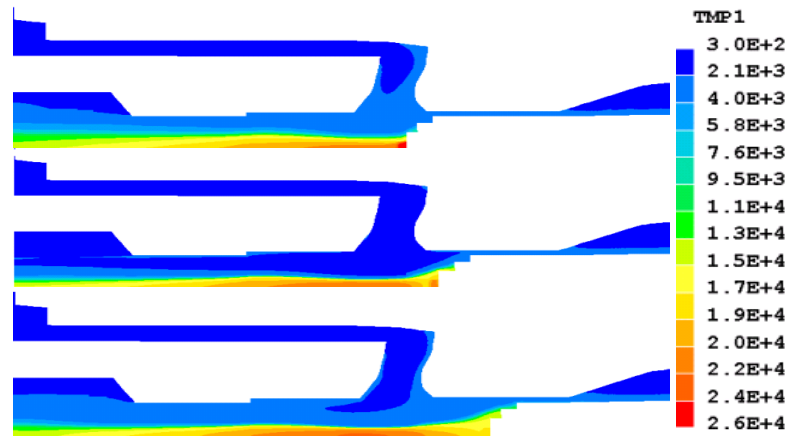


Figure 5.22: Temperature distribution at first current zero for short, medium, long arc duration cases at 21.8 ms, 23.6 ms and 25.5 ms, respectively

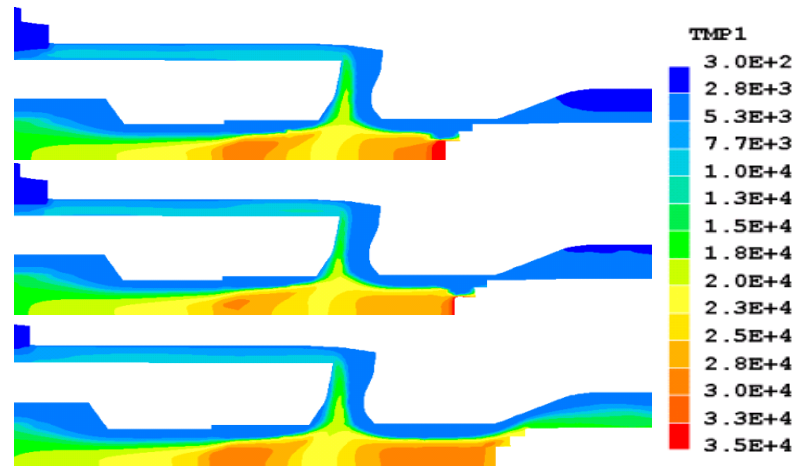


Figure 5.23: Temperature distribution at final current peak for short, medium, long arc duration cases at 27.1 ms, 28.9 ms and 30.8 ms, respectively

5.5.2.2 Comparison of pressure in the arcing space

Because of the pressure fluctuation after flow reversal, the pressure change in the arcing space has different pattern from that in the expansion volume. However it bears much of the patterns described in Section 5.5.1 and will not be analysed in details. At current zero, the pressure in the expansion volume for the long arc duration is the lowest, while the pressure in the arcing space (P5 with its location given in Figure 5.4) for short arc duration becomes the lowest (Figure 5.24). This matches well with Figure 5.25 that displays the pressure on the axis at current zero. The axial velocity on the axis for the three cases is given in Figure 5.26.

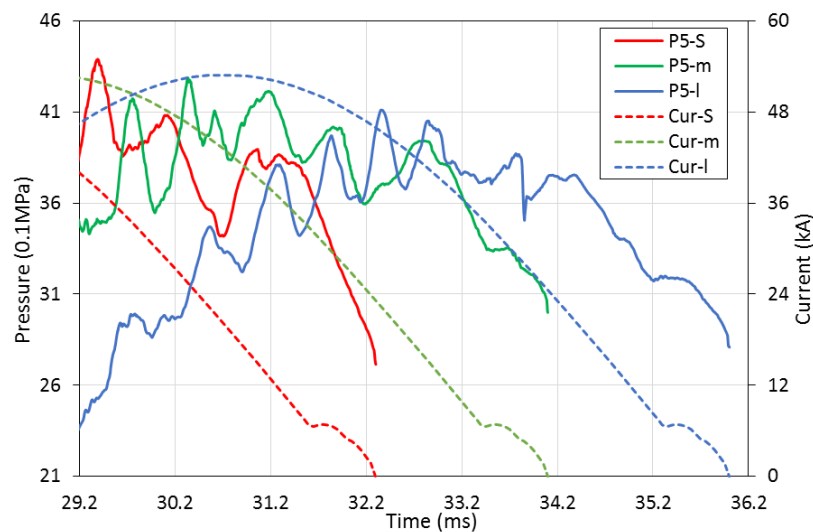


Figure 5.24: Pressure variation in the arcing space for different arc durations

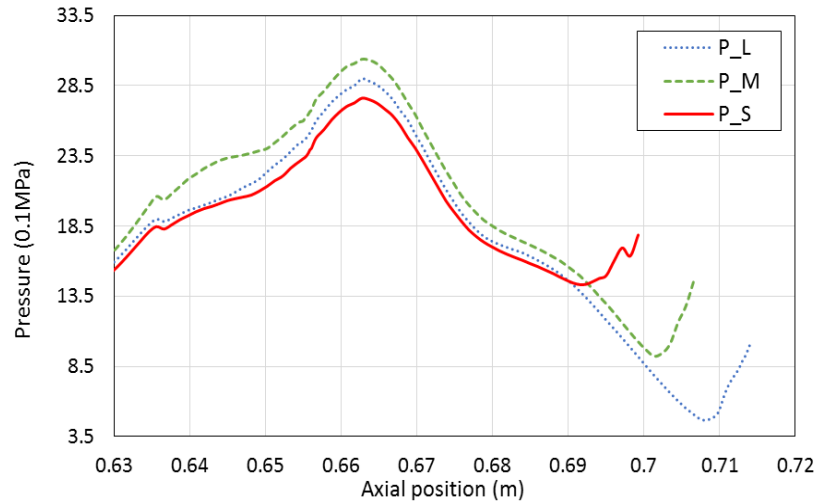


Figure 5.25: Axis pressure at current zero for different arc durations

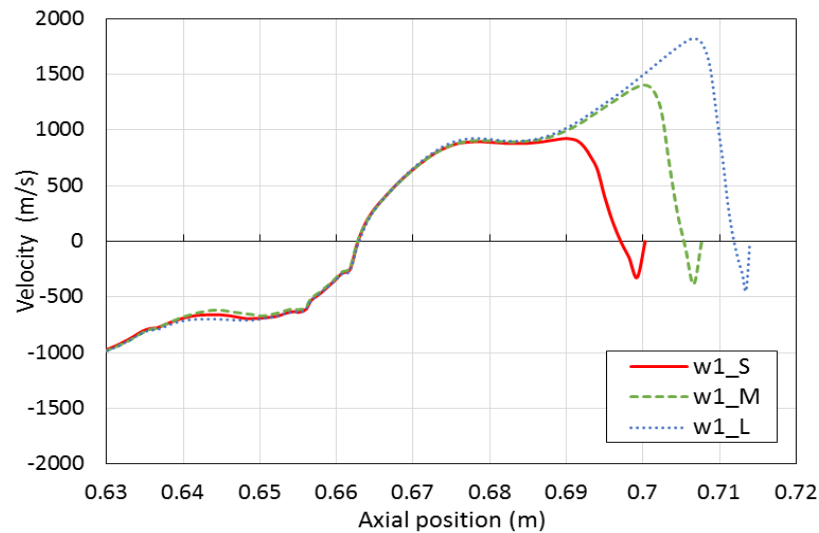


Figure 5.26: Axial direction component of axis velocity at current zero for different arc durations

To investigate the thermal interruption capability in terms of the critical rate of rise of recovery voltage (RRRV) of this circuit breaker, a linearly increasing voltage at a given rate of rise of the recovery voltage (dV/dt) is applied after current zero. The critical RRRVs for short, medium and long arc durations are, respectively, 7.5 kV/us, 9 kV/us and 9.5 kV/us. The critical RRRV not only depends on the pressure in the nozzles but also on the length of the arc column. Therefore a clear correlation between the pressure distribution and critical RRRV cannot be established, given the fact that the arc column size and temperature vary substantially along the axis.

After current zero, due to the strong turbulence cooling, the axis temperature at the arc region keeps decreasing as Figure 5.27 shows. The pressure on axis for the medium arc duration case is highest, while the axis temperatures for the other two cases are close to each other. Therefore, the critical breakdown voltage for the medium arc duration case should be initially larger than other two cases. The axis temperature is below 3000 K after 30 μ s. When the temperature is higher than 3000 K, the critical electrical field is low as Figure 5.28 shows [21], the breakdown voltage within 30 μ s therefore keeps at a constant value in Figure 5.29a. Only when the temperature drops to a particular value, around 3,000 K, the critical breakdown voltage starts to increase rapidly. The temperature on the axis decreases with a decreasing rate. Most temperature drop occurs within the first 5 μ s after current zero. However, the pressure does not have significant change within a short period after current zero [21]. Therefore, the pressure in the arcing space at current zero and the temperature decreasing rate after current zero are two critical factors for dielectric recovery.

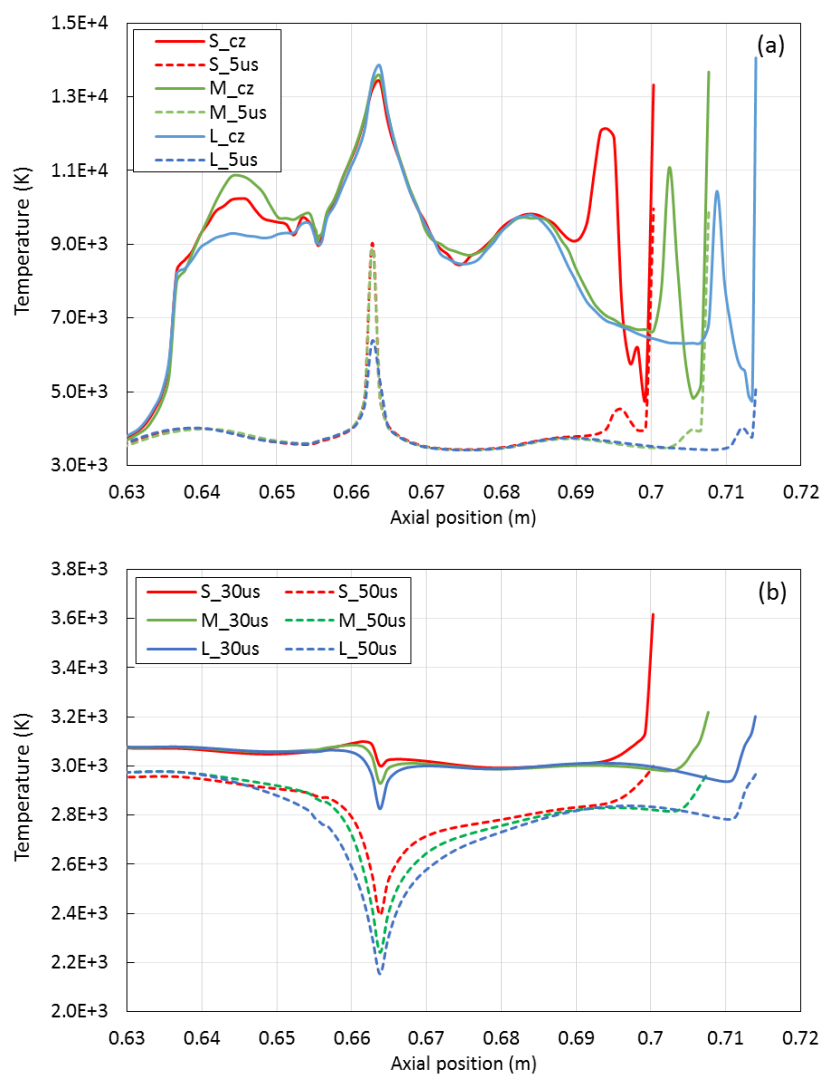


Figure 5.27: Axis temperature at current zero, and 5 us, 30us and 50 us after current zero for different arc durations.

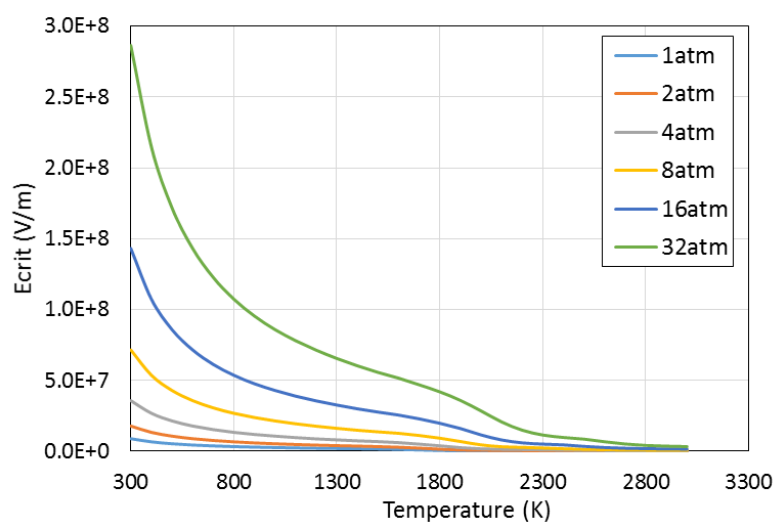


Figure 5.28: Critical electrical field E_{cr} at different pressures [21]

Gas from the expansion volume rushes into the arcing chamber after flow reversal and the flow separates at the space between the two nozzles with an axial position of 663 mm. This results in a stagnation region. Because of the large radial velocity of the cold flow from the expansion volume, temperature in the stagnation region decreases rapidly after current zero. At 30 μs , the stagnation region has the lowest temperature but still highest pressure region, which means the stagnation region has the fastest dielectric strength recovery rate. Therefore, the integrated critical breakdown voltage dramatically increases across the stagnation region which is shown in Figure 5.29b. On the contrary, the weakest region for breakdown is the region before the live contact, where the gas has the high temperature but lowest pressure.

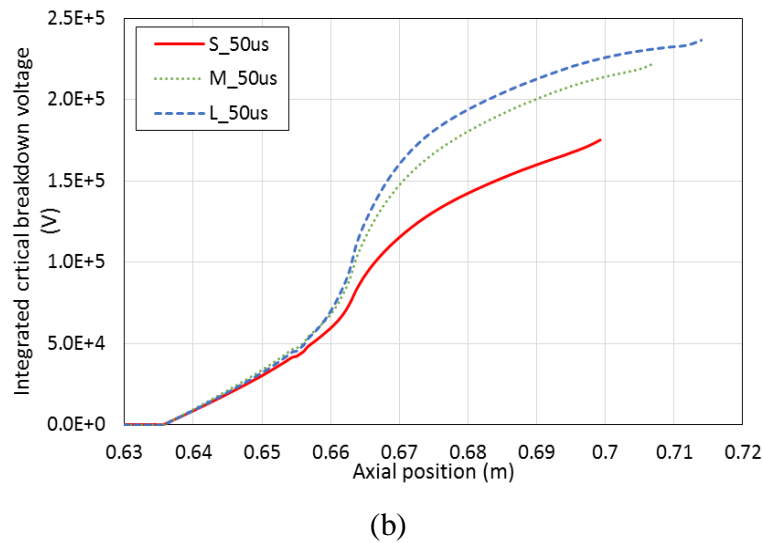
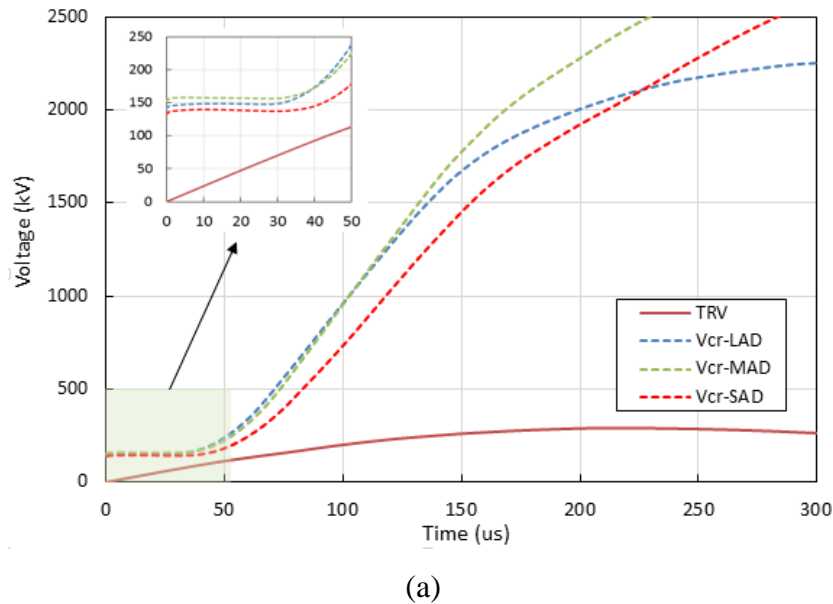


Figure 5.29. (a) Critical breakdown voltage at axis for different arc duration (b) Integrated critical breakdown voltage along the axis 50 μs after current zero

30 us after current zero, the axis temperature for different arc duration cases are almost the same except the small stagnation region, while the pressure for medium arc duration is higher than other two cases. Thus, the medium arc duration case has the best dielectric recovery performance before 30 us. However, after 30 us, the temperature in the stagnation regions has decreased to the lowest level, the gas surrounding the stagnation region starts to be cooled down because of the strong axial convection. For the long arc duration case, it has the most efficient heat removal capability because of the largest mass flux through the hollow contact and main nozzle throat. As a result, the temperature in much of the contact space in the long arc duration case is lower than in the medium arc duration case, though the pressure of long arc duration is still lower than the medium one 50 us after current zero, the critical breakdown voltage of the former is lower than the latter.

5.5.3 Different current levels

The comparison of results for different current levels (L90 and L75) indicates that the flow reversal time and axis temperature profile does not have much variation. However, lower current levels means lower Ohmic heating which causes lower energy into the expansion volume so that the pressure peak for L75 case is only 74.2 % of that for L90 case. The pressure in the arcing space for L75 is 81.2 % of that of L90 case at current zero (Figure 5.30 and Figure 5.31). Larger pressure difference between the expansion volume and arcing space result in a larger convection and energy removal ability. Thus, the critical RRRV and breakdown voltage for L75 are both much lower than those of L90 case (Figure 5.32).

Combined with the result in section 5.5.2, in the optimum global flow and thermal dynamic environment for reliable thermal interruption and the subsequent dielectric recovery process, the pressure should be as high as possible in the contact gap when the current passes its final zero point. A high pressure would be beneficial to a better convection of energy away from the contact space since it will generate a high mass flow rate towards the nozzle exits. Furthermore, a high pressure would aid the dielectric recovery process since there will be more collision between the free electrons and the heavy particles leading to a high dielectric strength.

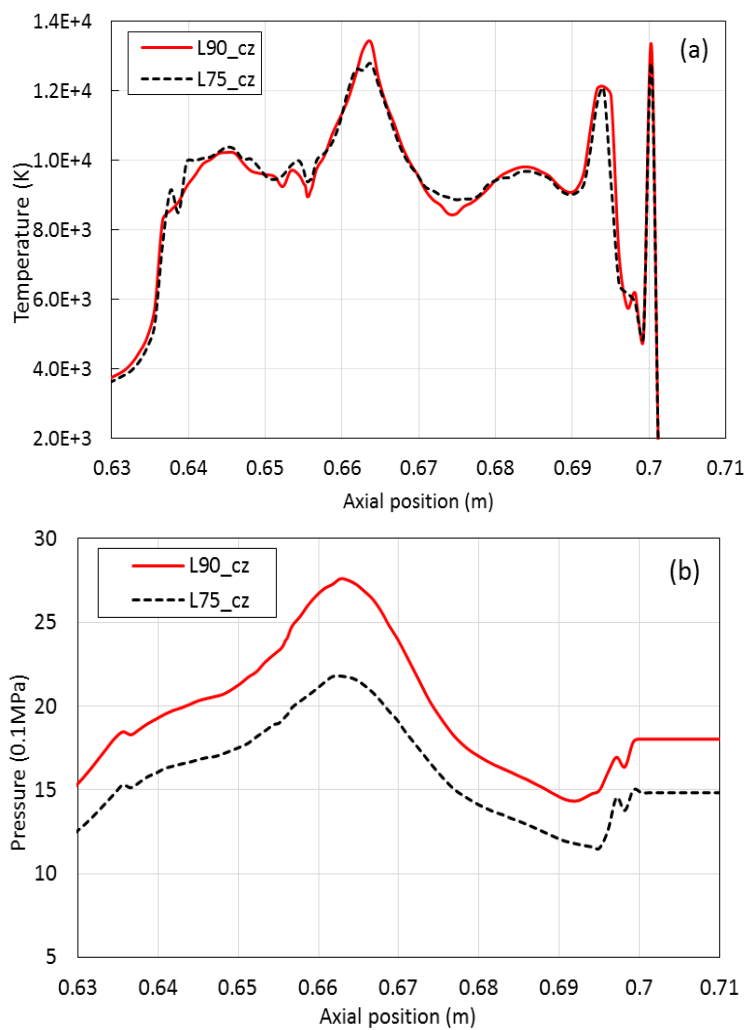


Figure 5.30: Temperature and pressure at axis at current zero for L90 and L75 cases

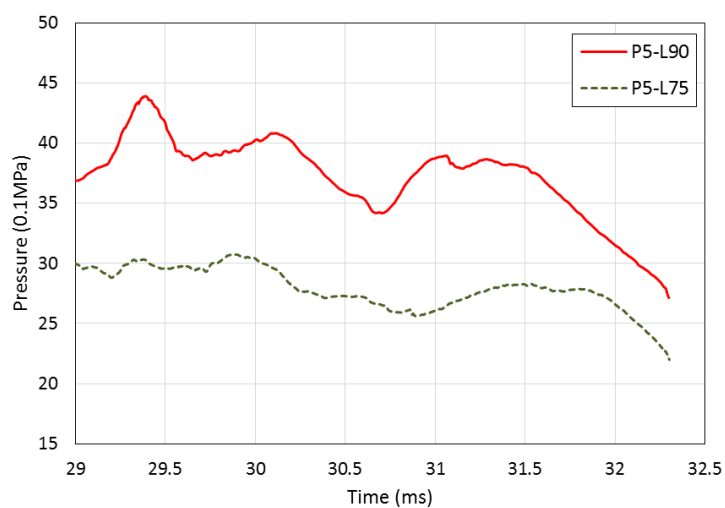


Figure 5.31: Pressure in the arcing space at current zero for L90 and L75 cases

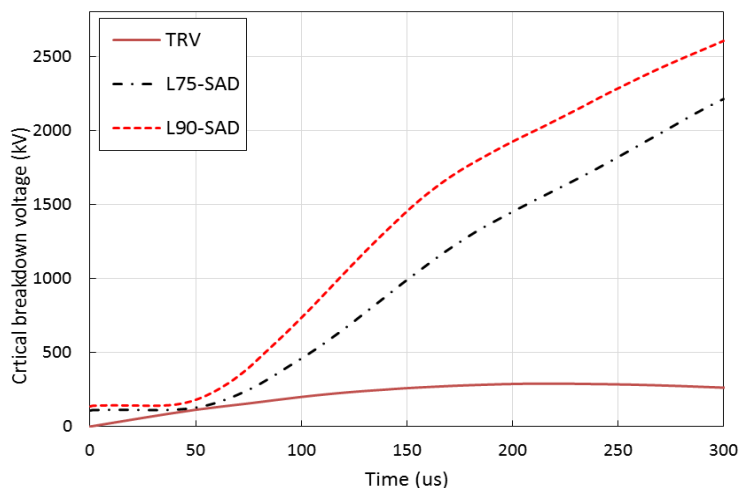


Figure 5.32: Critical breakdown voltage for L90 and L75

5.5.4 Design parameter-channel length

From Figure 5.31, the pressure in the arcing space for the L75 case is smooth than that of the L90 case. The pressure drop from Figure 5.31 for the L75 case is less than L90, which implies that the pressure fluctuation may be responsible for the difference in interruption performance in different test duties. It is expected to reduce the pressure fluctuation and in turn reduce the scattering in circuit breaker performance by changing the channel length. The respective length for short, original and long channels are 32mm, 65mm and 97 mm.

Figure 5.33 shows that shorten the heating channel slightly increases the pressure rise in the expansion volume. The reason might be that with a longer channel, more gas mixture is stored in the channel, which will not contribute to the pressure rise in the expansion volume. Furthermore, the pressure in the arcing space for long channel length performs more smoothly after flow reversal.

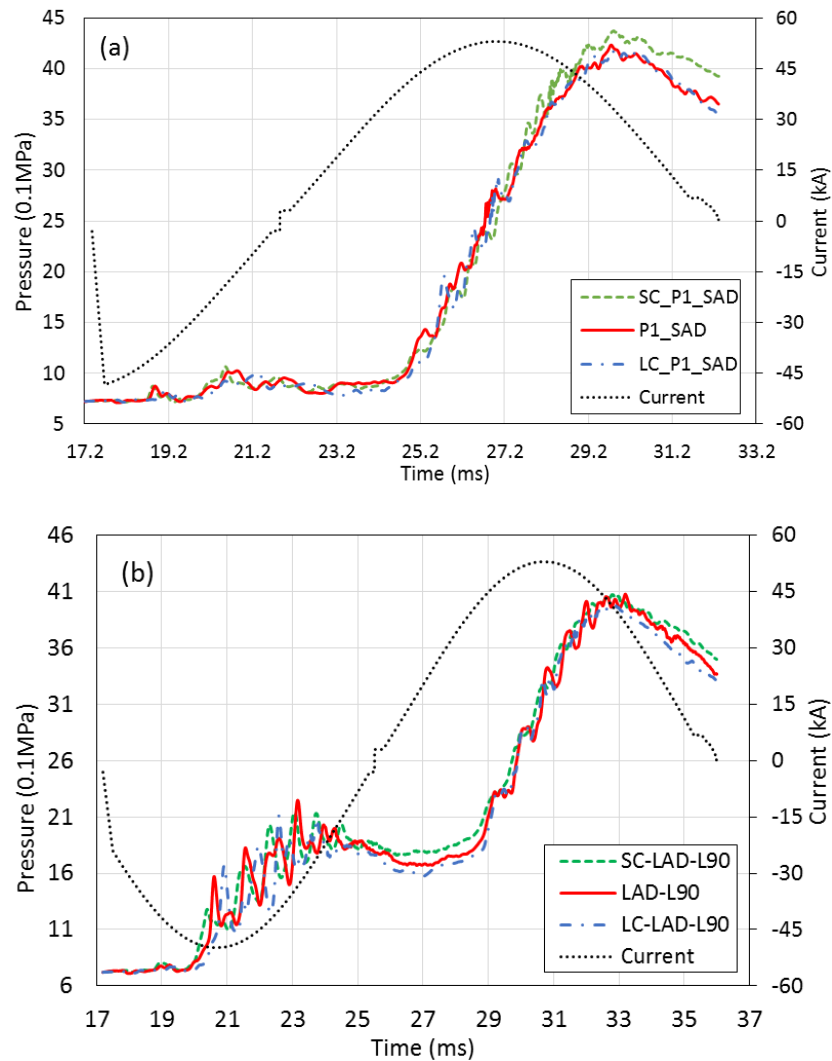


Figure 5.33. Pressure rise in the expansion volume for different channel length with (a) short arc duration (b) long arc duration

For the short arc duration case used in this study, the critical RRRV for short, original, long channel cases are 7.5, 7.5, and 9 kV/us, respectively. The pressure (Figure 5.34a) at current zero is just at a transient increasing state for long channel length, which enables the pressure in the arcing space for long channel length case to attain a higher instantaneous value than that for original channel length. Shortening the heating channel leads to the highest instantaneous pressure in the arcing space, however it does not increase the interruption capability of this circuit breaker. Figure 5.35a shows that shortly before flow reversal, in the arc region the mass of gas mixture keeps a very low value because the hot arc column expands and pushed away the gas mixture from the highlighted domain in Figure 5.4. Around 30 ms, the colder gas from the expansion volume starts to enter the arcing region and the mass

rapidly increases, especially for the long channel length case. Long channel length gives largest mass flux from the expansion volume. In addition, larger mass storage means the density in the arc region is higher, thus the collision between particles becomes more frequency, which will increase the dielectric strength.

For long arc duration, after flow reversal there is an obvious delay pressure profile in the arcing space for different channel length. The pressure (Figure 5.34b) difference between different channel lengths becomes quite small because of the smoother variation. In contrary to the short arc duration case, short channel length case has the largest mass storage in arc region (Figure 5.35b), but still highest pressure between the contacts when the interruption occurs. The critical RRRV for the short channel length case with long arc duration is the highest, 10 kV/us, compared with other two cases, both 9.5 kV/us as expected.

Therefore, changing the length of heating channel could improve the instantaneous pressure in between the contacts for the short arc duration in Figure 5.36a, but has no significant effect on long arc duration. Further extending the channel into the heating chamber may remove the oscillation and results in a smoothly decreasing pressure in the arcing space. Results for long arc duration here suggest that removing pressure fluctuation will result in a slowly decaying but lower pressure when thermal interruption takes places because it takes more time for gas to reach the arcing space. The length of the heating channel is a critical design parameter in controlling the mass flux from the expansion volume and shaping the pressure fluctuation after flow reversal. The choice of the appropriate channel length, apart from mechanical considerations, should be guided by results from computer simulation of different arc durations.

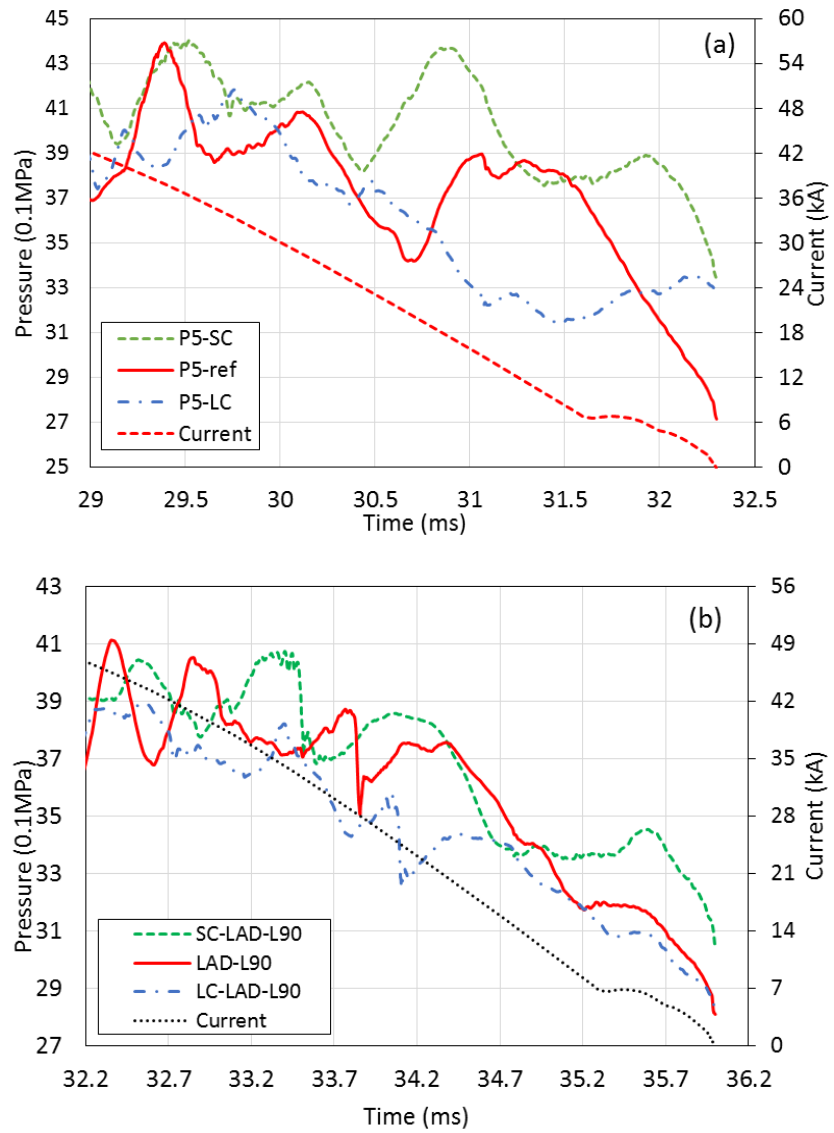


Figure 5.34: Pressure in the arcing space for different channel length with (a) short arc duration (b) long arc duration

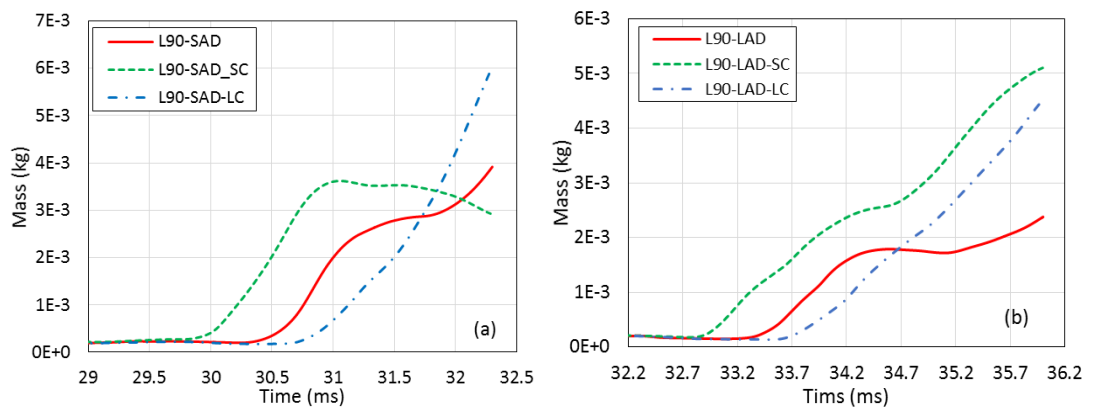
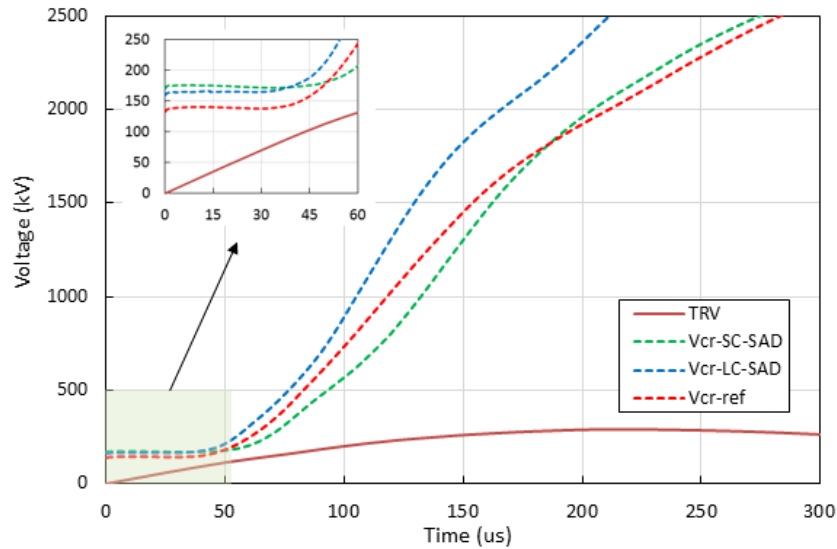
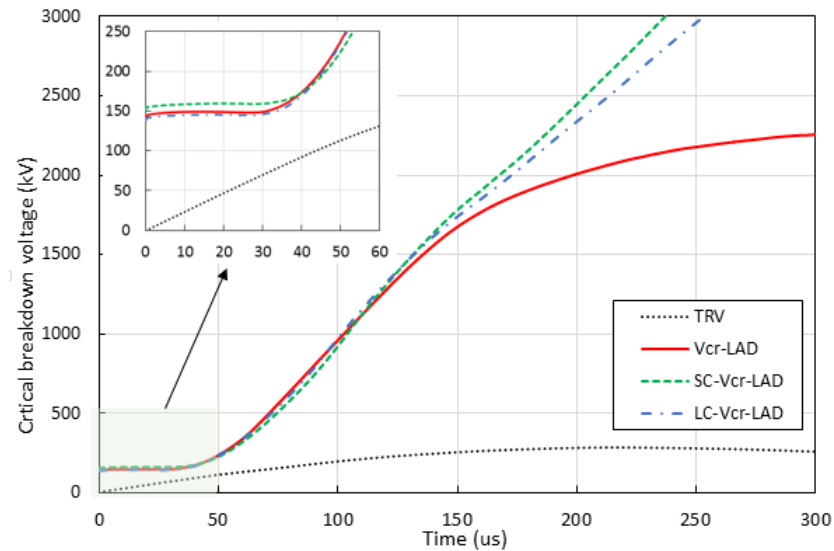


Figure 5.35: Total mass in the highlighted region with dash line in Figure 5.4 for different channel length with (a) short arc duration (b) long arc duration



(a)



(b)

Figure 5.36: Critical breakdown voltage at axis for different channel length with (a) short arc duration (b) long arc duration

5.6 Conclusions

Computer simulation of the arcing process in a self-blast circuit breaker with different arcing durations, current levels and channel lengths were carried out and typical results analysed. The systematic studies performed in this chapter lead to some important findings which are of interest to circuit breaker designers.

- a) Pressure oscillation always occurs as a result of changing current and movement of contact and piston. It has been shown that immediately after the current peak,

the reduction in electrical power input is the direct cause for the onset of pressure drop in the arcing space. This results in a reversed flow and cool gas from the expansion volume starts to rush towards the contact space. This mass flow creates a surplus of mass in the contact space with respect to the mass exhaustion from the nozzles and results in a temporary pressure peak. Following this the pressure and flow field adjusts themselves to create the final flow field at current zero. Changing the heating channel length can substantially affect the profile and timing of this oscillation, which could increase the pressure in the arcing space when interruption occurs.

- b) Optimum design in terms of the global pressure and temperature environment in the arcing space should aim at an efficient and timely supply of gas into the arcing space when the current decreases towards its final zero. With long arc duration, the main nozzle is normally cleared when pressurisation associated with the second current peak takes place. Pressure variation in the arcing space before the final current zero is much smooth. Therefore, the problem associated with pressure transient is less critical.

The density in the arc region rapidly increases after flow reversal in a self-blast circuit breaker, which highly depends on the mass flux from the expansion volume through the heating channel. The pressure variation in the contact space can be regulated by controlling the gas flow from the expansion volume if in future mechanisms can be developed to control the gas flow from the expansion volume.

References

- [1] S. Tominaga, H. Kuwahara, K. Yoshinaga, S. Sakuma. Investigation on Gas Flow of Puffer-Type Gas Circuit Breaker Based on Observation of Arc and Pressure Measurement, *IEEE Transactions on Power Apparatus and Systems*, Vol. PAS-99, pp2040 – 2049, 1980.
- [2] J.L. Zhang, J.D. Yan, A.B.Murphy, W. Hall, and M.T.C. Fang. Computational investigation of arc behaviour in an self-blast circuit breaker contaminated by ablated nozzle vapour. *IEEE Trans. on Plasma Science*, Vol. 30, pp. 706–719, 2002.
- [3] Yonggang Guan, Weidong Liu, Junhui Wu and Junyong Wu, Pressure measurement and characteristic analysis on a 252-kV puffer-type SF₆ circuit breaker, *IEEE transaction on power delivery*, Vol.28, No. 4, October 2013.
- [4] N. Osawa and Y. Yoshioka, Influence of puffer volume and operating force on puffer pressure built up in thermal puffer type gas circuit breaker taking nozzle ablation into account, *Proceeding of Power System Technology*, Vol. 3, pp. 1624-1629, 2002.
- [5] Y. Pei, Q. Zhang, J. D. Yan, M.T.C. Fang, Intelligent computer simulation tools for HV circuit breakers and issues related to simulation, *Electric power equipment-switching technology (ICEPE-ST) 1st international conference* pp. 435-439, 2011.
- [6] J. L. Zhang, J.D. Yan; M.T.C. Fang, Investigation of the effects of pressure ratios on arc behavior in a supersonic nozzle, *IEEE Transactions on Plasma Science* Vol.28 , pp. 1725 – 1734, 2000.
- [7] J.Y. Trepanier, M. Reggio, Y. Lauze etc. Analysis of the dielectric strength of an SF₆ circuit breaker, *IEEE Transactions on Power delivery*, pp. 809-815, 1991.
- [8] D W SHimmin, G R Jones and S M G Ali, Transient pressure variations in SF₆ puffer circuit breakers, *J. Phys. D: Appl. Phys.* Vol.23, pp533-541, 1990.
- [9] J.L. Leclerc, M. R. Smith and G. R. Jones, Pressure transients in a model gas-blast circuit breaker operating at extra high current levels, *IEEE transaction on plasma science*, Vol. 8, No. 4, 1980.
- [10] Y. Yoshioka, M. Tsukushi, K. Natsui, A method and applications of a theoretical calculation for on-load pressure rises in puffer type gas circuit breakers, *IEEE transaction on Power Apparatus and Systems*, Vol. 98, No. 3, pp. 731-737,

1979.

[11] S. Tominaga, H. Kuwahara, K. Yoshinaga, S. Sakuma, Estimation and performance investigation on SLF interrupting ability of puffer-type gas circuit breaker, IEEE Transactions on Power Apparatus and Systems, Vol. 98, pp. 261-269, 1979.

[12] A. M. Rahal, H. Delacroix, A. Gleizes etc. Pressure transients in a self-blown circuit breaker, proceeding of gas discharge and their applications, Oxford, pp. 95-98, 1985.

[13] P. Scarpa, B. Dauby, J.M. Defise etc. “SF₆ auto-expansion circuit breaker design: numerical and experimental investigations of arc-gas interaction”, IEEE Transactions on Power Delivery, Vol. 7, pp.339-345, 1992.

[14] J. Kim; C. Yeo ;Y. Yoshioka, Effects of Various Factors on Gas Blast Characteristics of Auto-Expansion Type Gas Circuit Breaker, IEEE Transactions on Power Delivery, Vol. 25, pp. 1538 – 1546, 2010.

[15] Y. Guan, W. Liu, J. Wu and J. Wu, Pressure measurement and characteristic analysis on a 252-kV puffer-type SF₆ circuit breaker, IEEE transaction on power delivery, Vol.28, No. 4, pp. 2616-2622, 2013.

[16] S. Tominaga, H. Kuwahara, K. Yoshinaga, S. Sakuma, Estimation and performance investigation on SLF interrupting ability of puffer-type gas circuit breaker, IEEE Transactions on Power Apparatus and Systems, Vol.98, No.1, pp. 261-269, 1979

[17] N. Osawa and Y. Yoshioka , Calculation of transient puffer pressure rise takes mechanical compression, nozzle ablation, and arc energy into consideration, IEEE Transactions on Power Delivery, Vol. 20, pp. 143-148, 2005.

[18] J.D. Yan, M.T.C. Fang, and W. Hall. The development of pc based cad tools for self-blast circuit breaker design, IEEE Transactions on Power Delivery, 14(1):176–181, 1999.

[19] J.D. Yan, S.M. Han, Y.Y. Zhan, H.F. Zhao and M.T.C Fang, Computer simulation of the arcing process in high voltage puffer circuit breakers with hollow contacts, Proceedings of XVIIIth Symposium on Physics of Switching Arcs, Brno Czech Republic, pp. 99-108, 2009.

[20] C.B. Ruchti and L. Niemyer, Ablation controlled arcs. IEEE Trans. on Plasma Science, Vol. 14, pp. 423–434, 1986.

[21] X. Jiang, X. Li, H. Zhao etc. Analysis of the dielectric breakdown

characteristics for a 252-kV gas circuit breaker, IEEE transactions of power delivery, Vol. 28, 2013.

[22] T. M. Wong, J.D. Yan, X. Ye, J. Abrahamsson and M.T.C Fang Global Thermal and Aerodynamic Environment in High Voltage Auto-Expansion Circuit Breakers. Proceedings of XVII Symposium on Pysics of Switching Arc. Local Organisation Committee, Brno, pp. 37-46, 2007.

Chapter 6

Conclusions and Future Work

6.1 Major Contribution and Achievements

There are four major contributions of the present work in the field of arc modeling and investigation on interruption capability of circuit breakers.

Firstly, the improved Liverpool arc model was built in a newly developed software package, which is called the Integrated Simulation and Evaluation Environment (ISEE). This intelligent simulation tool enables automation in model set up with a time saving of 90%, and allows easy and rapid identification of problems in new models through visual monitoring of the intermediate results in real time mode, which is extremely important for academic research staff.

The second contribution is that it is the first time that the turbulence parameter for the Prantl mixing length model is calibrated using real commercial circuit breaker geometries and test conditions. The fact that a single value of the turbulence parameter is applicable to three types of auto-expansion circuit breakers paves the way forward towards quantitative prediction of the thermal interruption performance of commercial circuit breakers.

The third contribution gives a detailed study on how the arc durations affect the interruption performance, which is the first time that this type of work is performed. It is shown that the mass flow rate surrounding the arc column is a key factor affecting the thermal interruption capability of the auto-expansion circuit breaker. Detailed knowledge gained from this research will be useful to the optimization of circuit breaker design in terms of identifying the weakest arc cooling situation and achieving maximum energy removal under different switching conditions.

The final contribution is an investigation of the pressure transient in the operation of auto-expansion circuit breaker. It presents a detailed analysis of the onset of pressure variation in the contact space and the time lag between the current peak and pressure peak in the expansion volume is explained using an energy flow rate balance. The reason for the pressure variation in the contact space before the final current zero is also identified by analyzing the mass flow balance in the contact space.

6.2 Summary and Conclusions

The Integrated Simulation and Evaluation Environment (ISEE) has been shown to be an efficient tool for optimum design studies of high voltage circuit breakers and similar arcing devices [1]-[6]. It eliminates the need for programming in the setup of arc model and its operation is intuitive by mapping the design process in practice into the simulation environment. With the help of ISEE the time scale for flow to reach quasi-steady state in a newly designed arcing device was obtained to help optimise the experimental conditions in [4][7]. It has been shown that such an environment should result in huge savings in time and cost for switchgear manufacturers [1][3][5]. It is equally helpful for academic researchers as a tool for improving arc models because of the advantages provided by the Visual Monitor. Using ISEE, the conventional k-epsilon turbulence model was modified to take into account of steep radial temperature gradient at the arc edge with much improved results in [3]. Investigations of computational convergence and the effects of initial arc conditions with sufficient accuracy can be achieved with the Liverpool arc model [3].

Another turbulence model, the Prantl mixing length model, has also been calibrated using real circuit breaker type test results in Chapter 3, which is hardly done by other researchers because of the scarce in test results from manufacturers, lack of reliable arc model and long computational time. In order to calibrate the turbulence parameter of the Prantl mixing length model, real arcing conditions including interrupting currents, contact travels, and transient recovery voltages of two commercial circuit breakers, 145 kV and 245 kV, are used to do the prediction. The range of applicable turbulence parameters in the current zero period are found for

converge-flat-diverge nozzles in different circuit breakers. The turbulence parameter changes linearly with the interrupting current from 0.05 at 15 kA to Tp_{I0} at current zero based on argument of the physical process. For the three circuit breakers the ranges overlap at 0.35, implying that a single turbulence parameter is able to make satisfactory prediction of the thermal interruption performance of different breakers. During the calibration process, the PTFE ablation was calculated and compared with published measurement, which gives a reasonable agreement.

The Liverpool arc model has been proved and verified, and then used to investigate the effect of arcing duration and pressure transient on the interruption capability of real commercial auto-expansion circuit breakers in Chapter 4 and Chapter 5.

The investigation shows that in some auto-expansion circuit breakers, the pressure peak in the expansion volume has a delay of 2.8 - 3.4 ms with reference to the current peak when the arc duration varies. It has been found that a reasonable indicator of the interruption environment is the average mass flow rate in the main nozzle. The short arc duration case (12.25 ms) is the most difficult case with the lowest critical rate of rise of recovery voltage (RRRV) of 10 kV/ μ s, just above the initial system applied RRRV of 9 kV/ μ s. This is a result of insufficient gas flow cross sectional area between the live contact and the main nozzle to develop rapid gas flow for arc cooling. The auxiliary nozzle plays two roles. It provides blockage in the high current phase to reduce gas exhaustion from the main nozzle into the hollow contact; after current zero the hollow contact shares a considerable portion of the system recovery voltage, especially for the short arc duration case (36%). Therefore the proper design and use of an auxiliary nozzle is key to enhancing the thermal interruption capability of high voltage auto-expansion circuit breakers.

There are also important findings in the study of the transient pressure variation in auto-expansion circuit breakers. The time lag between the current peak and pressure peak in the expansion volume was explained by using an energy flow rate balance method, which is flow reversal occurs when the enthalpy exhaustion rate from the contact space equals the electrical power input. The pressure changes in the arcing space under different arc durations, different current levels and different length of the heating channel have also been studied in details.

The thermal recovery and dialectical recovery ability of the investigated circuit breaker were both calculated under different arcing conditions. It is found that optimum design in terms of the global pressure and temperature environment in the arcing space should aim at an efficient and timely supply of gas into the arcing space when the current decreases towards its final zero.

At present there is no technology available to control the mass flow rate from the expansion volume, restricted by the mechanical design. However once this can be done conditioning the arc quenching environment in future intelligent circuit breakers will become a reality. It becomes clear that for the design of new generation of circuit breakers, two aspects are most important, the use of a more accurate and controllable driving mechanism and the control of mass flow from the expansion volume using advanced mechanical devices that satisfy the insulation requirement.

6.3 Future Work

6.3.1 Improvement for arc model based on measurement

As Figure 3.2 shows, it is difficult to measure the contact erosion and nozzle ablation because of the uneven contact and nozzle surface. To make the verification of radiation model and turbulence model more accurate, it is strongly needed to make a criterion to find an equivalent model including contact length, nozzle diameter etc following the interruption operations. As discussed in Chapter 2, after each test, the nozzle diameter varies with different extent. Because of the lack of accurately measured ablated mass, the predicted results on nozzle ablation need further verification. Contact erosion and nozzle ablation measurement remain as important topics in the field of arc research.

6.3.2 Parallel processing

With the increasing of computation domain, more grids are needed. It significantly increases the computation cost especially for three dimensional model. The computer simulation with more than 100,000 grid cells have to be on parallel processing in

order to keep computational time within an acceptable value for research and development. In an arc simulation, a large portion of computation time is used to do the interpolation to find the density and transport properties (laminar viscosity μ_l , laminar thermal conductivity divided by specific heat k/C_p , and electric conductivity, σ) of arcing gas mixture. Parallel computation can be realised by using the multitasking capability of modern computers. A trial on the parallel calculation of material properties has been carried out and it is feasible.

6.3.3 Radiation transfer and nozzle ablation

For auto-expansion circuit breakers, nozzle ablation is caused by arc radiation. The emission from the arc core is partly absorbed at the arc edge. Radiation-reabsorption in the arcing gas is a fundamental process affecting the arc temperature distribution and also the ablation of PTFE nozzles.

In the present work a one dimensional and semi-empirical model is used with an assumed percentage of 50% for the radiation flux from the arc core to be absorbed at the arc edge. A more accurate radiation model is expected to further improve the simulation accuracy. Relevant work is on-going at Liverpool to tackle this problem. There is work on the use of more complex model such as the Discrete Ordinate Method (DOM) [8] but the computation time is not affordable for simulation of commercial circuit breakers. Furthermore basic radiation data for complex gas mixtures may not be available. However, it is a direction for improving the overall accuracy of arc modelling.

In most models of arc modelling, PTFE ablation is assumed to be caused by arc radiation based on a constant ablation energy. Therefore ablation by hot gas in contact with the PTFE surface is not considered. A more universal ablation model will help improve the prediction accuracy of pressurization in the expansion volume.

References

- [1] Y. Pei, J. Zhong, J. Zhang, J.D. Yan, A comparative study of arc behavior in an auto-expansion circuit breaker with different arc durations, *J Physics D: Applied Physics*, Vol. 47, pp. 335201, 2014.
- [2] J.D. Yan, Y. Pei and M.T.C. Fang, The development of an object based simulation tool for switching arcs, *Proceedings of XIX Symposium on Physics of Switching Arc*, Brno Czech Republic, 2011.
- [3] Y. Pei, Q. Zhang, J.D. Yan, M.T.C. Fang, Intelligent computer simulation tools for HV circuit breakers and issues related to simulation, *Electric power equipment-switching technology (ICEPE-ST) 1st international conference* pp. 435-439, 2011
- [4] Y. Pei and J.D. Yan, An object based approach for defining and implementing switching arc models, *Proceedings of the XIX International Conference on Gas Discharges and Their Applications*, Beijing, China, pp. 138-141, 2012.
- [5] Y. Pei, J.D. Yan and J. Zhang, Interruption Capability of an Auto-expansion Circuit Breaker with Different Arc Duration, *International conference: Gas Discharge*, France, pp. 147-150, 2014.
- [6] J.D. Yan, Y. Pei, Q. Zhang and H. Wang, The influence of product design parameters on the performance of high voltage circuit breakers, *Proceedings of XX Symposium on Physics of Switching Arc*, Brno Czech Republic, 2013.
- [7] F. Yang, Y. Pei, J.D. Yan, J. Humphries, J.W. Spencer, An experimental investigation of nozzle arcs under turbulent conditions, *International conference: Gas Discharge*, France, pp. 63-66, 2014.
- [8] T. T. Stefan, Discrete-ordinates method in radiative heat transfer, *International journal of engineering science*. Vol. 36, pp. 1651-1675, 1998.